DOE/MC/28176 – 5727
(DE97005441)

The Atlas of Major Appalachian Gas Plays

Final Report
February 1997

Work Performed Under Contract No.: DE-FC21-91MC28176

For
U.S. Department of Energy
Office of Fossil Energy
Federal Energy Technology Center
Morgantown Site
P.O. Box 880
Morgantown, West Virginia 26507-0880

By
West Virginia University
P.O. Box 879
Morgantown, West Virginia 26507-0879

Disclaimer

DISCLAIMER

Portions of this document may be illegible electronic image products. Images are produced from the best available original document.

Abstract

This project will evaluate the technical, economic and environmental feasibility of filling abandoned underground mine voids with alkaline, advanced coal combustion wastes (Fluidized-Bed Combustion, FBC ash). Both pneumatic and hydraulic injection methods will be investigated. Success will be measured in terms of technical feasibility of the approach (i.e. % void filling), cost, environmental benefits (acid mine drainage and subsidence control) and environmental impacts (noxious ion release).

Phase I of the project is scheduled for 18 months starting in February, 1994 and is concerned with the development of the grout and a series of predictive models. These models will be verified through the field phases and will allow the results to be packaged in such a way that the technology can be easily adapted to different site conditions. Phase I will also redesign a pneumatic ejector, that was developed to stow limestone, to efficiently stow FBC ash. Bench scale testing will verify the redesign in Phase I.

The 12 month Phase II is a small scale field test at Anker Energy's Fairfax mine. An inactive panel will be used to evaluate flow, strength, and pressure requirements for hydraulic (grout) injection. The Phase II pneumatic injection activities willl take place at an Anker Energy mine in Preston County, West Virginia. Air flow requirements, pressure requirements, stowing rate (tons per hour), and stowing efficiency (distance blown) will be determined.

Phase III is to take 26 months and will be a full scale test at Anker's eleven acre Long Ridge mine site. The mine will be filled using both pneumatic and hydraulic injection methods.

It is expected that the FBC ash will replace what is now an acid mine pool with an alkaline solid so that the ground water will tend to flow around rather than through the previously mined areas. The project will demonstrate whether FBC ash can be successfully disposed of in underground mines. Additionally, the project is directed towards showing that such disposal can lead to the reduction or elimination of environmental problems associated with underground mining such as acid mine drainage and subsidence.

Acknowledgements

The authors would like to acknowldege the following organizations and persons for their support with this project:

Scott Renninger, Project Manager, US DOE/METC
Mr. Steven J. Bossart, DOE Project Officer
John Faltis, President & CEO, Anker Energy
Kim Burke, Vice President Northern Operations, Anker Energy
Jeff Kelly, Vice President Engineering, Anker Energy
Gerald Ramsburg, President, Patriot Mining Corporation, Inc.
Duane Maust, Superintendent, Patriot Mining Corporation, Inc.
Troy Titchenell, Land Agent, Anker Energy Corporation
The Analytical Laboratory at the National Research Center for Coal and Energy

Graduate Research Assistants:
Mr. Scott Putnam, Bench-Scale Grout Rheology Model
Mr. John Adkinson, Grout Rheology Model
Mr. Ramamurthy S. S. Kannan, Subsidence Control
Mr. Michael J.Main, Grout Formulation

Dr. Robert Eli , WVU
Dr. Rakesh Gupta, WVU
Dr. Ismail Celik, WVU

Table of Contents

List of Tables

List of Figures

Executive Summary

The purpose of this document is to report on the progress of Phase I of this project. Phase I involves laboratory scale experimentation and modelling to optimize the use of circulating fluidized-bed combustion ash in a grout to fill complex underground mine voids. The report is oraganized to report on each task separately. Task 1 Grout Formulation, perfromed by Dr. William A. Head of the Civil and Environmental Engineering Department, is concerned with the formulation of a grout with appropriate strength and consistency to be used to meet the goal of the project. Working with Dr. Head, Dr. Donald D. Gray is concerned with Grout Rheology (Task 2 and 3). Dr. Gray optimized the flowability of the grout with admixtures and by adjusting water content. Dr. Gray used both computer models and bench-scale experimentation to test the rheological properties of the grout. Task 5 Subsidence Control performed by Dr. Hema J. Siriwardane set a threshold strength that the grout must exceed in order to control subsidence. All grouts tested to date have exceeded the 500 p.s.i. threshold. Task 6 Contaminant Transport also performed by Dr. Siriwardane is concerned with the formation of acid mine draiange and the migration of the contaminants into the groundwater. The task will model contamainat transport both before and after the Phase III mine is filled with the alkaline grout. Dr. William A. Sack is performing Task 4 Water Quality Monitoring. He is collecting samples at the Phase III mine to establish a baseline to be compared against data collected after the mine is filled with alkaline cFBC ash grout. The final set of tasks deals with Pneumatic Transport of cFBC ash. Mackenzie Burnett of Burnett Associates, Inc. has designed a pneumatic device that will stow ash in an underground mine from the surface above the mine. The device will be tested in the filed as will the hydraulic grout methods in later Phases of this project.

Introduction

The United States currently has over 480 billion tons of mineable demonstrated reserve base of coal. Two thirds of this reserve is mineable by underground methods. Unfortunately coal contains a number of components such as sulfur and nitrogen that form undesirable oxides during combustion. Coal also contains incombustible mineral matter that is converted into ash and leads to suspended particles in air and degradation of downstream components. Several technologies designed to prevent the release of sulfur dioxide and nitrogen oxides have been developed. One such technology is Circulating Fluidized-Bed Combustion (cFBC). The cFBC technique combines limestone and coal in a circulating combustion chamber. The limestone burnt with the coal will capture the sulfides and a low combustion temperature prevents nitrogen oxides from being formed. However, this technique produces a large quantity of waste that has free lime or slaked lime with a large portion of fly ash. This material can present a disposal problem, and due to its high pH, landfill costs can be quite high.

Coal mining areas have been subjected to a series of problems. The legacy of coal mining has been ground collapse due to subsidence, and acid mine drainage due to dissolved pyrite forming sulfuric acid where abandoned mine workings drain underground water pools. The combined subsidence and acid mine drainage problems due to abandoned coal mines prompted the enactment of the Surface Mining and Control and Reclamation Act of 1977. This act was passed in order to accomplish the reclamation of abandoned coal mine lands. This reclamation includes the abatement of acid mine drainage, the prevention of mine subsidence, and reclamation of surface mines. The act also places strict regulations on coal companies, requiring them to take responsibility for the lands left behind after mining.

The combined problems of advanced coal combustion byproduct disposal, mine subsidence, and acid mine drainage create a ready made market. The problem of FBC ash disposal can be solved by stowing the material in abandoned mines. The matrerial may be made into a grout or steowed pneumatically. When stowed pnuematically, the ash, which is typically is highly pozzolonic, will achieve a reasonable compressive strength in the humid underground environment without additives. In addition, the neutralizing capability of the material makes it an ideal candidate for acid mine drainage prevention. When grouts are utilized, the flowability characteristics of the FBC grout will fill the complex mine voids. This solution carries the multiple benefit of creating a market for the FBC byproducts and providing mine closure engineers and abandoned mine authorities a new tool to combat abandoned mine land problems. The potential market for the FBC byproducts includes every active coal and non-coal mine, and every abandoned mine that state and federal agencies are in the process of reclaiming. The potential market is such that future coal contracts may include clauses to backship the FBC material to the mine. Full implementation of this application of the FBC material will change it from a waste product to a valuable product to be sold. This will help electric companies and other large and small scale coal burners to make the decision to use FBC or other Advanced Coal Combustion technologies.

This report will individually report on the six main tasks of this research project. The first

section is Task 1 Grout Formulation. Dr. William J. Head is the principal investigator for Task 1. Experiments have been conducted to determine the optimum mix of ash, water, and admixtures to give the grout optimum flowability and strength. Dr. Donald D. Gray is the Principal Investigator for Task 2 Grout Rheology Model and Task 3 Bench-Scale Rheology Tests. Task 2 involves the computer modelling of grout flow given formualtions provided by Dr. Head. The model will also aid in the design and verification of the Becnh-Scale testing. Under Task 3 Dr. Gray and his team are concerned with the flowability of the grout and modelling it on a bench scale. Task 4 Water Quality Modelling is concerned with gathering background water 1quality data for the Phase II and Phase III field demonstration sites. Dr. William A. Sack is the Prinicpal Investigator for Task 4. Task 5 Subsidence Control and Task 6 Contaminant Transport research efforts are lead by Dr. Hema J. Siriwardane. Dr. Siriwardane's research focusses on determining the minimum strength requirement for the grouts to be placed into the mine void and to develop the borehole drilling patterns for both Phase II and Phase III mines. Task 6 will modelling the change in transport of contaminants into the groundwater below the mine before and after grouting. Additional work performed includes investigating the use of pnuematic devices to inject FBC into a mine void. A separate section reports on the progress of this worked performed by Mackenzie Burnett of Burnett Associates, Inc.

TASK 1 GROUT FORMULATION

Purpose

The prime purpose of the work reported here is to develop grouts that are suitable for injection into selected underground mines. The grouts consist of fluidized bed ash, water, and other ingredients that may be necessary to achieve desirable mixture characteristics.

Methodology

The laboratory program associated with grout development focused on attainment of mixtures which were structurally adequate, appropriately durable, placeable in the field, and economical. Assessments of underground cavities with the aid of finite element computer codes aided in determination of desirable mixture properties. Such properties were adequate strength for subsidence control and appropriate permeability which affects grout durability and transport of contaminants through grout media. Considerations of flow and spreadability of fluid grout informed the development program of properties necessary for fresh grouts so that they may be properly and economically placed in underground cavities. Effort was expended in the program to employ water from mine pools as grout mix water as an example of an economic consideration.

The laboratory program entailed mixing varying proportions of Morgantown Energy Associates (MEA) ashes with water and other ingredients and casting the mixtures into cylinders and beams for future testing. To date, the test have dealt with strength, strength development, consistency/flowability, and durability. Strength tests were unconfined compression test of three inch diameter by six inch high cylindrical specimens conducted at selected time intervals after casting. Specimens were covered after casting to prevent egress of water. Triplicate samples were tested and average strengths were reported. A few beam specimens were fabricated to determine representative flexural strengths of selected mixtures. Strength development was assessed by monitoring in compressive strength with time. Based on previous experience, a target consistency of ten to twelve inch slump of the fresh grout was selected for all mixtures. Tests were also performed to determine changes in mixture consistency with time.

In sum, employed in the laboratory program were tests to determine relationships among grout water content, age, strength, consistency, flowability, and durability. Strength tests were conducted in accordance with provisions found in ASTM Standard test methods C 39 (compression test) and C 78 (flexure test). Consistency (slump) test were conducted according to ASTM C 143.

Results and Discussion

Results of the laboratory program appear in Figures 1-18; a discussion of the Figures follows. Figures 1 and 2 represent particle size distribution curves for the coarse fraction (3/8 in to # 200 sieve) and the fine fraction (-200 sieve) of the MEA fluidized bed ash. The coarse fraction resembles a sandy particulate material while the fine fraction resembles a silty substance.

Information from MEA plant personnel indicates that the average production of ash is about evenly split between coarse (bottom ash) and fine (fly ash) particles. However, production of ash is nonuniform both in terms of particle sizes available and with respect to physical characteristics of the ashes. The former point is illustrated in Figure 1, the latter in following Figures.

Figure 3 is a plot of compressive strength as a function of water content and age for specimens whose solids contents were 50 percent bottom ash and 50 percent fly ash. The results are typical: strength increases with age for a given water content and decreases with increasing water content for a given age. Tap water was used in fabricating these specimens. Water content here and in following plots was measured in terms of percent of total weight of specimen.

Figure 4 is a plot of compressive strength versus age for specimens fabricated with a 38 percent tap water and 4.6 percent bentonite, a commercially available clay material. Bentonite was used to enhance the flow characteristics of the grout mixture. Strength increased with age as anticipated.

Figure 5 contains plots of compressive strength versus age for specimens containing various combinations of water content and admixtures. WRDA-19 is a commercially available high-range water reducer employed on occasion in concrete technology to enhance consistency or strength characteristics of concrete mixtures. WRDA-19 was used here in attempts to enhance flow characteristics of grouts. Darafill is a commercially available air entraining admixture used to entrain air bubbles in concrete mixtures. It was used here to enhance mixture flowability. The plots indicate that the water reducing agent had little effect on mixture strength while the air entraining agent produced notably weaker mixtures compared to the mixtures containing tap water only. The fourth plot indicates that the mixtures containing bentonite may gain strength relatively slowly. The higher (39 percent) water content for this latter mix was necessary to achieve the target slump of ten to twelve inches for the fresh grout.

Figure 6 indicates that grouts can be successfully fabricated using mine water as mixing water. Specimens were made using 31 percent acidic water from the Longridge mine. The strengths of such specimens were essentially the same as strengths of specimens made using tap water both in the short term and over about a six-month period.

Figure 7 strength versus age plots are shown for specimens fabricated from ashes collected from the MEA plant at various times. Evident here is that ashes differ in cementitious characteristics.

Figure 8 portrays strength/age plots for specimens whose solids component were fly ashes only. Such mixes generally require more water than mixes containing bottom ash; additionally, strengths of fly ash only mixes varies with production time. Two mixes were fabricated with small (three or six percent) amounts of Portland cement. Such mixes were not as strong as a mix containing less water. The cement containing mixes required a relatively high water content to achieve the specified initial slump.

In Figure 9 are shown results of flexure tests. Flexural strengths vary directly with age and with

composition. Flexural strength of grouts is relatively low which reflects the brittle behavior associated with cement bound materials.

Figure 10 portrays slump as a function of water content for a mix consisting of a 50-50 blend of bottom ash and fly ash. As anticipated, slump varies directly with water content . Water contents of about 33 to 35 percent of total weight of specimen are required to achieve target slumps of ten to twelve inches for mixes containing both bottom ash and fly ash only.

In Figures 11 and 12 are shown slump versus age or time after mixing for various grouts. As anticipated, slump decreases with time after mixing. Noteworthy is that significant slump (about three inches) remained for most mixes after two hours had elapsed.

Figure 13 contains plots of compressive strength versus age for specimens whose solids content were 50/50 bottom ash/fly ash and with 31 percent water contents. Specimens were made with tap water. Some specimens were simply covered to prevent water loss until tested while other specimens were submerged in acidic mine water until tested. No differences were noted between the submerged and unsubmerged specimens.

Compared in Figures 14 and 15 are results of slump and flow tests for grouts containing tap water, high-range water reducer, an air entraining admixture, and the clay material, bentonite. The flow used here employed a cylindrical container, four inches in diameter and six inches high. The container was filled with fresh grout and then moved vertically upward allowing the grout to flow outward. The diameter of the sample after flow ceased was the flow. This test was believed to provide a better measure of grout flowability than the slump test. As indicated in the plots, the water reducing and air entraining admixtures did enhance flow characteristics slightly. Of note was that mixes containing bentonite and water reducer exhibited both enhanced flow and cohesion compared to the other mixes. Cohesion is the property of a mix to "stick together" and not experience particle segregation.

Illustrated in the last three plots, Figures 16, 17, and 18 is the swelling tendency of mixes with various ingredients as a function of age. The plots indicate that the grouts have little propensity to change volume with increasing age.

Conclusions

Based on results discussed above and observations made in the laboratory, the following **tentative** conclusions appear to be warranted:

1. The MEA ashes, products of modern coal-burning and gas cleaning technologies, are self-hardening materials. The ashes will form a hard, coherent, concrete-like substance when mixed with water. Setting and hardening times range from several tens of minutes (initial stiffening and significant loss of initial slump) to a few days (material capable of supporting small load), respectively. Setting and hardening times are functions of water content and composition of the

ashes which is variable. The coarse ash (bottom ash) has particle size distributions which are similar to coarse sands while the fine ash (fly ash) resembles silty soils.

2. Most of the blends of MEA ashes employed in the laboratory have consisted of 50 percent bottom ash and 50 percent fly ash as percent of total weight of ash. These proportions were chosen because they represent the average production quantities from the MEA plant.

3. Compressive strengths of blends of MEA bottom ash and fly ash are functions of water content, time, ash composition and type and quantity of admixture present, if any. Flexural strengths of such mixtures are probably affected by similar variables in similar ways.

4. Mixture water contents, as percent of total weight of sample, to achieve ten to twelve inch slump range from about 31 percent to about 43 percent for "straight" mixes (no admixtures) and mixes containing bentonite, respectively.

5. Mixes containing three to five percent bentonite seem to exhibit superior flow and cohesion characteristics when compared to straight mixes. Compressive strengths of bentonite mixes are lower than strengths of straight mixes at similar ages. However, attainment of 500 psi unconfined compressive strength over short (30 days or less) time periods appears feasible with properly constituted bentonite mixes. Five hundred psi was chosen as a benchmark compressive strength based on previous experience with strength levels needed to ameliorate subsidence problems in shallow underground cavities.

6. Incorporation of conventional air entraining agents into grouts at moderate to high dose rates seems to offer little advantage in enhanced consistency when compared to straight mixtures. High-range water reducers may enhance consistency to a useful degree; however, such admixtures are expensive and would be required in large dose rates. Utilization of a high-range water reducer appears not to be cost-effective at this time.

7. It seems feasible to employ mine pool water as mixing water. Strength appears to be unaffected when mine pool water is used as mixing water. In addition, mixtures will harden when submerged in mine pool water.

8. Consistency (slump) of mixes decreases with time. However, the time rate at which mixtures stiffen appears to be moderate. Consequently, mixes should remain pumpable in the field for sufficient time to allow proper installation of the grouts in underground cavities.

9. Grouts made with MEA ash experience little change in volume with time.

10. At the present time, the following "recipe" is recommended for disposal of MEA ashes in underground cavities: the ash component should consist of about 50 percent each of bottom ash and fly ash. The water content should be approximately 43 percent of the total weight of mixture with adjustments made on site to yield a grout with ten to twelve inch slump. Three to five percent of the total weight of the mixture should be bentonite. These proportions were employed in a recent

field trial which demonstrated that such grouts could be successfully mixed and that they exhibited satisfactory flow and cohesion characteristics. It must be emphasized that these proportions are tentative; final proportions will be established based on results of current flow characterization test and test of other admixtures.

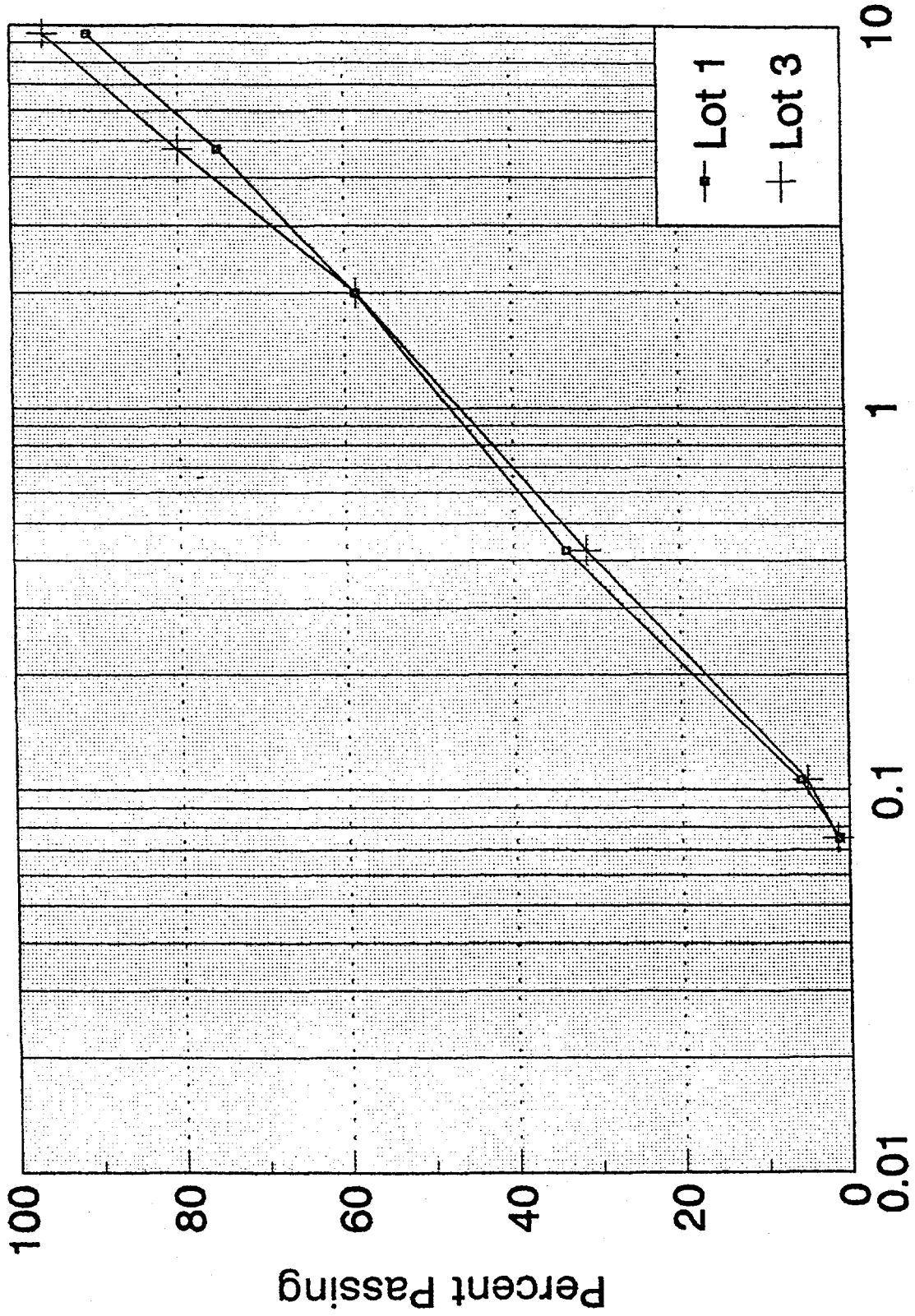

Figure 1 Grain Size Distribution of MEA Bottom Ash.

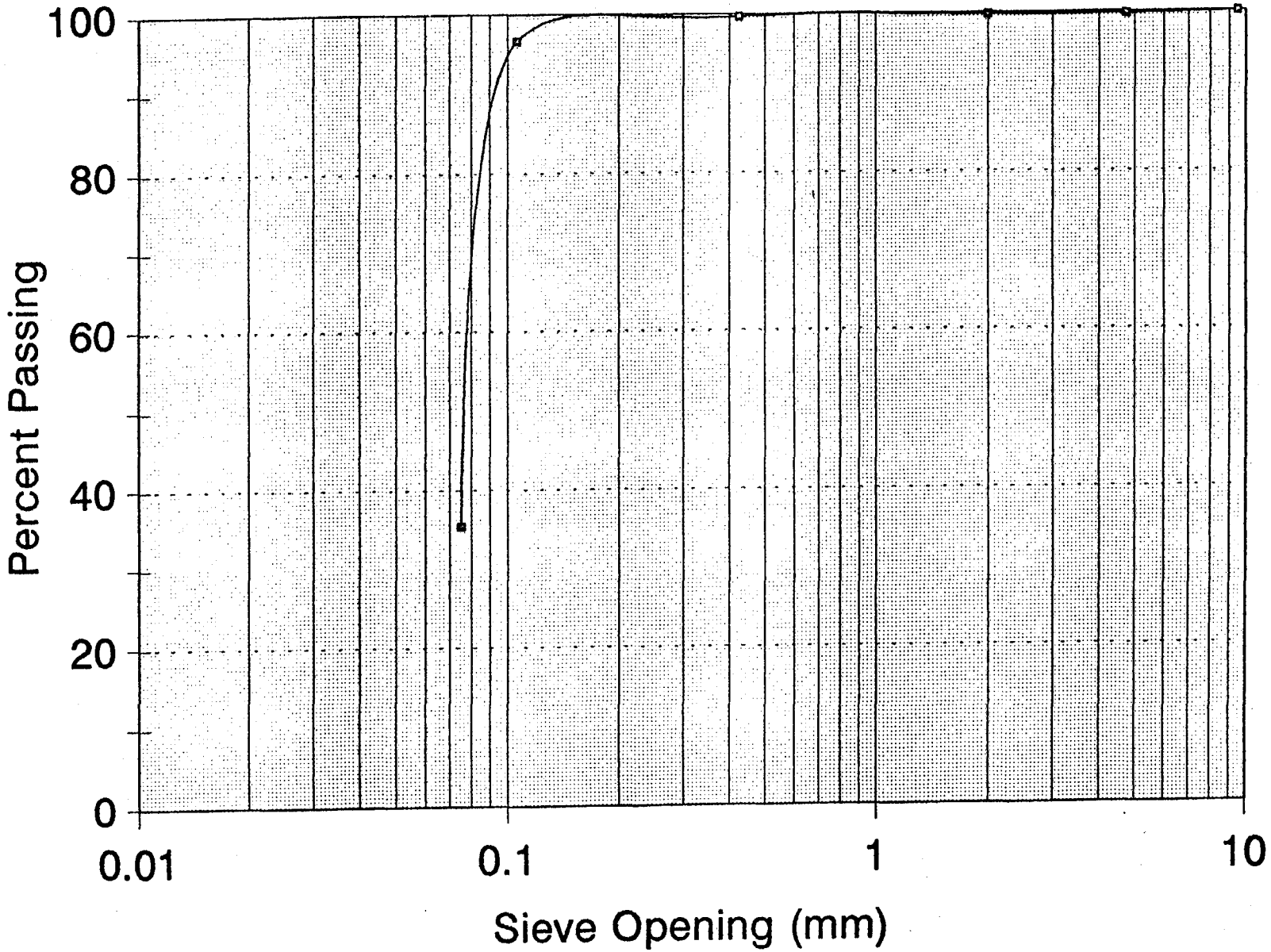

Figure 2 Grain Size Distribution of MEA Fly Ash.

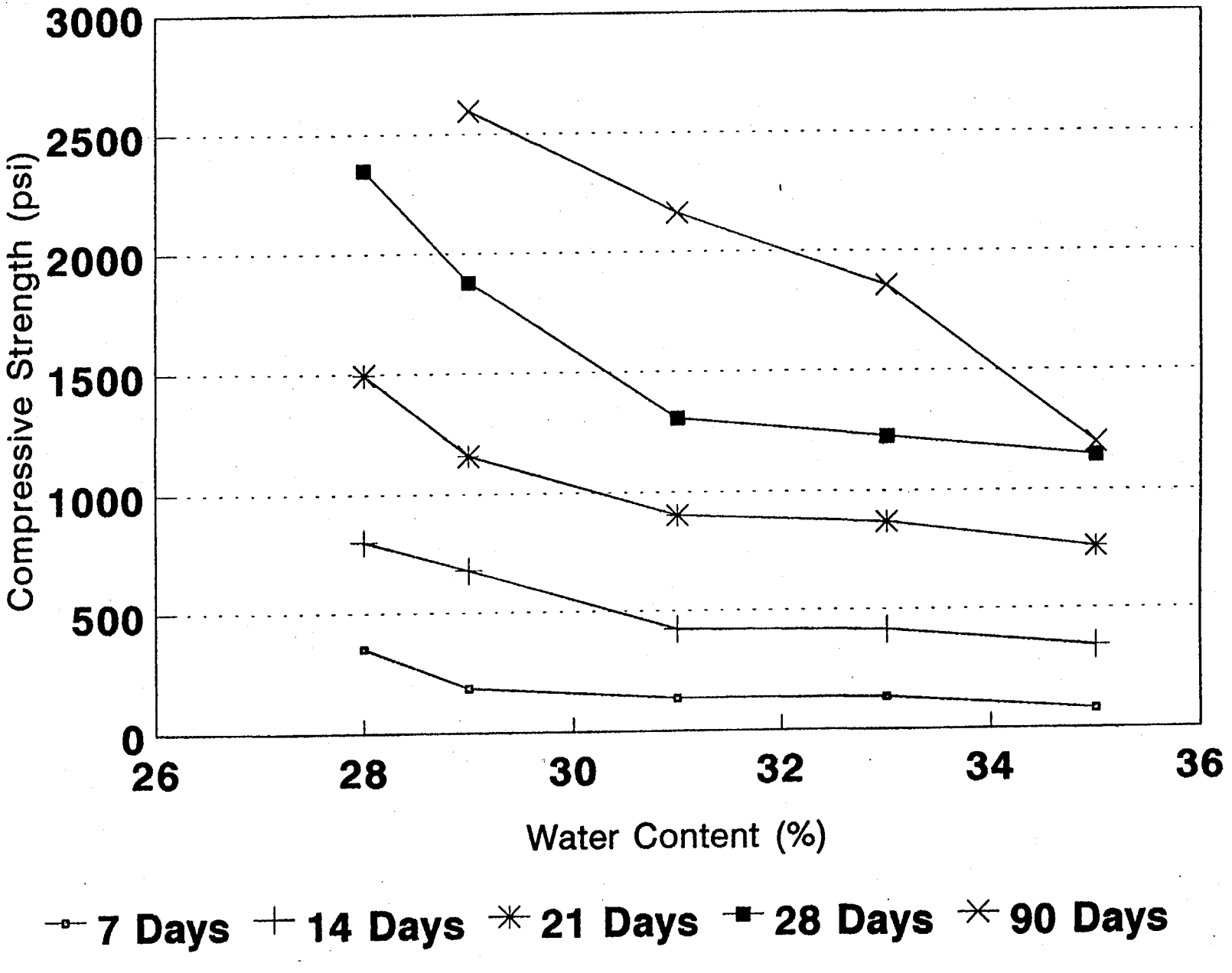

Figure 3 Compressive Strength vs. Water Content at Various Specimen Ages.

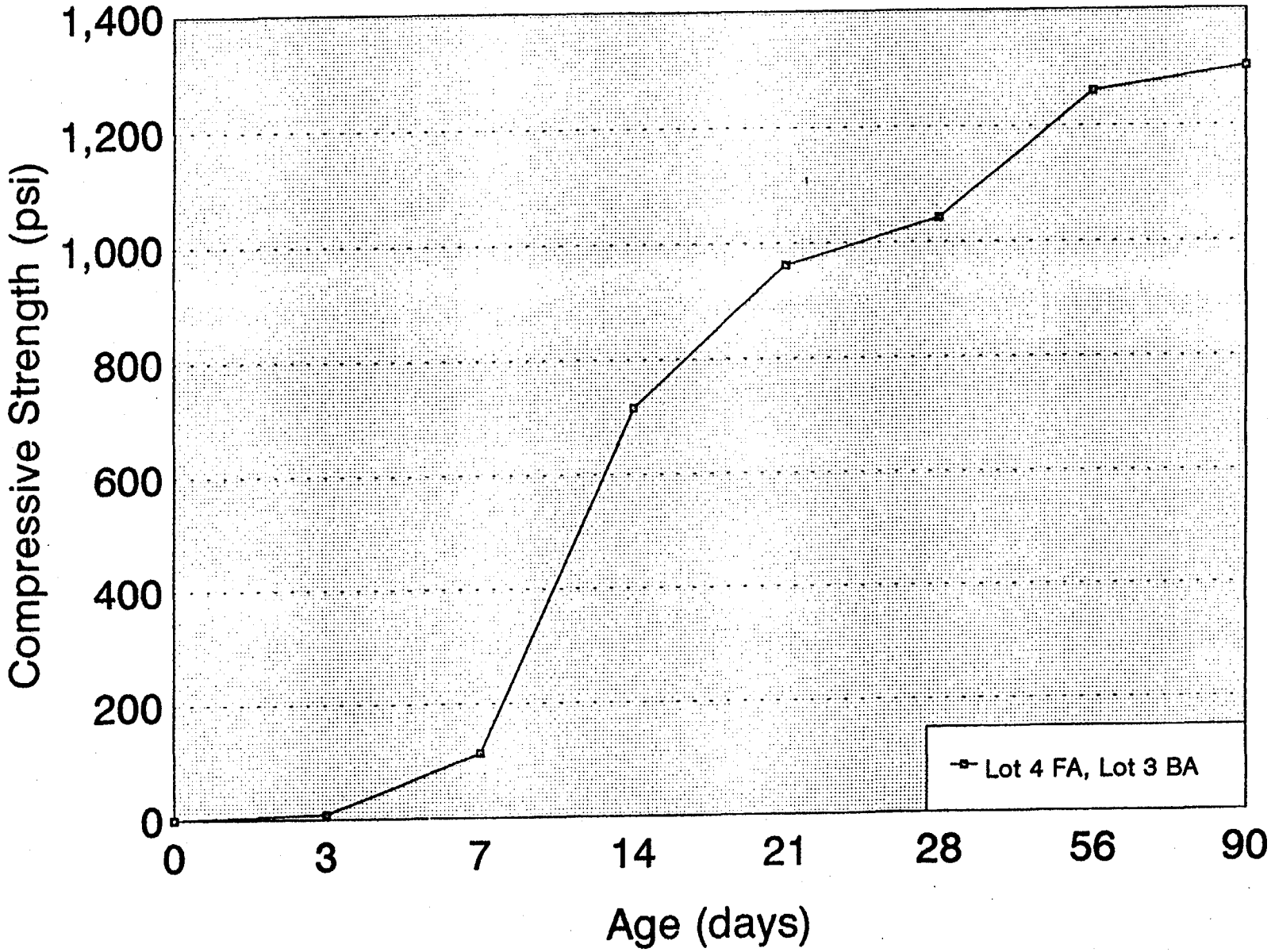

Figure 4 Compressive Strength vs. Age of 38% Tap, 4.6% Bentonite Specimens.

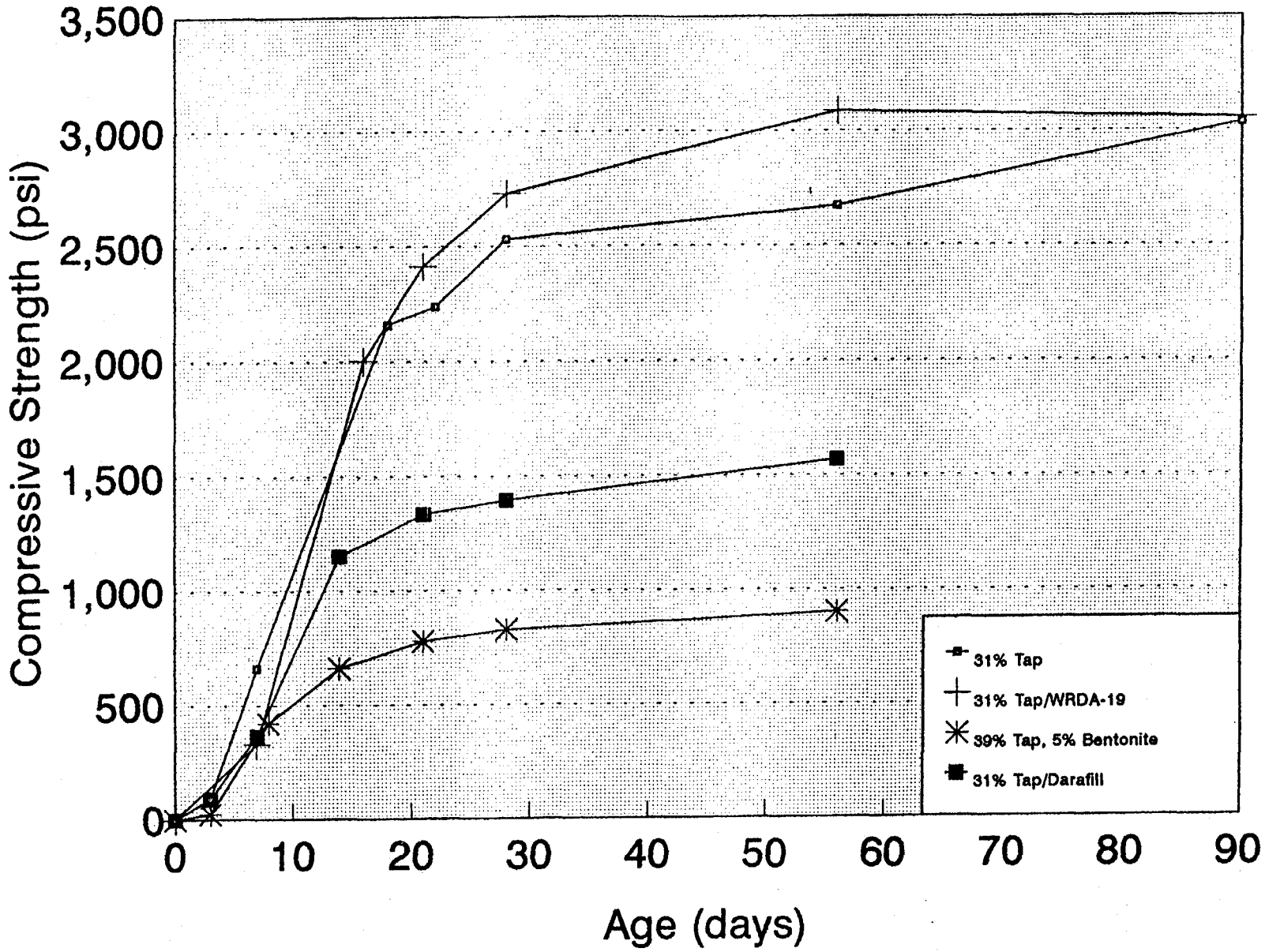

Figure 5 Compressive Strength vs. Age of Various Lot 5 FA,Lot 5 BA Specimens.

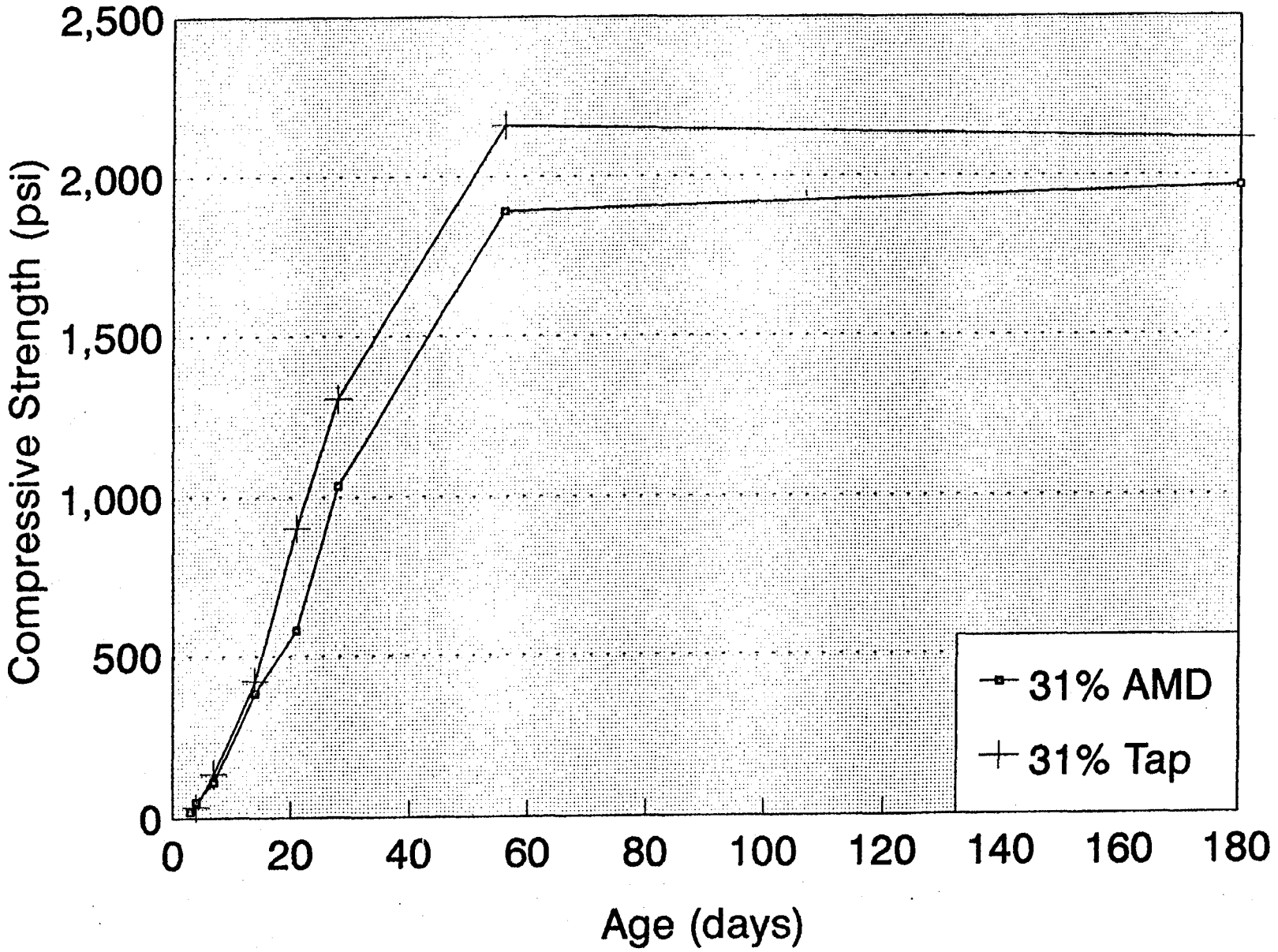

Figure 6 Compressive Strength vs. Age of 31% Tap & AMD Specimens.

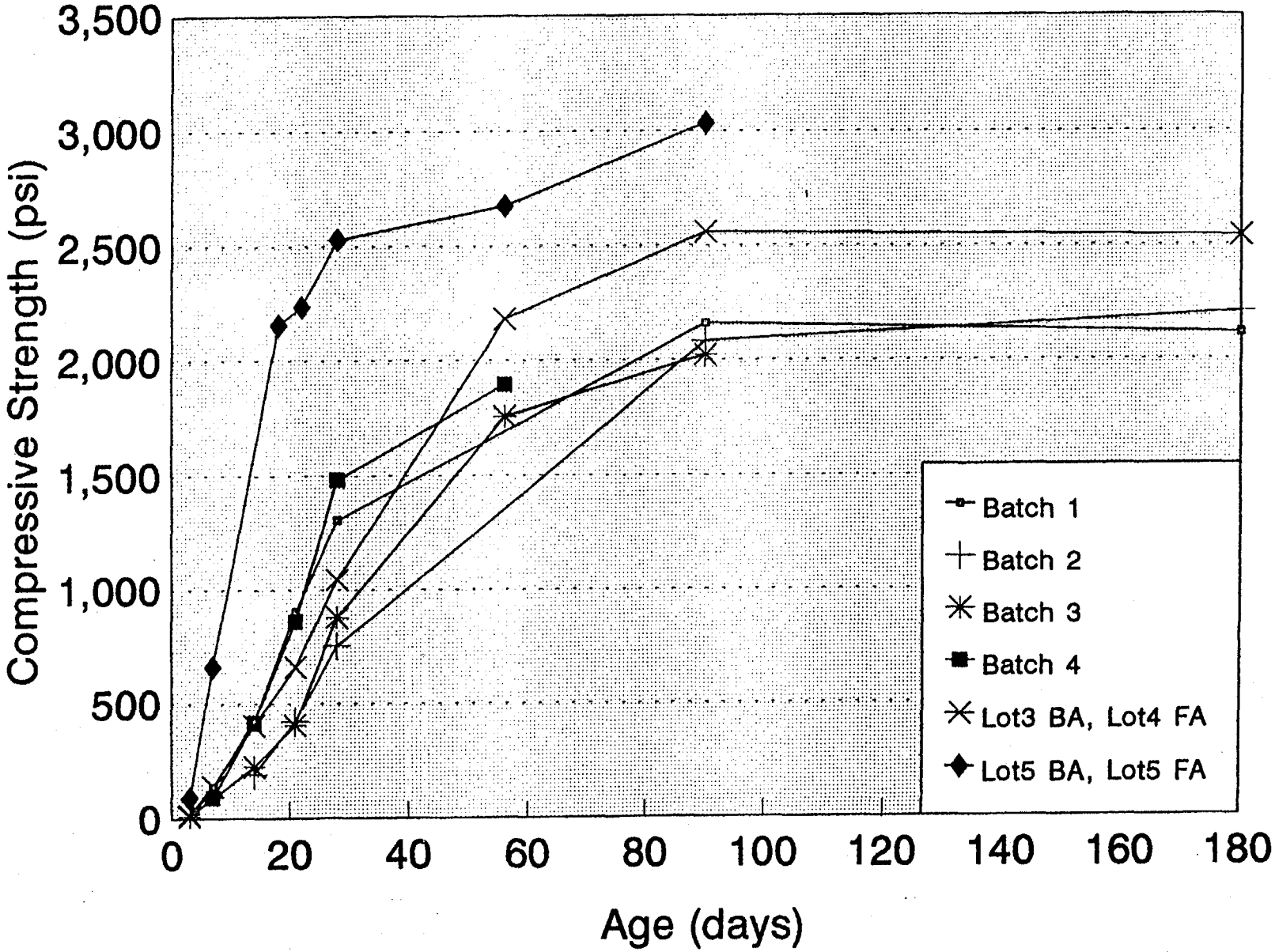

Figure 7 Compressive Strength vs. Age of Various 31% Tap Specimens.

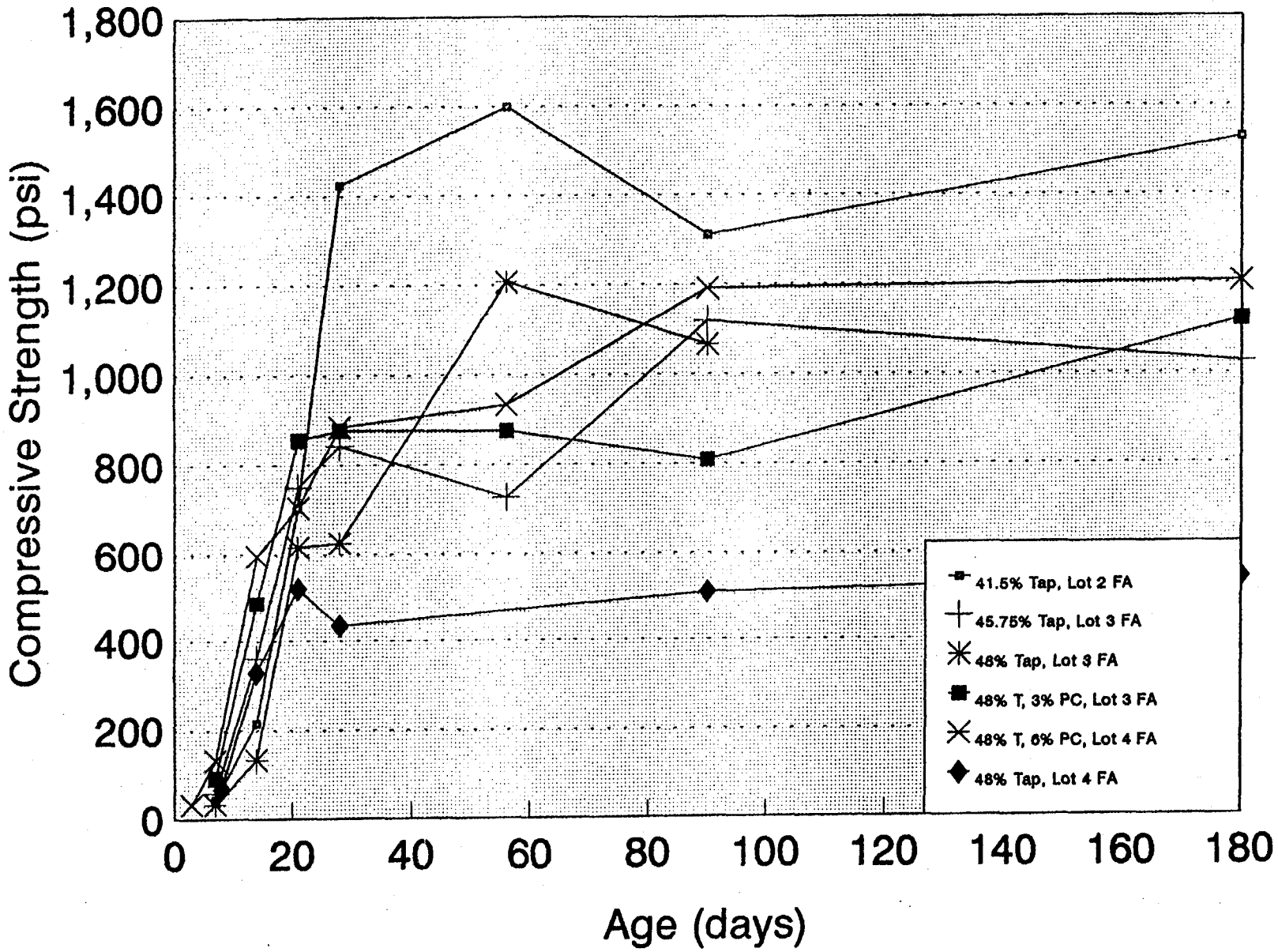

Figure 8 Compressive Strength vs. Age of Various Fly Ash Only Specimens.

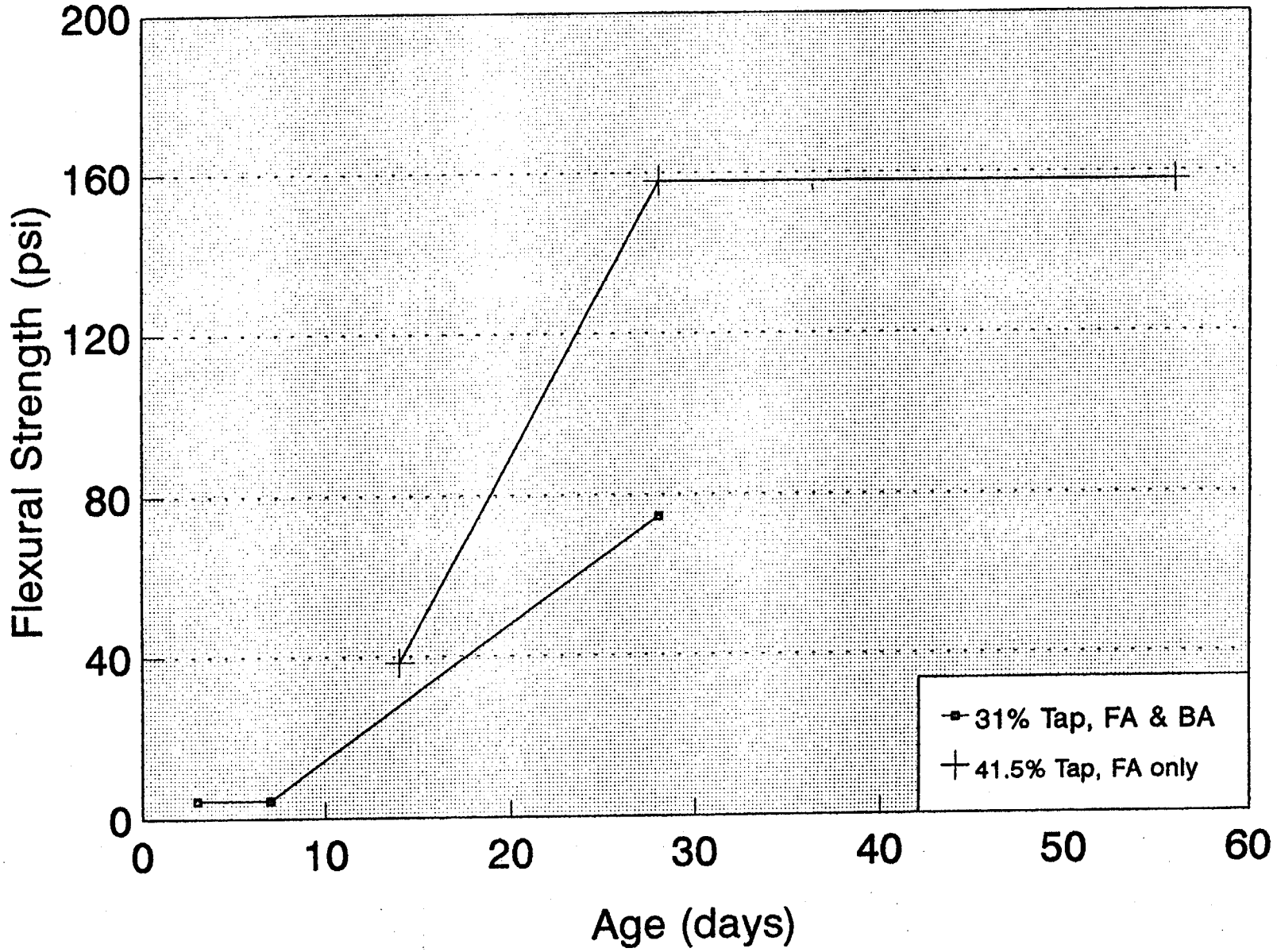

Figure 9 Flexural Strength vs. Age of Specimens.

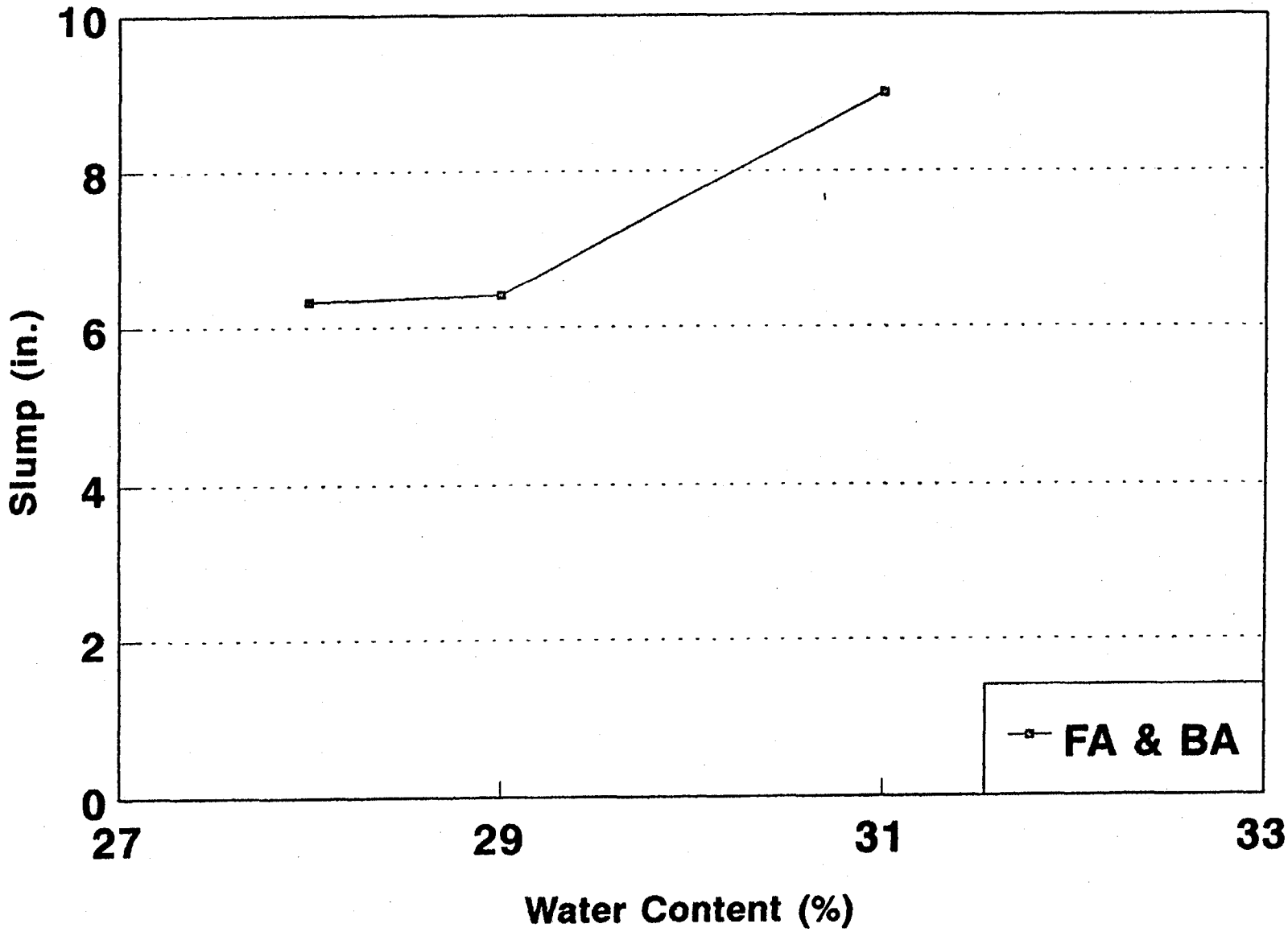

Figure 10 Slump vs. Water Content of Specimens.

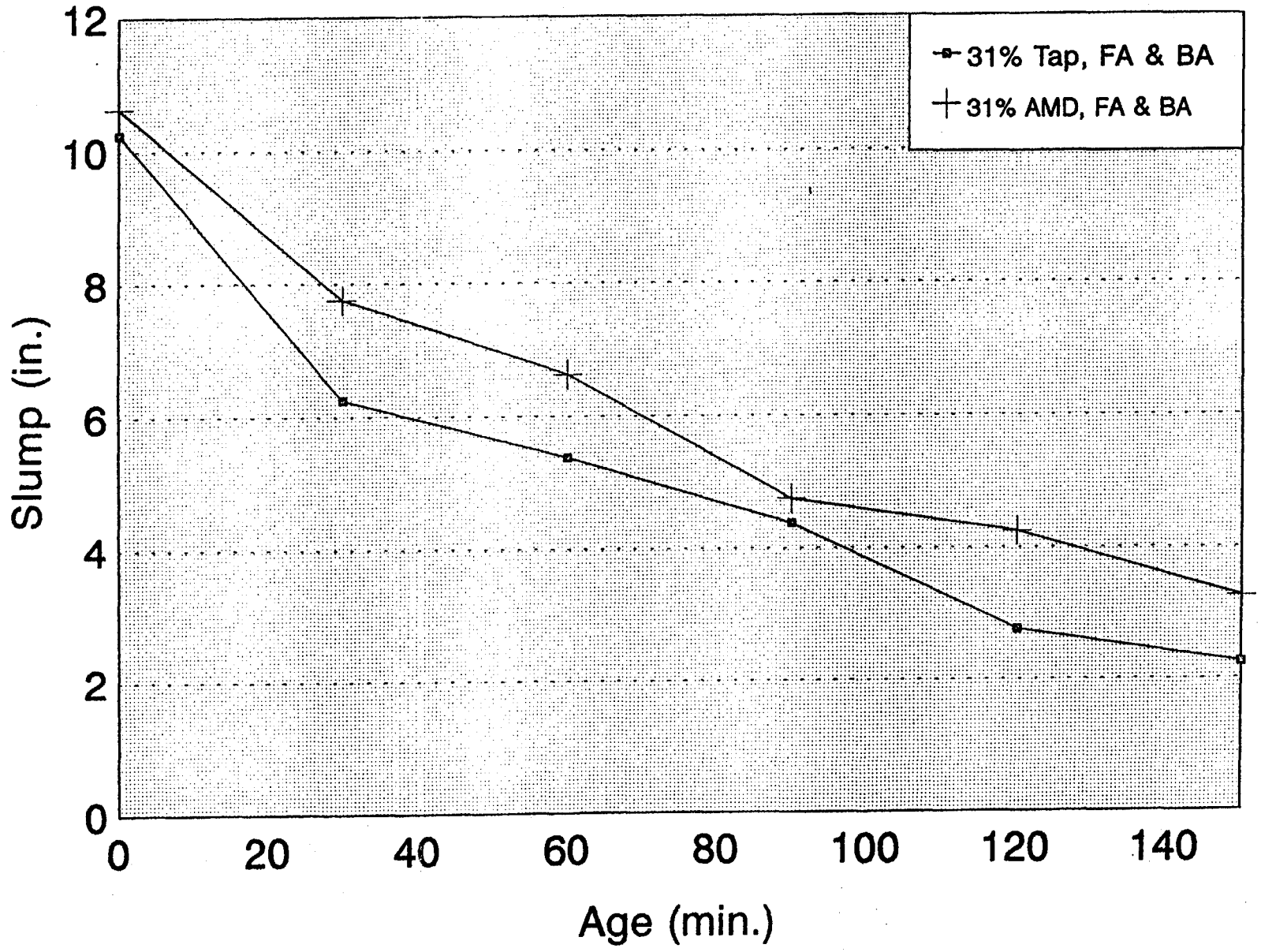

Figure 11 Slump vs. Age of Specimens.

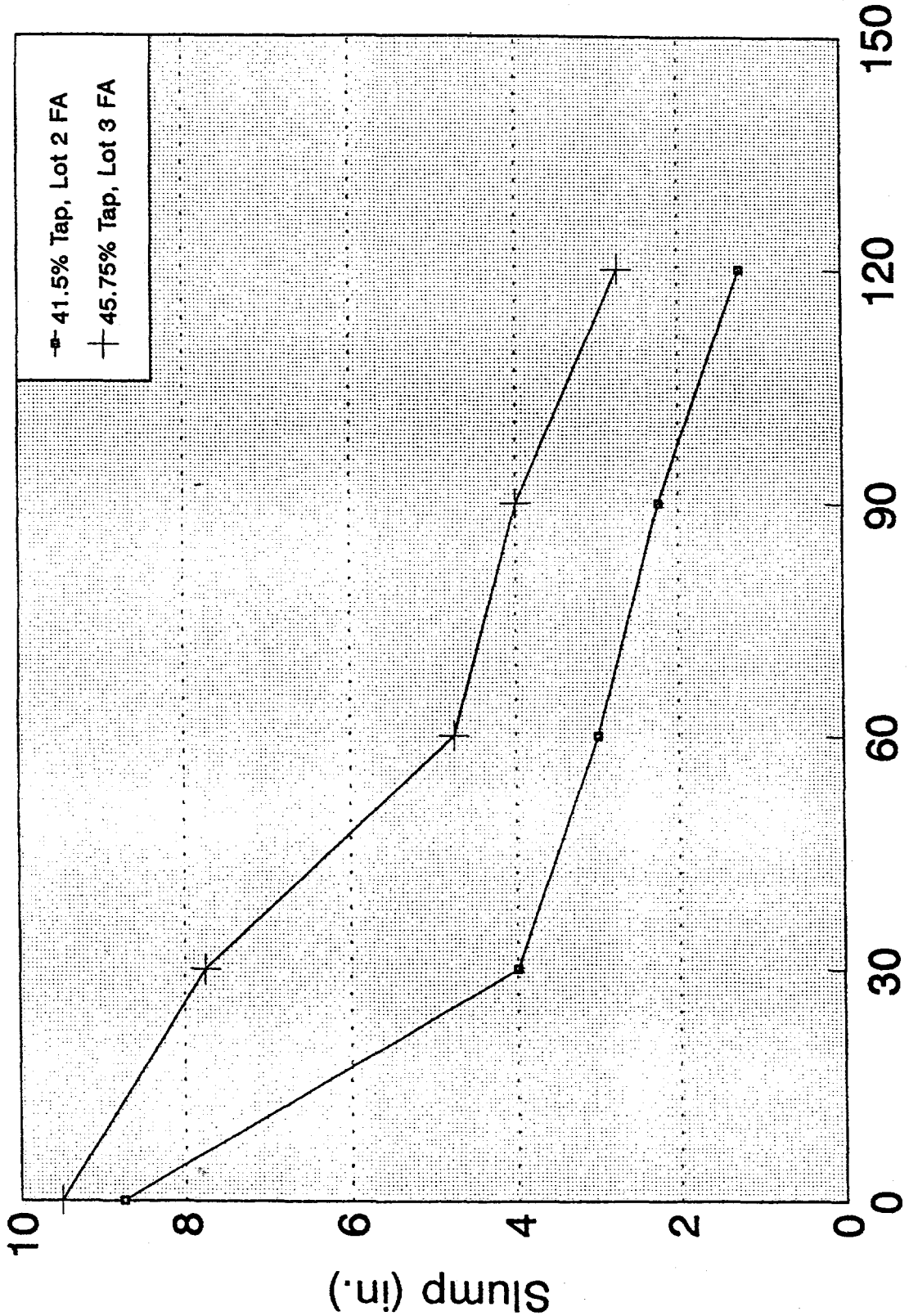

Figure 12 Slump vs. Age of Specimens.

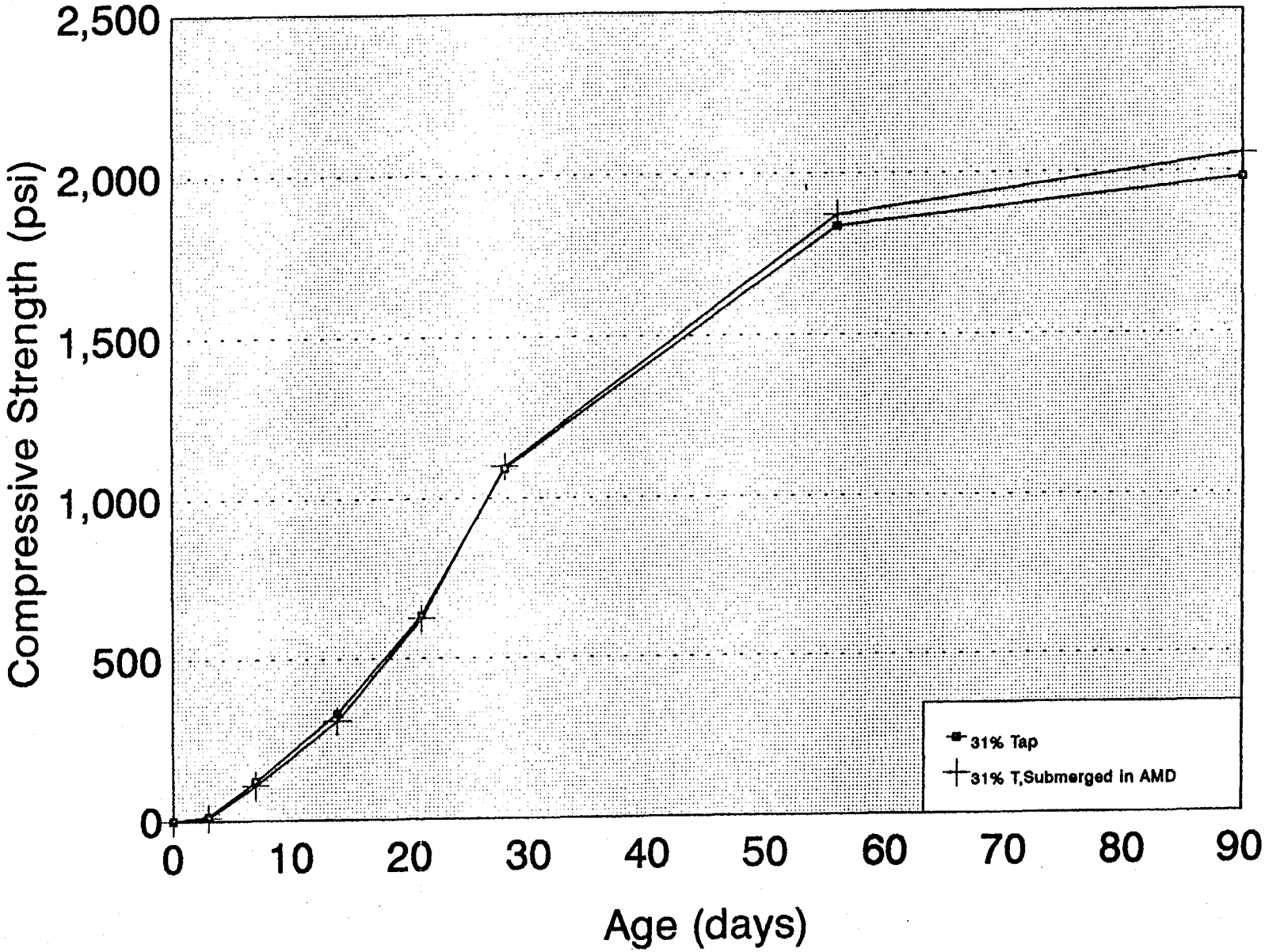

Figure 13 Compresive Strength vs. Age of Normal & AMD Submerged Specimens.

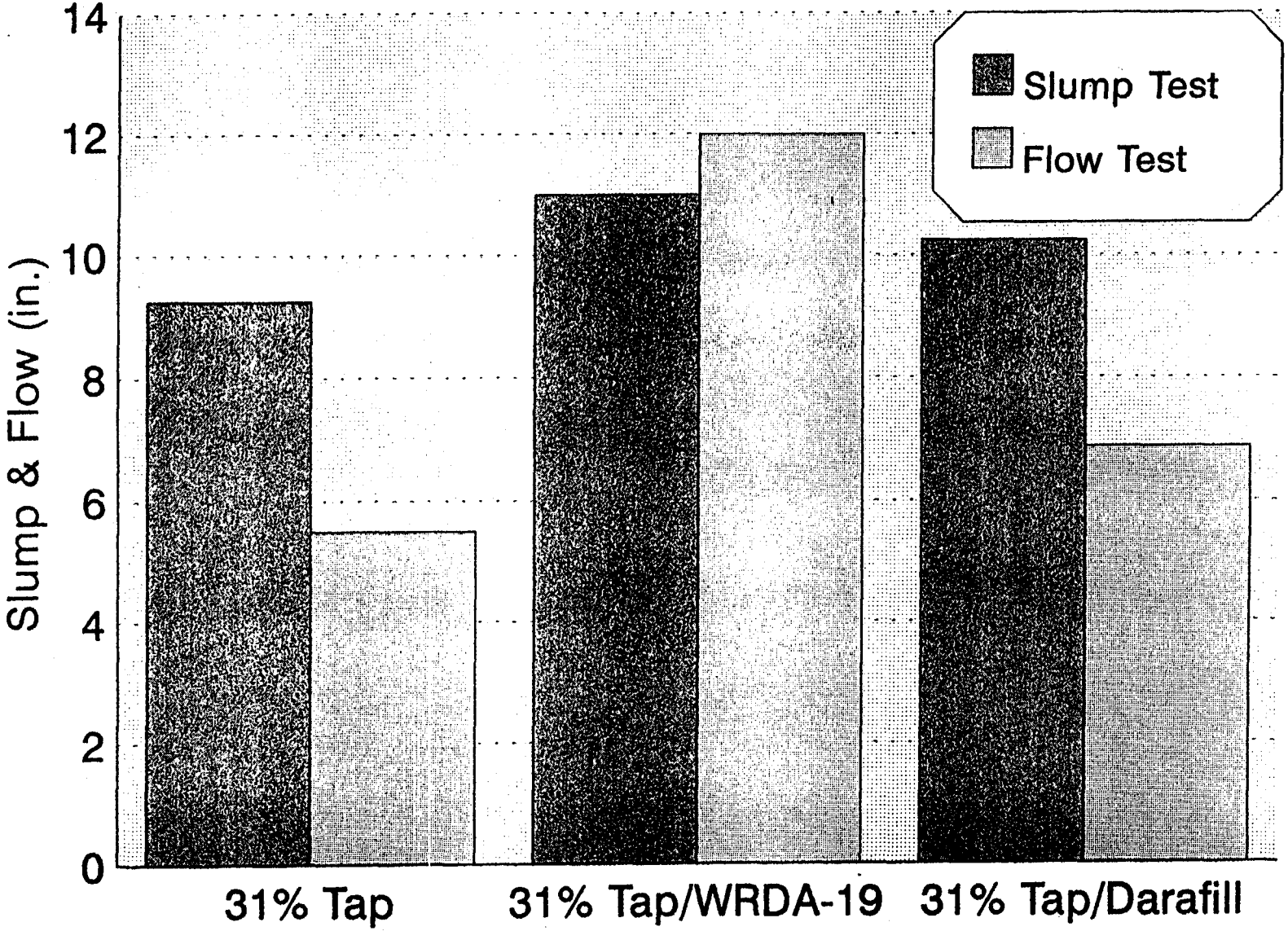

Lot 5 FA, Lot 5 BA

Figure 14 Comparison of Slump and Flow Tests.

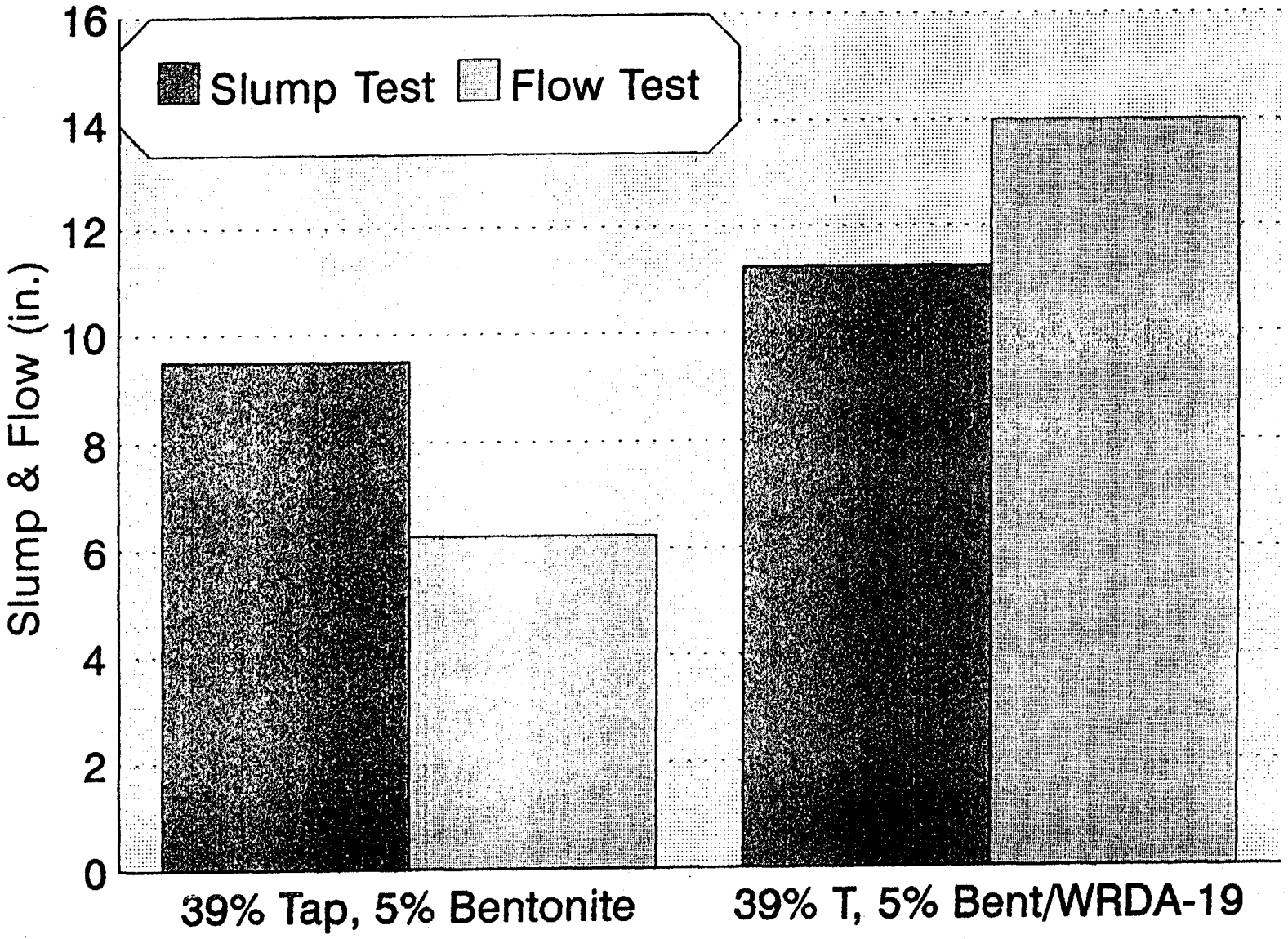

Lot 5 FA, Lot 5 BA

Figure 15 Comparison of Slump and Flow Tests.

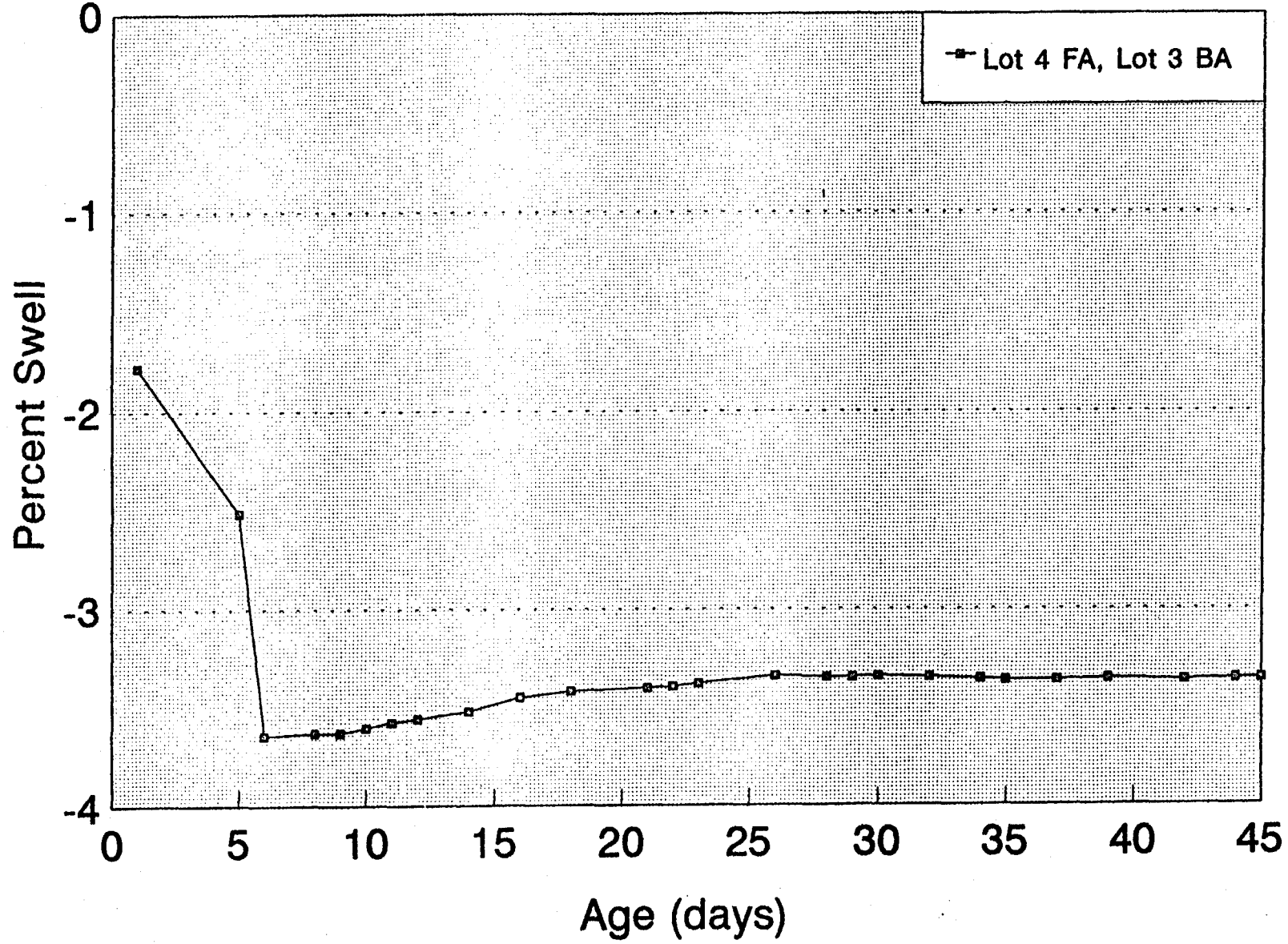

Figure 16 Swell vs. Age of 31% Tap Specimens.

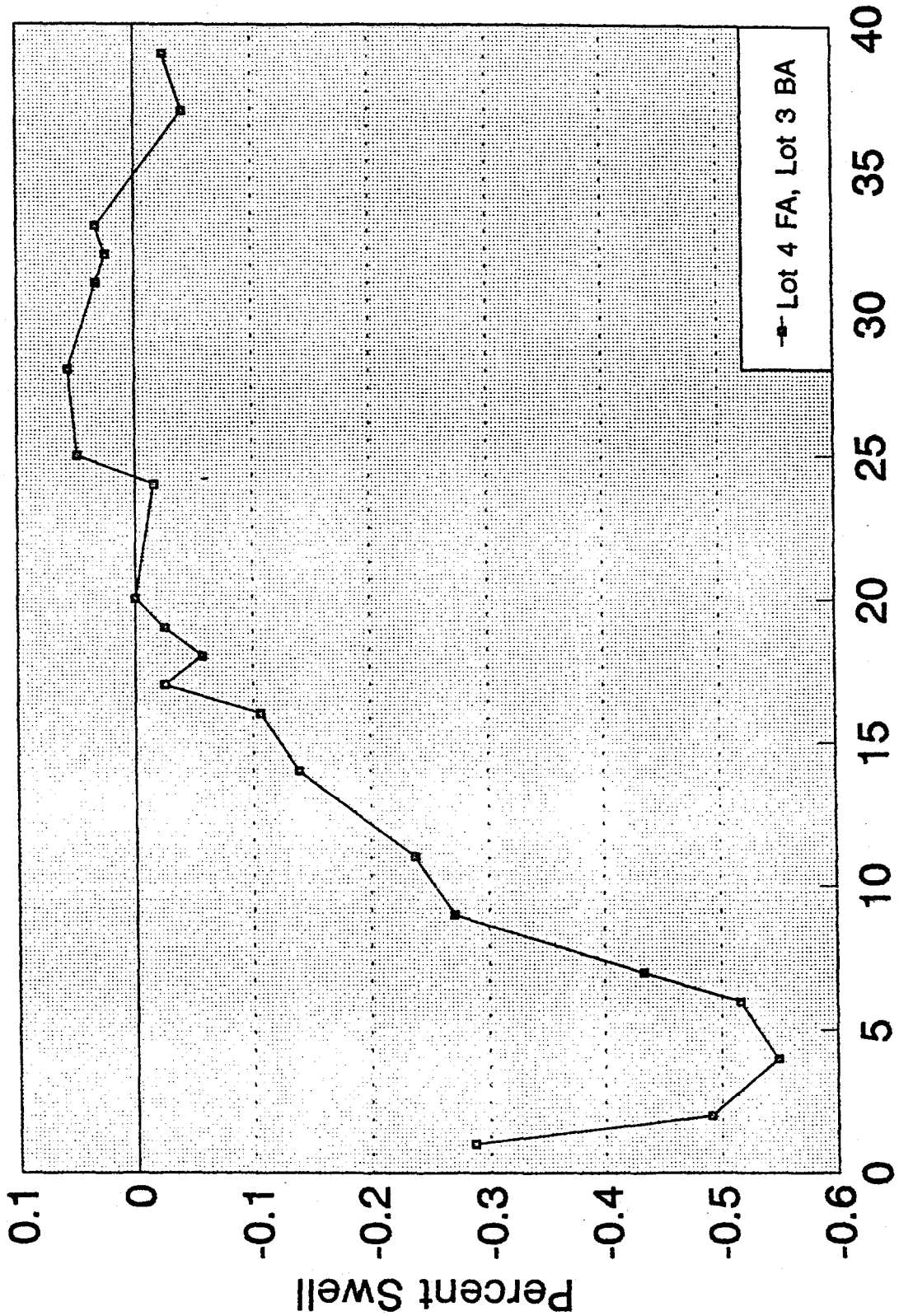

Figure 17 Swell vs. Age of 31% AMD Specimens.

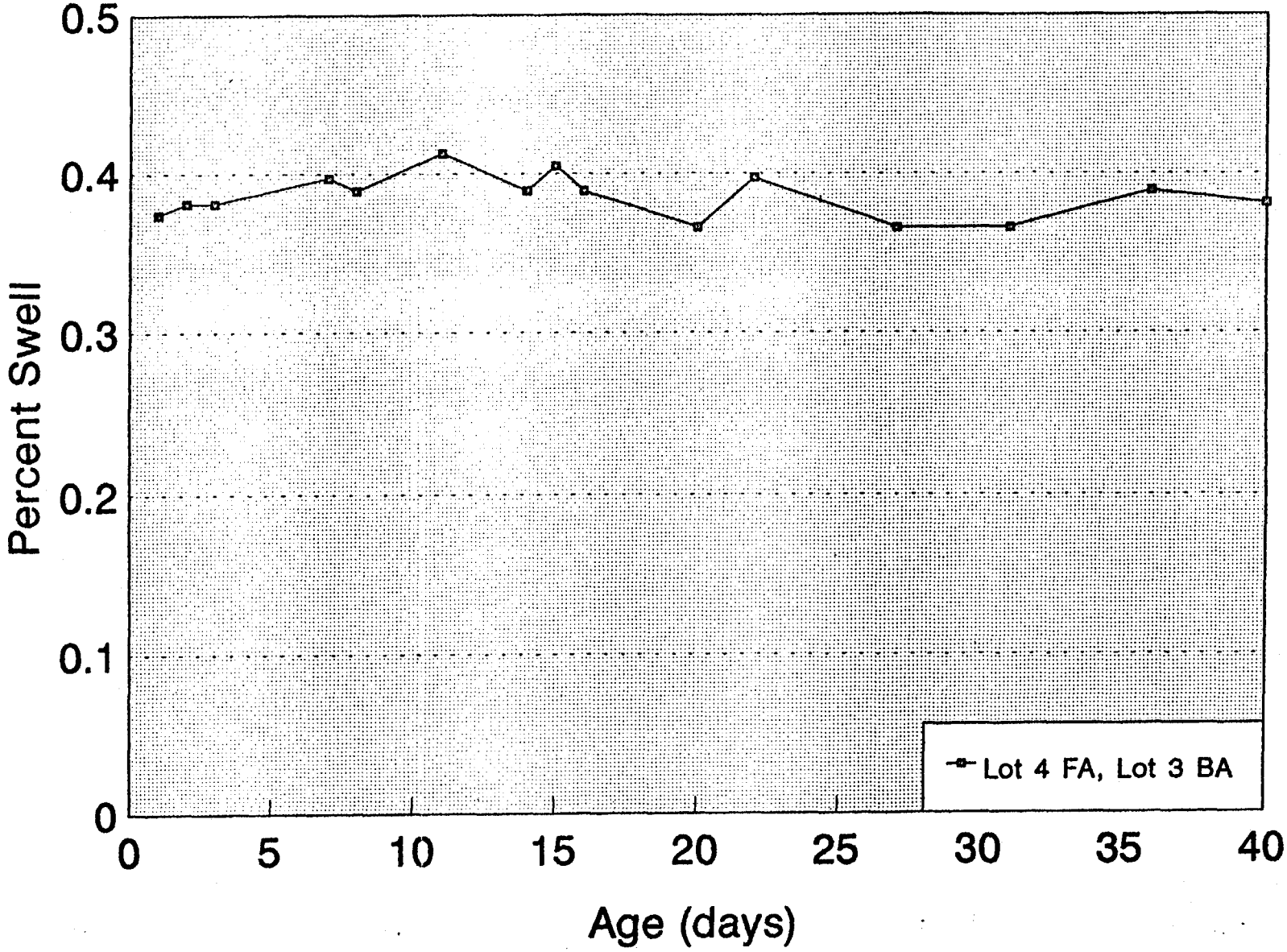

Figure 18 Swell vs. Age of 38% Tap, 4.6% Bentonite Specimens

TASK 2 GROUT RHEOLOGY MODEL

Purpose

Throughout much of Appalachia, abandoned coal mines have caused subsidence damage by collapse, and environmental damage by acid mine drainage into local watersheds. In addition, the local use of coal combustion for generating electricity has led to a large quantity of ash waste which is currently being disposed of in landfills. It has been proposed that these environmental problems may be eliminated by injecting a grout material, made from the ash waste product, into the abandoned mines. The grout would prevent subsidence by filling the empty mines, would reduce acid mine drainage by preventing groundwater and oxygen from coming into contact with exposed minerals and by neutralizing acid that is produced, and would provide an environmentally safe location for disposal of the coal combustion waste ash. The grout, a mixture of fly ash, bottom ash, water, and possibly other additives, would be injected into the underground mines through bore holes that would be drilled from the surface. Such a project would be economically feasible if the cost of disposing of the ash waste as a grout is less than the cost of the present practice (landfill disposal). Drilling the bore holes is the costliest part of this project, so to minimize project cost, the required number of bore holes must be minimized. To this end, a reliable computer model is needed to predict how the grout will flow in the subsurface environment, and to predict the total number and location of bore holes that will be required for successful placement of the grout in the mines. Once a suitable prediction method is developed, an efficient grout placement strategy can be developed.

The grout that is investigated in this project is produced from the ash waste of the Morgantown Energy Associates-Beechurst Avenue power plant. The MEA-Beechurst power plant uses an atmospheric pressure fluidized bed reactor for the combustion of coal and gob, and the waste that is generated is called FBC-ash. Gob, a combination of rejected rock, waste coal, and other impurities from the mining process, cannot be used in all coal combustion power plants. Limestone is added to the coal-gob mixture during combustion to reduce sulfur emissions. The FBC-ash particles have a higher calcium content and a more irregular shape than ash generated by traditional combustion processes. The grout mixtures made from the FBC-ash are similar in appearance to other flyash slurries, cement mortar, and concrete. All of these fluids exhibit non-Newtonian behavior. The behavior of these fluids has been described by other investigators with the power-law, Bingham, or Herschel-Bulkley fluid models.

The computer model used for this project is an adaptation of the commercially available code, PHOENICS. PHOENICS is a computational fluid dynamics code which has the capability to simulate three dimensional, unsteady, multi-phase flows with a free surface. However, user generated subroutines were needed to describe the non-Newtonian flow behavior exhibited by the grout mixtures. Rheological testing of the grout suggests that a Herschel-Bulkley fluid model may be used to describe the shear stress-shear rate relationship in the grout mixtures. The Herschel-Bulkley fluid model has been encoded in a subroutine added to the PHOENICS code. The parameter values obtained by laboratory testing of the grout can be used in the PHOENICS

computer model to correctly simulate the physics of flowing grout. Numerical simulations have been compared to analytical solutions and bench scale laboratory experiments. The computer model is intended as a design tool to make decisions about the mine filling process.

Background

The FBC-ash grout is a suspension of fly ash, bottom ash, and other additives in water. The flow and deformation of suspensions may be drastically different than that of Newtonian fluids as shown by a great deal of previous research.

RHEOLOGY OF SUSPENSIONS

When dealing with suspensions of solid particles, it is sometimes possible to treat the suspension as a homogeneous mixture by ignoring the particle-fluid interaction and ascribe effective fluid properties to the suspension. *Darby* (1984) stated that suspensions containing greater that 30-40% solids concentration by volume may be considered homogeneous and subject to description by the laws of continuum mechanics. *Jeffery and Acrivos* (1976) have described when suspensions may be treated as homogeneous fluids and have identified some of the factors that are responsible for non-Newtonian behavior. Jeffery and Acrivos further noted that even when suspensions may be considered homogeneous, it is not sufficient to simply modify the viscosity of the suspending medium as a function of the solid particle concentration. *Gupta* (1994) states that for all but very small volume fractions, suspensions will exhibit non-Newtonian behavior, and something more complicated than a viscosity value will be required to adequately describe the suspension behavior. Both Jeffery and Acrivos and Gupta have described the fundamental origin of the non-Newtonian behavior as a competition between hydrodynamic and non-hydrodynamic forces. Depending upon their size, shape, and concentration, particles in suspension may be subjected to a variety of non-hydrodynamic forces such as thermal (Brownian) forces, electrical forces due to surface charges, London-van der Waals forces, and hydrodynamic (i.e. viscous) forces from shearing at the particle-fluid boundary. As a consequence, the behavior of the suspension will often depend not only upon the concentration of particles but also on the particle size and aspect ratio, size distribution, the strength of the non-hydrodynamic forces, and the strength of the viscous forces. Fortunately, when it is valid to treat the suspension as a homogeneous fluid, the underlying reasons for the non-Newtonian behavior can be ignored, and attention can be focused on the macroscopic behavior of the homogeneous fluid. The macroscopic description of flow and deformation is therefore usually not based on theoretical considerations, but rather on empirical observations of behavior. Such observations are the foundation of the field of rheology: the science of deformation and flow.

Patel(1984) provides a useful survey of rheology. In the field of rheology, a fluid is defined as any material that deforms continuously for some range of applied shearing stress. Although the classical definition of a fluid is a material that exhibits continuous deformation under *any* applied shearing stress, there are materials that deform continuously only after a "yield" stress is exceeded. Below the yield stress, the material behaves like a solid. Such materials are still treated as fluids in

the field of rheology. The macroscopic description of a fluid's behavior is summarized by a constitutive law which relates the stress in a material to the rate of strain experienced by the fluid. It is therefore the primary goal of rheology to identify the constitutive law that is appropriate for a given fluid material.

Examples of constitutive laws may be found in any textbook on continuum mechanics, see for example *Mase and Mase* (1992). It is desired to find a constitutive law that can be used to describe the state of stress in a fluid by relating the stress tensor to the rate of deformation tensor. The state of stress is given by the stress tensor which can be decomposed as follows:

$$\sigma_{ij} = -p\delta_{ij} + \tau_{ij}$$

where σ_{ij} is the total stress in the fluid, p is the pressure, δ_{ij} is the Kronecker Delta, and τ_{ij} is the viscous stress tensor. The viscous stress tensor is a function of the gradients of fluid motion and, for a fluid without a yield stress, must be equal to zero when the fluid is at rest or in solid body motion. For a yield stress fluid, there may be a non-zero stress residual when the fluid is at rest because the fluid behaves like a solid until the yield stress is exceeded. For yield stress and non-yield stress fluids, the function that describes the stress tensor is called the constitutive law. It is usually assumed that the viscous stress tensor is related to the fluid motion through some function involving the rate of deformation tensor,

$$\tau_{ij} = f_{ij}(D_{kl})$$

where D_{ij} is the rate of deformation tensor defined by the velocity gradients:

$$D_{ij} = \frac{1}{2}\left(\frac{\partial v_i}{\partial x_j} + \frac{\partial v_j}{\partial x_i}\right)$$

The rate of deformation tensor is symmetric, thus $D_{12}=D_{21}$. If the function is linear, the fluid is called a Newtonian fluid and the relationship may be expressed as:

$$\tau_{ij} = C_{ijkl}D_{kl}$$

With the assumption that the fluid is isotropic, the fourth order tensor C_{ijkl} is an isotropic tensor. Because of the symmetry properties of D_{ij} and the isotropic nature of C_{ijkl}, the 81 components of C_{ijkl} may be reduced to two. The viscous stress tensor appropriate for an isotropic Newtonian fluid is:

$$\tau_{ij} = 2\mu D_{ij} + \lambda D_{kk}\delta_{ij}$$

The two constants, μ and λ, are properties of the fluid. μ is the dynamic viscosity and λ is the dilatational or second coefficient of viscosity. The compressibility of most liquids is negligible, so the trace of the rate of deformation rate tensor is zero. Consequently the last term in the above equation is usually neglected, leaving:

$$\tau_{ij} = 2\mu D_{ij}$$

With this relation, the constitutive equation for an incompressible Newtonian fluid may be expressed as:

$$\sigma_{ij} = -p\delta_{ij} + 2\mu D_{ij}$$

The Newtonian model described by this constitutive law is valid for many fluids, including water. The behavior of such materials may be described by the single parameter, μ, the dynamic viscosity. Each component of the viscous stress tensor, τ_{ij}, may be seen to be proportional to the

corresponding component of the rate of deformation tensor. The dynamic viscosity, μ, is the constant of proportionality, for instance:

$$\mu = \tau_{12}/2D_{12}$$

There are, however, many non-Newtonian fluids whose flow behavior cannot be adequately described by one constant. There exists a large class of materials whose constitutive relations fall under the class of generalized Newtonian fluids. For this class of materials, an *apparent* viscosity, η, is defined by analogy with the constant Newtonian viscosity and is used in place of the constant μ. The apparent viscosity is assumed to be a function of the magnitude of the rate of deformation. *Crochet and Walters* (1983) give the stress tensor for a generalized Newtonian fluid as:

$$\sigma_{ij} = -p\delta_{ij} + 2\,\eta(I_2)\,D_{ij}$$

where I_2 is a suitable form of the second invariant of the rate of deformation tensor, D_{ij}. Different forms of the function η describe different fluid behavior. Patel and *Govier and Aziz* (1972) list many of the common forms of the function η.

Relationships between a component of the stress tensor and the corresponding component of the rate of deformation tensor may be displayed graphically in stress vs. strain rate plots (see Figure 19). In such a plot, the slope of the curve is the viscosity. For Newtonian fluids, the line passes through the origin and the slope is constant. Pseudoplastics are fluid materials whose viscosity decreases with increasing rate of strain. Dilatant materials exhibit an increase in viscosity with increasing rate of strain. Dilatant and pseudoplastic behavior are often modeled with the power-law model. The power-law model is a two parameter model that relates the viscous stress to the magnitude of the rate of deformation rate tensor. In two dimensions, with one non-zero component ($D_{12} = D_{21} = \gamma/2$) of the rate of deformation tensor, the power-law model is:

$$\tau = k\gamma^n$$

where k is the consistency index, n is the behavior index, and τ here represents the only non-zero component ($\tau_{12} = \tau_{21} = \tau$) of the viscous stress tensor. For n>1, the behavior is dilatant, for n<1 the behavior is pseudoplastic, and for n=1, the power-law model reduces to the Newtonian model. In general, there will be more than one non-zero component of the viscous stress tensor and the rate of deformation tensor. *O'Donovan and Tanner* (1983) give the appropriate form of the generalized Newtonian constitutive relation in three dimensions. The symbol, γ, then represents the magnitude of the strain rate, and is interpreted as the square root of the second invariant of the rate of deformation tensor. γ is given by:

$$\gamma=[2(D_{ij}D_{ij})]^{1/2}$$

The expansion of the second invariant is:

$$2D_{ij}D_{ij} = 2(D_{11}^2 + D_{22}^2 + D_{33}^2) + 4(D_{12}^2 + D_{23}^2 + D_{13}^2)$$

By analogy with the Newtonian definition of viscosity, the apparent viscosity is defined by using the power-law model as follows:

$$\eta = \frac{\tau}{\gamma} = \frac{k\gamma^n}{\gamma} = k\gamma^{(n-1)}$$

The apparent viscosity can be interpreted as the slope of a chord from the origin to a point on the

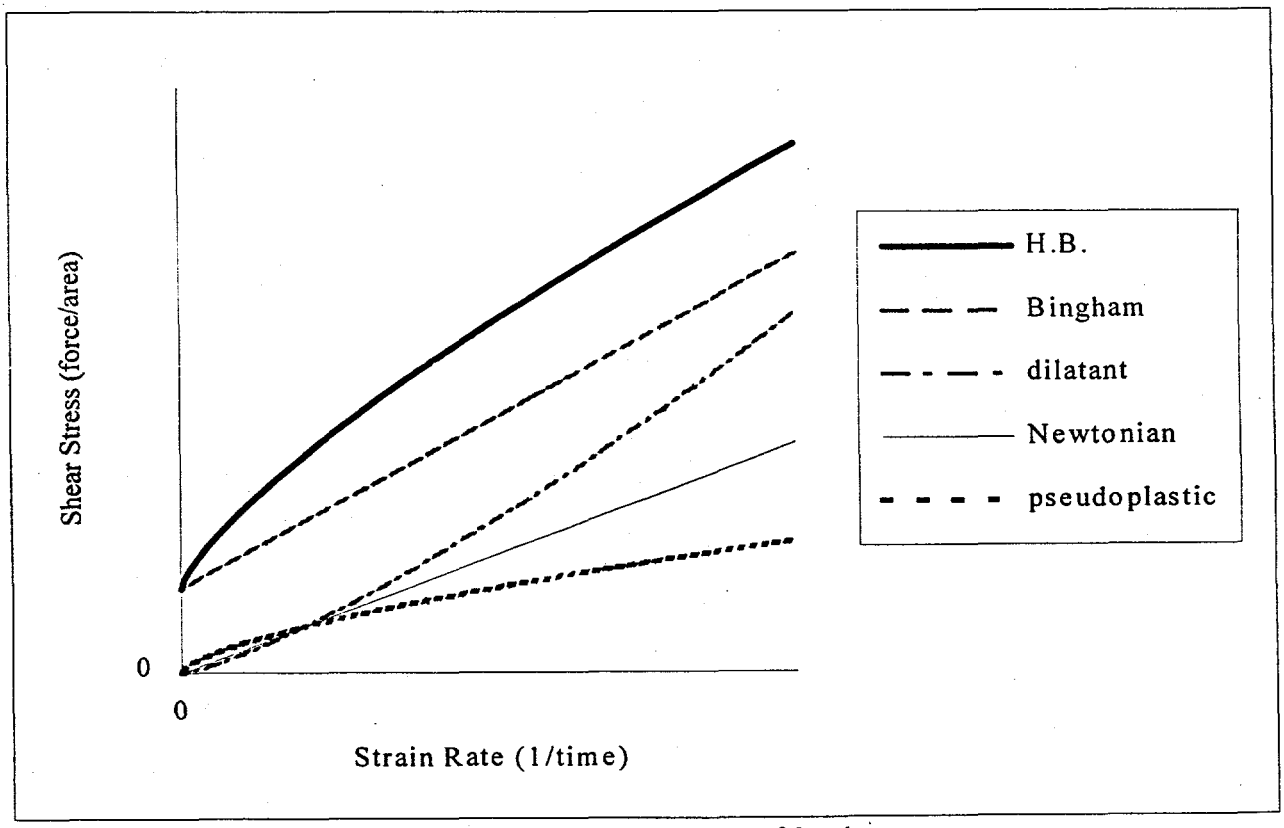

Figure 19 Stress vs. Rate of Strain

plot of stress vs. strain rate, as shown in Figure 20. The general three dimensional stress tensor for a fluid whose behavior may be described with the power-law constitutive relation is:

$$\sigma_{ij} = -p\delta_{ij} + 2(k\gamma^{n-1})D_{ij}$$

For those fluid models that include a yield stress, such as the Bingham and Herschel-Bulkley models, the stress vs. strain rate curve does not go though the origin (see Figure 19). The intercept on the stress axis denotes a stress value that must be exceeded in order to initiate continuous fluid deformation. The Bingham fluid model describes a fluid behavior that is linearly dependent on the strain rate once the yield stress has been exceeded.

The two dimensional form of the Bingham constitutive relation is given by:

$$\begin{aligned} \tau &= \tau_y + k\gamma \qquad \textit{for} \quad \tau > \tau_y \\ \gamma &= 0 \qquad\qquad\quad \textit{for} \quad \tau < \tau_y \end{aligned}$$

where k is the plastic viscosity and τ_y is the yield stress. As the yield stress approaches zero, the Bingham model will also reduce to the Newtonian model.

The Herschel-Bulkley (HB) fluid model uses the power-law model to describe fluid behavior after the yield stress is exceeded. In two dimensions, the viscous stress is given by:

$$\begin{aligned} \tau &= \tau_y + k\gamma^n \qquad \textit{for} \quad \tau > \tau_y \\ \gamma &= 0 \qquad\qquad\quad \textit{for} \quad \tau < \tau_y \end{aligned}$$

An apparent viscosity can also be defined for the yield stress fluids. For the Herschel-Bulkley model, the apparent viscosity is defined as follows:

$$\eta = \frac{\tau}{\gamma} = \frac{\tau_y}{\gamma} + k\gamma^{(n-1)} \qquad \textit{for} \quad \tau > \tau_y$$

The appropriate extension of the Herschel-Bulkley model to three dimensions is:

$$\sigma_{ij} = -p\delta_{ij} + \left(\frac{\tau_y}{\gamma} + k\gamma^{n-1}\right)\left(\frac{\partial v_i}{\partial x_j} + \frac{\partial v_j}{\partial x_i}\right) \qquad \textit{for} \quad \tau > \tau_y$$

where again the symbol, γ represents the magnitude of the rate of deformation tensor. Notice that the Herschel-Bulkley constitutive law will reduce to the power-law model when $\tau_y \to 0$, to the Bingham model when $n \to 1$, and to the Newtonian model when $\tau_y \to 0$ and $n \to 1$. It is

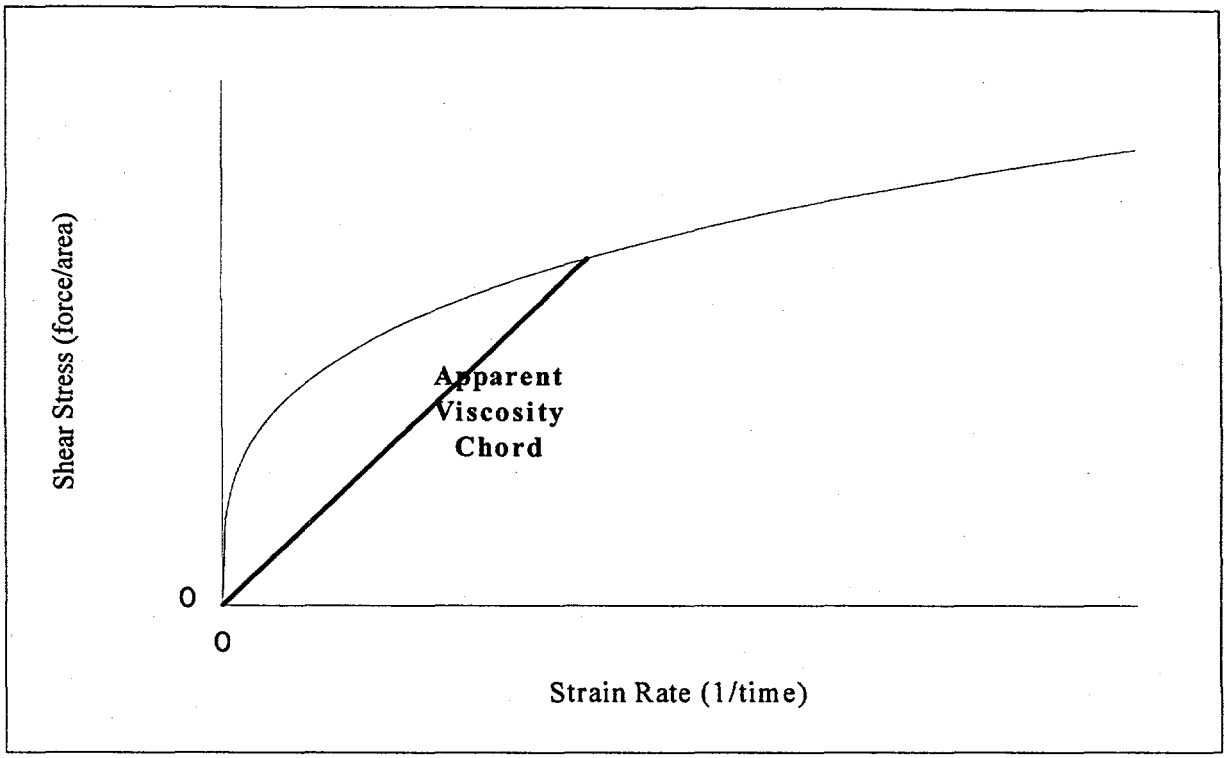

Figure 20 Apparent Viscosity

important to emphasize that the above constitutive laws are empirical descriptions of observed fluid behavior. This means that it may be possible that more than one model of fluid behavior could be used to describe how a particular fluid behaves depending on the range of shear stresses. The power-law, Bingham, and Herschel-Bulkley models have all been used to describe the behavior of suspensions. Other fluid models such as the Casson and the Prandtl-Eyring fluid models have also been used in attempts to describe such materials. *Bunn, Chambers, and Goh* (1991) have measured the rheological properties of fly ash slurries with solids concentration greater than 60% by weight. They showed that both the power-law and Bingham models could be used to fit data obtained with a tube viscometer. *Panda, Parida, Murty and Mitra* (1994) used the Bingham model to describe the behavior of a slurry of coarse and fine coal particles. *Håkansson, Hässler, and Stille* (1992) showed that the Bingham model was also able to describe flow of cement grouts. *Sakuta, Yamane, Kasami, and Sakamoto* (1979), and *Mori and Tanigawa* (1992) also used the Bingham model to characterize the flow of fresh concrete. *Hanks and Hanks* (1984) fit the Herschel-Bulkley model to experimental data for slurries of coal particles.

Although the Bingham and Herschel-Bulkley rheological models are widely used, some controversy appears in the literature as to the validity of the yield stress concept. *Barnes and Walters* (1985) have argued that if measurements can be made accurately enough, then continuous, but very slow, deformation will be observed at even the smallest of applied stresses. They contend that previous experimenters have not carefully evaluated the fluid behavior at low shear stresses, but have merely extrapolated a curve through the stress axis on a plot of experimentally obtained stress vs rate of strain data. They claim that a yield stress only defines what cannot be measured under the conditions of experimentation. Further controversy arises when considering the

existence of unyielded regions within a flow domain. O'Donovan and Tanner investigated the location of a yield surface within a parallel-plate plastometer and discuss the disagreement in the literature. They point out that the existence of an unyielded region, although required for a yield stress fluid, is kinematically impossible. Therefore, while yield stress models are a useful empiricism, care should be given when declaring a yield stress value for a fluid.

UNSTABLE SUSPENSIONS

The fluid models described above are based on the assumption that the fluid is homogeneous, and as such, are not adequate to describe the behavior of settling (unstable) suspensions in which the constitutive relation may change with position. *Lombardi* (1985) investigated the rheology of unstable grouts. As the solid particle concentration increases, friction will develop between the solid particles that are in contact. This friction is an additional resistance to flow and must be included in the rheological model of the grout. Lombardi modified the two dimensional Bingham fluid model to account for internal Coulomb friction in an unstable grout suspension:

$$\tau = \tau_y + \eta\gamma + p\mu_f \qquad \text{for } \tau > \tau_y$$

with p denoting the fluid pressure, and μ_f is the Coulomb friction coefficient. The friction coefficient is the tangent of the angle of internal friction between the solid particles. The above rheological model is the same as the Bingham model except for the addition of the last term on the right side. Similarly, the Herschel-Bulkley model could be modified to account for internal friction with the inclusion of the same extra term. The extra term shows that an additional stress is present that is proportional to the local fluid pressure and the tangent of the internal friction angle. This implies that the shear stress will differ throughout the fluid because the pressure will vary throughout the flow domain. An additional complication arises because the internal friction is a function of solid particle concentration which varies in space and time. The yield stress and plastic viscosity are also dependent upon solid particle concentration, and as such, will not remain constant. The result is a constitutive law that is a function of time, space, and flow strength. It is more illustrative to write the two dimwnsional constitutive law of an unstable suspension as an explicit function of space, $\mathbf{x}$, time, t, and flow strength as measured by the magnitude of the rate of deformation, γ:

$$\tau(\mathbf{x},t,\gamma) = \tau_y(\mathbf{x},t) + \eta(\mathbf{x},t)\gamma + p(\mathbf{x})\mu_f(\mathbf{x},t)$$

Thus, the rheological model needed to describe unstable suspensions is much more complex than the corresponding constitutive relation for stable suspensions.

Any yield stress fluid that is pumped, with a finite initial pressure head, into a closed, infinitely long channel will inevitably come to rest. As the pressure head is converted into velocity head, the loss of head due to friction will cause the stress in the fluid to continually decrease downstream. At some distance downstream, the stress in the fluid will fall below the yield stress and a solid plug will completely fill the channel resulting in cessation of flow. The Coulomb friction present in unstable suspensions will further limit the extent of flow. Lombardi compared the distances that

a stable and unstable grout could be made to flow in idealized, two-dimensional, bounded channels. Equations that describe the pressure drop and maximum flow distance were derived from a balance of forces on a fluid element that has stopped moving. For stable grouts, the maximum flow distance is a function of initial pressure, channel size, and yield stress. For unstable grouts, the maximum flow distance depends also on the coefficient of friction, and is much smaller than the maximum flow distance of stable grouts. Lombardi's results are not accurate because axisymmetric and two dimensional results were incorrectly combined.

THE WALL BOUNDARY CONDITION

Non-Newtonian fluids mechanics may also differ from Newtonian fluids mechanics by the inclusion of wall slip into the statement of the wall boundary condition. *Schowalter* (1988) used the term *slip* to describe behavior which violates the usual wall boundary condition of Newtonian fluid mechanics, which states that there must be no relative motion between an impenetrable boundary and a flowing fluid. Schowalter warns that the behavior of non-Newtonian fluids can be so unpredictable near a solid boundary that the statement of the boundary condition is often part of the solution being sought. Schowalter further claims that when dealing with complex fluids, continuum mechanics must be coupled to microscale physics because macroscopic effects can be caused by the microscopic physical and chemical nature of the boundary.

Some of the possible microscopic mechanisms responsible for slip are reviewed in *Silliman and Scriven* (1980). First, while not slipping locally on the microscopic irregularities of the actual surface, a fluid could appear to slip at a mathematical surface passed through the mean elevation of the solid surface roughness. Second, the normally submicron scale of intermolecular forces between the solid and fluid may locally reduce the apparent viscosity. Third, in fluids whose viscosity is highly dependent upon shear rate, apparent slip could occur in a thin layer of high shear near a solid surface. Fourth, the presence of solid boundaries may result in a migration of suspended solid particles away from the walls. As a result a thin low-viscosity fluid layer is formed near the wall in suspensions whose apparent viscosity is a function of solid particle concentration. The last two mechanisms create a "lubrication" layer that enhances flow without causing true slip. Fifth, "true" slip may occur at the molecular level, implying that there may be an appreciable departure from thermodynamic equilibrium within a few molecular diameters. Layers of molecules may slide past each other in a coordinated manner. Finally, apparent slip may occur in suspensions due to contact between the suspended solid phase and the solid boundary surface. While the velocity of the suspending fluid may still be zero at a solid wall, the solid particles in the suspension may slide on the wall. A combination of any of these mechanisms may generate a macroscopic appearance of slip at the wall.

The most easily observed macroscopic effect of wall slip are flow rates that are higher, for a given pressure, than predicted assuming no slip. *Barkat, Shaughnessy, and Clark* (1988), *Lawal, Kalyon, and Yilmazer* (1993), *Yilmazer and Kalyon* (1992), *Yoshimura and Prud'homme* (1988), and *Cohen and Metzner* (1985) have all reported apparent slip of suspensions in capillary and torsional viscometers. These researchers have concluded that the formation of a thin lubrication

layer is the cause of the apparent slip. It has been shown that above a critical shear stress, a plug of nearly undeformed fluid can be made to flow through a capillary due to slippage at the wall. As a consequence of the variation of slip layer thickness compared to capillary diameter, experimental pressure vs. flowrate data from different diameters of capillary or torsional viscometers will not overlap. An attempt to empirically quantify the magnitude of the wall slip is given by Navier's slip condition:

$$\beta\, u_s = \eta \frac{\partial u}{\partial n}$$

where β is Navier's formal slip constant, η is the apparent viscosity, u_s is the slip velocity, and n is the normal to the surface into the fluid. Barkat, Shaughnessy, and Clark have shown that particle migration does occur in pipe flows of cement slurries, and have measured the parameter, β, for cement slurries.

Methodology

PHOENICS

The computer simulations were performed using a PC version of the commercially available PHOENICS software. The computer had an Intel Pentium cpu operating at 90 MHZ, with a 500 MB hard disk, 16 MB RAM, and the MS-DOS operating system. PHOENICS is a general purpose Computational Fluid Dynamics (CFD) code developed by *Ludwig, Qin, and Spalding* (1989). Figure 21 illustrates the organization of the program. The flow parameters, domain, grid, and boundary conditions are specified using PHOENICS Input Language (PIL) in the Q1 file. SATELLITE is a pre-processor that translates the user's specification of a flow simulation into a format that is understood by EARTH, the computational program that solves the conservation and transport equations. The user has access to the solution process at specific points via the GROUND subroutine, which is written in FORTRAN. A specific GROUND subroutine provided by the vendor, GREX3.FOR (GRound EXample 3), contains many of the most frequently needed capabilities. By modifying GREX3.FOR, the user can customize the solution method, implement various fluid models, change fluid properties, or solve for user defined variables. AUTOPLOT and PHOTON are two post-processors that provide graphical display of the simulation results. The numerical solution is performed by EARTH. The relevant equations are solved using the well known finite volume method of discretization and the SIMPLE algorithm for coupling the velocity and pressure.

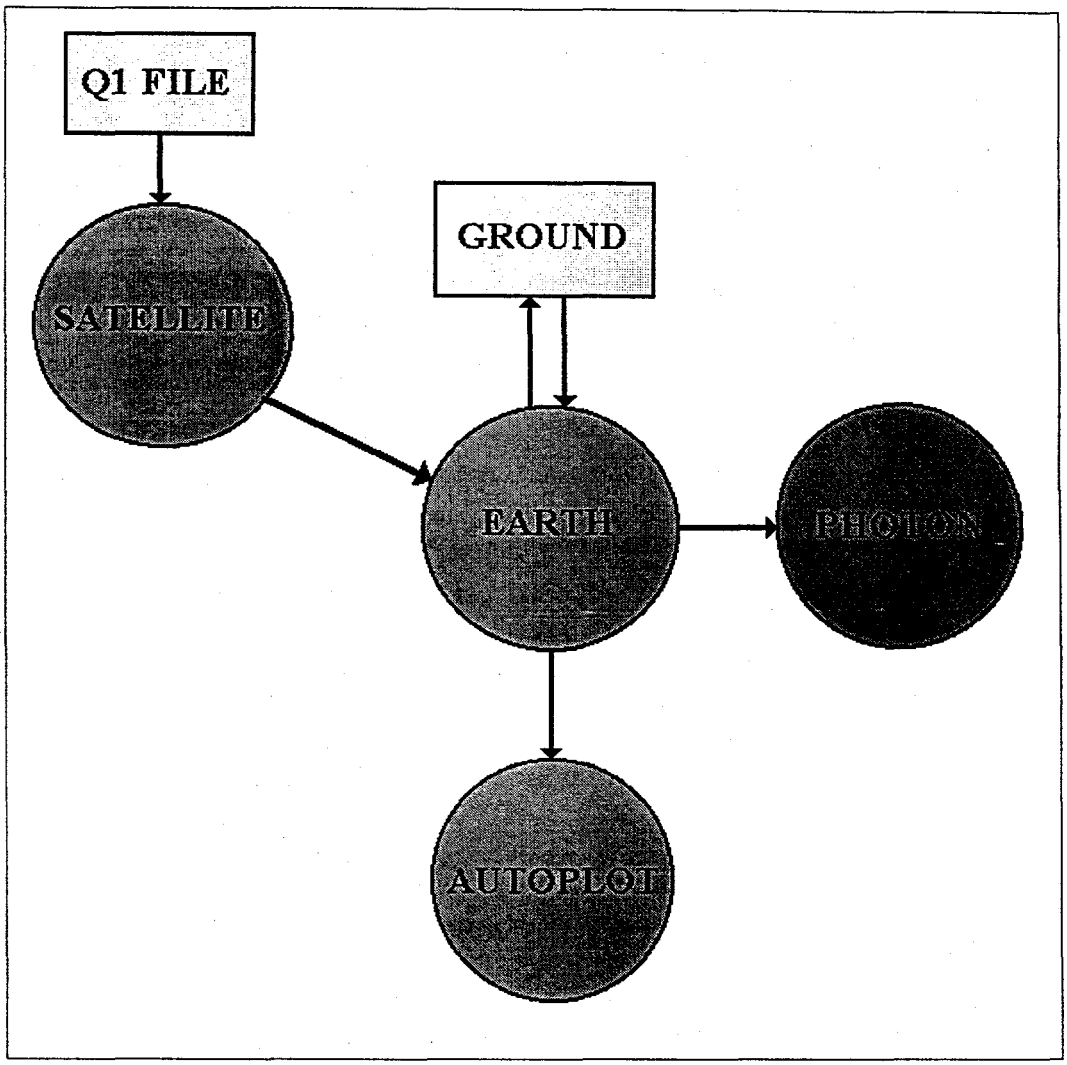

Figure 21 The PHOENICS Structure

THE FINITE VOLUME METHOD

In order to obtain a numerical solution it is necessary to replace the continuous governing differential equations with discrete equations for the dependent variables at a finite number of locations within the calculation domain. The locations where the dependent variables are calculated are called grid points. The equations that relate the grid point values to each other are finite difference equations, and the process by which the finite difference equations are extracted from the differential equations is called discretization. The discretization method employed by PHOENICS is the finite volume method. The finite volume method is well explained by *Patankar* (1980). In the finite volume method, the calculation domain is discretized into a number of finite volumes or cells. The primary grid points are located at the geometric center of the cells, and secondary grid points are located at the centers of the cell faces. These are the locations where the values of the dependent variables are calculated according to the staggered grid convention. Figure 22 shows a typical finite volume discretization in two dimensions.

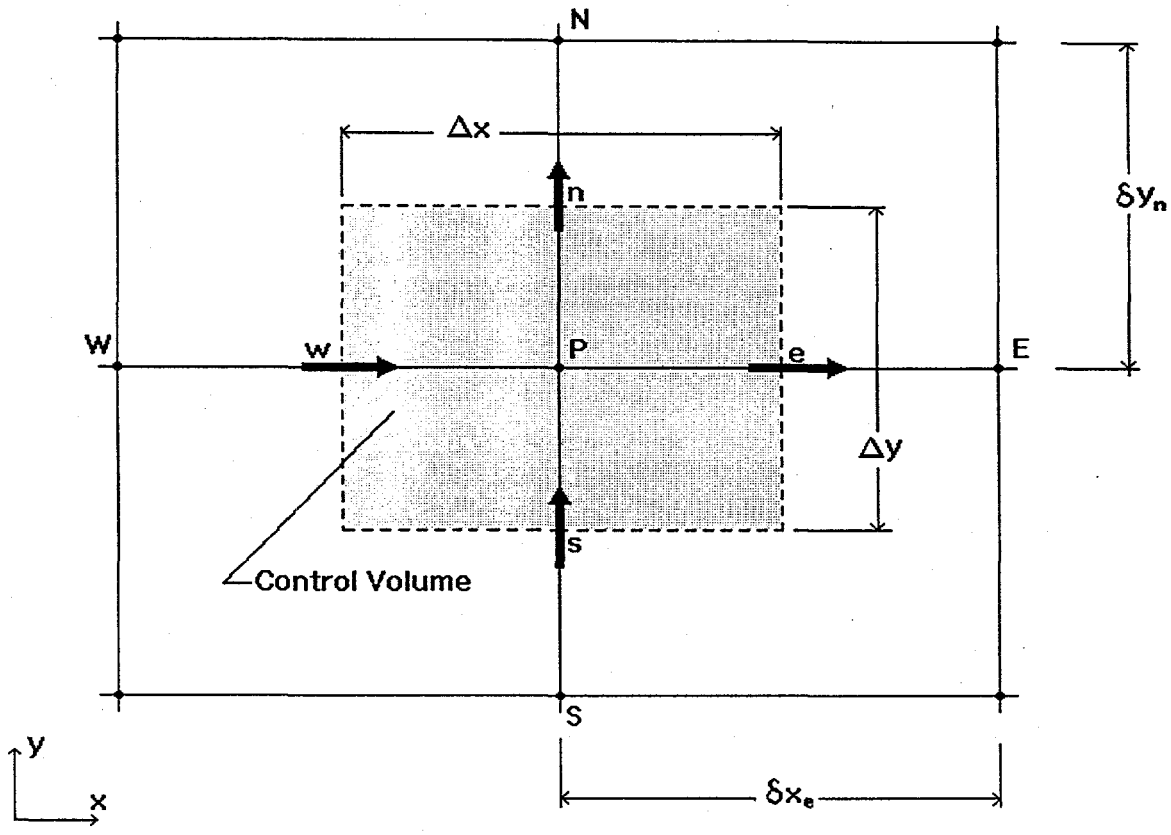

Figure 22 The Staggered Grid Arrangement

The finite difference equations are created from the differential equations by integrating the differential equations over the finite volume of a cell and, for transient problems, a finite time interval. The integrals are evaluated by making assumptions about how the dependent variables change between grid points. A significant advantage of the finite volume method is that it insures integral conservation of the dependent variables over every cell.

The authors of PHOENICS wished to create a general discretization scheme that could be applied to all of the governing differential equations. Therefore, all of the governing equations are cast into the following peculiar form:

$$\frac{\partial}{\partial t}(\rho\phi) + \nabla\cdot(\rho\vec{V}\phi - \Gamma\nabla\phi) = S_\phi$$

where ρ is the density, V is a velocity vector, Γ is the diffusion coefficient, S_ϕ is a source term, and ϕ may represent any conserved quantity such as enthalphy or a velocity component. The quantities Γ and S_ϕ have unique meanings for a particular meaning of ϕ. The first term on the left hand side

is called the transient term, the second term is the advection term, the third is the diffusion term, and the term on the right hand side is the source term. The continuity equation is obtained by setting ϕ=1 thus obtaining:

$$\frac{\partial}{\partial t}\rho + \nabla\cdot(\rho\bar{V}) = S_\phi$$

When ϕ denotes the x-velocity component, the associated meanings of Γ and S are:

$$\Gamma = \eta_{app}$$

$$S_\phi = -\frac{\partial p}{\partial x}$$

where η_{app} is the apparent viscosity. With this notation, the general equation becomes the x-direction momentum equation:

$$\frac{\partial}{\partial t}(\rho u) + \nabla\cdot(\rho u\bar{V}) = -\frac{\partial p}{\partial x} + \frac{\partial}{\partial x}(\eta_{app}\frac{\partial u}{\partial x}) + \frac{\partial}{\partial y}(\eta_{app}\frac{\partial v}{\partial y})$$

The conservation and transport equations cannot be solved directly. They need to be discretized. The discretization of the general equation is accomplished by formally integrating over a control volume. For a steady flow, the transient term is zero and the integration over a control volume yields:

$$\int_{\delta\forall}\left[\frac{\partial}{\partial x}(\rho u\phi - \Gamma\frac{\partial\phi}{\partial x}) + \frac{\partial}{\partial y}(\rho v\phi - \Gamma\frac{\partial\phi}{\partial y})\right]d\forall = \int_{\delta\forall} S_\phi\, d\forall$$

The above result is for two dimensions such where $d\forall=\delta x\delta y$, but all of the following results can be extended to three dimensional transient simulations by integrating over δx, δy, δz and a finite time step, δt. The restriction to two dimensions is only to simplify the explanation.

The left hand side may be converted to a surface integral by the application of Gauss' theorem:

$$\int_s^n\left[(\rho u\phi - \Gamma\frac{\partial\phi}{\partial x})_e - (\rho u\phi - \Gamma\frac{\partial\phi}{\partial x})_w\right]dy + \int_w^e\left[(\rho v\phi - \Gamma\frac{\partial\phi}{\partial})_n - (\rho v\phi - \Gamma\frac{\partial\phi}{\partial})_s\right]dx = \int_{\delta\forall} S_\phi\, d\forall$$

The integration limits, e, w, n, s refer to the east, west, north, and south cell faces as defined in Figure 22. To evaluate the integrals in the above equation, some assumptions must now be made about how ϕ varies between grid points. The first assumption is that the fluxes through the control volume faces can be expressed as the product of a mean flux at the cell face center times the cell face area. This enables the previous equation to be written as:

$$[\ (\rho u\phi - \Gamma\frac{\partial\phi}{\partial x})_e - (\rho u\phi - \Gamma\frac{\partial\phi}{\partial x})_w\ ]\Delta y + [\ (\rho v\phi - \Gamma\frac{\partial\phi}{\partial y})_n - (\rho v\phi - \Gamma\frac{\partial\phi}{\partial y})_s\ ]\Delta x = S_\phi \Delta\forall$$

The diffusive fluxes are then approximated as follows:

$$(\frac{\partial\phi}{\partial x})_e = \frac{\phi_E - \phi_P}{\Delta x_e} \qquad (\frac{\partial\phi}{\partial x})_w = \frac{\phi_P - \phi_W}{\Delta x_w}$$

$$(\frac{\partial\phi}{\partial y})_n = \frac{\phi_N - \phi_P}{\Delta y_n} \qquad (\frac{\partial\phi}{\partial y})_s = \frac{\phi_P - \phi_S}{\Delta y_s}$$

This ultimately leads to central differencing being applied to the diffusion terms.

The advective fluxes; $\rho u\phi$, are discretized using either the second order exponential scheme (Patankar, 1980) or traditional first order upwinding. This combination is called the HYBRID scheme. The Peclet number

$$Pe = uL / \Gamma$$

is a ratio of the strengths of advection and diffusion. The Peclet number is evaluated for each cell.

When $|Pe| < 2$, diffusion dominates the flow and the HYBRID scheme uses exponential differencing for the advection terms. When $|Pe| > 2$, advection is strong and the HYBRID scheme reduces to upwind differencing of the advection terms. As a consequence, the discretization applied to the advective fluxes may vary through the computational domain. The solution order of a method is the rate at which errors decrease as the cell size decreases. A method whose solution error decreases linearly with the cell size is called a first order method, while a method whose solution error decreases like the square of the cell size is called a second order method, and so on. Therefore, the solution order will also vary from first to second order throughout the computational domain.

The source term, S_ϕ is assumed to be constant within a cell. Non-linear source terms must be linearized because the solution method used on the system of algebraic equations is for linear equations. Therefore, the discretized equations must be linear. Source terms are linearized as follows:

$$S_{\phi,p} = S^*_{\phi,p} + (\frac{\partial S_{\phi,p}}{\partial \phi_p})^* (\phi_p - \phi_p^*)$$

where $S_{\phi,p}$ is the source value of ϕ at the p^{th} cell and the starred values are those from the previous iteration. The above equation is put into the following form:

$$S_{\phi,p} = S_c + S_p\phi_p$$

where:

$$S_c = S_{\phi,p}^{\star} - \left(\frac{\partial S_{\phi,p}}{\partial \phi_p}\right)^{\star}\phi_p^{\star}$$

$$S_p = \left(\frac{\partial S_{\phi,p}}{\partial \phi_p}\right)^{\star}$$

For unsteady simulations, all values are assumed to be constant within a cell and for each cell, the integral over a finite time step is replaced with:

$$\int \frac{\partial}{\partial t}(\rho\phi)\, dt = \frac{[(\rho\phi)_{new} - (\rho\phi)_{old}]}{t_{new} - t_{old}}$$

With the above approximations, a set of algebraic equations may be constructed relating the value of the dependent variable at the P^{th} grid point, ϕ_P, to the values of the dependent variable at the surrounding grid points and the value at the previous time step. The algebraic equations are of the following general form (in two dimensions):

$$a_P \phi_P = a_E\phi_E + a_W\phi_W + a_N\phi_N + a_S\phi_S + b_P$$

The 'a' coefficients are calculated for each cell using:

$$a_E = [\![-F_e, D_e-(F_e/2), 0]\!]$$
$$a_W = [\![F_w, D_w-(F_w/2), 0]\!]$$
$$a_N = [\![-F_n, D_n-(F_n/2), 0]\!]$$
$$a_S = [\![F_s, D_s-(F_s/2), 0]\!]$$
$$a_P = a_E + a_W + a_N + a_S + (F_e - F_w) + (F_n - F_s)$$
$$b_P = \text{contribution of source terms}$$

where:

$$F \equiv \rho\phi \qquad \text{and} \qquad D \equiv \Gamma/\delta x$$

The function $[\![x,y]\!]$ means the maximum of x and y, and is analogous to the AMAX1 function in FORTRAN. This set of equations is must be solved iteratively. Each meaning of ϕ has it's own set of equations for which a solution must be obtained.

The SIMPLE Method

A special method is required to solve for the above equations when ϕ represents a velocity

component. This is because of the indirect link between the velocity field and the pressure field. While the pressure gradients appear in the momentum equation source terms, there is no an explicit equation for solving the pressure field. As a consequence, the coupling of pressure and velocity is accomplished by using the Semi-Implicit Method for Pressure Linked Equations (SIMPLE) method described by Patankar (1980). The SIMPLE method is based upon the idea that the velocity field will satisfy the continuity equation only when the correct pressure field is used to solve the momentum equations. The staggered grid approach must be followed to appropriately represent the pressure gradient term in the momentum equations and the velocity gradient terms in the continuity equation. Use of the staggered grid arrangement avoids unrealistic checkerboard solutions and divergence. Pressure and velocity correction equations are used to adjust the pressure and velocity values during the iterative SIMPLE procedure as follows:

1. Guess the pressure field.
2. Solve the momentum equations.
3. Solve the pressure correction equations with the current velocity values.
4. Calculate new velocity values that satisfy continuity.
5. Solve for all other dependent variables.
6. Use the corrected pressure field as the next guess and return to step 2.

This iterative procedure is continued until pressure and velocity values are obtained that satisfy both the momentum equations and the continuity equation within a set tolerance.

CONVERGENCE CRITERIA

PHOENICS solves the flow equations using the algebraic equations and the SIMPLE method described above. The algebraic equations are implicit. Therefore, PHOENICS will "sweep" through the simulation domain many times, updating the dependent variables in each iteration. During three dimensional simulations, PHOENICS sweeps through the domain in a slab-wise fashion in the z-direction, solving for the dependent variables at each grid point in one x-y slab, then for each grid point in the next x-y slab, and so on. For transient problems, many sweeps are performed for each time step so that a converged solution is obtained for each time step. The sweeps through the domain continue until the specified maximum number of sweeps is reached, or the residuals fall below the convergence criteria. For this project, the convergence criteria was chosen to be 10^{-4}. During some simulations, it was not possible to make the residual fall below the convergence criteria, even though further iterations produced no change in the values of the dependent variable. Such solutions appeared to be converged, but no explanation can be given for the high residuals.

GRID REFINEMENT STUDY

A grid refinement study was performed to assess the accuracy and verify the solution order of a PHOENICS solution. In such a study, numerical solutions are computed for a particular flow using two or more grids of different grid spacing. By computing the difference between the

numerical solutions, their dependence upon grid spacing can be quantified. The grid refinement ratio, GR, is the ratio between the coarse grid spacing, Δx_c, and the fine grid spacing, Δx, as follows:

$$GR = \frac{\Delta x_c}{\Delta x_f}$$

The relative difference, ϵ, between ϕ_f, the fine grid solution, and ϕ_c, the coarse grid solution, is expressed as:

$$\epsilon = \frac{(\phi_f - \phi_c)}{\phi_f}$$

This quantity by itself is not a good estimate of the error in the solution because it does not take into account the grid refinement ratio, GR, and the solution order, p, of the numerical method. For instance, with a very small GR, the two solutions would be very close and ϵ may falsely indicate that the fine grid solution is very close to the converged solution. *Roache* (1993) proposes the use of a Grid Convergence Index (GCI) that includes both GR and p. Roache states that within the CFD community, there is confidence that the ϵ obtained by a grid doubling with a second order method (ie: GR= p= 2) is indicative of the solution error if both solutions are within the asymptotic range. Thus, the idea behind the GCI is to relate the ϵ obtained from any grid refinement study with arbitrary GR and p, to the ϵ that would be obtained with the same base grid but with GR and p = 2. The GCI defined as:

$$GCI = 3\frac{\epsilon}{(GR^p - 1)}$$

where ϵ, GR, and p are the values obtained from the actual grid refinement study. If the solution order is unknown, it can be found with solutions from three grids as follows:

$$p = \ln\left(\frac{\phi_1 - \phi_2}{\phi_2 - \phi_3}\right)\frac{1}{\ln(GR)}$$

The three solutions, ϕ_1, ϕ_2, and ϕ_3, are obtained from two grid reductions with the same GR such that:

$$GR = \Delta x_1/\Delta x_2 = \Delta x_2/\Delta x_3$$

This definition of the GCI is only valid for solutions that are within the asymptotic range. Determination of whether or not the asymptotic range has been achieved can be accomplished as

follows. If an exact solution is known for the simulated flow, then an Error Indicator, E, is defined as:

$$E = \frac{\phi_{exact} - \phi_{numerical}}{\Delta x^{p}}$$

and is monitored as the grid spacing, Δx, is decreased. If E remains constant the solutions are within the asymptotic range. If an exact solution is not known, then the numerical solution must be calculated with three different grid spacings. From these two GCI values are computed. If the solutions are within the asymptotic range, the following relationship will be true for GCI_{12} (the GCI found using solutions ϕ_1 and ϕ_2) and for GCI_{23} (the GCI found using solutions ϕ_2 and ϕ_3):

$$GCI_{12} = (GR)^{p} \cdot GCI_{23}$$

The ϕ values used to compute the GCI may represent any of the solution variables or any function of the solution variables. For example, ϕ may represent individual velocity values at a specific location or a flow rate obtained by integrating a velocity profile. The only restriction is that the comparison must be made at the same physical location within the domain. Thus care must be taken when choosing GR to insure that each grid contains nodes for at least a few of the same points in physical space.

The grid refinement study was performed with results from a steady, axi-symmetric pipe flow simulation. The pipe flow was used in the grid refinement study because the exact solution for this flow is well known, even for fluids that exhibit non-Newtonian behavior. The simulated pipe flow domain and boundary conditions were as follows:

Dimensions:

radius = 1.0 m
length = 25 m

Boundary Conditions:

uniform entrance velocity = 2 m/s
exit pressure = 0.0 Pa
no slip condition at the pipe wall

Fluid Properties (Newtonian):

density = 1.0 kg/m^3
dynamic viscosity = 0.1 N·s/m^2 (SAE 30 oil @ 38°C)

These parameters resulted in a Reynolds number of $R_e = 20$, which guarantees laminar flow. The entrance length was found to be 3 meters using an empirical relationship in *White* (1991). Simulations of this flow were performed with three different grids: 3x12, 9x36, and 27x108 cells in the radial and downstream directions. In this grid refinement study, both refinement ratios are 3. PHOENICS grid points are cell centered, thus the first grid point is only a half grid spacing from

the boundary and a grid refinement ratio of three was necessary to insure that nodes existed in the coarse and fine grids which represented the same points in physical space. The results from the three PHOENICS simulations and the exact solution are shown in Figure 23. The velocity and flowrate data were used to determine the solution order and the rate at which grid refinement leads to a converged solution. Figure 24 shows root-mean-square (RMS) error vs. grid spacing for the velocity profiles.

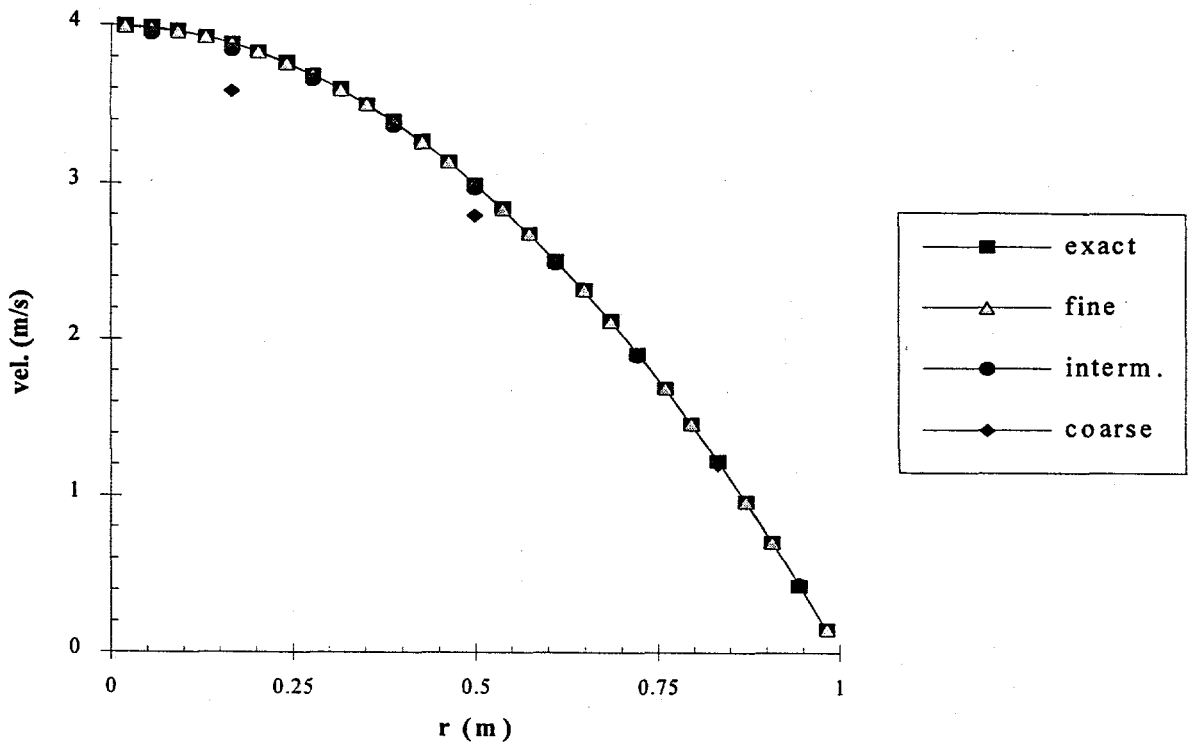

Figure 23 Comparison of PHOENICS and Exact Solutions.

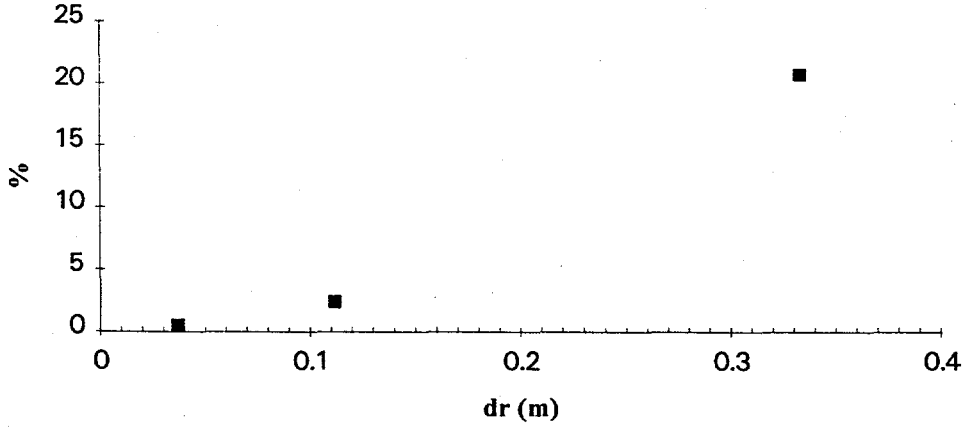

Figure 24 RMS error vs. Grid spacing.

The solution order, determined using velocity values at several locations, was found to vary across the pipe radius within the entrance length from p=1.0 at r=0.167 (near the pipe centerline), to p=1.5 at r=0.500, and p=1.85 at r=0.833 (near the pipe wall). The solution order is nearly first order where convection terms dominate the flow (near the centerline), and closer to second order where viscous terms dominate the flow (near the pipe wall). This behavior is attributed to the hybrid discretizing employed by PHOENICS. The solution order variation found within the entrance region is consistent with this explanation and is within the theoretical limits for the solution order of this method. In the fully developed region, the solution was second order for all positions across the pipe. This is expected because the convective terms are negligible when the flow is fully developed. For these flow conditions, the HYBRID scheme is functioning as a second order central differencing scheme. The fully developed velocity profiles were integrated using Simpson's rule and compared to the flowrate specified at the inlet boundary. The error indicator between the computed and exact flowrate decreased as a second order method such that:

$$E = \frac{Q_{exact} - Q_{numerical}}{\Delta x^2} = constant$$

The same result was obtained when flowrate values and discrete velocity values were used in the above equation.

The results of this grid refinement study clearly indicate that the solution is second order within the fully developed region, and is between first and second order throughout the rest of the domain. While the GCI does not provide information about the overall solution, the computed GCI can be used as an estimate of how close the fine grid solution is to the converged solution. Using the method of Roache (1993), the GCI was computed with data from the flowrate values obtained by integrating the fully developed velocity profiles. The GCI computed for the finest grid using GR=3 and p=2 was 0.002346. This indicates that the fine grid solution is within 0.23% of the converged solution. The GCI was computed at a location within the entrance region using velocity values and was found to be higher than the GCI in the fully developed region. Within the entrance region, the GCI was found to vary from 0.024 near the wall (where p=2) to 0.118 near the centerline (where p=1). This implies that the finest solution at this sampling location within the entrance length may be expected to lie within 2.4% of the converged solution near the pipe wall, and within 11.8% of the converged solution near the centerline. The solution was more converged in the developed region than in the developing region. This verifies that the HYBRID discretizing scheme is functioning as a second order method in the developed region, but as a lower order method within the entrance length.

TRACKING A FREE SURFACE

PHOENICS has two built in methods for tracking a moving interface between two fluid phases during a transient flow simulation. The two methods are the Scalar Equation Method (SEM), and the Height Of Liquid method (HOL). Both are coded within the GREX3.FOR subroutine, and may be "turned on" by making the appropriate setting within the Q1 file. Both the SEM and HOL

methods treat the flow as one phase, i.e. two sets of velocity and pressure are not calculated. Rather, the methods permit fluid properties such as density and viscosity to vary throughout the domain to represent the spatial distribution of the two phases. A definite interface must exist, therefore dispersed phase simulations are not possible with the SEM and HOL methods. There are advantages and disadvantages to each model, but for flow simulations where both models are applicable, they yield the same result.

SCALAR EQUATION METHOD

The SEM simulates the transient convection of a scalar variable throughout the simulation domain. The scalar variable is given a value of unity in fluid A, and a value of zero in fluid B. Use of this kind of marker variable is analogous to seeding a flow domain with a dye (fluid A is purple, fluid B is clear), except that the numerical dye is transported only by convection. The convection of the scalar variable, ϕ, is governed by:

$$\frac{\partial \phi}{\partial t} + u\frac{\partial \phi}{\partial x} + v\frac{\partial \phi}{\partial y} + w\frac{\partial \phi}{\partial z} = 0$$

The solution of the flow is obtained by solving the governing differential equations in conjunction with the transport equation for the scalar marker variable. The simulation is a one phase simulation of a fluid whose properties vary throughout the domain. The value of the scalar variable at each grid point will establish the fluid properties for that control volume. For control volumes with intermediate values of the marker variable, fluid properties are assumed to vary linearly. The variation of the density, ρ, and viscosity, μ, are:

$$\rho = \rho_a + (\rho_b - \rho_a)\phi$$
$$\mu = \mu_a + (\mu_b - \mu_a)\phi$$

Upwind discretization of the above transport equation creates unphysical smearing of the discontinuity at the interface. The upwind scheme used in PHOENICS evaluates the flux at a cell face by using the information at the cell that lies "upwind" of the cell to be evaluated. For instance, to evaluate the advective flux at the east face of cell P:

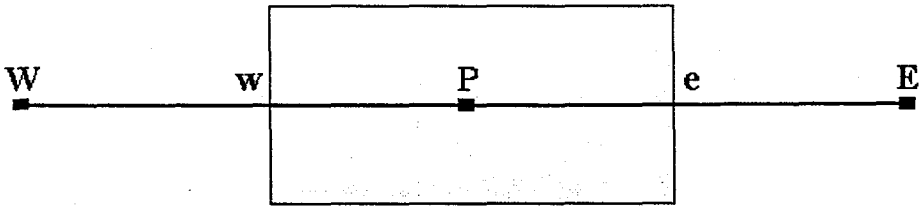

for $u_e > 0$; $\phi_e = \phi_P$ for $u_e < 0$; $\phi_e = \phi_E$

and for the west face:

$$\text{for } u_w > 0 \;\; ; \;\; \phi_w = \phi_W \qquad\qquad \text{for } u_w < 0 \;\; ; \;\; \phi_w = \phi_P$$

The smearing associated with the above discretization scheme is combated with the discretization scheme proposed by *Van Leer* (1981). The Van Leer approach is an explicit scheme which modifies the first order upwind formulation using characteristics. The flux at the east face is modified as follows:

for $u_e > 0$:

$$\phi_e = \phi_P + (\frac{\partial \phi}{\partial x})_P (dx - udt)$$

for $u_e < 0$:

$$\phi_e = \phi_E + (\frac{\partial \phi}{\partial x})_E (dx + udt)$$

The gradient of ϕ is based upon the values at the start of the time step, thus making the scheme explicit. Therefore, the Courant criterion places a restriction upon the size of a time step to avoid instability. Physically the time step restriction prevents the interface from moving through a full cell during a time step. The following limit must be satisfied for every cell in the computational domain:

$$dt < \min(\frac{dx}{u} , \frac{dy}{v} , \frac{dz}{w})$$

The Van Leer scheme is incorporated into the SEM subroutine in the GREX3.FOR file. The SEM has been used successfully by *Hirt and Nichols* (1981) and *Chan, Pericleous, and Cross* (1991). Both have interpreted a surface of ϕ=0.5 in the computational solution as the location of the fluid interface. This interpretation of the surface location was verified by measuring the area under the ϕ=0.5 curve for a simple two dimensional test case that will be discussed later.

HEIGHT OF LIQUID METHOD

The HOL method determines the location of a fluid interface by evaluating the mass of liquid that exists in a vertical column of cells. An "up" direction must be specified along which only one intersection of the interface is permitted. Flows with overturning surfaces can **not** be simulated using the HOL method. A volume fraction of liquid, ϕ, is defined for each cell. The inflows and outflows of fluid to each column of cells in the up direction are calculated from the convective mass fluxes multiplied by the upwind values of ϕ. The net flux of fluid mass into a column of cells is used to calculate the total mass within the column. Since the cell volumes are known, the height of liquid within a cell can be calculated by dividing the total mass by the density and cell volume. Cells below the interface have a volume fraction of unity (filled with fluid A), and cells above the interface have a volume fraction of zero (filled with fluid B). The cell where the interface occurs is given an intermediate volume fraction defined by:

ϕ = (Total Mass - Lower Mass)/(ρ_a*cell volume)
Total Mass = Old mass in column + inflow - outflow
Lower Mass = Mass below the interface cell

Fluid properties will have an intermediate value at the interface cell and are defined by the same linear variation as used in the SEM. A surface of ϕ=0.5 is interpreted as the interface of the two fluids and was verified with a simple test case that will be discussed below. The HOL method does not generate numerical smearing of the interface, nor does it have a restriction on time step. The coding for the HOL method is included in the GREX3.FOR file.

DAM BREAK SIMULATION

The following "dam break" simulation was used to evaluate the two surface tracking methods in PHOENICS. An imaginary restraining wall is instantaneously removed and the volume of initially static fluid contained behind it is permitted to slump under the influence of gravity. The simulation domain is 1.0 m in the x-direction and 0.3 m in the vertical y-direction. Initially, the fluid occupies a 0.2 m wide by 0.275 m high area at the left end of the domain. The simulation begins just after the wall has been removed. The simulation is transient and two dimensional. The grid has 50 uniform cells in the x-direction and 20 non-uniform cells in the y-direction expanding exponentially at a rate of 1.4 in the positive y-direction. The Herschel-Bulkley fluid model was used with the following parameters: $n = 0.8$, $k = 1.0$ ($N \cdot s^n/m^2$), $\tau_y = 5$ Pa. The time step was 0.001 s and 200 iterations were specified per time step. A 0.5 second simulation required 5 hours and 9 minutes of cpu time when the SEM was used. The same simulation has been run using the SEM and the HOL method.

At each time step, the surface of $\phi = 0.5$ is used to mark the location of the fluid interface as shown in Figure 25. To check the validity of this as a true indicator of the free surface, the area under each of the curves was computed by numerical integration using Simpson's rule. The area under the $\phi = 0.5$ curve at each time step was the same as the initial area occupied by the fluid. Thus, the $\phi = 0.5$ curve is a good representation of the free surface location.

The results predicted by the SEM and the HOL method agree. The smoothness of the free surface predicted by the HOL method is more susceptible to grid coarseness. A coarse grid may produce a free surface that has steps coinciding with the grid columns. This is because the HOL method "fills up" each columns of cells. When the grid is finer, the HOL method produces free surface curves that are as smooth as those produced by the SEM. To achieve realistic results with the SEM, small times steps are needed. If the Courant criterion is exceeded for any cell in the domain, large errors occur that spread quickly throughout the domain, ultimately leading to divergence. This can be a problem when the velocity magnitudes cannot be predicted before the simulation is run because the size of

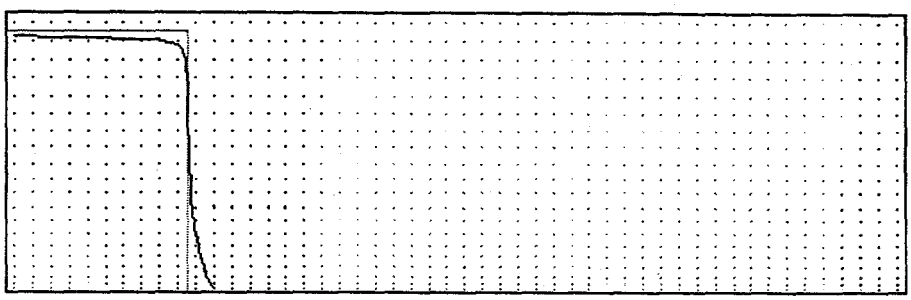

y
x

Time = 0.05 sec

y
x

Time = 0.15 sec.

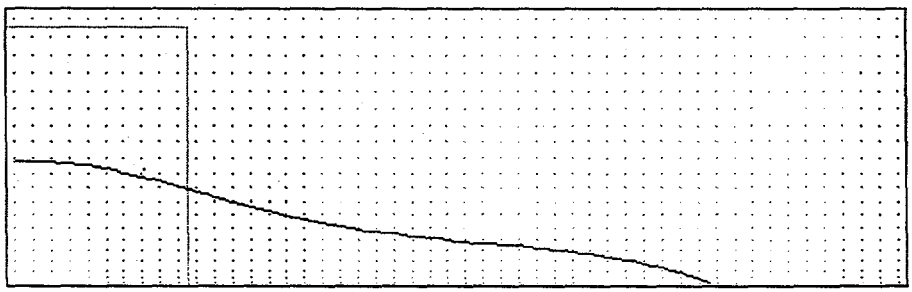

y
x

Time = 0.30 sec.

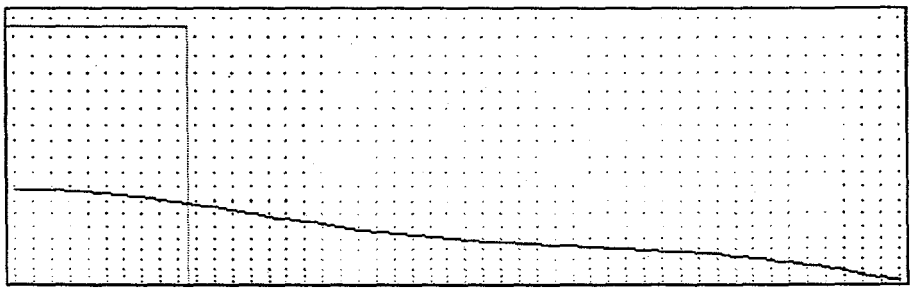

y
x

Time = 0.37 sec.

Figure 25 Dam-Break Simulation Results Using SEM

the time steps must be set before the run. PHOENICS does not have the ability to change time step duration once the simulation is started. Thus, both methods have a dependency on the discretization of the continuum. The HOL method requires a fine spatial grid while the SEM requires fine temporal discretization. With the appropriate grids, both methods yield the same results.

A second test case to evaluate the SEM and HOL methods used a flow that is similar to the mine filling flow. Fluid is introduced into the domain by a fixed mass flux boundary condition through the "roof" of the axisymmetric domain shown in Figure 26. Gravity is in the negative y-direction. The SEM is able to satisfactorily simulate the flow, but the HOL method cannot be used in such a simulation. The reason is that no correct "up" direction can be used. For each of the four possible choices, ±x-direction and ±y-direction, unrealistic results are produced. The reason for the unrealistic results is that the HOL method always "fills up" columns of cells from the bottom based upon the specified "up"direction. For this simulation (and the mine filling simulation) some of the columns of cells are actually filled from the "top". Mine filling cannot be represented using the HOL method. Therefore, the SEM must be used in the mine filling simulations.

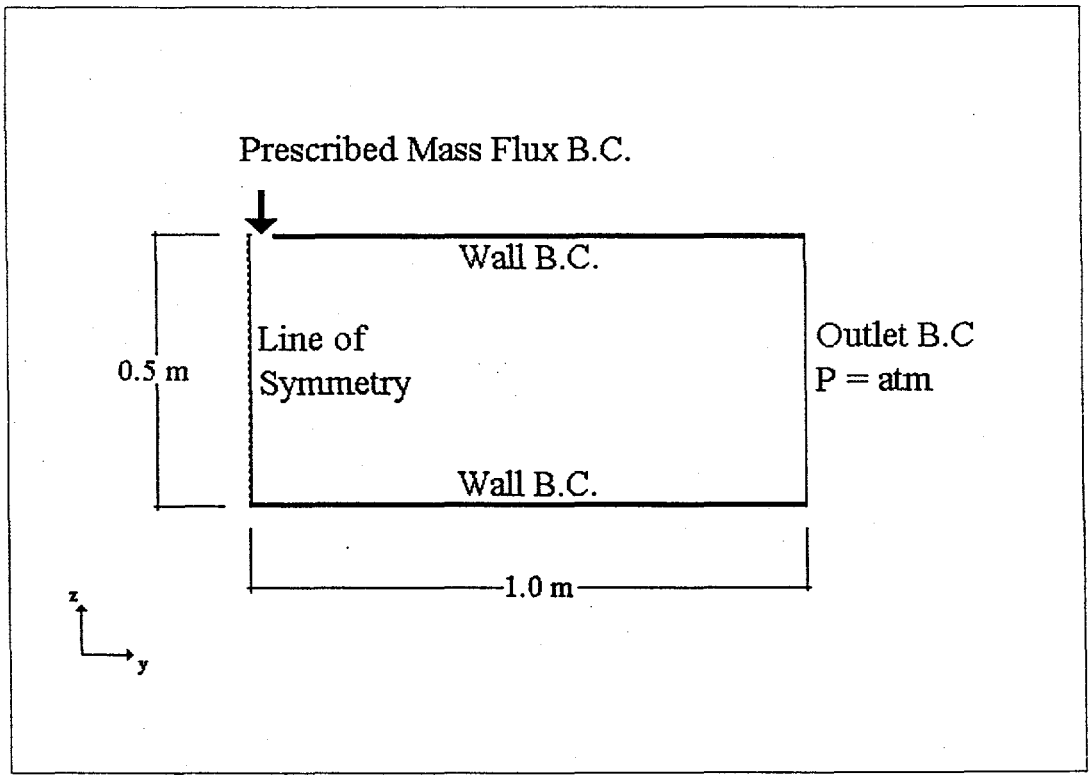

Figure 26 Axisymmetric Simulation Domain

SAMPLE Q1 FILE

This section presents a typical Q1 file which is used to specify the flow simulation parameters for PHOENICS. The Q1 file is an ASCII file that PHOENICS SATELLITE reads and interprets for use by EARTH. There are 24 groups in a Q1 file, some or all of which may contain information. The groups only serve to assist the user in organizing the simulation data. Commands may be placed anywhere within the file, but subsequent commands supersede earlier commands. SATELLITE will only recognize commands that begin in the first or second space; all other commands are interpreted as comment lines. The meaning of all the PIL commands and their associated groups may be found in the CHAM manual TR200a (Ludwig, et.al.). The Q1 file shown below contains all the information that must be submitted to SATELLITE so that EARTH will simulate the "dam break" problem described above using the SEM method to track the interface. The command that activates the SEM subroutine is SURF=T. If the HOL method was used,the appropriate subroutine would be activated by replacing SURF=T with HOL=T. The other settings that are necessary for both methods to function properly are described in the PHOENICS documentation.

```
 TALK=T;RUN( 1, 1);VDU=VGAMOUSE

    GROUP 1. Run title and other preliminaries
TEXT(DAM BREAK ; H-B FLUID ; NO Friction
TITLE

    GROUP 2-5. Grid specification
STEADY=F
GRDPWR(T,500,0.5,1.0)
GRDPWR(x,50,1.0,1.0)
GRDPWR(y,20,0.30,1.4)

    GROUP 7. Variables stored, solved & named
STORE(DEN1,PRPS,ENUL,GENK);SOLVE(VFOL,SURN,btau)
SOLUTN(P1,Y,Y,Y,N,N,N)
SOLUTN(U1,Y,Y,N,N,N,N)
SOLUTN(V1,Y,Y,N,N,N,N)

    GROUP 8. Terms (in differential equations) & devices
  ** activate the "gas-and-liquid algorithm", ie volumetric
     continuity equation, and allow convection fluxes to be
     modified in GROUND
GALA=T
TERMS(VFOL,N,N,N,N,P,P)
TERMS(SURN,N,N,N,N,P,P)
GENK=T
SURF=T

    GROUP 9. Properties of the medium (or media)
RHO1=GRND10 ; ENUL=grnd6
enula=0.00083 ; enulb=0.0042 ; enulc=0.8

    GROUP 11. Initialization of variable or porosity fields
FIINIT(P1)=0.0;FIINIT(V1)=0.0;FIINIT(SURN)=0.0
FIINIT(DEN1)=1.2;INIADD=F
  ** place the initial "pile" of liquid of which the slumping
     is to be simulated
PATCH(LIQUID,INIVAL,1,10,1,ny-1,1,nz,1,1)
COVAL(LIQUID,SURN,ZERO,1.0)
COVAL(LIQUID,DEN1,ZERO,1200)
```

```
    GROUP 13. Boundary conditions and special sources
  ** try an actual open top boundary
OUTLET(TOPOUT,NORTH,1,NX,1,NY,NZ,NZ,1,LSTEP)
  ** provide for the gravity-force source of w1
PATCH(GRAV,PHASEM,1,NX,1,NY,1,NZ,1,LSTEP)
COVAL(GRAV,v1,FIXFLU,-9.81)
  ** time patch for transient term
PATCH(TCON,CELL,1,NX,1,NY,1,NZ,1,LSTEP)
COVAL(TCON,SURN,GRND,GRND)

    GROUP 15. Termination of sweeps
LSWEEP=500
LITER(SURN)=1

    GROUP 16. Termination of iterations
RESREF(P1)=1.E-4 ; RESREF(V1)=1.E-4 ; RESREF(u1)=1.E-4

    GROUP 17. Under-relaxation devices
relax(p1,linrlx,0.3)
RELAX(u1,FALSDT,0.0001);RELAX(v1,FALSDT,0.00008)
    GROUP 19. Data communicated by satellite to GROUND
IPRPSA=68 ; IPRPSB=0 ; IDISPA=10 ; CSG1=y
VARMIN(SURN)=0.0 ; VARMAX(SURN)=1.0
RLOLIM=0.4 ; RUPLIM=0.6

    GROUP 22. Spot-value print-out
TSTSWP=50 ; ECHO=F ; IYMON=NY/2 ; IZMON=NZ/2 ; IXMON=NX/2

    GROUP 23. Field print-out and plot control
  ** provide contour-plot output for EXCELL manipulation
       PATCH(tboSURN,CONTUR,1,1,1,ny,1,NZ,1,LSTEP)
       PLOT(tbosurn,SURN,ZERO,10)
OUTPUT(P1,Y,n,n,n,Y,Y);OUTPUT(u1,Y,n,n,n,Y,Y)
OUTPUT(V1,Y,n,n,n,Y,Y);OUTPUT(SURN,Y,N,N,N,N,N)
OUTPUT(DEN1,Y,N,N,N,N,N);OUTPUT(vfol,y,N,N,N,N,n)
OUTPUT(btau,y,N,N,N,N,N)
STOP
```

MODIFICATIONS TO THE PHOENICS CODE

SUBROUTINE FOR HERSCHEL-BULKLEY FLUID MODEL

The capability to simulate power-law and Bingham fluid behavior is already contained within PHOENICS. However, preliminary rheological testing indicated that the Herschel-Bulkley fluid model would be needed to describe the flow behavior of the FBC-ash grout. It was therefore desired to implement a procedure within PHOENICS to simulate flows of Herschel-Bulkley fluids. The Herschel-Bulkley fluid model in two dimensions is as follows:

$$\tau = \tau_y + k\,\gamma^n \qquad \textit{for} \quad \tau > \tau_y$$

The apparent viscosity that corresponds to the Herschel-Bulkley constitutive law is:

$$\eta_{app} = \frac{\tau_y + k\gamma^n}{\gamma} = \tau_y\gamma^{-1} + k\gamma^{n-1} \qquad for \quad \tau > \tau_y$$

The behavior expressed by the above constitutive law is included in a flow simulation by evaluating the apparent viscosity at every cell and using that value as the viscosity when solving the momentum equations. The form of the apparent viscosity equation is very similar to that of the power-law and Bingham fluid models which are already included in a PHOENICS subroutine called GXPROPS.FOR. The subroutine GXPROPS.FOR is called by the GREX3.FOR subroutine when the laminar viscosity, ENUL, is set equal to a "ground flag" rather than a viscosity value in the Q1 file. A ground flag is a PHOENICS device for calling a specific subroutine. Ground flags may be used for calling a wide range of subroutines for many of the flow simulation parameters that need to be specified in the Q1 file. The PHOENICS manuals CHAM tr200a and CHAM tr200b (Ludwig, et.al.) provide in-depth discussions of the ways to use the GREX3.FOR subroutine to call other subroutines.

These viscosity settings in the Q1 file invoke the following fluid models and parameters.

ENUL = GRND4 → Power-Law Apparent Viscosity Calculated
ENULA = k
ENULB = n

ENUL = GRND5 → Bingham Apparent Viscosity Calculated
ENULA = k
ENULB = τ_y

The ground flags (e.g. GRND4, GRND5, etc.) specify unique subroutines. The subroutines that calculate an apparent viscosity according to the power-law and Bingham fluid models were used as patterns for developing a subroutine to calculate an apparent viscosity value based upon the Herschel-Bulkley model.

The existing GXPROP.FOR file was copied to GXPROP2.FOR, and the GREX3.FOR file was copied to GREX4.FOR. The original files are in the \D_PHOE20\D_EARTH directory. All modifications were made to the two copied files in the \D_PHOE20\D_JOHN directory, thus leaving the original files unmodified. The new subroutine was given a ground flag of GRND6. It appears in the GXPROP2.FOR file immediately following the GRND5 code. The FORTRAN variables used in the new subroutine are:

VISL = η_{app}
LGEN1 = γ^2
ENULA = k
ENULB = τ_y

ENULC = n

The symbol, γ, denotes the magnitude of the rate of strain. In PHOENICS, the rate of strain is the square root of the variable LGEN1. The calculation of apparent viscosity with these variables is obtained with the following:

VISL=ENULA*LGEN1**(0.5*(ENULC-1.)) + ENULB*LGEN1**(-0.5)

This is broken up into four steps:

1. EXPN = 0.5*(ENULC-1.)
2. VISL = ENULA
3. VISL = VISL * LGEN1 ** EXPN
4. VISL = VISL + ENULB * LGEN1**(-0.5)

Using built in PHOENICS function statements, these steps become:

1. EXPN = 0.5*(ENULC-1.)
2. CALL FN1(VISL,ENULA)
3. CALL FN37(VISL,LGEN1,EXPN)
4. CALL FN35(VISL,LGEN1,ENULB,-0.5)

These function statements are explained in appendix 4 of CHAM tr200b.

Printout of stress is enabled by computing the stress as BTAU according to the actual constitutive law. The following three steps compute the stress magnitude for each cell in the domain.

1. EXPN = 0.5*(ENULC-1.)
2. CALL FN1(VISL,ENULB)
3. CALL FN35(VISL,LGEN1,ENULA,EXPN)

The GXPROP2.FOR file is partially listed below. Modifications to the file are in bold.

```
C!!!!!!!!!!!!!!!!!!!!!!!!!!!!!!!!!!!!!!!!!!!!!!!!!!!!!!!!!!!!!!!!!!!!!!!
C**** SUBROUTINE GXENUL is called from section 6, group 9 of
GREX3,
C     and is entered only when ENUL is set to GRND options.
C
C.... The arguments VISL,and TEMP1 are integer names used in the
C     SATELLITE, indicating which whole-field store will be used
C     for the laminar kinematic viscosity and the temperature of
C     phase 1; ENUL is the laminar kinematic viscosity, and set to
C     GRND(n).
```

.
.
.

REMOVED FOR BREVITY OF PRESENTATION

```
C.... ENUL=GRND4 selects laminar kinematic viscosity as a linear
C     function of the strain rate to the power 0.5*(ENULB-1), as
is
C     appropriate for a power-law non-Newtonian fluid.
C.... ENUL=GRND5 selects Bingham laminar kinematic viscosity.
C.... ENUL=GRND6 selects Herschel-Bulkley viscosity law.
C     NOTE that ENUL or VISL must be stored in Q1. This is checked
C     for in GREX.
       ELSEIF(GRNDNO(4,ENUL).OR.GRNDNO(5,ENUL).OR.GRNDNO(6,ENUL))
THEN
        IF(ISWEEP.EQ.FSWEEP) THEN
          IF(QEQ(FIINIT(VISL),READFI)) THEN
C.... On first sweep of restart, copy viscosity from internal 2D
C     store KDUMM to prevent 'kick'
            CALL FN0(VISL,-KDUMM)
          ELSE
C.... On sweep 1, set VISL to ENULA, as no sensible strain rate
available
            CALL FN1(VISL,ENULA)
          ENDIF
        ELSE
C.... ENUL=GRND4: power-law laminar kinematic viscosity
          IF(GRNDNO(4,ENUL)) THEN
C           FN1(Y,A) Y = A ; FN37(Y,X,A,B) Y = Y * A*X**B
            CALL FN1(VISL,ENULA)
              IF(NEZ(ENULB).AND.QNE(ENULB,1.0)) THEN
                CALL FN22(LGEN1,TINY)
                CALL FN37(VISL,LGEN1,0.5*(ENULB-1.))
              ENDIF
          ELSEIF(GRNDNO(5,ENUL)) THEN
C.... ENUL=GRND5: Bingham laminar kinematic viscosity
            CALL FN22(LGEN1,TINY)
C     Option to printout square-root of the second invariant of
C     deviatoric stress tensor, i.e.tau = enulb+enula*sqrt(lgen1)
C     where enulb=yield stress & enula=Bingham plastic viscosity
          IF(LBNAME('BTAU').NE.0) THEN
   CALL FN1(VISL,ENULB)
   CALL FN35(VISL,LGEN1,ENULA,0.5)
   CALL FN0(LBNAME('BTAU'),VISL)
 ENDIF
                              C  Compute  kinematic  viscosity,visl  =
[enula+enulb/sqrt(lgen1)]/rho
C           FN(Y,A) Y=A   ; FN35(Y,X,A,B) Y=Y+A*X**B
            CALL FN1(VISL,ENULA)
            CALL FN35(VISL,LGEN1,ENULB,-0.5)
**
**  Modification on 16-May-1995 to simulate H-B fluid behavior
**
          ELSEIF(GRNDNO(6,ENUL))THEN
```

```
            CALL FN22(LGEN1,TINY)
            EXPN=0.5*(ENULC - 1.0)
C     Option to printout square-root of the second invariant of
C     deviatoric stress tensor, i.e.tau = enulb+enula*sqrt(lgen1)
C     where enulb=yield stress & enula=Bingham plastic viscosity
            IF(LBNAME('BTAU').NE.0) THEN
              CALL FN1(VISL,ENULB)
              CALL FN35(VISL,LGEN1,ENULA,EXPN)
              CALL FN0(LBNAME('BTAU'),VISL)
            ENDIF
C     Compute kinematic viscosity from HB fluid model
C      FN1(Y,A) Y=A   ;   FN35(Y,X,A,B) Y=Y+A*X**B   ;   FN37(Y,X,A)
Y=Y*X**A
            CALL FN1(VISL,ENULA)
            CALL FN37(VISL,LGEN1,EXPN)
            CALL FN35(VISL,LGEN1,ENULB,-0.50)
          ENDIF
**
**  End of modification from 16-May-1995
**  Original grnd6 routine has been removed
**
        ENDIF
**
```

A modification was also required in the GREX3.FOR file to include storage for LGEN1 and the velocity gradients needed for calculating LGEN1 when GRND6 is called from the Q1 file. A logic statement on line 172 is modified to include GRND6. The following is an excerpt from the GREX4.FOR file that contains the modification, indicated in bold face.

```
C-------------------------------------------------------LGEN1
C.... Provision of storage for square-of-velocity-gradient
C      expressions for viscous-dissipation or turbulence-
C     energy source. First ensure that strain-rate is calculated
C     for ENUL=GRND4 and GRND5.
C

GENK=GENK.OR.((GRNDNO(4,ENUL).OR.GRNDNO(5,ENUL).OR.GRNDNO(6,ENUL))
```

The modification activates a call on line 216 which is also modified as follows:

```
C-------------------------------------------------EASP5 TO EASP18
C
      IF(GRNDNO(4,ENUT).OR.GENK.OR.DUDX.OR.DVDX.OR.DWDX.OR.

     1        DUDY.OR.DVDY.OR.DWDY.OR.DUDZ.OR.DVDZ.OR.DWDZ) THEN
```

Once the two files were modified, a "private" version of the executable, EARTH, needed to be compiled. This was accomplished by updating the BLDEAR.BAT batch file in the \D_PHOE20\D_UTILS directory. By including the path and file name of the new subroutines to be included, a new EARTH file was "built" in the \D_PHOE20\D_JOHN directory by running the BLDEAR.BAT batch file. The FORTRAN compiler used to

compile and assemble the various subroutines was the Salford Software FTN77 compiler version 2.74. When the user tries to run EARTH, a choice of "public" or "private" is now given to permit selection of the EARTH version that is desired. The public version is the original commercial version of PHOENICS, the private version contains the modifications discussed above.

FULLY DEVELOPED PIPE FLOW

The exact solution is known for the fully developed velocity profile and flowrate of a Herschel-Bulkley fluid in a pipe. A pipe flow simulation was performed to evaluate the accuracy of the new subroutine. The velocity profile and flow rate are functions of fluid properties, pipe radius, and pressure gradient, and are given by the following equations.

r = radial coordinate
R = tube radius
r_{plug} = radius of the unsheared plug
$\Delta P/\Delta L$ = pressure gradient

For $R > r > r_{plug}$, the velocity profile is:

$$u = \left(\frac{1}{k}\right)^{\frac{1}{n}} \left(\frac{-2\Delta L}{\Delta P}\right)\left(\frac{n}{n+1}\right) \cdot \left[\left(-\frac{r\Delta P}{2\Delta L} - \tau_y \right)^{\frac{n+1}{n}} - \left(-\frac{R\Delta P}{2\Delta L} - \tau_y \right)^{\frac{n+1}{n}} \right]$$

When $r < r_{plug}$ the fluid moves as a plug. The plug velocity is obtained by replacing r with r_{plug} in the above equation. The plug radius is given by:

$$r_{plug} = \frac{2\,\tau_y\,\Delta L}{\Delta P}$$

The flowrate is:

$$Q = \frac{\pi R^3 n}{k^{(1/n)}} \left(\frac{R\Delta P}{2\Delta L}\right)^{-3} \left(\frac{R\Delta P}{2\Delta L} - \tau_y\right)^{\frac{n+1}{n}} \cdot \left[\frac{\left(\frac{R\Delta P}{2\Delta L} - \tau_y\right)^2}{1+3n} + \frac{2\tau_y\left(\frac{R\Delta P}{2\Delta L} - \tau_y\right)}{1+2n} + \frac{\tau_y^2}{1+n} \right]$$

A FORTRAN program named PIPEFLOW.FOR was written to compute the exact velocity profiles for flow of an HB fluid, Bingham fluid, power-law fluid, and Newtonian fluid for comparison to the numerical model.

The Q1 file that was used previously in the pipe flow grid refinement study was changed to call the HB subroutine. The pipe radius is 0.1m and the pipe length is 5 m. A uniform entrance velocity of 2.5 m/s is specified at the upstream end of the pipe. Thus, the specified velocity corresponds to a volume flowrate of 0.07854 m^3/s. From the exact solution, the pressure gradient that would produce a flowrate of 0.07854 m^3/s is 39525 Pa/m for fully developed flow. This is the pressure gradient used to compute the exact velocity profile. The pressure at the pipe exit was set to zero. A uniform grid with 9 divisions in the radial direction and 60 divisions in the axial direction was used in the numerical simulation.

Care must be taken to properly correlate the material property values specified in the PHOENICS simulation with those used in the corresponding analytical solution. All three non-Newtonian subroutines, power-law, Bingham, and Herschel-Bulkley, return a value for the kinematic viscosity. This means that the parameters used as input in the Q1 file must be interpreted as kinematic properties. To illustrate this, the four dummy variables DENS, VISC, EXP, and TAUY are used to relate the PHOENICS input with the values used in the exact solution. Note that VISC has different meanings for different fluid models.

	Q1 File	Exact Solution
Newtonian:	RHO1=DENS	ρ = DENS
	ENUL=VISC	μ = DENS*VISC
Power-Law:	ENUL=GRND4	
	ENULA=VISC	k = DENS*VISC
	ENULB=EXPN	n = EXPN
Bingham:	ENUL=GRND5	
	ENULA=VISC	k = DENS*VISC
	ENULB=TAUY	τ_y = DENS*TAUY
Herschel-Bulkley:	ENUL=GRND6	
	ENULA=VISC	k = DENS*VISC
	ENULB=TAUY	τ_y = DENS*TAUY
	ENULC=EXPN	n = EXPN

If the above correlation between the PHOENICS input and the exact solution is not made, the numerical and exact solutions will not agree.

In the axisymmetric pipe flow simulation of a Herschel-Bulkley fluid, the following fluid properties were specified:

$\rho = 1200\ kg/m^3$
$k = 12\ N \cdot s^n/m^2$
$n = 0.8$

$$\tau_y = 1200 \text{ Pa}$$

The appropriate variables in the Q1 file are:

DENS=1200.
VISC=0.01
EXPN=0.8
TAUY=1.0

Following is the Q1 file used to simulate the flow described above of a HB fluid in a pipe:

```
TALK=T;RUN( 1, 1);VDU=VGAMOUSE
TEXT(non-Newtonian Pipe Flow
REAL(LENGTH,RAD,WIN,REYNO,VISC,DENS,EXPN,TAUY,flsfact,falsev,fals
ew)

RAD=0.10 ; LENGTH=5.0
NY=9  ;  NZ=60

DENS=1000.0  ;  VISC=0.01
TAUY=1.0  ;  EXPN=0.80
WIN=2.5

    GROUP 2-5. Grid specification
STEADY = T
CARTES = F
GRDPWR(y,NY,RAD,1.0)
GRDPWR(Z,NZ,LENGTH,1.0)

    GROUP 7. Variables stored, solved & named
SOLVE(P1,V1,W1) ; SOLUTN(P1,Y,Y,Y,N,N,N)
STORE(ENUL,BTAU,GENK,lgen1)
genk=t

    GROUP 9. Properties of the medium (or media)
RHO1=DENS
ENUL=grnd6
enula=visc ; enulb=tauy  ;  enulc=expn

     Group 11. Initial Values
         INIADD=F
 fiinit(w1)=win ; fiinit(v1)=0.0

     GROUP 13. Boundary conditions and special sources
     Inlet
 INLET(IN,LOW,1,1,1,NY,1,1,1,1)
 VALUE(IN,P1,WIN*RHO1)
 VALUE(IN,W1,WIN)
     Outlet
 PATCH(OUTLET,HIGH,1,1,1,NY,NZ,NZ,1,1)
 COVAL(OUTLET,P1,1000,0.0)
```

```
    North wall
WALL(PSIDE,NORTH,1,1,NY,NY,1,NZ,1,1)

    GROUP 15. Termination of sweeps
LSWEEP=5000
RESREF(P1)=1.E-4;RESREF(V1)=1.E-4;RESREF(W1)=1.E-4

    GROUP 17. Under-relaxation devices
varmax(v1)=0.00
RELAX(P1,LINRLX,0.6)
flsfact = (length/nz)/(1.5*win)  ;  flsfact
falsev = 0.01*flsfact  ; falsev
falsew = 0.1*flsfact  ; falsew
          RELAX(V1,FALSDT,falsev) ; RELAX(W1,FALSDT,falsew)

    GROUP 22. Spot-value print-out
IYMON=ny/2 ;IZMON=3*nz/4
TSTSWP=-1

    GROUP 23. Field print-out and plot control
NXPRIN=1 ; NYPRIN=ny/5 ; NZPRIN=nz/10
OUTPUT(P1,N,N,N,N,Y,N)
OUTPUT(V1,N,N,N,N,Y,N)
OUTPUT(W1,N,N,N,N,Y,N)
OUTPUT(ENUL,N,N,N,N,N,N)
OUTPUT(GENK,N,N,N,N,N,N)
OUTPUT(BTAU,N,N,N,N,N,N)
OUTPUT(lgen1,N,N,N,N,N,N)
patch(tbop1,contur,1,1,ny/2,(ny/2)+1,1,nz,1,1)

plot(tbop1,p1,0.0,10)
patch(tboend,contur,1,1,1,ny,nz-6,nz-2,1,1)
plot(tboend,w1,0.0,10)
plot(tboend,genk,0.0,10)
plot(tboend,enul,0.0,10)
ECHO=F
STOP
```

Figure 27a shows that the velocity profile calculated with the Herschel-Bulkley subroutine agreed very well with the exact solution. The RMS error between the exact and numerical velocity profile was 1.601%. The numerical velocity profile was integrated using Simpson's rule to obtain a flowrate of 0.07898 m^3/s. The relative error between the exact and numerical flow rate is 0.555%. Although the velocity profile agrees very well with the exact solution, the relative error between the exact and numerical pressure gradient is large. The pressure gradient predicted by PHOENICS was 45857 Pa/m , but the exact pressure gradient is 39525 Pa/m. The relative error between the PHOENICS and exact pressure gradient is 13.8% for the 9x60 grid solution. The large discrepancy has been attributed to insufficient grid resolution. To verify this, solutions were also obtained with a 6x40 grid and a 3x20 grid. Figure 27b shows the relative error decreasing as the as the

number of grid point increases. The 9x60 grid is sufficient to demonstrate that the Herschel-Bulkley subroutine is functioning properly, but an even more accurate solution would be obtained with a more refined grid.

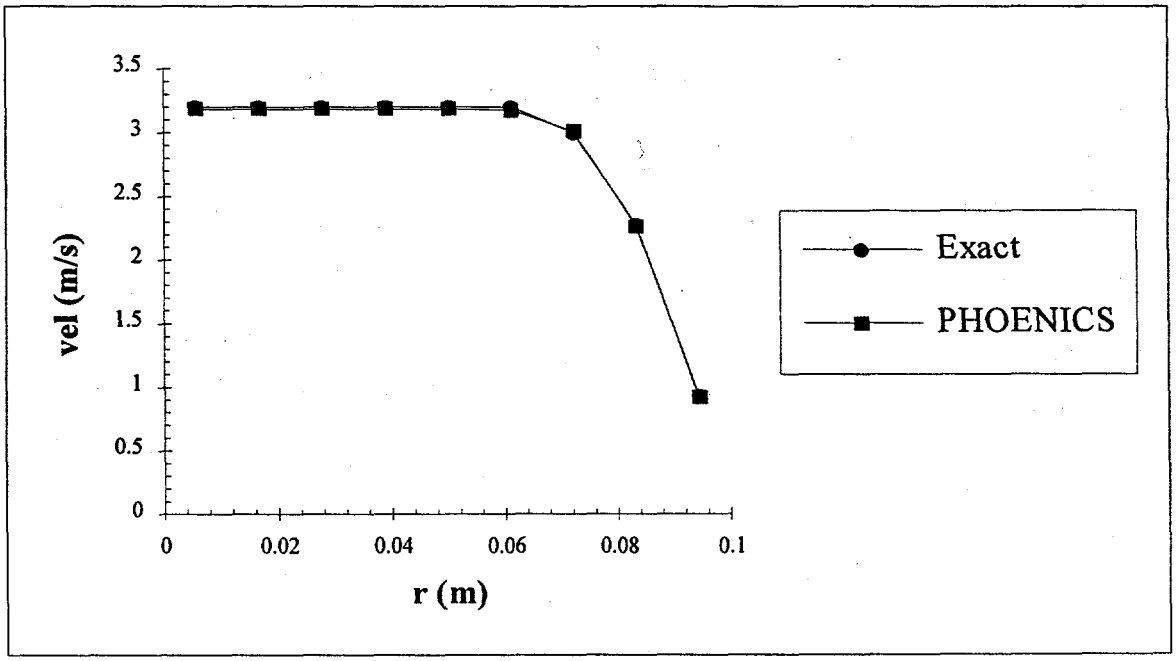

Figure 27a Numerical and Exact Solution of Herschel-Bulkley Velocity Profile

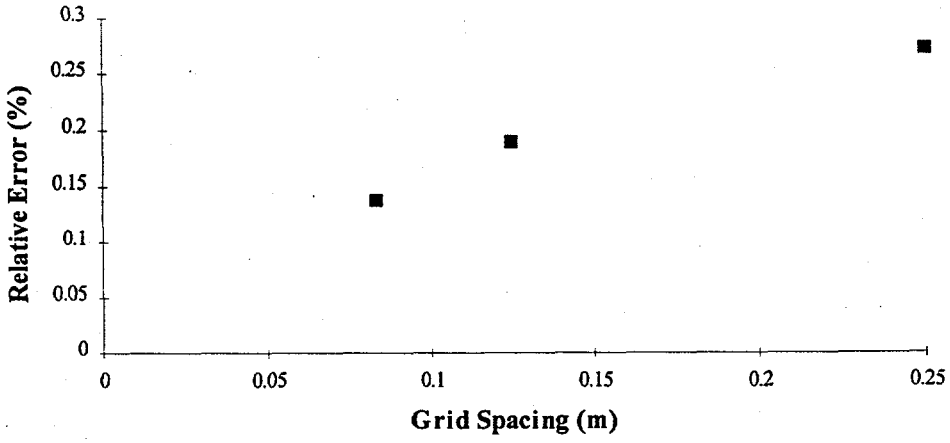

Figure 27b Relative Error in Calculated Pressure Gradient vs. Grid Spacing

Results

UNSTABLE GROUT

It has become apparent from rheological testing, that the FBC-ash grouts under investigation are unstable unless suitable additives are used. The concentration of solid particles varies with time and space because of gravity settling, implying that the grout becomes inhomogeneous. As the concentration of particles increases at the bottom of the grout mixture, contact develops between the solid particles. This permits Coulomb friction to act as an additional resistance to flow of the grout which must be included in the rheological constitutive law that is used to define the grout mixture. The Herschel-Bulkley model for two dimensional parallel shear flow with the effect of Coulomb friction included is:

$$\tau = \tau_y + k(\gamma)^n + P\mu_f$$

When there is no flow (i.e. γ=0) the residual shear stress may be as large as:

$$\tau = \tau_y + P\mu_f$$

The following analysis uses this as a starting point for determining the maximum distance that an unstable grout may be pumped.

RELEVANCE TO PROJECT

The project goal is to fill an underground mine with FBC-ash grout using as few drilled holes as possible, because drilling the injection holes is the costliest part of the project. As a consequence, the distance underground that the grout may be made to flow is of direct importance to the project outcome. It is anticipated that as grout is injected into the mine through the mine roof, the grout will form a conical pile that will eventually reach the mine roof. The pumping pressure will then expand the pile in a radial direction until the maximum spreading distance is reached as shown in Figure 28. The maximum flow distance of unstable grouts may be so limited that the project is rendered impractical due to the large number of injection wells needed will be cost prohibitive.

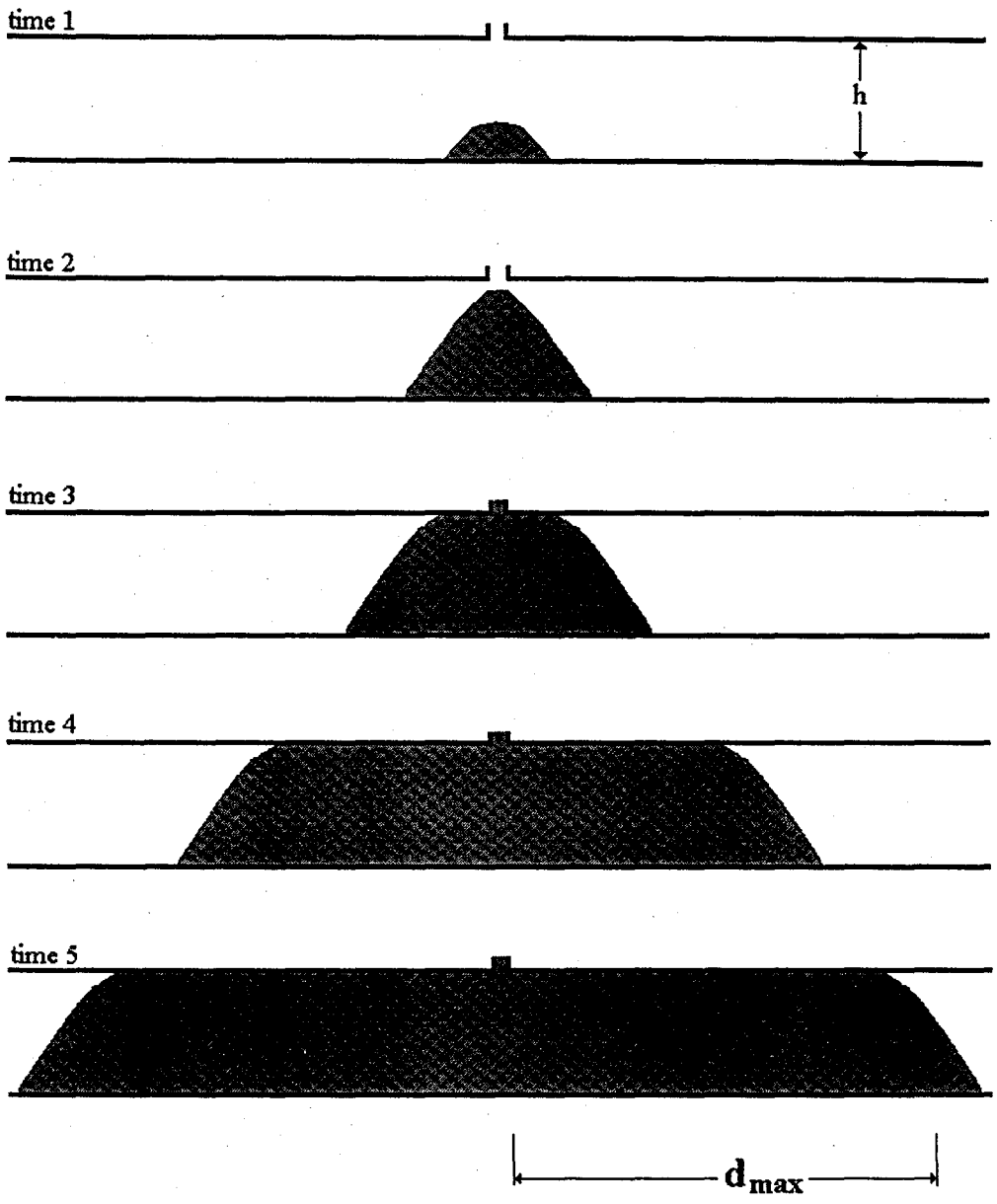

Figure 28 How Grout May Fill Mine Passage

PUMPING DISTANCE

A look at how stable and unstable grouts behave in an idealized channel provides a preliminary evaluation of the flow of the FBC-ash grouts in underground mine voids. The underground cavities are idealized as a two dimensional and an axisymmetric cavity of finite

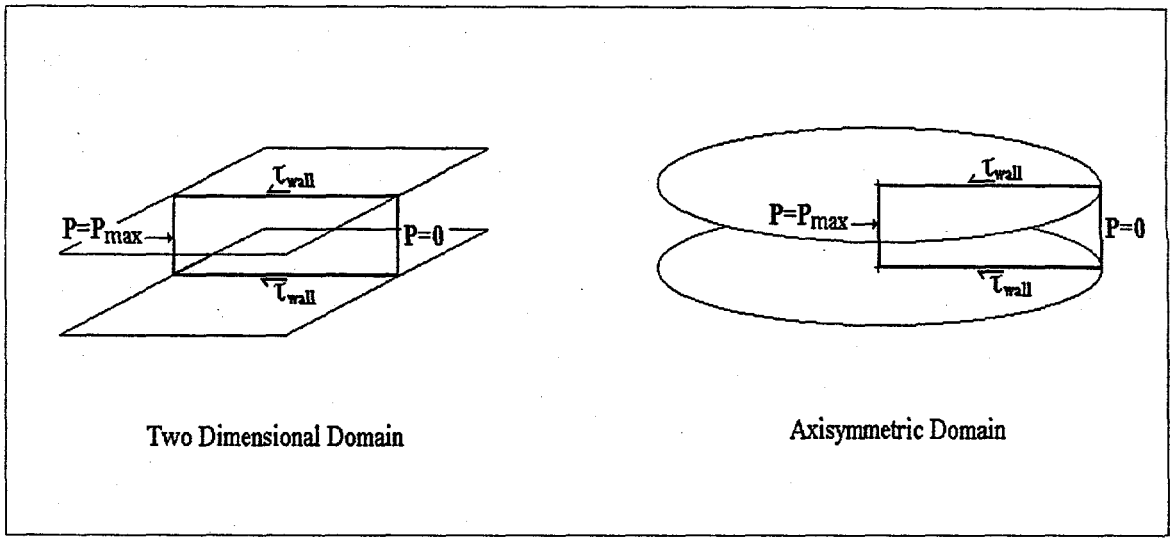

Figure 29 Simplified Geometry Used in Deriving Maximum Flow Distance

thickness as shown in Figure 29. The floor and ceiling are considered but not the walls.

As discussed earlier, any yield stress fluid, stable or unstable, that is injected into a pipe or closed channel with a finite initial pressure head, will eventually stop moving. Inevitably there will be a location downstream where the stress in the grout will fall below the yield stress at all points across the cross section, a solid plug will completely fill the pipe or channel, and flow will cease. For an unstable grout, Coulomb friction will further limit the extent of flow. The hardening of the grout has been neglected because the time required for hardening is much greater than the time scale of the flow.

Lombardi compared the distances that stable and unstable grout can be made to flow in idealized bounded channels, but axisymmetric and two dimensional results were incorrectly combined. Lombardi's results have been corrected here to find the equations that describe the pressure gradient along a channel and the maximum flow distance. The equations have been derived from a balance of forces for a fluid that has stopped moving. When flow has stopped, the wall shear will be balanced by the internal stress in the grout. The internal shear stress in the grout is found from the constitutive relation given previously. All of the derived equations are presented below. It can be seen that the pressure gradient along the channel for both the two dimensional and axisymmetric cases is a function of initial pump pressure, channel thickness, and yield stress. For unstable grouts, the pressure gradient depends also on μ_f, the coeficient of friction.

The equations for pressure as a function of downstream distance and for the maximum flow distance are given below for stable (no Coulomb friction) and unstable (with Coulomb friction) grout in a two dimensional geometry and in an axisymmetric geometry.

The following variables appear in the maximum flow distance equations:

P_o = inlet pressure
r_o = inlet pipe diameter
h = ½ channel thickness
d = maximum flow distance
$\mu_f = \tan(\phi)$
τ_y = yield stress
$a = \mu_f / h$
$b = -\tau_y / h$

1. Stable Grout, yield stress only:

2D Case

$$P = P_o - \frac{\tau_y}{h}(r - r_o)$$

$$d = \frac{P_o\, h}{\tau_y}$$

Axisymmetric Case

$$P = \frac{r_o}{r} P_o - \frac{\tau_y}{2h}\left(r - \frac{r_o^2}{r}\right)$$

$$d = \sqrt{r_o^2 + \frac{2h\, r_o\, P_o}{\tau_y}}$$

2. Unstable Grout, yield stress and Coulomb friction:

2D Case

$$P = -\frac{\tau_y}{\mu_f} + \frac{1}{\mu_f}(\tau_y + \mu_f P_o)\, \exp\left[\, \mu_f \frac{(r_o - r)}{h} \,\right]$$

$$d = \frac{h}{\mu_f} \ln\left[\, \frac{\tau_y + \mu_f P}{\tau_y + \mu_f P_o} \,\right]$$

Axisymmetric Case

$$P = \frac{b}{a}\left(1-\frac{1}{ar}\right) - \frac{b}{a}\frac{r_o}{r}\left(1-\frac{1}{ar_o}\right)\exp[\,a(r_o-r)\,] + P_o\frac{r_o}{r}\exp[\,a(2r_o-r)\,]$$

A closed form solution for the maximum flow distance was not found for the unstable grout in axisymmetric coordinates. However, the maximum distance may be found by plotting the pressure, P, vs. the distance, r. The maximum flow distance corresponds to the value of r for which the pressure is zero.

PARAMETRIC STUDY

A parametric study was performed with the equations listed above to determine how variations in the channel height, 2h, the pumping pressure, P_0, the yield stress, τ_y, and the friction coefficient, μ_f, affect the maximum pumping distance. Each of the parameters was varied over a wide range and the corresponding flow distance computed with the following constants: $P_0 = 1$ MPa, h = 0.75 m, $\tau_y = 50$ Pa, and $\mu_f = 0.20$. The results are shown in Figures 30-39. It was found that the maximum pumping distance was least sensitive in changes to pumping pressure, and most sensitive to changes in the yield stress and friction coefficient. As can be seen from all the figures, the maximum pumping distance of an unstable grout is always less than that of stable grouts, usually substantially so.

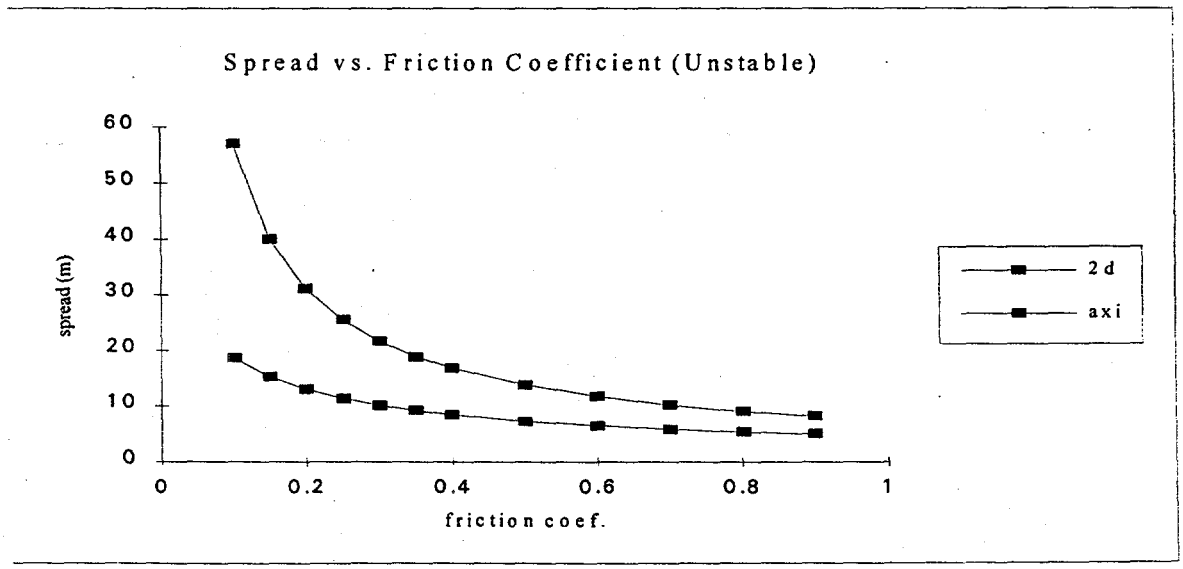

Figure 30

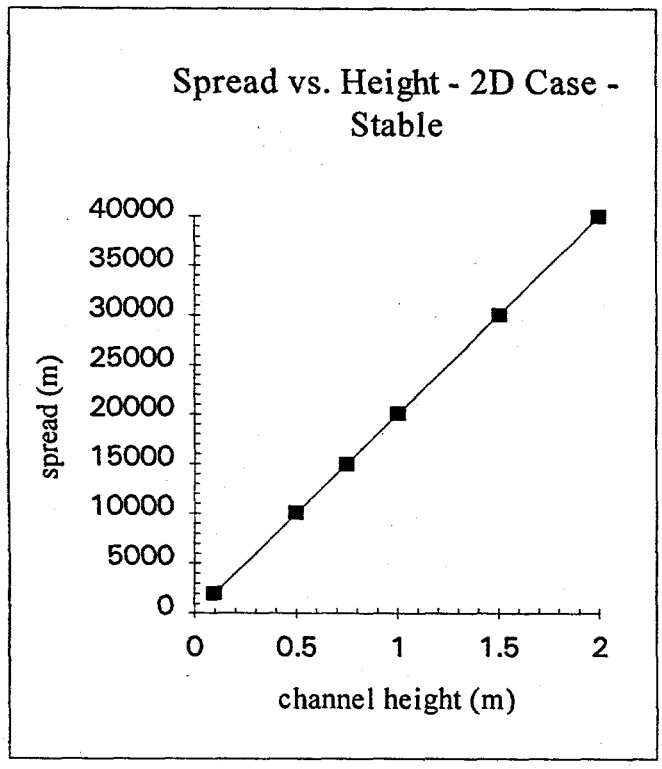

Figure 31

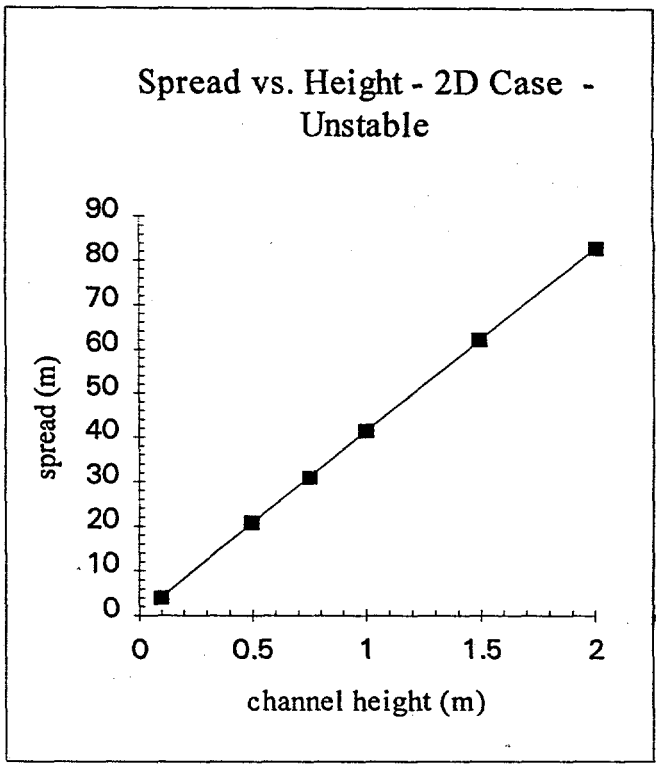

Figure 32

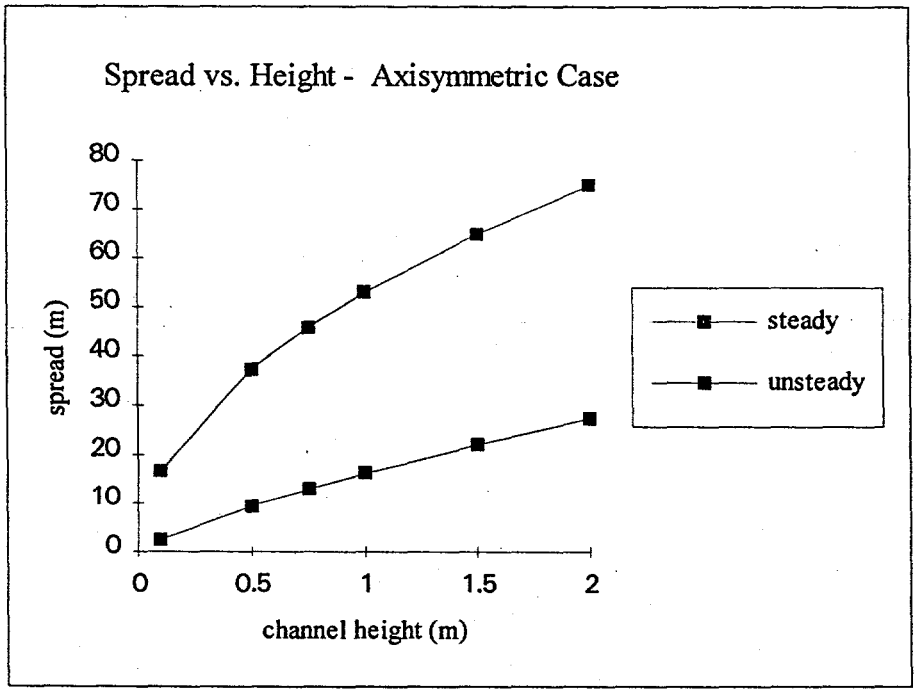

Figure 33

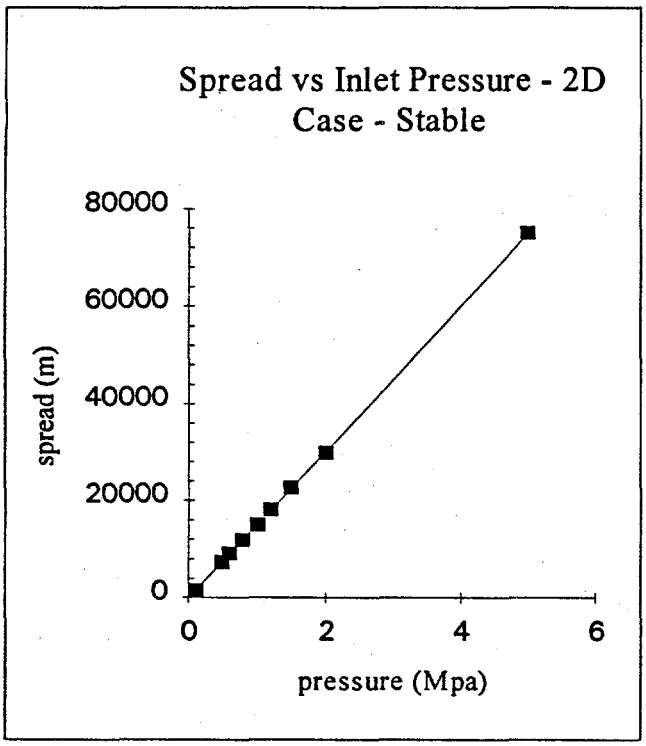

Figure 34

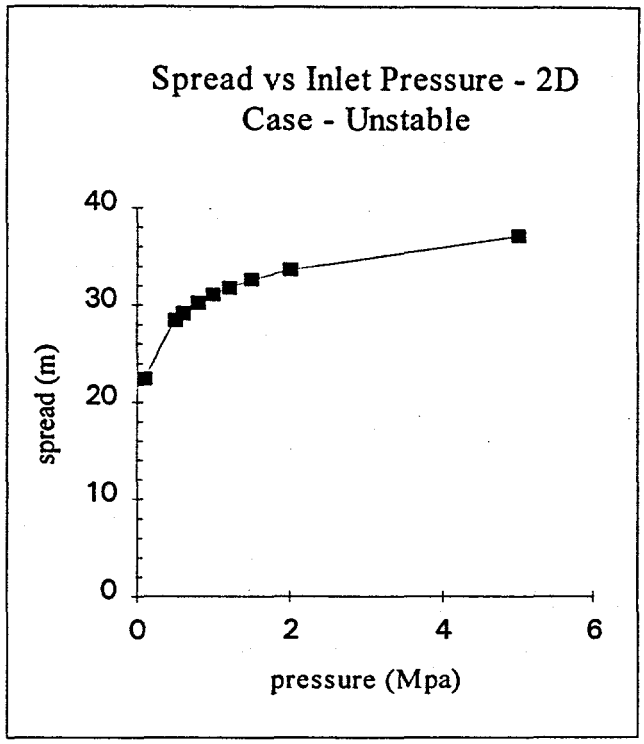

Figure 35

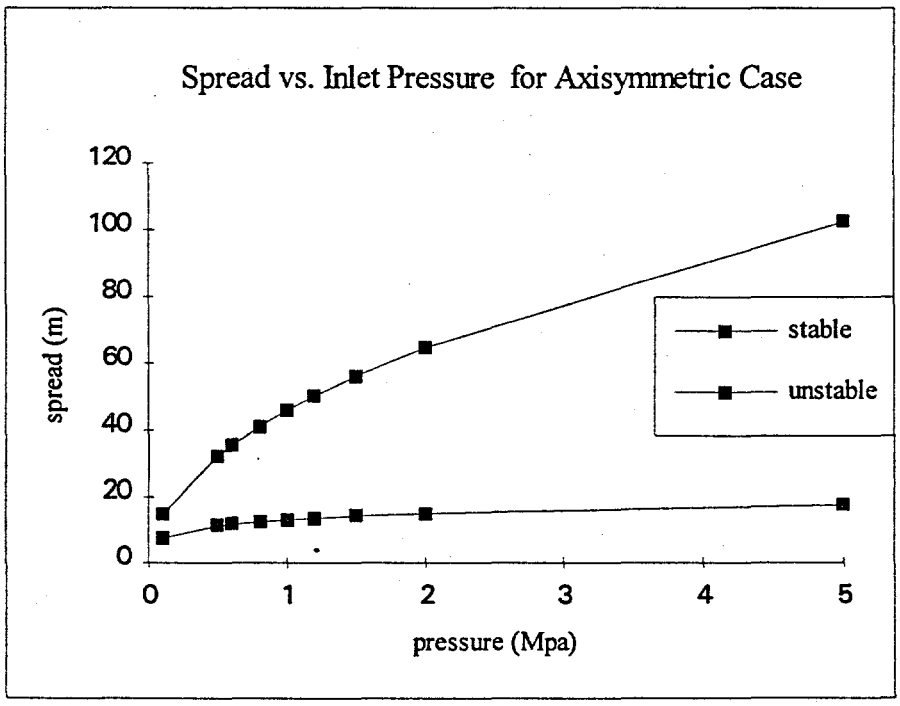

Figure 36

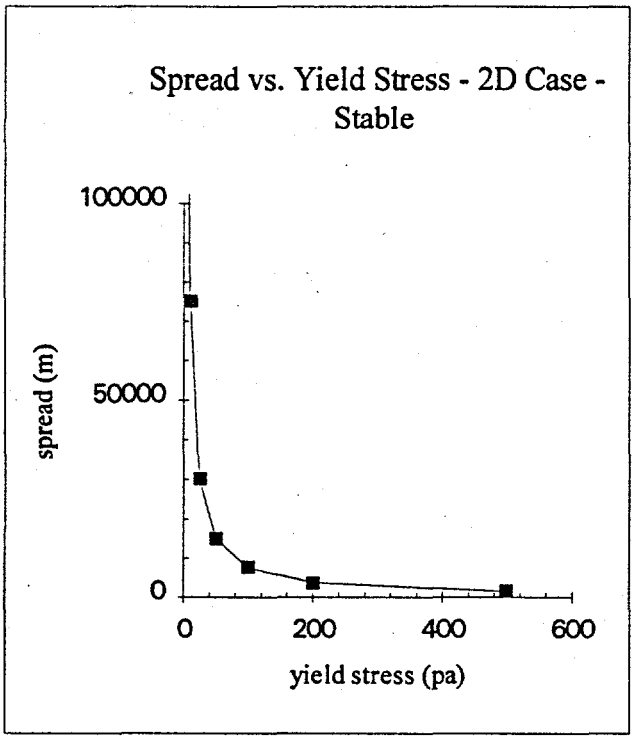

Figure 37

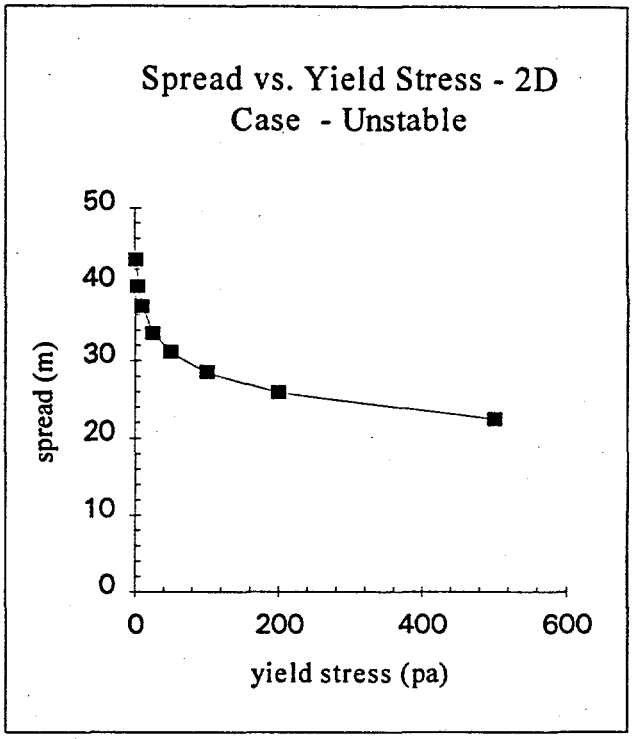

Figure 38

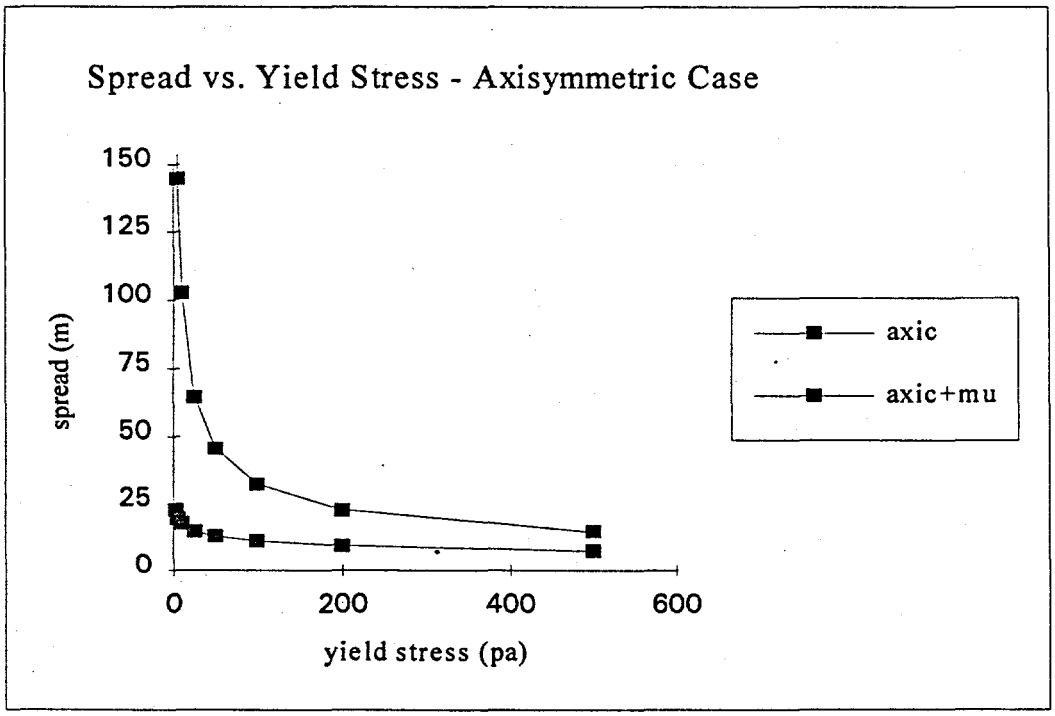

Figure 39

ILLUSTRATIVE EXAMPLE

Grout is to be injected at the intersection of two mine corridors. The geometry of the mine corridors and coal pillars is idealized as shown in Figure 40. It is desired that the grout injected at the center of the intersection shall fill the mine corridors at least half the distance to the next intersection so that injection wells can be drilled only at the corridor intersections. The flow of the stable and unstable grout in the vicinity of the intersection is described by the axisymmetric flow equations given previously.

The following example uses the same data for calculating the stable and unstable flow distances:

$P_o = 0.5$ MPa
$r_o = 0.076$ m
$2h = 1.524$ m
$\tau_y = 100$ Pa
$\mu_f = 0.5$

Maximum Flow Distance:

Stable Grout:	$r_{max} = 22.3$ m
Unstable Grout:	$r_{max} = 2.89$ m

Thus the stable grout could be made to fill the desired volume, but the unstable grout would not even flow out of the intersection area. This example does not take into account the slope of the mine floor, debris and obstructions in the mine, and segregation of the water and solids due to impact of the grout on the mine bottom. In addition, the actual pumping pressure available at the injection site may be significantly greater than assumed here, and the material property values are uncertain.

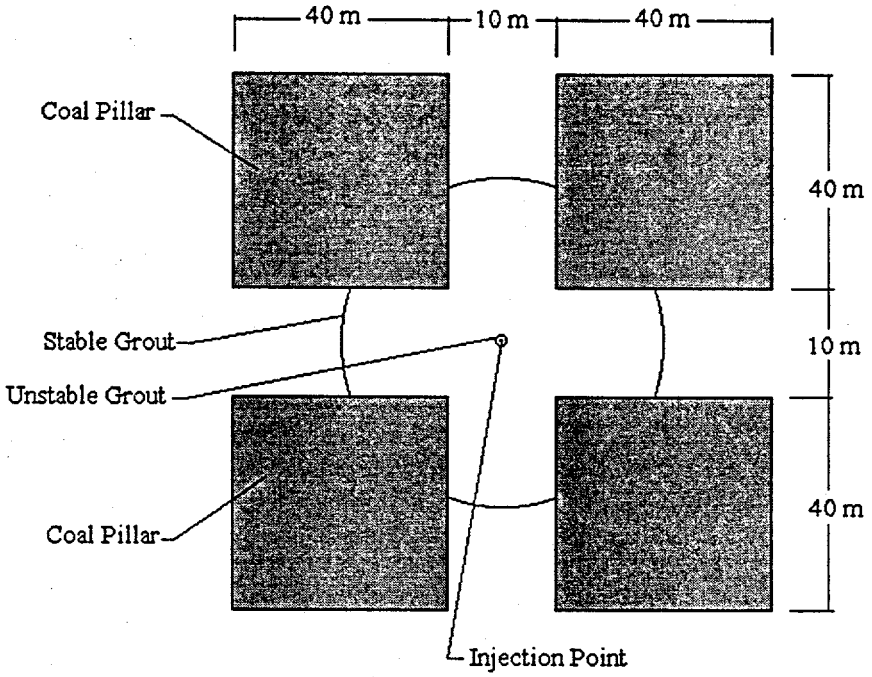

Figure 40 Idealized Mine Intersection (Plan View)

IMPACT ON SIMULATIONS

It was intended that knowledge of the grout rheology could be incorporated into a computer model in order to obtain a numerical simulation of the injection process. PHOENICS can simulate the behavior of several non-Newtonian fluid models. However, these fluid models treat the grout as a one phase homogeneous fluid. The FBC-ash grouts that are unstable cannot be modeled as a single phase due to the inhomogeneities that arise from settling. In order to accurately simulate flows of such unstable suspensions, the fluid model and the computer simulation must take into account the interaction between the suspended phase and the liquid phase within the grout. To be accurate, this would entail simulating the movement of each solid particle within the grout mixture. Such a complex task is outside the capabilities of the PHOENICS software and is beyond the scope of this project. PHOENICS can only be used to simulate the flow of stable FBC-ash grouts.

STABILIZATION

It is clear that unstable grout mixtures are not desirable for practical application and are beyond the scope of the numerical model. Therefore, a method must be found to stabilize the grout mixtures. The addition of bentonite to the grout mixtures has been shown to stabilize the grout (Putnam, 1995). Preliminary rheological testing of the stabilized grout indicates that the power-law fluid model may represent the stabilized grout's flow behavior as well as the Herschel-Bulkley fluid model. The simulation results that will be presented make use of both the power-law fluid model and the Herschel-Bulkley fluid model to simulate flow of the stabilized grout.

ATTEMPT TO DETERMINE GROUT PROPERTIES WITH PHOENICS

The grout mixtures used in preliminary testing were all prepared with the same recipe. The initial grout samples were mixed with water fractions ranging from 31 to 37 percent. The water fraction is defined as the ratio of the weight of water to the total weight of the grout mixture. The solid material contained equal parts by weight of fly ash and bottom ash. The size of the fly ash particles ranged in size from 5 to 50 μm. The maximum particle size in the bottom ash is approximately 1 cm. No additives were used when preparing the initial grout mixtures.

The desire to simulate the flows of the FBC ash grouts has been frustrated by difficulties in fully characterizing the grout rheology. Several attempts were made to quantify rheological constants such as yield stress, consistency index, and flow behavior index, by performing well known viscometric flow experiments. Before additives were used, the ash solids would settle very quickly and the subsequent inhomogeneous mixture was not amenable to traditional rheological testing. In addition, the equipment used to perform the viscometric experiments, the cone and plate, parallel plate, and squeeze plate rheometers, are too small to permit large particles in the grout. While the grout to be used in the field

will contain large particles from the bottom ash, rheological testing can only be performed with grouts devoid of large particles. Therefore, it was suggested that the material properties could be obtained by reversing the traditional procedure of *first* defining the constitutive relation, quantifying the rheological constants with viscometric flows, and *then* using the constants as input in a numerical model for more complex flows. The proposed method was to match numerical simulations to experimental results. PHOENICS would be used to simulate an actual flow experiment. The fluid properties used as input in PHOENICS would be updated until the PHOENICS output closely matched the actual flow. The use of PHOENICS to determine the flow properties of the grout would generate confidence that PHOENICS simulations can accurately represent the grout behavior. Unfortunately this method was not successful.

A bench scale flow model of the "dam break" flow (Figure 25) was constructed of plexiglass and is described by *Putnam*, (1996). The bench scale model was 0.2 m in width, 0.3 m in height, and 1.0 m in length. Grout flow in the bench scale model was recorded with a video camera such that the flow as a function of time was clearly captured. The PHOENICS software was then used to simulate flow with the same geometry. Two and three dimensional models were used in conjunction with the Herschel-Bulkley subroutine. Attempts to match the experimental data were not successful. However, the inability to match the experimental data provided illuminating insight into some grout characteristics that were previously unrecognized.

First, the flow behavior (and thus also the grout properties) were different each time a grout sample was mixed. The grout samples were all prepared by combining equal parts by weight of fly ash, bottom ash, and water. The same grout recipe was used for all grout samples and the same procedure was used to prepare each grout sample. The physical flow test was performed many times, but flow time, flow distance, and shape of the free surface varied greatly. The variability has been attributed to variations in the solid material (ash) used to prepare the grout. Although all the ash material used in this project originated in the same power plant, the power plant does not discharge a uniform waste product. The power plant continually varies the amount of lime, coal, and gob in the combustion reactor to maximize efficiency and minimize pollution. In addition, larger bottom ash is extracted from the reactor and stored at a different rate than the finer fly ash. The trucks that are used to haul the waste material away are loaded with varying amounts of fly ash and bottom ash. Thus, within a given sample of ash, solid properties and size distribution may vary greatly. The bench scale flow test has demonstrated the sensitivity of flow to the variations in solid particle properties.

Second, it was discovered that several combinations of fluid properties produced the same or nearly the same results. In other words, a specific flow behavior could be independent of some of the fluid model constants. The time required to impact the far tank wall was the flow property that was used to initially evaluate simulation results. Comparisons were also made of velocity at impact and free surface shape. The Herschel-

Bulkley model was used when trying to match the experimental results. This model has three flow parameters, the yield stress, τ_y, the consistency, k, and the flow behavior index, n. It was found that within the range of properties used in the parametric study, $\tau_y = 1 \rightarrow 50$ Pa, $k = 0.1 \rightarrow 500$ $(N \cdot s/m^2)^n$, and $n = 0.5 \rightarrow 1.0$, the flow was most influenced by the k value. Varying k resulted in large changes in time required to impact the opposite wall and velocity at impact, but a small changes in free surface shape. The τ_y value did somewhat influence the shape of the interface, but its effect on the flow time was negligible, perhaps due to the small range of values over which it varied. An estimate of the yield stress was provided by measurements of the residual slope of the grout-air interface after flow had stopped. Thus, the actual grout yield stress is thought to lie within the range of values used in the numerical simulations. Variation of the n value had negligible effect on all the flow parameters evaluated. Very low n values generated only a slight increase in impact velocity. However, slight n variations do have a large impact on flow behavior in other geometries, such as the pipe flow geometry. As a consequence, there must be something about the flow in this geometry that negates the influence of n. The n value is responsible for the deviation from a linear stress vs. rate of strain curve. It is the exponent of the rate of strain magnitude. If the magnitude of the rate of strain did not vary greatly across a large portion of the domain, the effect of n would be small. Since most of the shearing occurred in a small region near the tank floor, it is conceivable that the effect of n could be limited to this small region. This is consistent with the slight increase in impact velocity because shear thinning would occur in this small region. The conclusion is that, whatever the mechanism, the flow in the dam break model is not suitable for reliably evaluating fluid constants.

Finally, observations of the actual grout flow indicated that there may be very large wall slip behavior. As soon as the grout material was placed behind the retaining wall (the dam) bleeding began. Bleeding is the separation of water from the grout. Bleeding is identified by the appearance of a layer of water on the surface of the grout mixture. The bleed water drained down the sides of the plexiglass containment walls, and out from underneath the retaining dam. Stabilized grout was not used in any of the physical model tests.

When flow was initiated by removal of the dam, the bleed water acted as a lubricant, and the grout would slide along this lubrication layer largely undeformed. The slip behavior was enhanced by the smooth plexiglass used to construct the dam break model. The amount of bleeding was sensitive to the properties of the solid ash used in the mix, as indicated by the different amounts of bleeding that occurred between several grout batches, all prepared according to the same recipe. Thus if the amount of bleed water released was not constant, the amount of wall slip was not constant. In the extreme case, a quantity of nearly clear water would quickly flow to the opposite wall, while the remainder of the grout would slump part way across the tank and remain stationary. The apparent wall slip had the effect of preventing the numerical model from matching the experimental data because a lubricating layer was not included in the simulations. Flow time across the tank was decreased because of the slip layer. The majority of the motion and deformation of the grout occurred very

quickly. After the initial slumping of the grout column, the motion continually decelerated until impacting the far wall. The actual impact velocity of the grout was less than the flow distance divided by the flow time. When fluid properties were specified in the numerical model to match the observed flow time, the simulated impact velocity was too large. When properties were specified to match the impact velocity, the flow time was too long. The slip layer also reduced the amount of deformation that occurred in the bulk of the grout. As a consequence, no combination of parameters were found that could match the observed free surface. The slip layer was below the spatial resolution of the numerical model. A non-uniform grid was employed in the vertical direction, with the cell size expanding in the positive z axis. The smallest vertical cell dimension was adjacent to the lower domain boundary with a thickness of 1.2 cm. The slip layer on the lower domain boundary is estimated to be on the order of 1 mm. Thus, in order to resolve the behavior of the lubrication layer, several rows of cells would be needed adjacent to the lower domain boundary with a thickness on the order of 0.01 mm. The physics at this scale could no longer be modeled as a one phase continuum, and the numerical model could not be expected to yield realistic results. Thus, PHOENICS was not able to accurately simulate this flow, partly because one of the physical mechanisms, wall slip due to grout instability, is not included in the numerical model.

MINE INJECTION SIMULATION

Predictions about how FBC-ash grout flows during injection into an underground mine must be based upon knowledge of the grout properties and the dimensions and geometry of the mine. Due to the sensitivity of grout rheology to solid ash properties, and the settling of the grout suspension as described above, a conclusive fluid model has not yet been obtained. It is believed that either the power-law or Herschel-Bulkley fluid model can be used to describe the grout rheology. While the grout properties are anticipated to lie within the range of:

$$\tau_y = 0 \rightarrow 50 \text{ Pa}$$
$$k = 0.1 \rightarrow 1000 \text{ (N·s/m}^2\text{)}^n$$
$$n = 0.25 \rightarrow 1.0$$

the actual fluid model constants are as yet unknown. Conversely, the geometry of an underground room and pillar mine is known from mine maps, but is of such irregularity that simplifications and idealizations are needed to facilitate the modeling process. As can be seen from the map of the Fairfax mine in Figure 41, large pillars of unexcavated coal form a nearly regular array. The pillars range in size from 16 m to 50 m per side. It is the series of interconnecting hallways and passageways that are required to be filled. The coal seam in the Fairfax mine averages 1.5 m in thickness, and the mine passageways are assumed to be the same thickness. The mine floor has a slope of approximately 4% that is oblique to most of the passageways. The floor slope has been neglected. The idealized mine passageway intersection shown in Figure 40 is regarded as typical of the mine geometry.

It is anticipated that the points of injection will coincide with the underground mine

corridor intersections. The passageway intersections are from 15 m to 70 m apart. It is assumed that one injection hole per intersection is the maximum drilling density that would be considered. Of course the goal is to minimize the number of holes that need to be drilled, but for the purposes of developing a numerical model, a minimum estimate of flow distance is needed. If the grout rheology is such that it could be made to flow further than the distance to one intersection, it may be possible to plan drilling injection holes at every other intersection, every third intersection, and so on. Figure 42 demonstrates the minimum distances that grout must be made to flow for various injection strategies. These conceptual injection schemes are based upon a mine with uniform geometry, square pillars, and negligible slope. Many factors not included in the conceptual model or the numerical model may impede or enhance grout placement. Such factors are the variability of the actual mine geometry, floor slope, obstructions from partial collapse of mine pillars or roof, and possible pooling of groundwater within the mine. Even with these simplifications, useful knowledge can be obtained by considering injection into the idealized geometry.

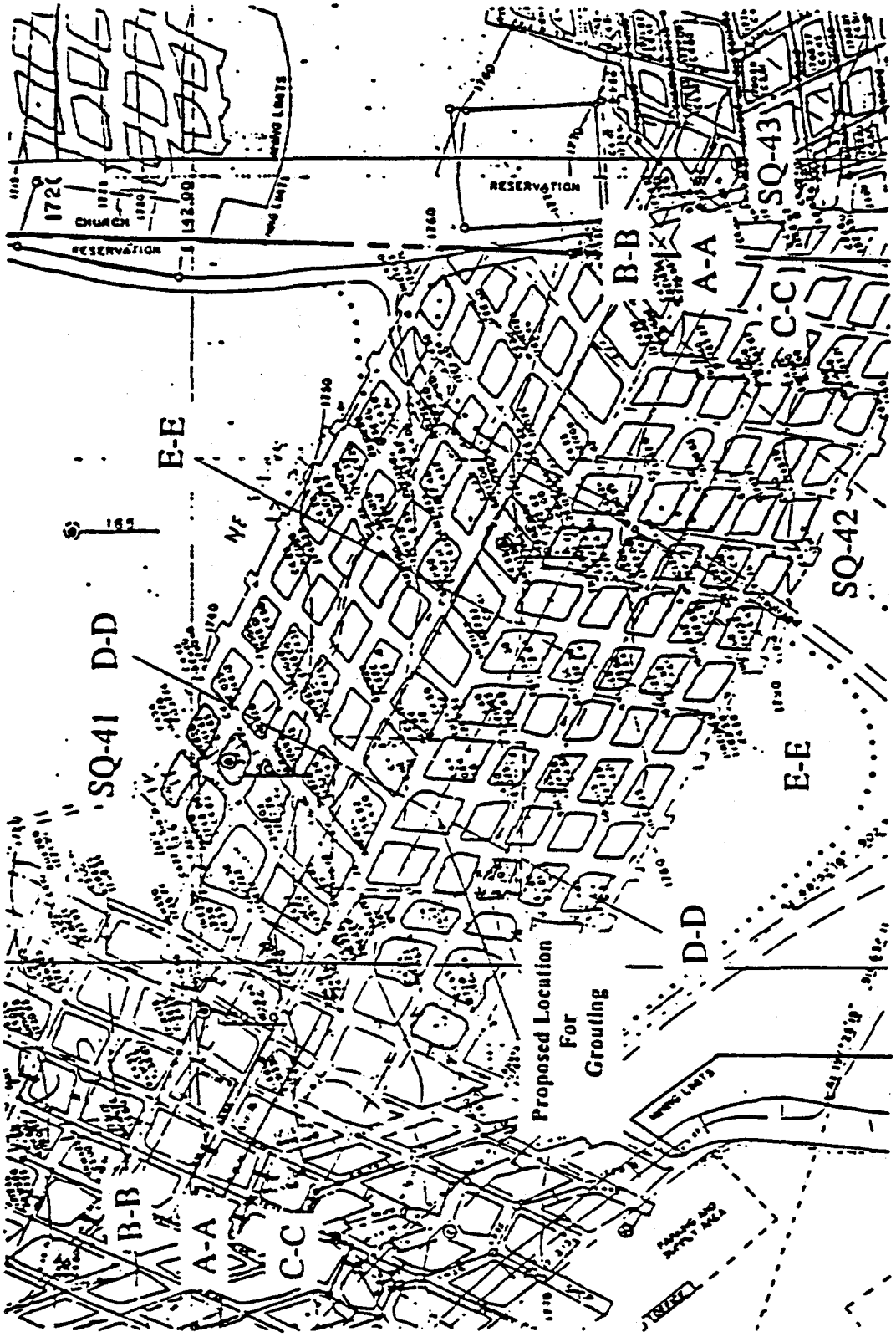

FIGURE 41 Map of the Fairfax Mine

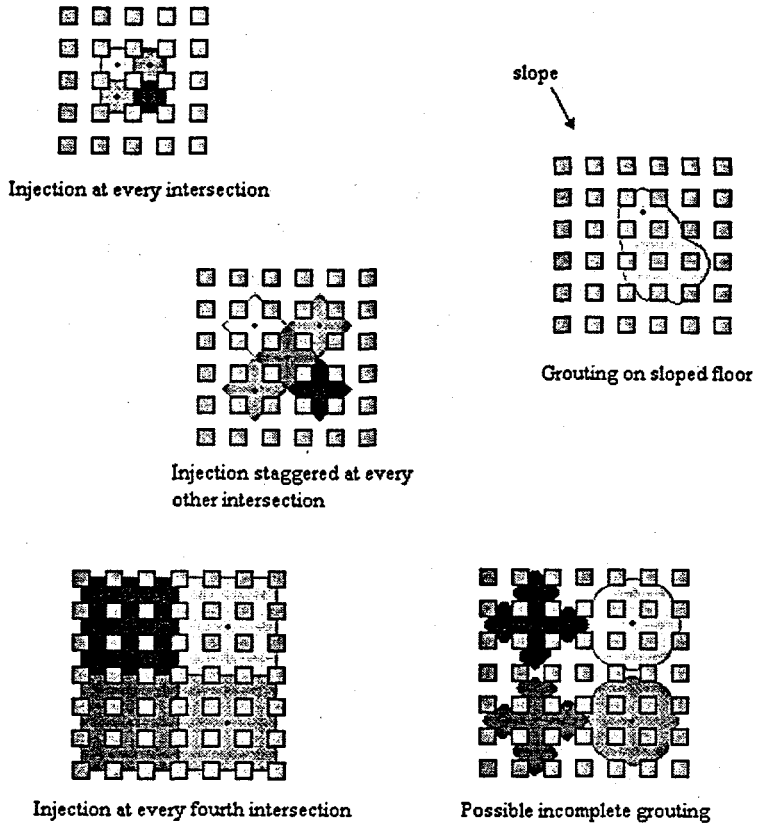

Figure 42 Grout Injection Schemes

AXISYMMETRIC SIMULATION

Axisymmetric simulations have been used to investigate how grout may be expected to pile up on the mine floor and spread outward. The axisymmetric cavity in Figure 43 represents one of the passageway intersections that extends outward from the injection point. Because the simulation is axisymmetric, there is no influence of the vertical mine walls. This should be a good approximation for flow within the intersection area where the grout that impacts on the floor should spread axisymmetrically. The influence of the walls is not important until the grout extends more than 5 m from the injection point.

The power-law model was used because the power-law model appears to fit stress-strain rate data from preliminary rheological tests of grout mixtures that have been stabilized with bentonite. Since the exact values of the power-law parameters are still unknown, several simulations have been performed with various combinations of power-law parameters. A simulation was also performed with the Herschel-Bulkley fluid model to compare to the power-law model results.

The mass flux boundary condition in the upper left corner of the domain represents grout injection at a rate of 0.2 m^3/s. Three simulations were performed with an open outlet, P = 0, along the right boundary. The outlet boundary condition on the right side of the domain was then changed to a no flow, wall boundary condition 5 m from the injection point. This wall boundary condition is used to simulate injection into one of the mine

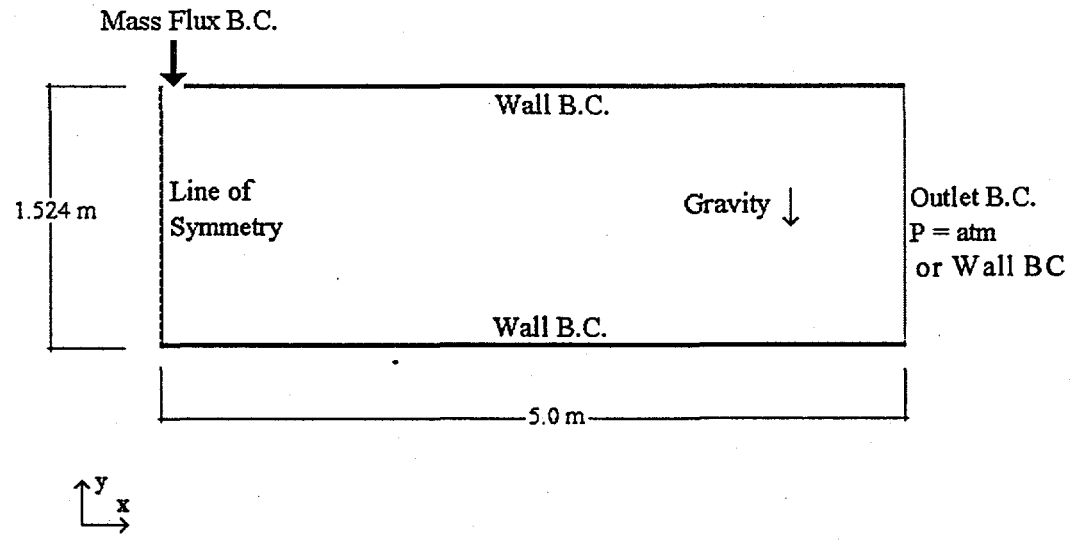

Figure 43 Axisymmetric Simulation Domain

passages between intersections. None of the simulations include resistance from walls that are parallel to the flow. A no-slip condition was specified on the floor and roof for all of the simulations. As mentioned before, the unstabilized grout exhibits apparent slip at the wall which implies that the no-slip boundary condition is not realistic. However, the wall resistance for a real grout flow must lie between the no-slip and no-friction conditions. Thus, simulation results obtained with a no-slip boundary condition and a frictionless wall boundary condition should bracket the real grout flow. The results of one simulation without friction on the floor and roof are included for comparison.

All the following simulations used a uniform grid with 50 cells was used in the radial y-direction, and a non-uniform grid in the vertical with 20 cells expanding exponentially in the positive z-direction. With a time step of 0.005 seconds and 50 iterations per time step, each simulation required more than 7 hours to simulate 10 seconds of injection. The results at six time steps are presented for the seven cases listed in Table 1.

Figure No.	B.C. @ Right	Fluid Model	n	k ($N \cdot s^n/m^2$)	τ_y (Pa)
44	Outlet	Power-Law	0.8	100.0	-
45	Outlet	Power-Law	0.8	1000.0	-
46	Outlet	Power-Law	0.3	25.0	-
47	Outlet	HB	0.3	25.0	25.0
48	Outlet	HB (no fric.)	0.3	25.0	25.0
49	Wall	Power-Law	0.8	1000.0	-
50	Wall	Power-Law	0.3	100.0	-

Table 1

The figures all show the grout-air surface as a solid line. The space beneath the solid line represents the grout. The area above the solid line contains only air. PHOENICS treats the entire simulation as a one phase fluid with spatially varying properties delineated by the solid line. The vector arrows shown in the figures illustrate the velocity vectors in either the grout or air phase.

It was assumed that the grout flows would be laminar because the grout is so viscous. No turbulence models were used in any of the simulations. Typically, the Reynolds number is calculated to verify that a flow is laminar, but for this flow geometry there is no obvious choice for a length scale or a representative velocity with which to calculate a Reynolds number. Moreover, even if a Reynolds number were calculated, no data is available for this geometry to suggest at what Reynolds number the transition to turbulence would begin. Thus, no Reynolds numbers have been calculated, and laminar flow has not been verified.

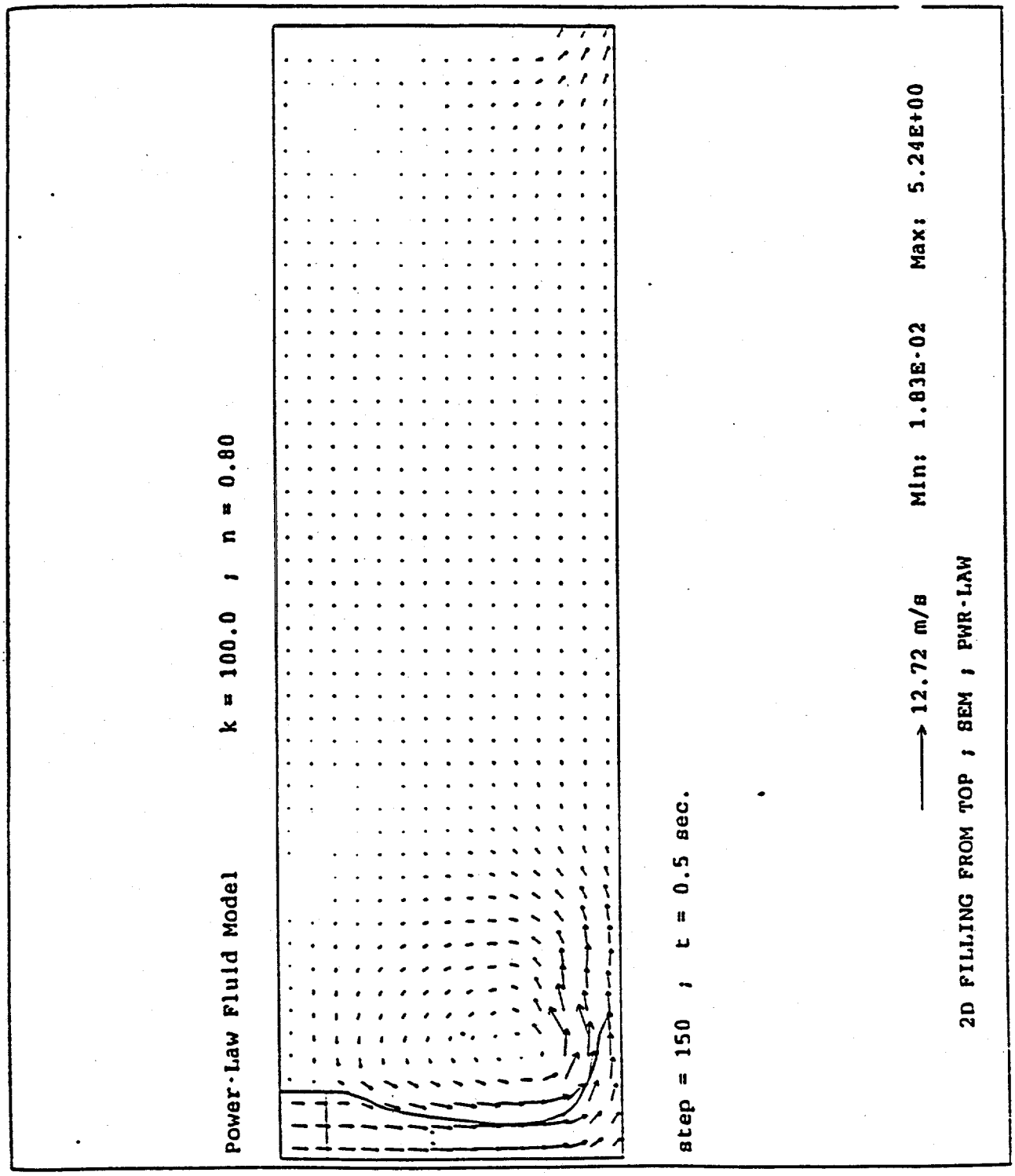
Power-Law Fluid Model
k = 100.0 ; n = 0.80
step = 150 ; t = 0.5 sec.
12.72 m/s
Min: 1.83E-02
Max: 5.24E+00
2D FILLING FROM TOP ; SEM ; PWR-LAW

Figure 44a

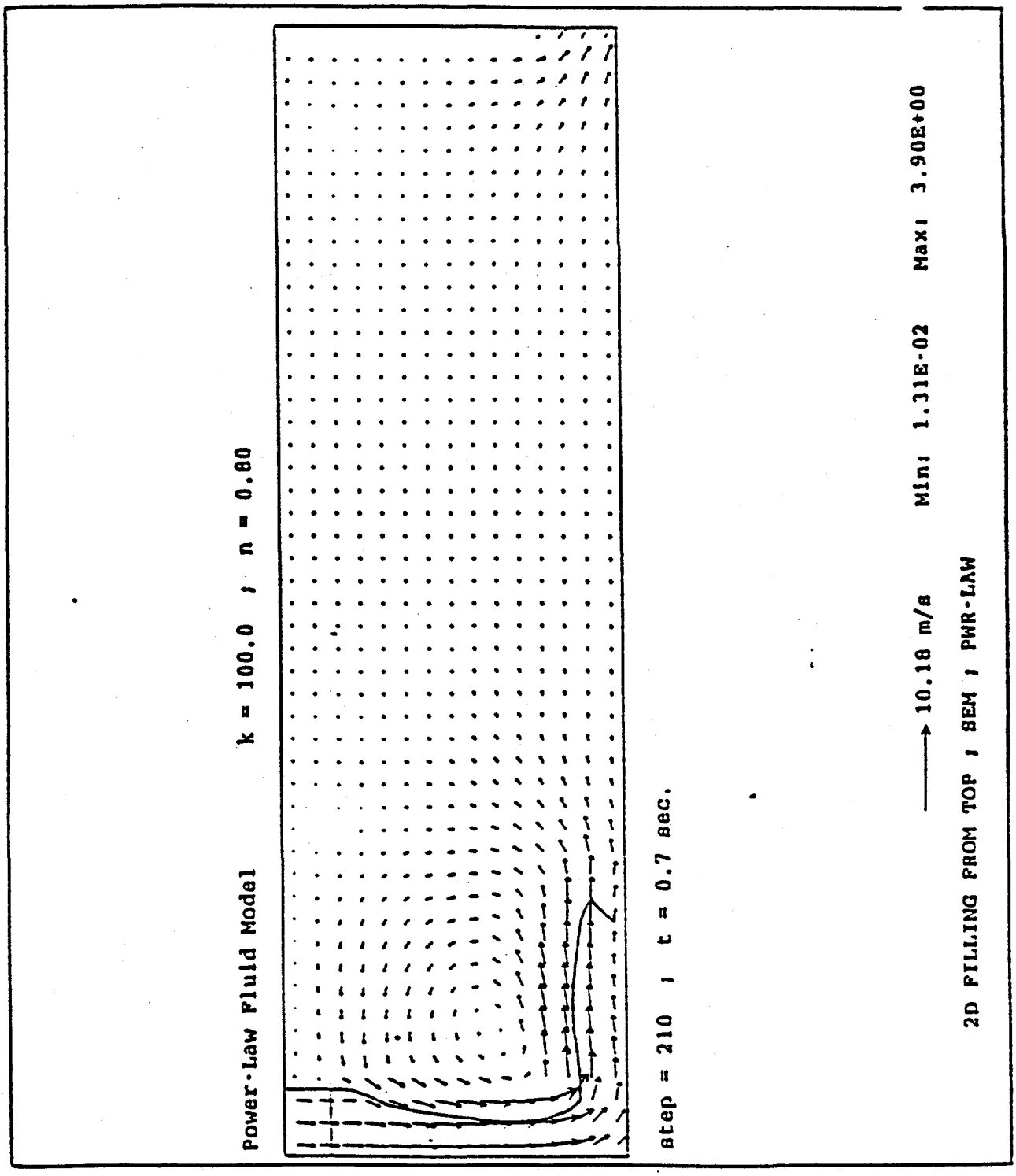
Power-Law Fluid Model
k = 100.0 ; n = 0.80
step = 210 ; t = 0.7 sec.
10.18 m/s
Min: 1.31E-02
Max: 3.90E+00
2D FILLING FROM TOP ; BEM ; PWR-LAW

Figure 44b

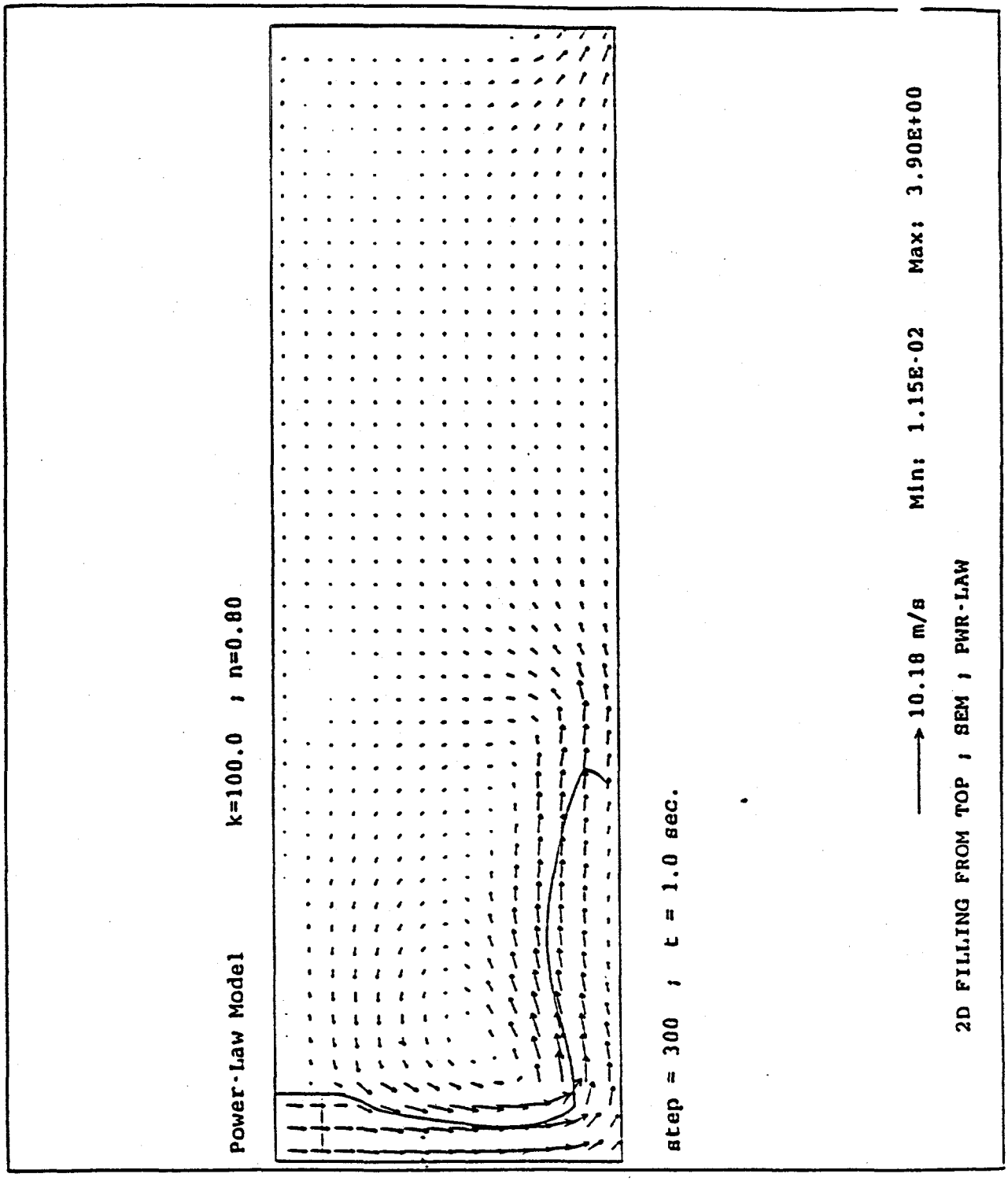
Power-Law Model
k=100.0 ; n=0.80
step = 300 ; t = 1.0 sec.
10.18 m/s
Min: 1.15E-02
Max: 3.90E+00
2D FILLING FROM TOP ; SEM ; PWR-LAW

Figure 44c

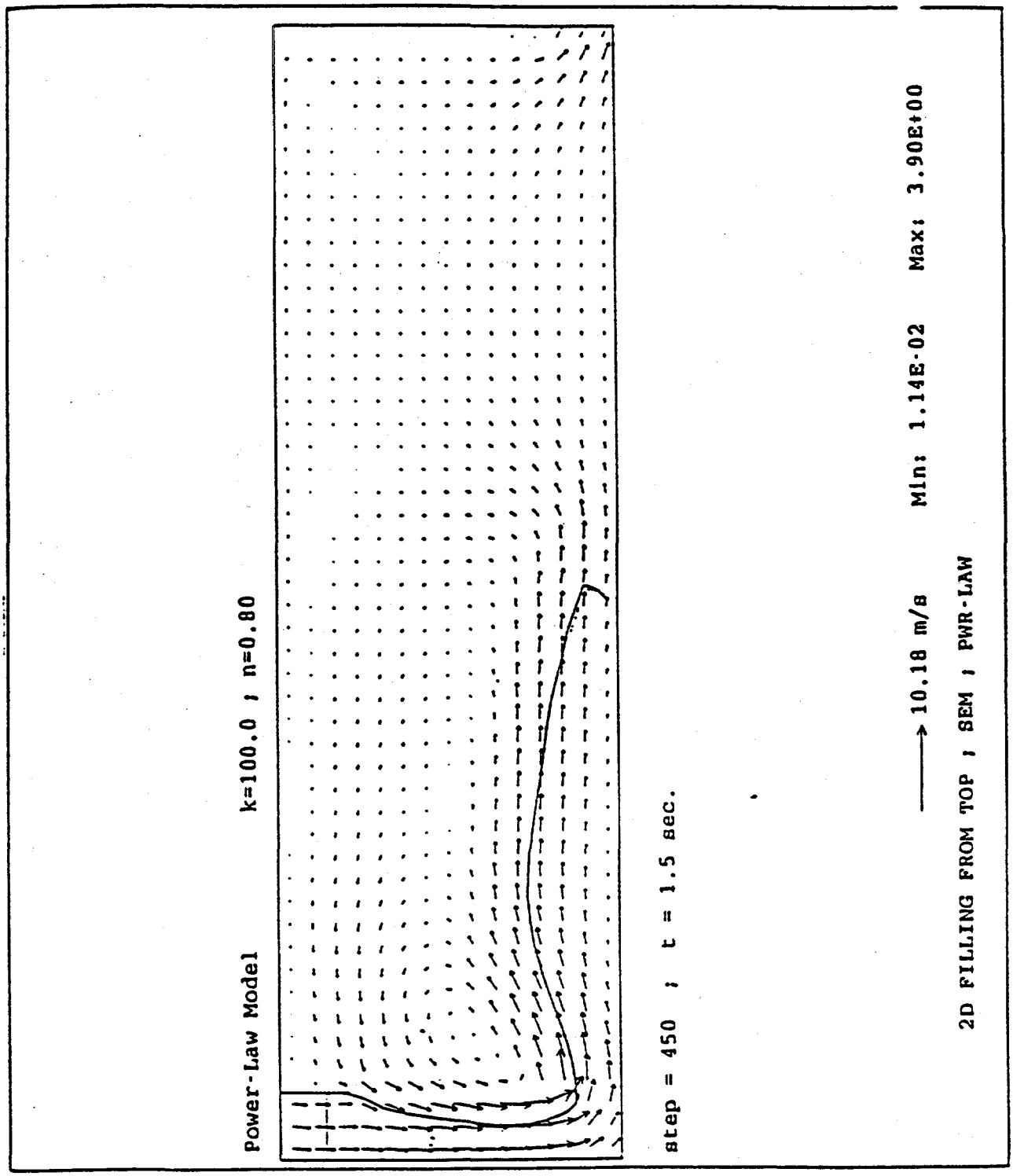
Power-Law Model
k=100.0 ; n=0.80
step = 450 ; t = 1.5 sec.
10.18 m/s
Min: 1.14E-02
Max: 3.90E+00
2D FILLING FROM TOP ; SEM ; PWR-LAW

Figure 44d

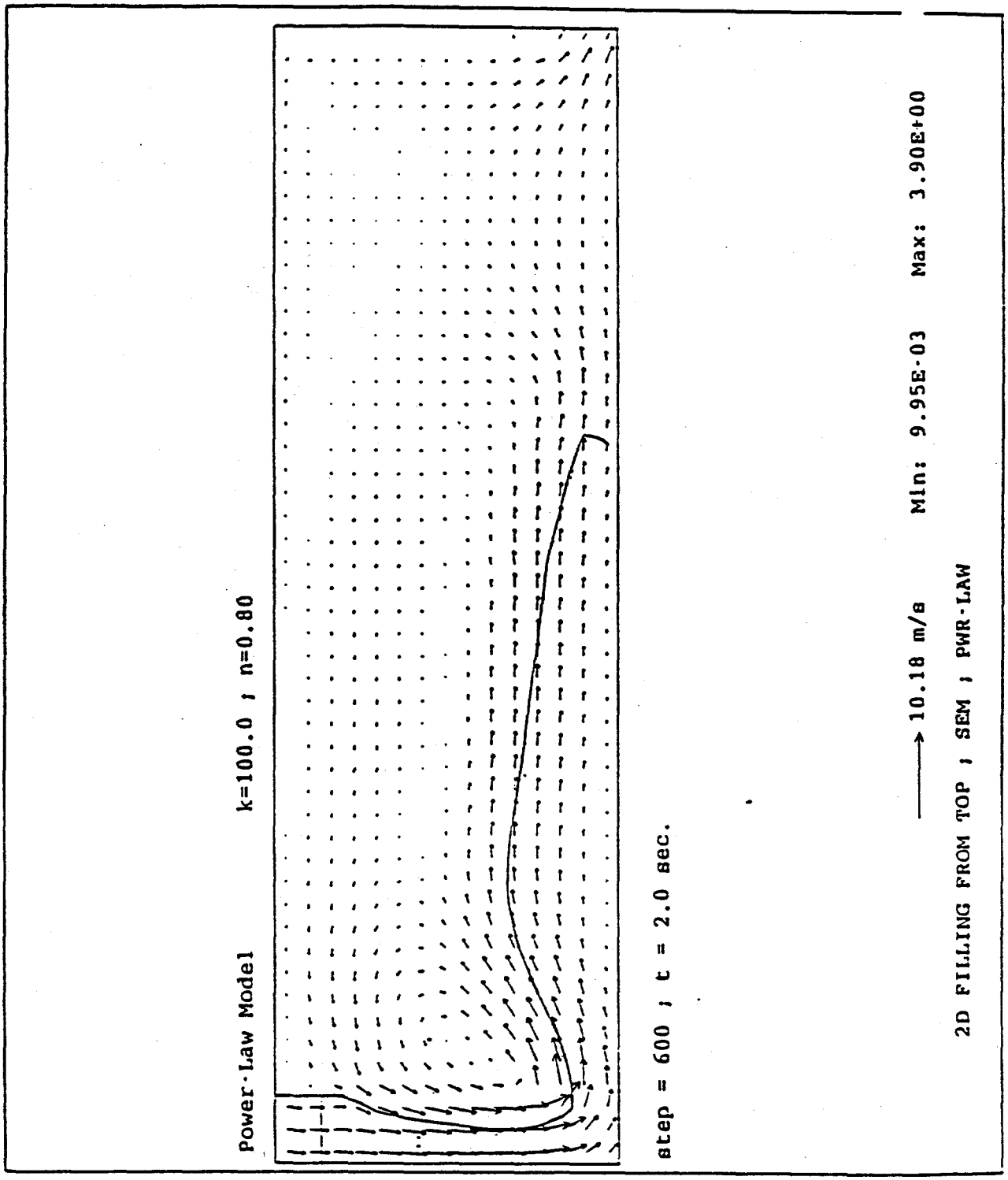
Power-Law Model
k=100.0 ; n=0.80
step = 600 ; t = 2.0 sec.
10.18 m/s
Min: 9.95E-03
Max: 3.90E+00
2D FILLING FROM TOP ; SEM ; PWR-LAW

Figurre 44e

The results demonstrate the how strongly the flow is dependent upon fluid properties. Figures 44 - 46 were all computed with the power-law fluid model, yet changing the material property constants resulted in changes in the flow field. As n and k increase, the grout is more viscous, and the depth of the grout on the mine floor increases. The model parameters used to generate Figure 46 simulated a less viscous grout that spreads out in a thin layer on the floor and quickly flows out of the simulation domain. The free surface depicted in Figure 46 is similar in appearance to supercritical profiles in open channel flow. Therefore, the Froude number was checked to determine if a hydraulic jump could occur at some location downstream of the simulation domain. A Froude number of 1.32 was calculated for the solution at 10 seconds at a location 4 m from the axis of symmetry. Although this indicates supercritical flow, the jumps associated with Froude numbers in the range of 1 to 1.5 are small undular jumps and standing waves which would have no influence on the project. Henderson(1966) presents figures and descriptions of these types of hydraulic jumps. All of the other simulations had Froude numbers less than one, indicating subcritical flow.

When the Herschel-Bulkley model is used, Figure 47 shows that the grout does not flow across the floor like the power-law models predict. Rather it piles up until it fills the entire height of the cavity and then begins moving outward as a nearly solid plug. Thus the power-law and Herschel-Bulkley fluid models generate very different predictions about how the mine may fill with injected grout.

Figure 48 illustrates a case in which there is no wall friction. Comparison with Figure 47 shows that the main effect of wall slip is to eliminate the overshoot at the floor and ceiling. With no friction, the leading edge of the spreading grout is nearly vertical, with a tendency to slump down and outward.

The simulations that produced Figures 49 and 50 used a wall boundary condition at the right of the simulation domain instead of an outlet condition. These simulations represent the flow that may occur if an injection well is drilled (perhaps inadvertently) in the middle of a mine passage, rather than in one of the passage intersections. These simulations represent the flow in a plane that is perpendicular to the closest mine pillar wall. Real flows that impact a wall would cease to be axisymmetric. Thus, Figures 49 and 50 do not give realistic predictions for flow after the grout impacts the wall.

It is evident that the choice of fluid model and model parameters have a direct impact on simulation results. This indicates that the choice of fluid model may greatly impact mine filling predictions and design decisions. Obviously it is important to use a numerical model that realistically simulates the actual grout rheology. Thus, thorough understanding of the grout rheology and accurate representation of the rheology in the computer model are vital to the success of the numerical simulation.

TWO DIMENSIONAL SIMULATION

A horizontal two dimensional simulation of a mine passage in plan view was attempted to demonstrate how the grout would flow once it has filled the intersection area and begun to move past the coal pillars. However, it was found that the inlet boundary condition could not be correctly implemented. The two dimensional simulation was to take place in the horizontal x-y plane, but the grout is actually to be injected vertically in the -z direction. In the actual three dimensional domain, the grout that comes down from the roof would impact the floor and begin to spread out in an, axisymmetric manner. A number of

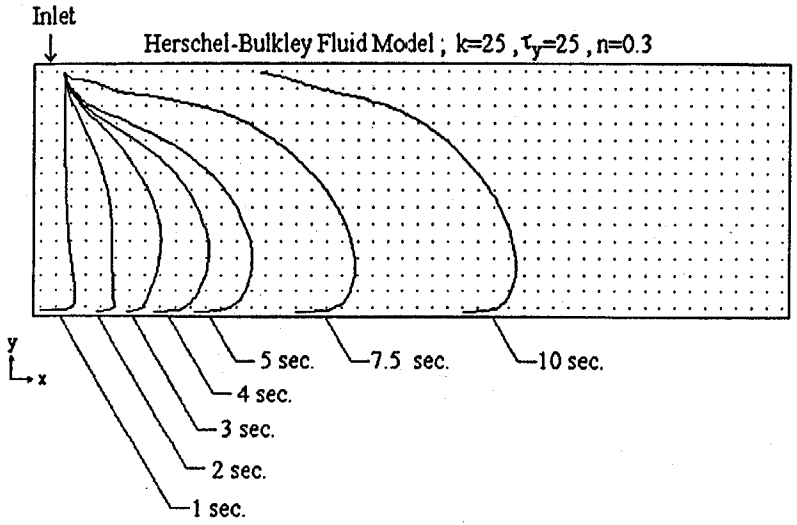

HB Fluid - Outlet B.C. - No-Slip B.C.

Figure 47

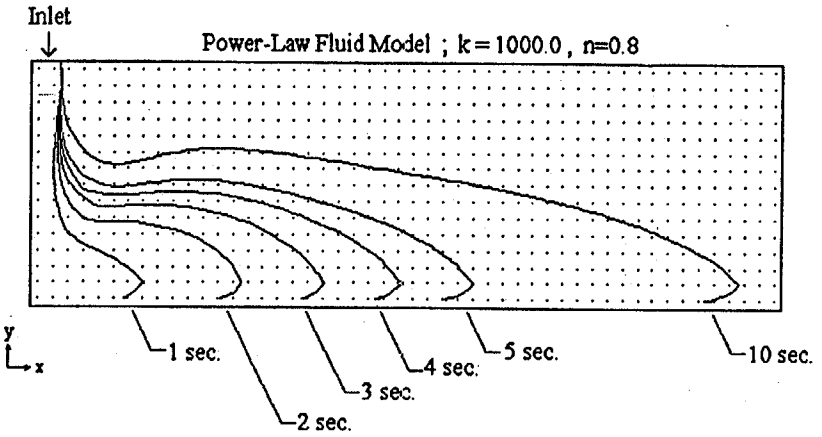

Power-law Fluid - Outlet B.C. - No-Slip B.C.

Figure 45

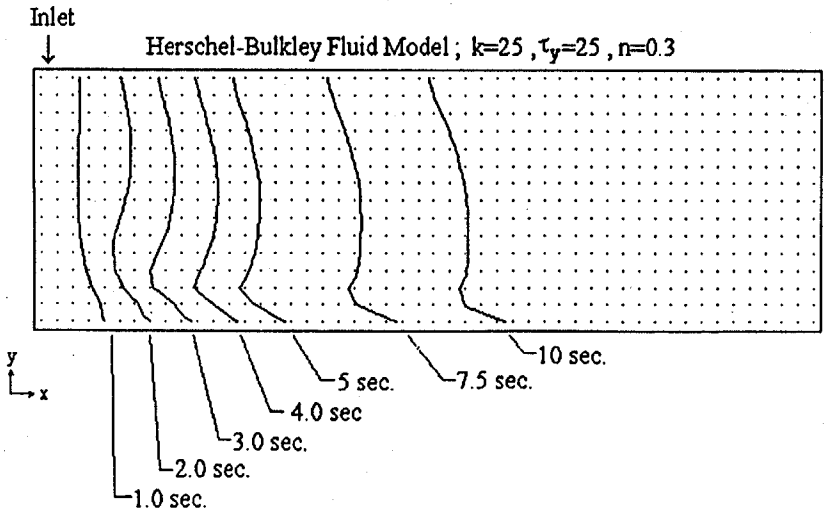

HB Fluid - Outlet B.C. - No Wall Friction

Figure 48

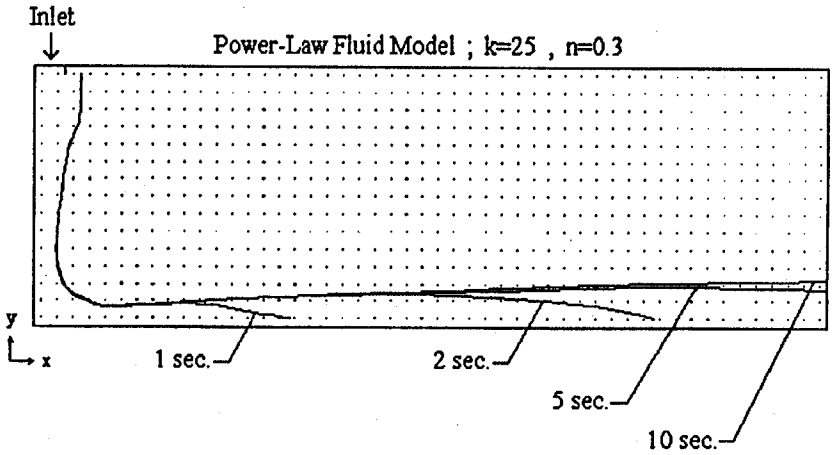

Power-law Fluid - Outlet B.C. - No-Slip B.C.

Figure 46

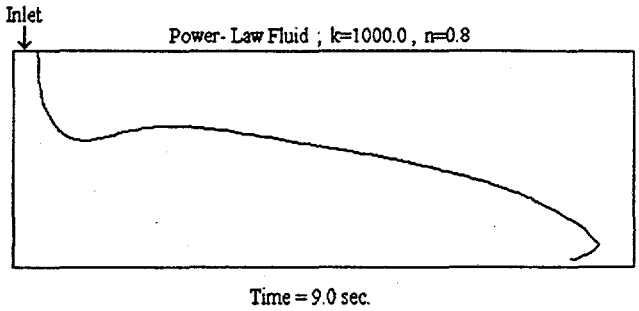

Figure 49a

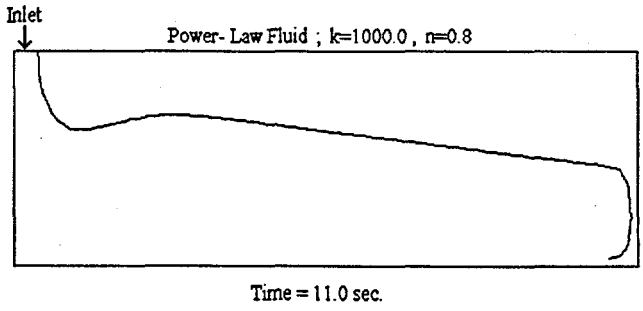

Figure 49b

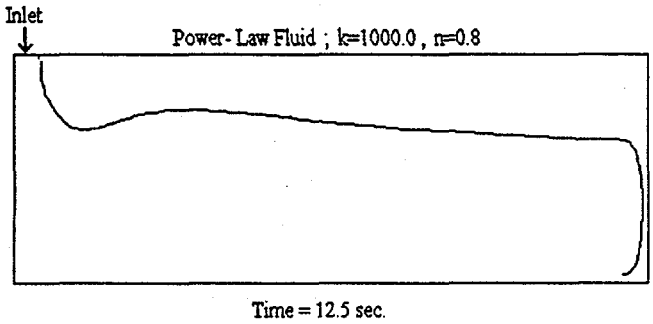

Figure 49c

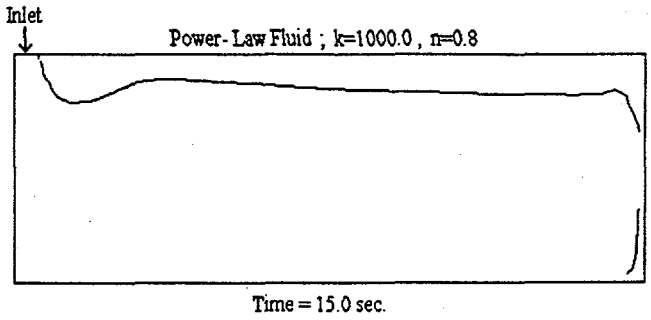

Figure 49d

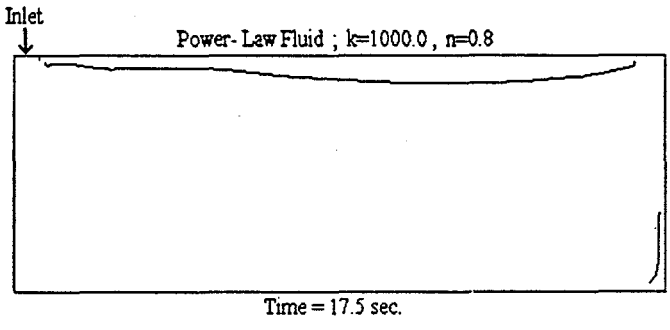

Figure 49e

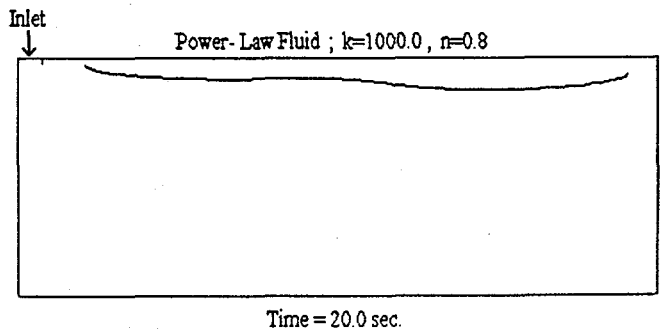

Figure 49f

Figure 49 Power-Law Fluid - No Outlet B.C. - No-Slip B.C.

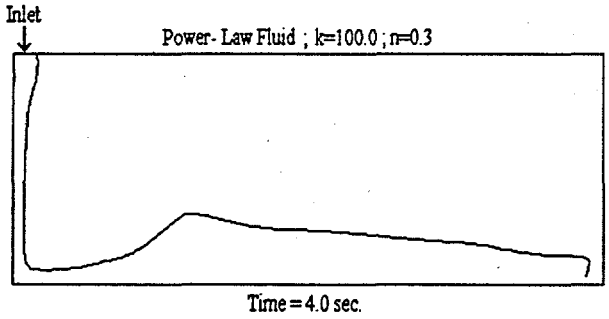

Figure 50a

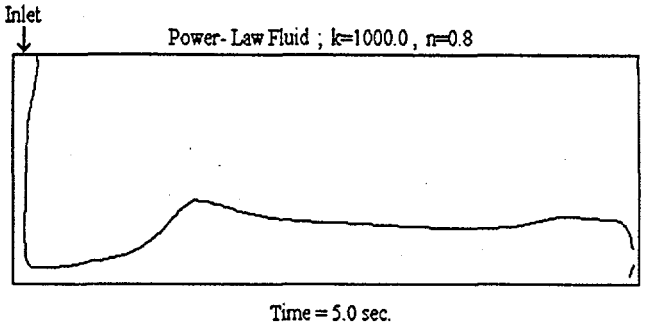

Figure 50b

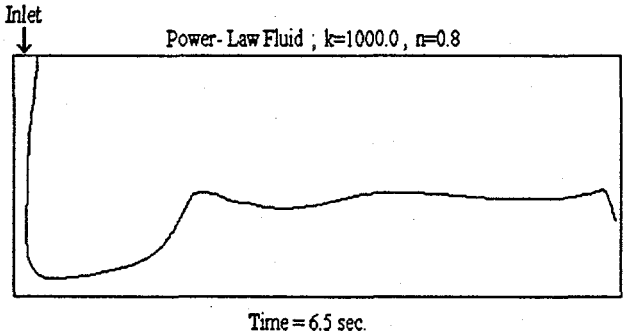

Figure 50c

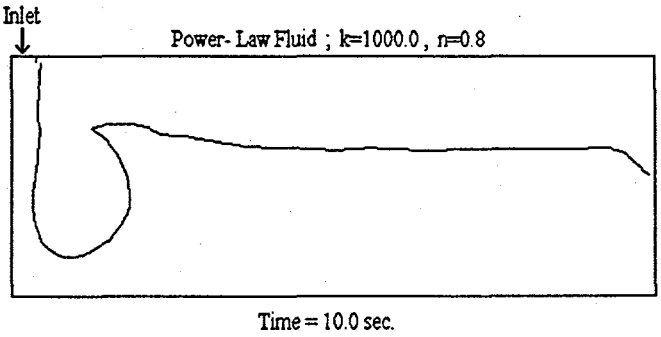

Figure 50d

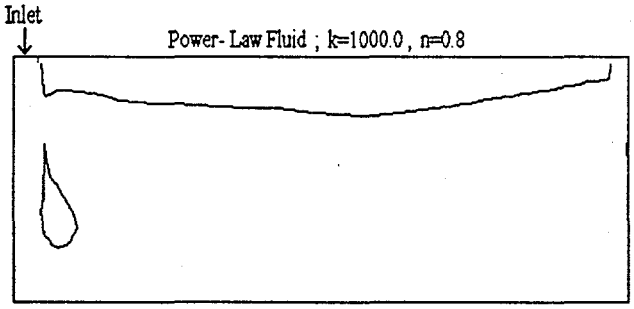

Figure 50e

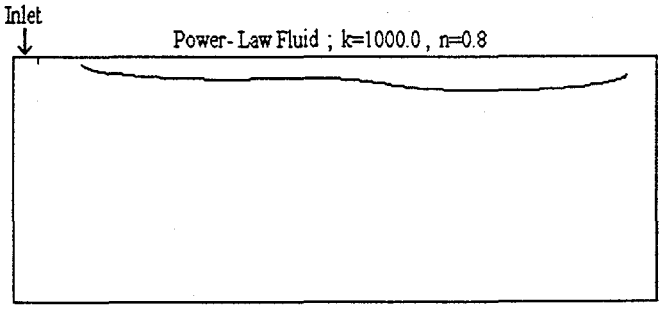

Figure 50f

Figure 50 Power-Law Fluid - No Outlet B.C. - No-Slip B.C.

attempts were made to represent this axisymmetric spreading by declaring mass inflow boundary conditions in the x and y directions near where the grout would impact the floor. Unfortunately, such boundary conditions did not produce the axisymmetric spreading that was expected. Rather, the grout interface developed irregular lobes as shown in Figure 51 because the grout was being injected into the domain in a non radial fashion. Thus, a two dimensional simulation of the area near the injection point is not meaningful because the inlet boundary condition cannot be defined realistically.

THREE DIMENSIONAL SIMULATION

A three dimensional domain was created to simulate the complete injection process. The symmetry of the mine passage geometry was exploited to minimize the size of the simulation domain. The x, y, and z dimensions of the domain were 50 m, 1.524 m, and 5.0

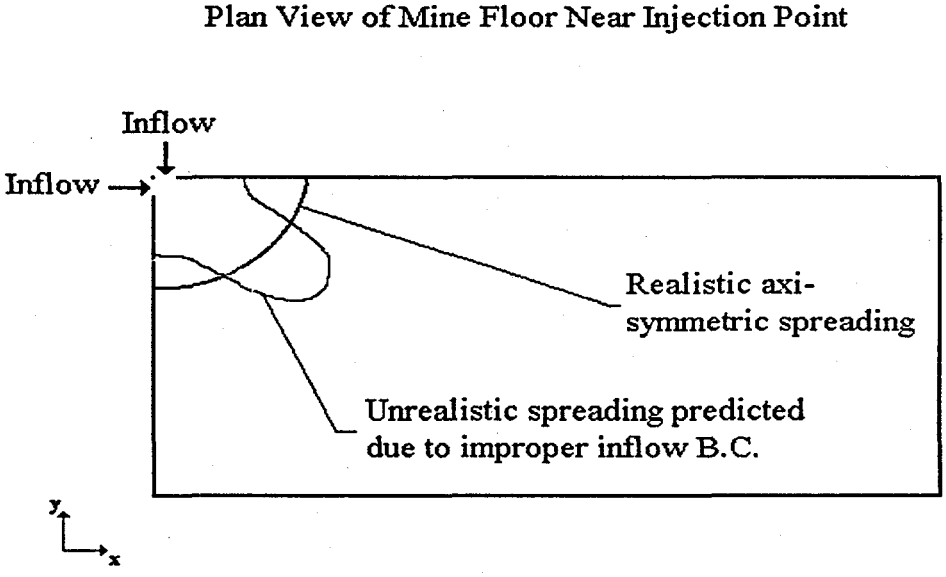

Figure 51 Unrealistic Simulation Result

m respectively, as shown in Figure 52. A uniform grid was used with 50, 12, and 15 divisions in the x, y, and z direction, for a total of 9000 grid points. A sample of the simulation results after 5 second of injection is shown in Figure 53. The figure depicts the grout-air interface near the injection point as represented by the three dimensional ϕ=0.5 surface. Figure 53 reveals that the grout is spreading axisymmetrically after it reaches the mine floor and before it impacts the walls, as expected. The grout properties used in the three dimensional simulation are the same as those used in the axisymmetric simulation represented by Figure 45. Although the results of both are qualitatively similar, a

quantitative comparison of the two results cannot be made because the specified flowrate boundary conditions are different.

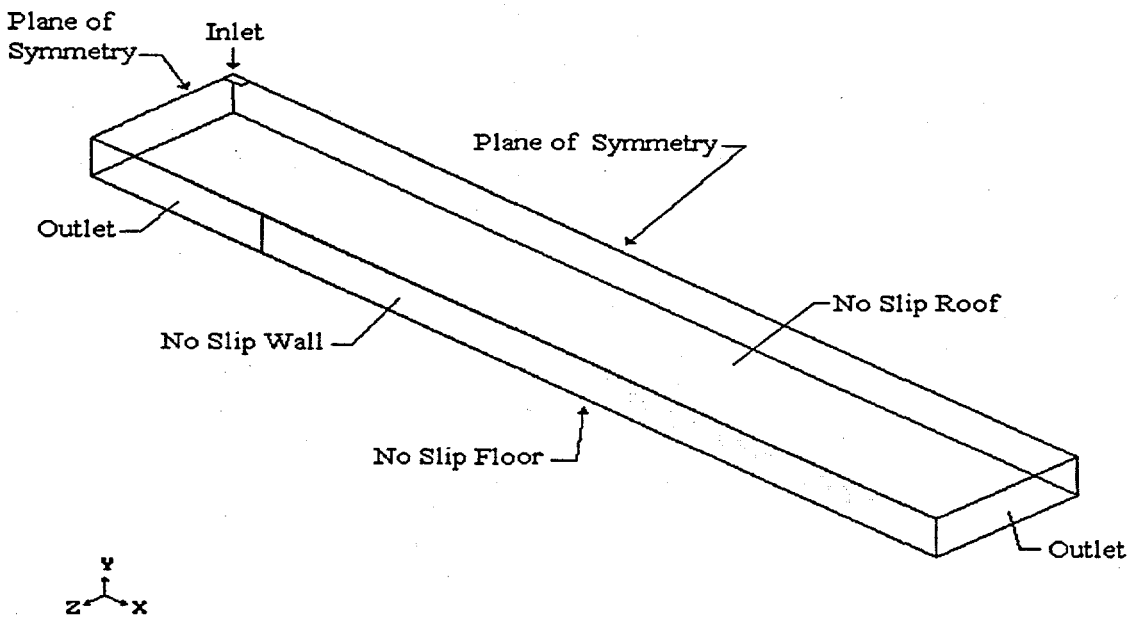

Figure 52 Three Dimensional Simulation Domain

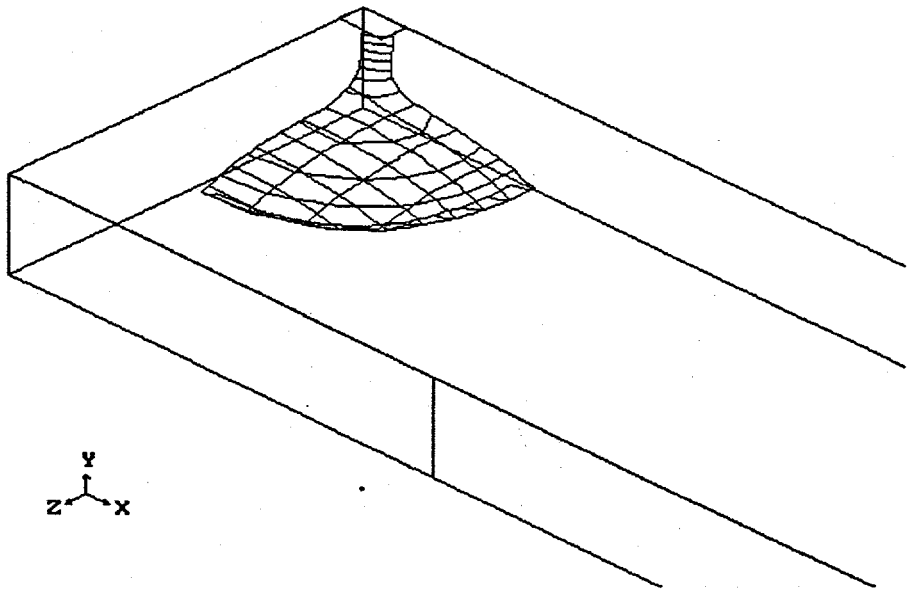

Figure 53 Three Dimensional Grout Interface after 5 s.

Although the results appear promising, the three dimensional simulation was stopped after 48 hours of cpu time. The small time steps required by the Scalar Equation Method of marking the grout-air interface, and the large number of computational cells in the three dimensional domain, result in a very slow simulation. With a 90 MHZ Pentium processor, it takes approximately 8 hours to simulate one second of the injection process. Because the time scale of the injection process is expected to be on the order of minutes or possibly hours, the three dimensional model cannot be considered to be a practical design tool with the present generation of personal computers.

Conclusions

1. It has been shown that the maximum flow distance of an unstable grout will always be less than the flow distance of a stable grout. As settling occurs in the unsteady grout mixtures, Coulomb friction between the suspended particles will generate an additional resistance to flow. Such mixtures may be so limited in their ability to flow that they would be impractical for the mine filling application under investigation.

2. A commercially available CFD code, PHOENICS, has been modified to include a specific non-Newtonian constitutive law. The Herschel-Bulkley apparent viscosity has been included in the GXPROP2.FOR subroutine and a new PHOENICS run version has been compiled. The subroutine has been compared to an exact solution and shown to produce accurate results.

3. Axisymmetric simulations of the mine injection process have been performed. The CFD software, in conjunction with the new subroutine, may be used to simulate the initial period of injection of stable grout mixtures into abandoned, underground mines.

4. The computer model has not been able to simulate flow beyond the mine passage intersections where the influence of the coal pillar walls transforms the axisymmetric flow into a truly three dimensional flow. Three dimensional simulations have been performed, but the execution times are excessive on the available hardware. More powerful computers are necessary to make three dimensional simulations a practical tool.

5. Simulation results using several non-Newtonian fluid models display strikingly different results. It is therefore very important that the correct fluid model be used to simulate the injection process, else the quantitative and qualitative information provided by numerical simulations will be useless. With the appropriate non-Newtonian model, fluid properties, and boundary conditions, numerical simulations can provide useful predictions of grout flow behavior.

RECOMMENDATIONS FOR FURTHER STUDY

Several aspects of this investigation are still unresolved. The correct wall boundary

condition is uncertain. It should be determined experimentally and incorporated into the PHOENICS code for future simulations. The variability of solid content from the Beechurst plant must be addressed. If no change is made to the current method of gathering the ash waste, it will not be possible to predict mine filling behavior because the grout properties will be subject to large and unknown variations. If a definitive grout recipe cannot be obtained, the computer model will not be a successful tool for designing injection well placement nor choosing an injection strategy. It is desirable to devise a simple field test, similar to the slump test used for concrete testing, to monitor the grout rheology during large scale injection operations. If the grout rheology can be determined in the field, field personal may be able to adjust the grout mix and injection well spacing to compensate for variations in the grout ingredients. Finally, the computer model developed here should be used to perform a thorough parametric study covering the range of expected grout property values.

TASK 3 BENCH-SCALE RHEOLOGY MODEL

Purpose

The purpose of this task is to determine the rheological properties of a grout composed of FBC byproducts, water, and bentonite, and also to simulate the flow of the grout into an abandoned mine using both computer models and bench scale lab tests. The goal of this task is to minimize the number of boreholes needed to completely fill abandoned subsurface mines using conventional pumping techniques. Therefore it is necessary to achieve maximum flowability while maintaining grout stability and meeting minimum strength properties.

Methodology

Grout Rheology

The first task was to establish a suitable range of water fractions for the FBC ash grouts. This was done by preparing grout samples at several water fractions and visually inspecting them for flowability. After doing preliminary tests to determine a suitable range of water fractions, rheological tests were performed. After the grout sample was prepared, a portion was tested using the Brookfield LVDV III rotational viscometer fitted with a T-bar spindle and a heli-path mount. A schematic of this setup is shown in Figure 54.

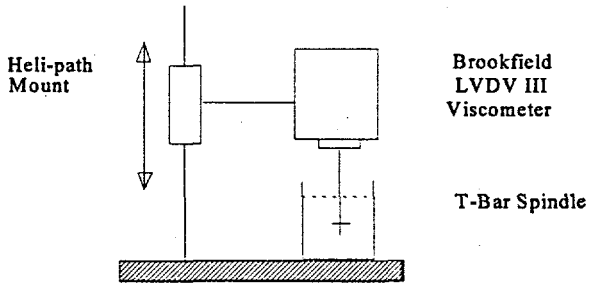

Figure 54: Schematic of viscometer with heli-path mount.

The principle of the rotational viscometer is to measure the torque required to turn a rotor submerged in the test fluid at a constant angular velocity. The heli-path device moves the entire viscometer up and down periodically so that the spindle cuts a helical path

through the sample. This continually puts the spindle in contact with new material. This is of particular importance when testing non-flowing samples where a spindle turned at the same depth could cut a groove into the sample. Tests were performed at variety of angular velocities with torque readings being taken when the T-bar was at a constant depth in the grout in order to eliminate the variation in the torque reading due to the changing length of the shaft that is submerged in the sample. The torque-rpm data were then reduced to shear stress and strain rate data using the mixer viscometer method introduced by *Metzner and Otto (1957)*, who were working with power law fluids, and by *Tattersall and Bloomer (1979)*, who extended this work to include Bingham plastics. This method was further extended by the present authors to include the Herschel-Bulkley fluid model. The mixer viscometer method uses the slope and intercept of the torque versus rpm plot (either on linear-linear or log-log paper) along with two machine constants, which are found by testing fluids of known properties. This method can be used to obtain parameters for Newtonian, power-law, Bingham and Herschel-Bulkley fluid models.

Mixer Viscometer Method

The basic principle of this method is that the torque T needed to maintain a constant rotational speed N is equal to N multiplied by the apparent viscosity of the substance at the corresponding rate of strain (η_a) and G, which is a device constant.

$$T = G\eta_a N$$

Case 1: Newtonian Fluid

For a Newtonian fluid, the constitutive equation for parallel shear flow is given by the equation

$$\tau = \mu\gamma$$

where τ is the shear stress, μ is the dynamic viscosity, and γ is the rate of strain. From this we can define an apparent viscosity which is equal to the shear stress divided by the strain rate. For a Newtonian fluid, this is a constant equal to the dynamic viscosity. By solving for the apparent viscosity, we get

$$\eta_a = \frac{\tau}{\gamma} = \mu = \frac{T}{GN}$$

The constant G can be found by testing Newtonian fluids with known viscosities and plotting the data as torque (T) versus rotational speed (N). This plot should yield a "straight" line through the origin with a slope equal $G\mu$. If a fluid of known μ is tested, G can be determined. This allows μ to be found for any other Newtonian fluid.

Case 2: Bingham Fluid

For the Bingham model, the constitutive equation which relates the shear stress to the strain rate in a parallel shear flow is

$$\tau = \tau_y + \mu_p \gamma$$

where τ_y is the yield stress of the fluid and μ_p is the plastic viscosity. Again we can define an apparent viscosity by dividing the shear stress by the rate of strain. Unlike the Newtonian, the apparent viscosity is not a constant, but depends on the rate of strain.

$$\eta_a = \frac{\tau_y}{\gamma} + \mu_p = \frac{T}{GN}$$

By assuming that the rate of strain (γ) is equal to a constant K multiplied by N and solving for the torque we get

$$T = \mu_p GN + \frac{G\tau_y}{K}$$

The assumption γ=KN has been verified for numerous Non-Newtonian fluids (*Skelland, 1983*). Like the Newtonian case, a plot of torque versus angular speed yields a straight line with the slope equal to μ_pG, only in this case the line does not pass through the origin (See Figure 55). The intercept on the torque axis is equal to τ_yG/K. By testing a Bingham fluid with known properties such as an 8% bentonite slurry (*Grim, 1978*), K, which is a device constant, can then be found.

Case 3: Power-law Fluid

For a power-law fluid, the constitutive relationship for parallel shear flow is

$$\tau = r\gamma^s$$

where r is the consistency index and s is the power number. By the definition of the apparent viscosity, we have

$$\eta_a = r\gamma^{s-1} = \frac{s}{GN}$$

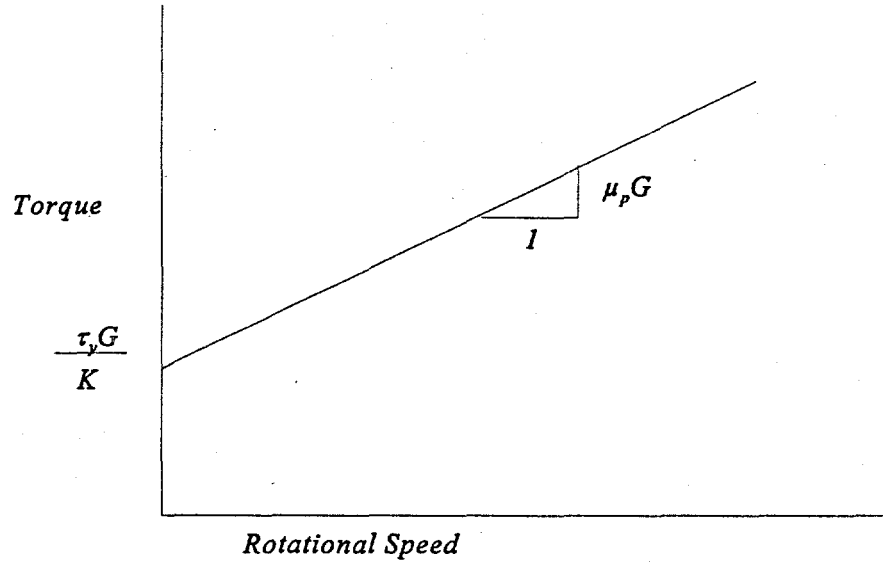

Figure 55: Torque versus rotational speed plot for a Bingham fluid.

Again substituting KN for γ and solving for T we get

$$T = GrK^{s-1}N^{s}$$

For this case the plot of T versus N does not yield a straight line on linear graph paper, but taking the natural log of both sides of the above equation gives

$$\ln T = \ln(GrK) + s\ln N$$

Plotting this equation on log-log paper then yields a straight line with the slope equal to the power number s and the intercept equal to GrK.

Case 4: Herschel-Bulkley Fluid

The constitutive equation for parallel shear flow for a Herschel-Bulkley fluid is

$$\tau = \tau_y + r\gamma^{s}$$

The constitutive equation for parallel shear flow for a Herschel-Bulkley fluid is For this relationship, the apparent viscosity is equal to

$$\eta_a = \frac{\tau_y}{\gamma} + r\gamma^{s-1} = \frac{T}{GN}$$

By making the same substitutions as before, and again solving for T, the result is

$$T = \frac{G\tau_y}{K} + GrK^{s-1}N^s$$

In order to fit the data to an HB model it is necessary to first have an independent measure of the yield stress of the liquid. This can be obtained by several procedures, of which the vane method is the easiest to perform and also one of the more reliable (*Nguyen and Boger, 1992)*. For this test a four-bladed vane is immersed in the liquid. The torque is then increased until the vane begins to rotate. Below this value of torque the material behaves like an elastic solid, and above the value, like a fluid. The maximum torque reached before rotation of the vane begins can be converted to the yield stress by

$$T = \frac{\pi}{2}d^3\left(\frac{l}{d}+\frac{l}{3}\right)\tau_y$$

where T = maximum static torque
l = length of the vane
d = diameter of the vane
τ_Y = yield stress

Substituting this value of the yield stress into the previous torque equation and moving that term to the left side of the equation gives

$$T - \frac{G\tau_y}{K} = GrK^{s-1}N^s$$

Taking the natural log of both sides of this equation gives

$$\ln\left(T - \frac{G\tau_y}{K}\right) = \ln\left(GrK^{s-1}\right) + s\ln(N)$$

Plotting the left hand side of the equation versus N on log-log paper gives a straight line with the slope equal to s and the intercept equal to GrK^{s-1}. This can then be solved for s and r if τ_y is already known. Thus all the parameters of the constitutive equation for the

Grout Stability

Before any viscometric tests could be performed, it was first necessary to produce a grout that was stable. By definition, an unstable grout is one that bleeds greater than five percent of its water during a two hour period. Bleed tests were done in accordance with ASTM standard C 232 - 87. Samples were prepared and placed in round containers which were covered to prevent evaporation. After two hours, any clear water that had bled to the surface was pipetted off and weighed. This weight, divided by the weight of water used in the mix and multiplied by 100 gives the percentage of bleed. Mixtures of pure FBC ash and water were found to be unstable. To combat the settling of the solid particles, various percentages of WYO-BEN 250 mesh bentonite were added to the grout mix. Figure 56 shows that the percentage of bleed increases linearly with an increase in water fraction,

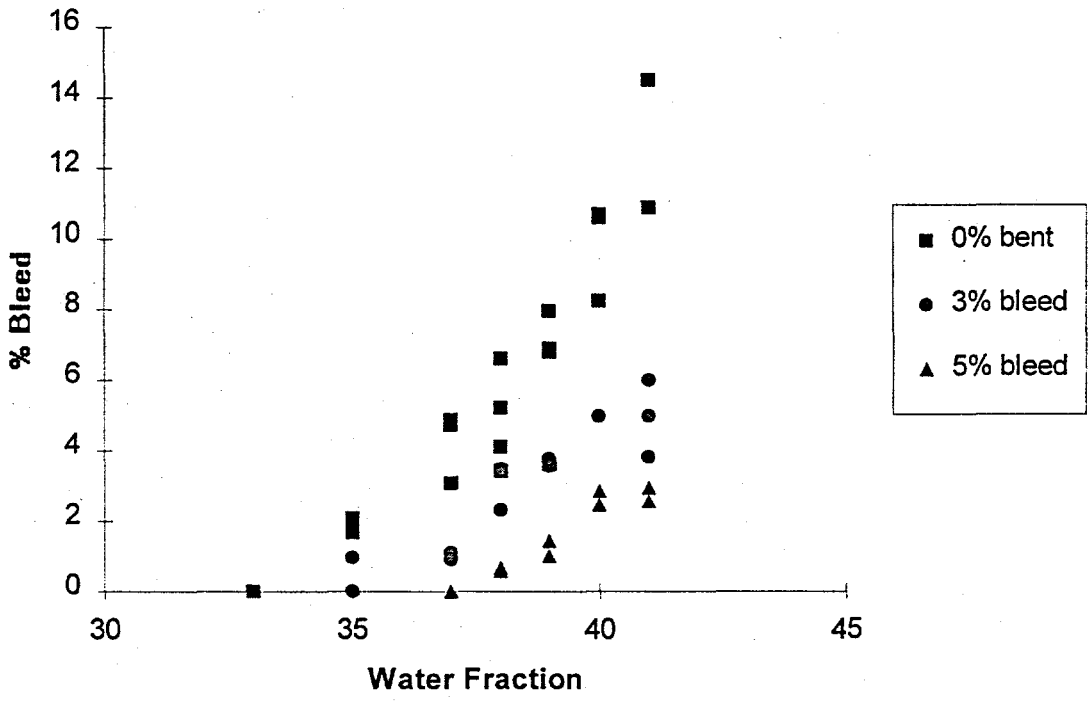

Figure 56: Results of bleed tests on mixes containing equal portions of fly ash and bottom ash.

while the amount of bleed is decreased by increasing the amount of bentonite added. It was found that 3% bentonite was sufficient to render the grout stable.

Other tests done on the rotational viscometer using the T-bar spindle gave proof that particles in the pure FBC ash - water grouts were settling. First a series of tests were done

Other tests done on the rotational viscometer using the T-bar spindle gave proof that particles in the pure FBC ash - water grouts were settling. First a series of tests were done in which the spindle was rotated at a constant speed while being moved through a helical path in a grout containing only fly ash. Torque readings were taken at five second intervals for the length of the test. When these readings were plotted versus time, the pattern showed that the torque increased as the spindle neared the bottom of its path , and decreased as it neared the top of the path, as seen in Figure 57. This periodic behavior is due to the variation in the length of the submerged shaft, but the increase in amplitude is due to the settling of the particles causing the lower portion of the sample to become more concentrated than the upper portion.

Tests were then done using different water fractions and different amounts of bentonite. At 7 % bentonite, there was very little settling. Another test where the spindle was rotated at a constant depth was performed with torque readings taken at a specified time interval. Figure 57 shows that with no bentonite used in a fly ash only grout, the torque increased with time, but with 7 % bentonite, the torque at the constant depth showed much less increase. The increase in torque for the no bentonite grout is due to the settling of the ash particles. As the particles come in contact with one another there is an additional frictional mechanism which increases the torque. Eventually, the T-bar formed a slip surface in the sample which effectively caused the torque to become constant. The sample containing bentonite, on the other hand, has less torque increase, showing that particle settling is not a problem. All of these tests have shown that bentonite is an effective additive in the reduction of particle settling and in increasing the stability of the grout.

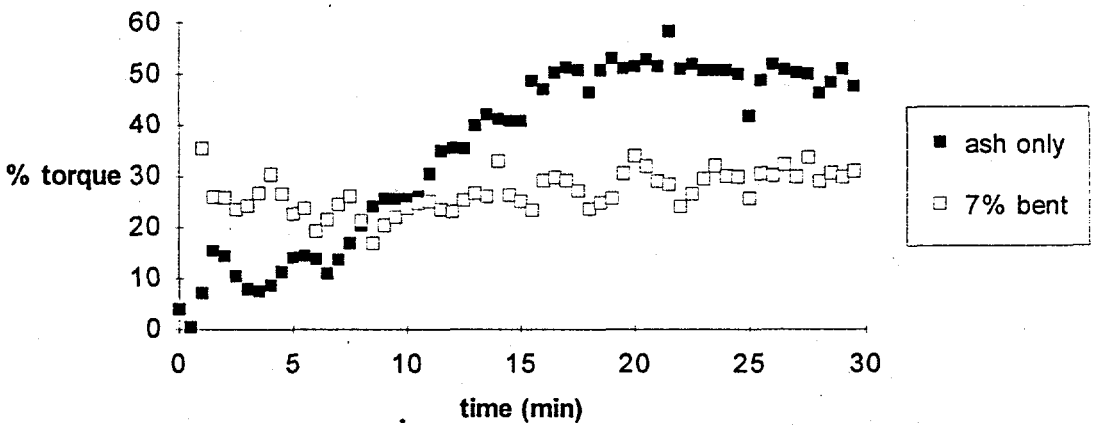

Figure 57: Plot showing increase in stability due to the addition of bentonite.

Ash Variability

Different samples of ash taken from the Beechurst Avenue power plant not only contain varying percentages of fly and bottom ash, but also vary considerably in flow characteristics. This was discovered when doing the "dam break" experiment. In this test a rectangular box 100 cm long by 20 m wide by 40 cm high with a removable wall 20 cm from the end was used. Grout was placed behind the wall to a depth of 30 cm. The wall was then quickly removed, and the grout was allowed to flow toward the other end of the box. Tests were done using grouts prepared using identical recipes but with ash taken from two separate ash lots. In one test the grout was very fluid and reached the end of the box in under 2 seconds, while the other sample failed to reach the end of the box at all. This difference in behavior is likely due to the variability of material that the plant is burning and also to the plant's method of collecting the ash. The power plant burns a mixture of pure coal, limestone, and "gob", which is refuse coal found in the overburden. Limestone is added to decrease the sulfur emissions from the exhaust stack. The percentage of gob burned is changed according to the output power requirements. Another cause of variability is due to the ash handling at the power plant. Every truck is filled from one of three ash holding hoppers. At any time these hoppers can contain any combination of fly and bottom ash.

The variability will become a problem when actually filling the mine. The operator will not be able to simply use the same grout recipe for each truckload of ash. For this reason work has been done to come up with an acceptable field test that the operator can perform to ensure that the grout has the proper flow characteristics. The proposed test uses a cylinder 3 inches in diameter by 6 inches in height open at both ends. The cylinder is placed vertically on a horizontal surface and filled with grout. The cylinder is then slowly lifted and the grout is allowed to spread in a radial fashion. The distance of spread is then measured in two perpendicular directions and an average is taken. Spread tests were done using varying amounts of bentonite and water. Figure 58 shows how the addition of bentonite reduces the spread of the grout. This reduction in spread may call for the use of a super-plasticizer or air entraining agent to counteract the effect of the bentonite. Work is currently being done to see how these additives will affect the flow of the grout, and to obtain a correlation between the spread and the appropriate flow parameters.

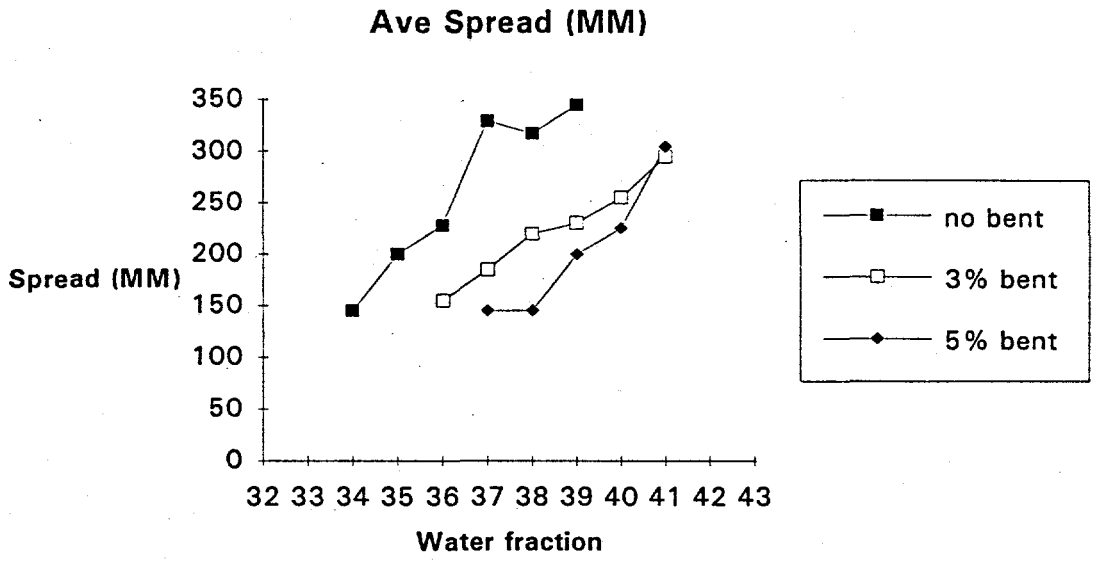

Figure 58: Spread versus water fraction for fly ash only samples at varying amounts of bentonite.

Results and Discussion

Tests have been done using the T-bar spindle on grouts with fly ash as the only combustion byproduct. The ash was taken directly from the ash collection flow stream before it was deposited in the collection hoppers. Work will eventually include grouts containing both fly and bottom ash. These tests have been done with varying water fractions and amounts of bentonite. When using bentonite it is necessary to dry mix the ash and the bentonite before any water is added to insure that the bentonite will be in contact with as much of the ash as possible. Figure 59 shows typical torque versus speed data for a fly ash only sample containing 7% bentonite along with the Bingham fit to the data (μ_p = 6.7 Pa-sec , and τ_y = 2.9 Pa)

One problem that has been discovered is the shear rates found using the T-bar spindles are on the order of 0.2 s^{-1}. This is far below the rates which will be found in the pumping and placing of the grout. During the placing, the maximum shear rate for the grout flowing in an injection pipe is approximately 60 s^{-1}. Therefore a series of tests have been done using a cylindrical spindle . With this particular geometry, it is likely that wall slip may occur, so that the results may not be reliable, but the shear rates that are generated in this geometry are in the range that will occur in the field. Future work will include tests to determine if wall slip has occurred and to correct for it if necessary. When the concentric cylinder data is combined with the data generated using the T-bar spindle, the best fit is given by an HB model as shown in Figure 60.

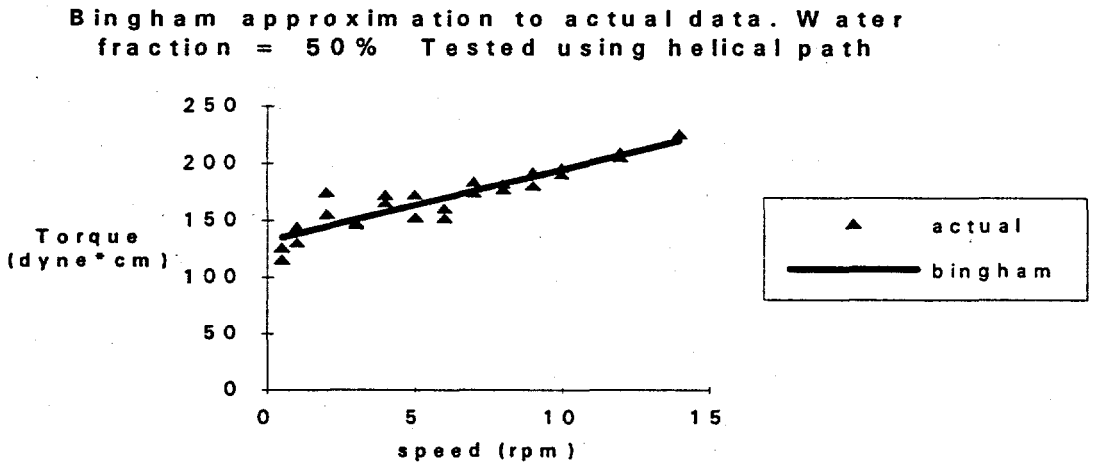

Figure 59: Torque versus speed plot for a sample with a water fraction of 50% containing 7% bentonite.

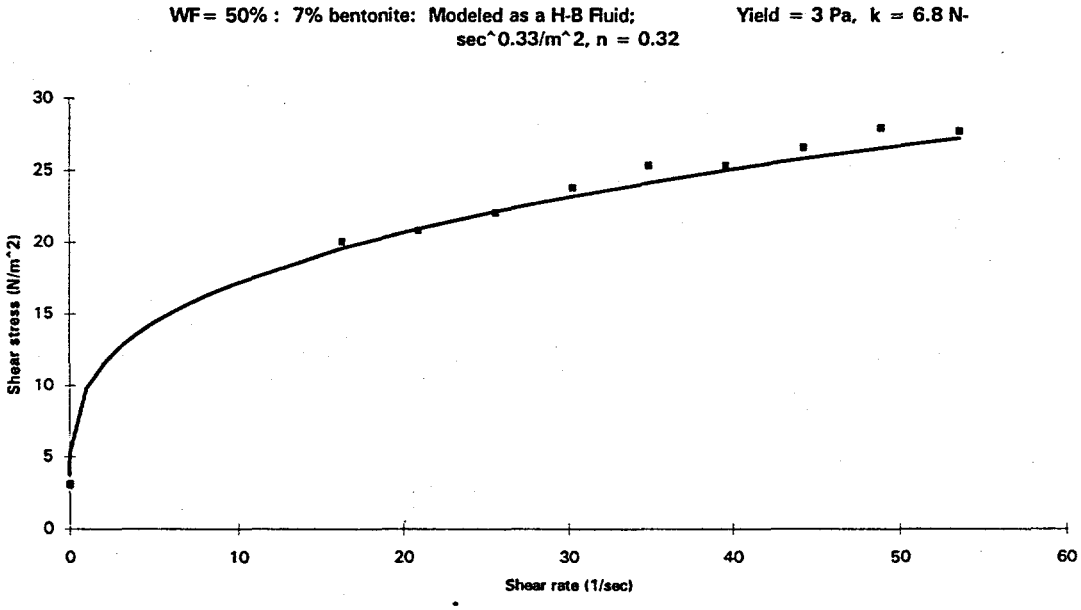

Figure 60: Shear stress versus strain rate for a sample tested using concentric cylinder geometry.

TASK 4 WATER QUALITY MONITORING

Purpose

This purpose of this task is to monitor baseline water quality and quantity of the acid mine drainage (AMD) from the Longridge and Fairfax Mines prior to grouting. The baseline data will be essential to evaluate and document the benefit of the grouting activity over time.

Background

The Longridge Mine is an ideal site for sampling since all water exits the mine from a single opening. It was relatively easy to modify the area near the opening so as to capture all the flow and then to direct it into a pipe for measurement and sampling. Several flow and water quality measurements were made on AMD from the mine in 1982. At that time the flow varied between 10 to 74 gallons per minute (gpm). This information was helpful in choosing a flow measurement system to monitor the expected large variation in flow over the project period. It was decided to set up a continuous sampling station for baseline monitoring of flow and water quality from the Longridge Mine. All water in the active Fairfax Mine has historically been collected in a sump and pumped out of the mine as required. It was planned that baseline samples would be taken of the pumped flow on a bi-monthly basis.

Methodology

In order to measure flow from the Longridge Mine, a rock and concrete dam was built at the entrance to back up water leaving the entrance to a depth of about 2 feet. The minewater was directed to flow through a 6 inch diameter PVC pipe built into the bottom of the dam and a variable gate flowmeter was attached to the end of the pipe to continually monitor the flow. Calculations show that the system should be able to monitor flows of from about 0.25 to 180 gpm which will cover the expected flow range both prior to and after the grouting.

The site is visited weekly to inspect the equipment and to collect the data and samples. Flow data from the meter is continuously recorded and a signal is sent to a sampler in order to allow collection of samples in proportion to flow. The flow data is both recorded on a stripchart and stored on flowlink software for weekly downloading to a portable computer. Samples of minewater are taken and sent to a weatherproof sampling station (heated and cooled) where they are stored in a polyethylene container at 4° C. The sampled AMD is picked up on a weekly basis and transported to the laboratory for analysis. The sampler is programmed to take as many as 100 aliquots of minewater per week based on a preset flow interval such as 1200 gallons. Thus when the flow is high, samples are taken more frequently than when flow falls off. The flow interval

between samples is adjusted from time to time depending on the flow at that period so as to spread sample collection over the entire week's period.

Seventeen constituents were analyzed in the weekly samples. The constituents were chosen based on contaminants known to be in AMD and their potential toxicity to the environment. Another factor in the choice were those pollutants which might be leached from the MEA FGD by-product sludge. The constituents chosen for analysis are as follows:

acidity	magnesium	specific conductance	arsenic
calcium	pH	acidity	lead
temperature	alkalinity	sulfate	cadmium
manganese	iron	aluminum	boron
selenium			

It may be seen that a variety of major AMD constituents were chosen such as acidity, sulfate and iron as well as 5 trace elements. All analyses were performed according to accepted standard methods and QA/QC procedures rigorously observed.

Since the amount of precipitation in a given time period will affect the volume of water moving through the mines and the strength of the AMD, a precipitation gauge was set up close to the mines. Precipitation is measured with a battery operated tipping bucket rain gauge located in a setting away from trees and wind currents. The data is continuously recorded on a data logger and downloaded weekly to a portable computer.

Results and Discussion

Set-up of the sampling equipment was completed on 8/3/94 and the first sample was taken at the Longridge Mine on that date. Table 2 presents the data obtained for each sample while Table 3 provides the average values and range for each parameter. Samples were taken weekly through the end of Phase 1 on 9/30/95 for a total of 56 samples. Several weeks of flow data were lost when the flow meter malfunctioned and was returned to the manufacturer for repair. It should be noted that no samples were taken from the Fairfax Mine during Phase 1 because no water was produced in the areas that had been targeted for sampling.

Flow and Precipitation Monitoring

As may be seen in Table 3, average weekly flow during the period varied from a low of 8.79 to a high of 121.4 gpm with and averaged 36.2 gpm. Figure 61 presents a plot of flow vs sample number and month. The months are shown to show influence of season on the flows. As noted above, sampling began in the late summer (August) of 1994 and the data shown continues through the end of Phase 1 (September 30, 1995). It may be

noted that the flow drops off significantly toward the end of each summer period with low flow periods extending into late fall.

Table 2. Weekly Data-Longridge Mine

Date	8/3/94	8/15/94	####	9/2/94	9/9/94	####	9/23/94	####	####	#####	#####	10/28/94	####	#####	#####	11/26/94	12/2/94	####	#####	12/23/94	#####	1/7/95	1/14/95	1/21/95	####	2/5/95
Sample #	1	2	3	4	5	6	7	8	9	10	11	12	13	14	15	16	17	18	19	20	21	22	23	24	25	26
Flow (gpm)	na	38.2	95.4	46.8	30.3	23.9	18.4	16	13.5	12.1	11.3	10.6	9.9	9.6	8.9	8.79	10	19.83	83.57	45.74	34.39	36.96	93.9	89.36	73.56	44.54
Temp (C)	na	na	na	11	10	10	10	10	10	10	10	8	10	8	10	6	6	10	10	10	10	10	10	10	10	9
Precip. (in) *	1.97	1.33	4.52	1	0	2.26	0.32	0.45	0.64	0.09	0.47	0.03	0.05	0.58	0.57	0.25*	0.78	1.28	1.72	0.24	0.04	1.5	0.62	0.91	0.51*	0.45*
pH	2.5	2.9	2.5	2.4	2.4	2.55	2.58	2.56	2.67	2.65	2.56	2.67	2.82	2.61	2.94	2.6	2.6	2.7	2.7	2.6	3	2.5	2.6	2.2	2.6	2.7
Conduc. (umo/cm)	2570	2870	2510	2600	1830	2530	2450	2510	2480	2560	2530	2620	2580	2590	2450	2780	2640	2390	2030	2630	2570	2550	2130	2110	2250	2290
Acidity (mg/L CaCO3)	1200	1100	950	1010	1100	1150	1150	1110	1020	1134	1188	1235	1176	1229	1264	1187	1187	1053	783	1072	1096	1179	861	847	831	935
Acid (lbs/d)	na	505	1088	568	400	330	254	213	165	165	161	157	140	142	135	125	143	251	786	589	453	523	971	909	734	500
Fe-tot (mg/L)	200	192	156	166	175	166	189	158	195	202	201	229	233	238	224	220	229	190	140	190	190	220	147	148	140	162
Mn (mg/L)	24.3	29.3	24.5	25.1	25	24.1	23.6	22.4	23.78	23.8	24	25.3	27.2	24.7	27.2	24.6	24.7	22	16	24	25	25	21.3	21.4	21.3	23.6
Al (mg/L)	79.1	80.8	64.5	70.5	75.1	76	77.2	78.3	71.2	74.5	71.75	90	95.6	96.8	98.3	96.6	95.2	80	53	75	73	83	53.7	51.9	52.1	58.6
Ca (mg/L)	198	189	149	161	178	182	187	185	182	190	192	219	229	236	238	235	233	190	120	170	160	190	119	114	112	133
Mg (mg/L)	95.1	105	80.55	84.9	84.9	94.8	93.1	91.6	96.1	95.3	94.8	98.3	110.2	112.5	114.1	120	119	87	52	87	92	95	68.6	66.6	65.8	75.9
SO4 (mg/L)	1740	2080	1850	1530	1500	1631	1471	2190	1600	1524	1788	1527	1894	2156	2156	1631	1839	1600	1100	1600	1700	1600	1223	1112	1179	1190
As (mg/L)	0.82	0.92	0.75	0.79	0.82	0.87	0.88	0.81	0.82	0.81	0.91	0.85	0.84	0.76	0.87	0.85	0.79	0.71	0.55	0.72	0.7	0.82	0.59	0.57	0.61	0.62
Se (mg/L)	0.69	0.71	0.57	0.63	0.62	0.68	0.75	0.54	0.65	0.62	0.67	0.59	0.62	0.84	0.78	0.57	0.75	0.44	0.3	0.6	0.63	0.57	0.5	0.52	0.44	0.5
Pb (mg/L)	0.27	0.28	0.23	0.24	0.24	0.27	0.25	0.24	0.34	0.33	0.34	0.3	0.33	0.31	0.33	0.27	0.32	0.21	0.17	0.19	0.23	0.25	0.22	0.21	0.2	0.2
Ba (mg/L)	<0.05	<0.05	<0.05	<0.05	<.05	<.05	<.05	<0.05	<.05	<.05	<.05	<.05	<0.05	<0.05	<0.05	<0.05	<0.05	<0.05	<0.05	<0.05	<0.05	<0.05	<0.05	<0.05	<0.05	<0.05
Cd (mg/L)	<0.05	<0.05	<0.05	<0.05	<.05	<.05	<.05	<0.05	<.05	<.05	<.05	<.05	<0.05	<0.05	<0.05	<0.05	<0.05	<0.05	<0.05	<0.05	<0.05	<0.05	<0.05	<0.05	<0.05	<0.05
B (mg/L)	0.22	0.26	0.19	0.14	0.23	0.17	0.2	0.21	0.2	0.2	0.2	0.22	0.23	0.22	0.21	0.21	0.22	0.2	0.13	0.63 (2)	0.19	0.24	0.13	0.13	0.13	0.16

* Data taken from Morgantown Lock & Dam (1) Flow meter not in operation for this sample

na = not available (2) This data judged in error and not used in calculations

sack\patriot.xls

Table 2. Continued

2/12/95	2/17/95	####	###	####	####	####	4/1/95	4/8/95	4/15/95	4/22/95	####	5/6/95	5/14/95	5/21/95	5/27/95	6/6/95	6/13/95	6/21/95	7/19/95	7/26/95	8/02/95	8/10/95	8/16/95	8/23/95	9/1/95	9/5/95	9/16/95	9/23/95	9/30/95
27	28	29	30	31	32	33	34	35	36	37	38	39	40 (1)	41 (1)	42 (1)	43 (1)	44	45 (1)	46	47	48	49	50	51	52	53	54	55	56
37.63	31.09	121.4	106.8	95.53	89.97	55.49	43.76	31.82	27.6	29.74	35.95	70.94	na	na	na	na	25.2	na	12.53	11.62	11.19	10.8	13	12.4	11.2	10.2	9.74	9.34	8.97
9	10	10	10	10	10	10	10	10	10	10	10	10	10	10	10	10	10	10	10	10	10	10	11	11	10	11	10	9	10
0.17*	0.63	0.54	0.54	0.64	0	0.64	0.15	0.2	0.67	0.23	0.77	1.03	1.59	1.46	0.16	0.5*	1.36*	0	0.82*	0.03	0.41	3.34*	0.43*	0.2	0.01	0	0.47*	2.44	0
3	3	2.7	2.7	2.7	2.7	2.7	2.7	2.83	2.9	2.8	2.7	2.7	2.7	2.5	2.5	2.9	2.7	2.7	2.74	2.72	2.74	2.71	2.69	2.69	2.69	2.73	2.61	2.69	2.8
2620	2390	2130	2250	2240	2240	2190	2200	2350	2200	2160	2190	2090	2090	1893	2010	1100	2000	1200 (2)	2780	2650	2720	2870	2650	3010	2910	3130	3310	2630	2740
959	956	753	754	693	694	823	844	888	898	870	1176	835	785	727	866	360	920	940	1002	1006	1035	1097	1151	1124	1124	907	1014	985	1221
433	357	1098	967	795	750	548	444	339	297	311	508	711	na	na	na	na	278	na	151	143	139	142	180	167	151	111	119	110	132
168	166	125	104	109	100	139	163	175	147	141	161	143	133	111	141	60.2	164	182	173	173	161	176	197	186	192	193	144	144	210
23.3	23.2	16.9	17.3	17.5	17.8	19	19.1	24.3	19.2	10.6	20.3	17.6	17.4	14.9	19.5	7.9	20.6	20.9	19	19.4	19.6	20.2	21.2	22	21.4	21.7	21.9	21.9	22.4
59.3	70.2	46.6	50.4	50.9	53	51.9	53.4	57.4	56.4	55	63.8	76.9	72.4	47	60.7	24.4	63.7	66.4	72.4	73.7	73.7	79.7	81.1	85.2	88.4	89.5	91.1	92.2	94.7
138	157	93	96.4	104	102	126	135	147	140	141	148	135	119	92	127	116	147	152	170	174	174	184	190	193	198	200	207	213	220
77.3	84.2	59	56.9	65	124	69.1	69.6	72.7	68.4	66.1	77.2	64.9	58.1	51.4	69	31.4	78.3	80	82.6	83.5	83.7	89.5	92.6	98.4	98.6	97.4	100	102	103
1329	1365	1360	1320	1390	1430	1580	1600	1850	1070	1120	1525	1409	1355	1173	1464	880	1900	1900	1639	1746	1788	1760	1840	2128	2188	2226	2102	2332	2372
0.65	0.64	0.48	0.56	0.57	0.64	0.71	0.77	0.77	0.73	0.7	0.54	0.46	0.42	0.33	0.59	0.24	0.6	0.9	0.59	0.67	0.73	0.68	0.74	0.77	0.85	0.7	0.73	0.7	0.81
0.56	0.55	0.4	0.49	0.48	0.58	0.49	0.53	0.53	0.45	0.48	0.54	0.48	0.48	0.39	0.63	0.32	0.59	0.6	0.63	0.63	0.55	0.64	0.6	0.53	0.67	0.61	0.63	0.63	0.63
0.25	0.29	0.19	0.22	0.27	0.19	0.21	0.2	0.25	0.25	0.26	0.18	0.12	0.13	0.14	0.18	0.09	0.27	0.28	0.24	0.25	0.24	0.24	0.29	0.27	0.32	0.32	0.31	0.3	0.37
<0.05	<0.05	<0.05	<0.05	<0.05	<0.05	<0.05	<0.05	<0.05	<0.05	<0.05	<0.05	<0.05	<0.05	<0.05	<0.05	<0.05	<0.05	<0.05	<0.05	<0.05	<0.05	<0.05	<0.05	<0.05	<0.05	<0.05	<0.05	<0.05	<0.05
<0.05	<0.05	<0.05	<0.05	<0.05	<0.05	<0.05	<0.05	<0.05	<0.05	<0.05	<0.05	<0.05	<0.05	<0.05	<0.05	<0.05	<0.05	<0.05	<0.05	<0.05	<0.05	<0.05	<0.05	<0.05	<0.05	<0.05	<0.05	<0.05	<0.05
0.19	0.2	0.1	0.07	0.07	0.07	0.13	0.13	0.15	0.16	0.17	0.19	0.15	0.12	0.08	0.1	0.06	0.16	0.17	0.15	0.15	0.15	0.16	0.16	0.16	0.22	0.2	0.17	0.17	0.22

Q11

Table 3. Summary Data-Longridge Mine

Parameter	Average	Range
Flow (gpm)	36.19	8.79-121.4
Temp (C)	9.8	8-11
Precipitation (inches)	0.62	0-4.52
pH	2.68	2.40-3.00
Conduc. (umo/cm)	2457	1830-3310
Acidity (mg/L CaCO3)	1002	693-1264
Acid (lbs/d)	360	110-1098
Fe-tot (mg/L)	171.0	100-238
Mn (mg/L)	21.80	14.9-29.9
Al (mg/L)	71.80	46.6-98.3
Ca (mg/L)	165.7	92-238
Mg (mg/L)	85.50	51.4-124.0
SO4 (mg/L)	1648.6	1070-2372
As (mg/L)	0.711	0.33-0.92
Se (mg/L)	0.577	0.30-0.75
Pb (mg/L)	0.251	0.12-0.37
Ba (mg/L)	<0.05	<0.05
Cd (mg/L)	<0.05	<0.05
B (mg/L)	0.170	0.07-0.26

Figure 61. Flow Vs Sample # and Month

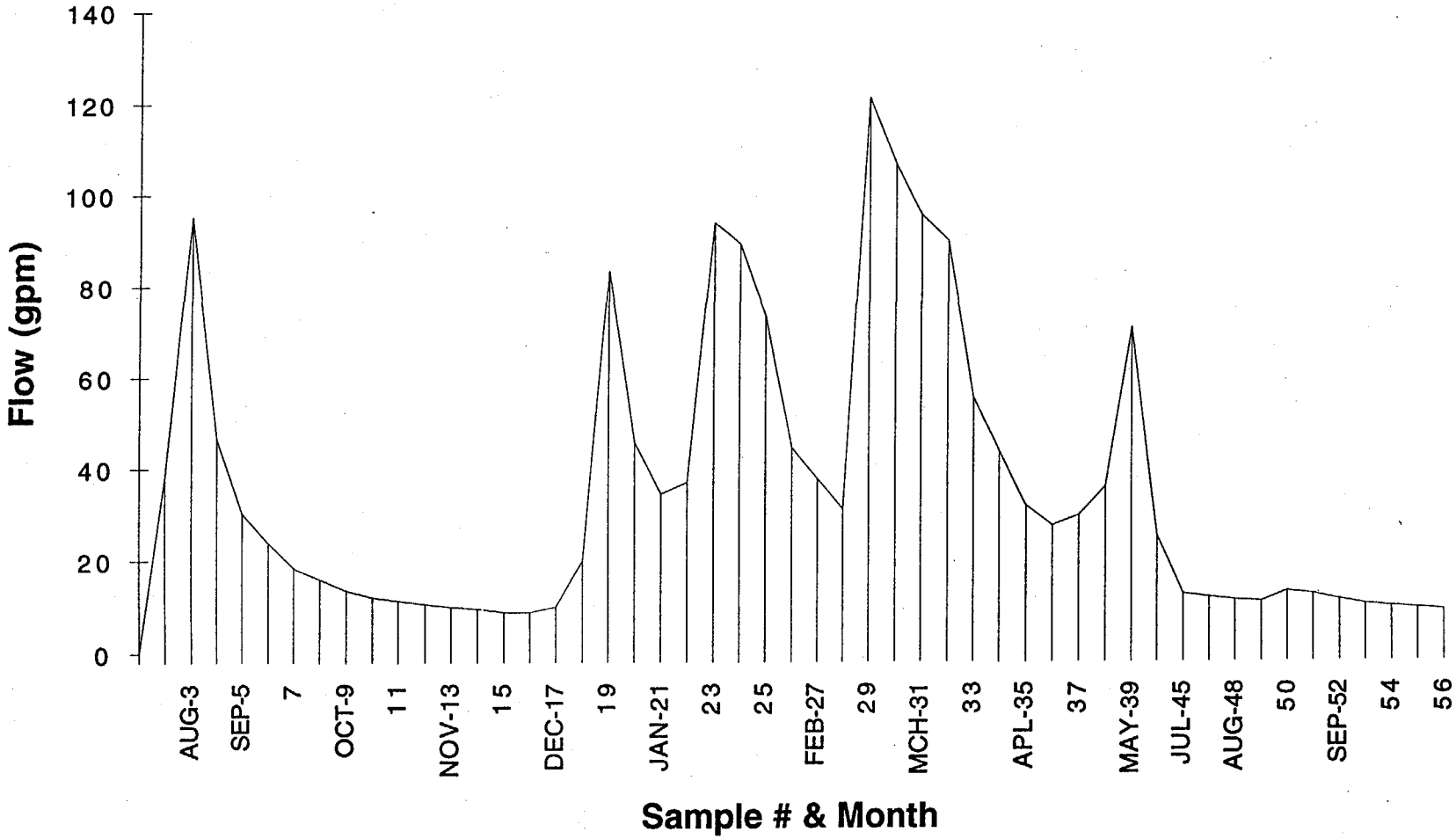

and early winter and producing low flows of 8 to 9 gpm. An example of a daily chart showing flow data (week of 3/18/95 to 3/25/95 (sample 33) is shown in Figure 62. It may be noted that the flow did not vary significantly during the week. Figures 63 and 64 present plots of rainfall intensity and the cumulative total as a function of time for the same period. It may be noted that 0.41 inches of precipitation occurred during the week. The rainfall was not sufficient to make a marked change in the AMD flow as may be seen from Figure 62.

As shown in Tables 2 and 3, rainfall rates varied from 0 to 4.52 inches per week. Unfortunately, the unheated rain gauge at the site was out of service for a number of weeks in the winter due to freezing. It also malfunctioned a few times during warmer weather with loss of data. For weeks where precipitation at the site was unavailable, precipitation records for the Morgantown Lock and Dam (MLD) are provided as indicated by an asterisk on Table 2. The Morgantown Lock and Dam Station is about 20 air miles from the site. Since storms can be very localized, especially in the summer period, it is not felt that the data from the MLD are truly reflective of the precipitation received at the site. A search is being made for an alternative precipitation station closer to the site for use in Phase 2 when the precipitation gauge at the site may not be functioning.

Water Quality Analysis and Parameter Interrelationships

Examination of Tables 2 and 3 shows that the AMD from the Longridge Mine has pH values ranging from 2.4 to 3.0 and an average acidity of 1002 mg/L (range; 693-1264 mg/L). Other important parameters include iron, sulfate, and aluminum averaging respectively 171 (range; 100-238), 1649 mg/L (range; 1070-2372), and 72 mg/L (range; 47-98). It is difficult to define an "average" quality AMD since quality varies with many factors. These include the particular coal seam and character of the surrounding strata, age of the mine and whether the mine is in an active or an inactive status, availability of oxygen, amount of water flowing through the mine and time of contact of the water with the exposed strata. Skousen and Ziemkiewicz (1995) reported the analysis of AMD samples from four different sites in West Virginia. They found that acidity, iron and sulfate values averaged respectively 1536 mg/L (range; 516-3152) , 409 mg/L (range; 7-1129), and 2472 mg/L (range ; 640-4300). James (1984) sampled 12 different sites for AMD from the Upper Freeport Seam. The average of the mean values from the 12 sites for acidity, aluminum and sulfate were as follows: acidity 808 mg/L (range; 62-1698), aluminum 77 mg/L (range 1 to 169) and sulfate 1509 mg/L (range 384-3426). The values from James may be readily compared to the Phase 1 values noted above since the Longridge Mine is also in the Upper Freeport coal. It may be noted that the Longridge Mine AMD strength falls in the middle to upper end of samples reported by James showing the Longridge AMD to be a typical, to relatively strong AMD for the Upper Freeport formation.

Figure 65 presents mg/L of acidity and iron as a function of flow. The influence of dilution at higher flows is clearly shown as both acidity and iron decrease significantly as flow increases. Over the flow range shown (10 to 120 gpm), the concentration of acidity falls about 38 % while the iron concentration fell about 49 %. While the concentration of the contaminants decreased as flow rose, the actual mass of contaminants released per day actually rose significantly as flow increased. Figure 66 compares acid concentration (mg/L) and acid mass discharged (lbs/d) vs flow. It may be seen that the acid mass entering the environment increased from about 150 lb/d at 10 gpm to about 1150 lbs/d at 120 gpm showing an almost 8 fold increase. It is interesting to note that James (1984) did not find a consistent trend when AMD parameters were plotted against flow. However, the author reported a variety of problems in obtained in obtaining reliable flow measurements. In addition, the Phase 1 samples are from a single mine while the samples that James collected were from 12 different sites.

As might be expected, most constituents rose and fell together from sample to sample. That is, a sample with a high concentration of acidity would also have a relatively high concentration of sulfate. Figure 67 compares the concentration of acidity, sulfate and iron as a function of sample #. It may be noted that there is a general tendency for the contaminants to rise and fall together. This trend is shown clearly in Figures 68 to 70. Figures 68 and 69 present the correlation between aluminum and sulfate and iron and acidity respectively. While there is a significant amount of scatter, the trends are unmistakable with the contaminants rising or falling together. A similar correlation is shown between calcium, iron and aluminum in Figure 70.

The AMD from the Longridge Mine also contains environmentally significant levels of trace elements. As shown in Table 3, the average arsenic, selenium, lead and boron concentrations were found to be 0.71, 0.58, 0.25, and 0.17 mg/L respectively. The trace elements also varied greatly with flow as shown in Figure 71 where arsenic, selenium and lead concentrations are presented as a function of flow. For example, it may be noted that lead fell from about 0.3 mg/L at 10 gpm to approximately 0.17 at 120 gpm for a reduction of about 43 %. As flow increased arsenic and selenium also fell off about 34 % each. These reductions in trace element concentration with flow are similar to those noted for the major AMD constituents above. While concentration decreased with flow, the actual mass rate of trace elements release actually increased with flow as depicted in Figure 72. It may be noted that the lbs/d of lead leaving the mine increased about 8 fold as flow increased from 10 to 120 gpm. Figure 73 presents the compares the concentration of three trace elements with acidity. It may be noted that all three trace metals (As, Se, & Pb) tend to increase in concentration as acidity increases.

Figure 62. Running Rain Fall Total: Week 48

Saved Recorder Status

Type: 674L-8K Range:-0.00 - 2.55 inches Recorder ID: 0001
Time at Recorder: 08/02/95 18:41:36 Accum Reset @:07/26/95 19:06:35
Signal process: Not Applicable Accum: 0.41 inches
Values being saved: Totals

Totalizing period: 00:02:30 Amount of data recorded: 6 days 23:37:30

Storage Capacity: 8140 values records: 14 days 03:10:00 Prescaler: 1
Output compressed by a factor of 100

Date	Time	Avg inches	Period Total	Running Total
07/26/95	19:04:05	-0.00	-0.00	-0.00 *
[illegible]/26/95	23:14:05	-0.00	-0.00	-0.00 *
[illegible]/27/95	03:24:05	-0.00	-0.00	-0.00 *
07/27/95	07:34:05	-0.00	-0.00	-0.00 *
[illegible]7/27/95	11:44:05	-0.00	-0.00	-0.00 *
[illegible]/27/95	15:54:05	-0.00	-0.00	-0.00 *
[illegible]7/27/95	20:04:05	-0.00	-0.00	-0.00 *
07/28/95	00:14:05	-0.00	-0.00	-0.00 *
[illegible]/28/95	04:24:05	-0.00	-0.00	-0.00 *
[illegible]/28/95	08:34:05	0.00	0.12	0.12 *
07/28/95	12:44:05	-0.00	-0.00	0.12 *
[illegible]/28/95	16:54:05	0.00	0.01	0.13 *
[illegible]/28/95	21:04:05	0.00	0.01	0.14 *
07/29/95	01:14:05	0.00	0.12	0.26 *
[illegible]7/29/95	05:24:05	0.00	0.10	0.36 *
[illegible]/29/95	09:34:05	0.00	0.01	0.37 *
[illegible]7/29/95	13:44:05	-0.00	-0.00	0.37 *
07/29/95	17:54:05	-0.00	-0.00	0.37 *
[illegible]7/29/95	22:04:05	-0.00	-0.00	0.37 *
[illegible]7/30/95	02:14:05	-0.00	-0.00	0.37 *
07/30/95	06:24:05	-0.00	-0.00	0.37 *
[illegible]7/30/95	10:34:05	0.00	0.01	0.38 *
7/30/95	14:44:05	-0.00	-0.00	0.38 *
07/30/95	18:54:05	-0.00	-0.00	0.38 *
[illegible]7/30/95	23:04:05	0.00	0.01	0.39 *
7/31/95	03:14:05	-0.00	-0.00	0.39 *
[illegible]7/31/95	07:24:05	-0.00	-0.00	0.39 *
07/31/95	11:34:05	0.00	0.02	0.41 *
7/31/95	15:44:05	-0.00	-0.00	0.41 *
[illegible]7/31/95	19:54:05	-0.00	-0.00	0.41 *
08/01/95	00:04:05	-0.00	-0.00	0.41 *
8/01/95	04:14:05	-0.00	-0.00	0.41 *
8/01/95	08:24:05	-0.00	-0.00	0.41 *
08/01/95	12:34:05	-0.00	-0.00	0.41 *
[illegible]8/01/95	16:44:05	-0.00	-0.00	0.41 *
8/01/95	20:54:05	-0.00	-0.00	0.41 *
[illegible]8/02/95	01:04:05	-0.00	-0.00	0.41 *
08/02/95	05:14:05	-0.00	-0.00	0.41 *
8/02/95	09:24:05	-0.00	-0.00	0.41 *
[illegible]8/02/95	13:34:05	-0.00	-0.00	0.41 *

Figure63. Flow Data; Sample 48

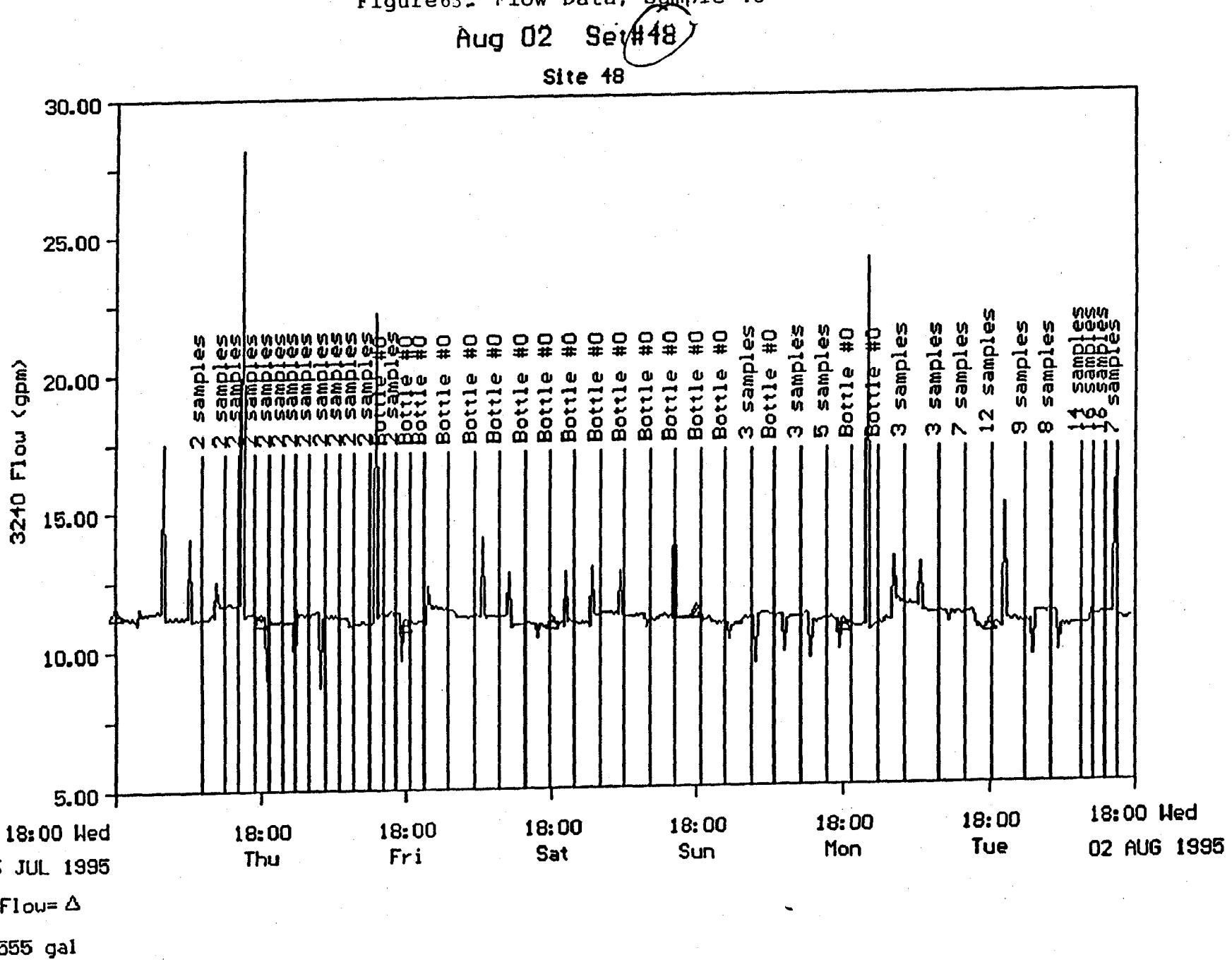

Figure 64. Rain Fall Plot; Week 48

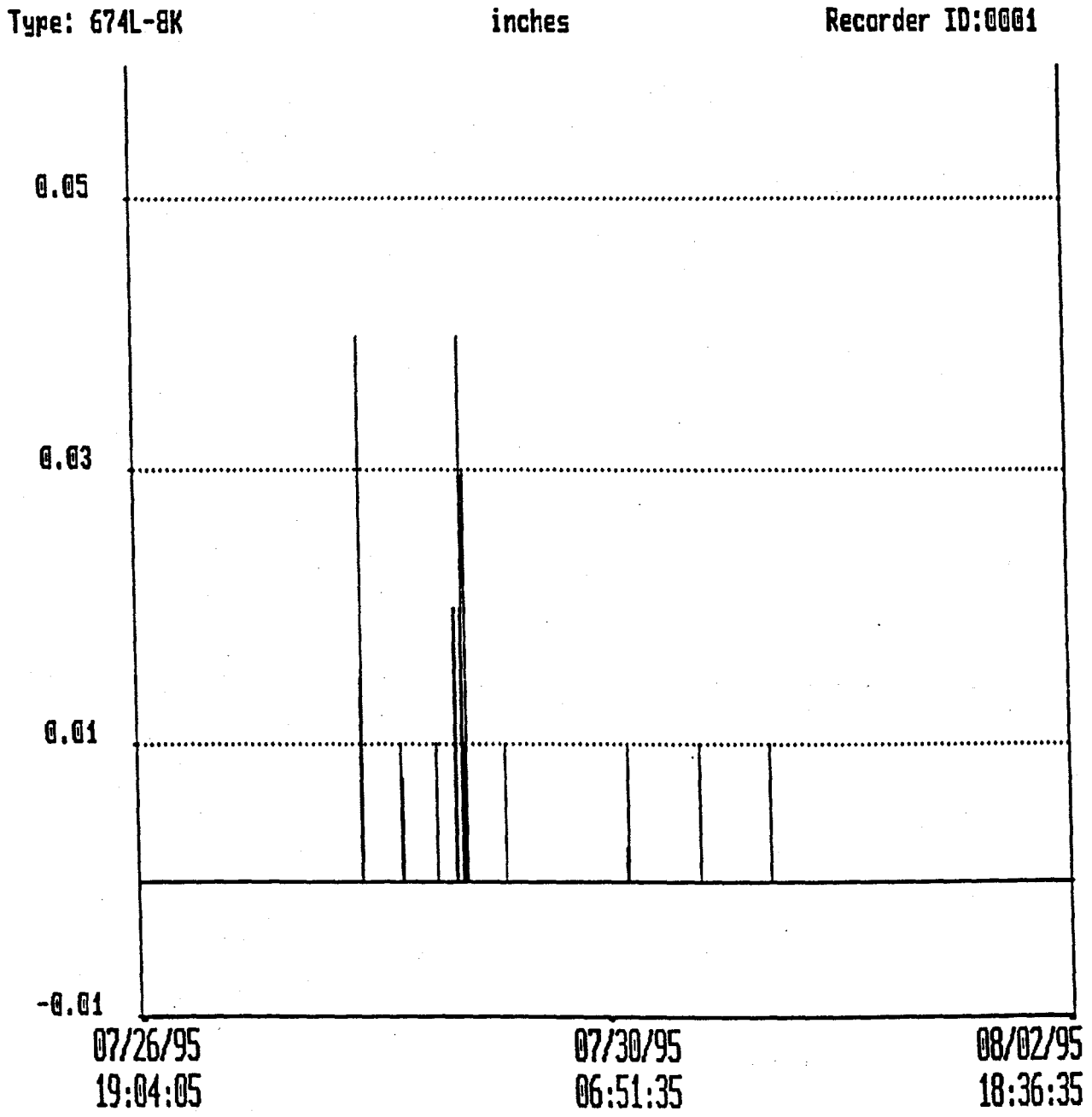

Figure 65. Flow Vs Acidity & Fe

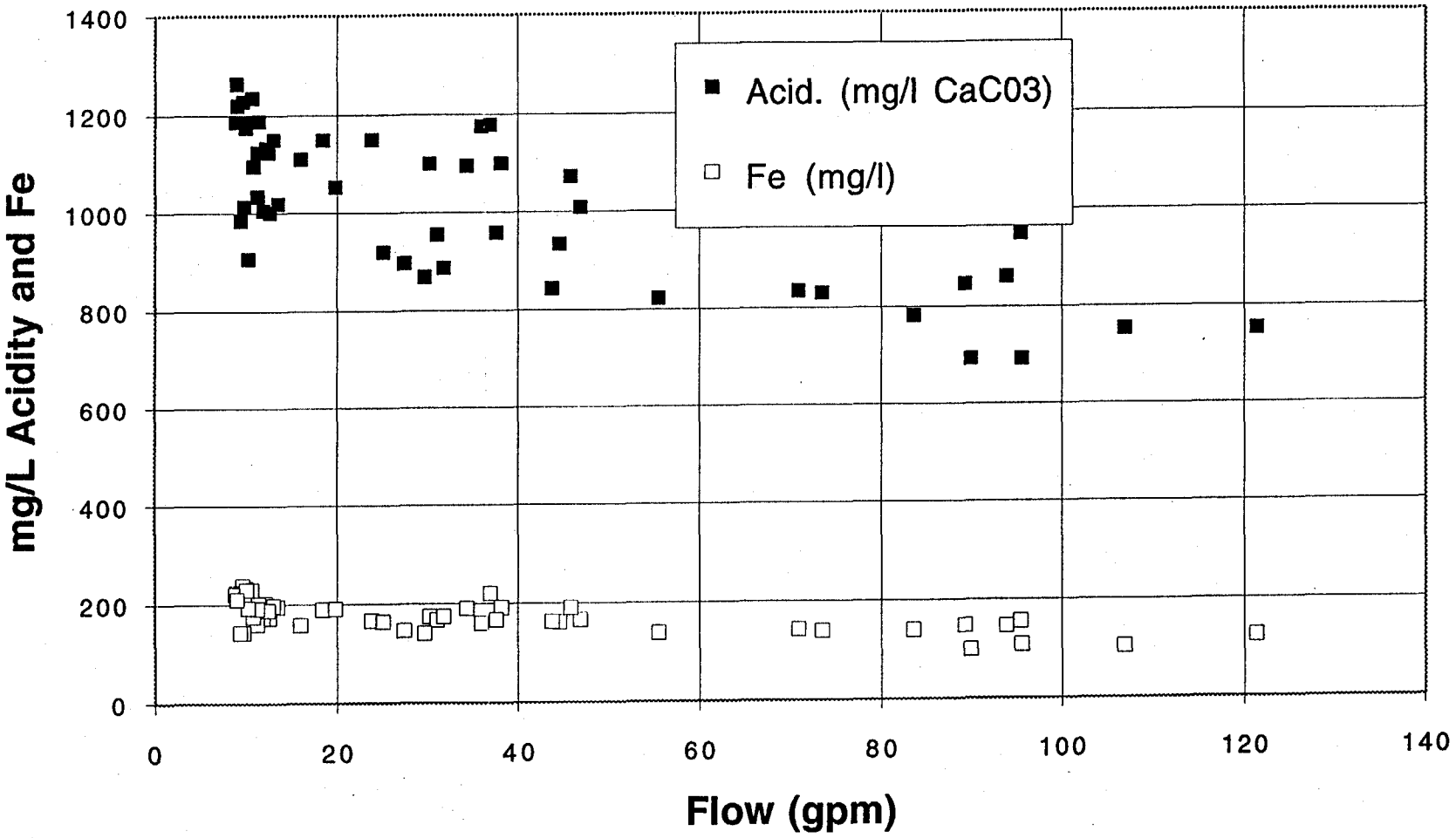

Figure 66. Flow Vs Acid Concentration & Acid Mass

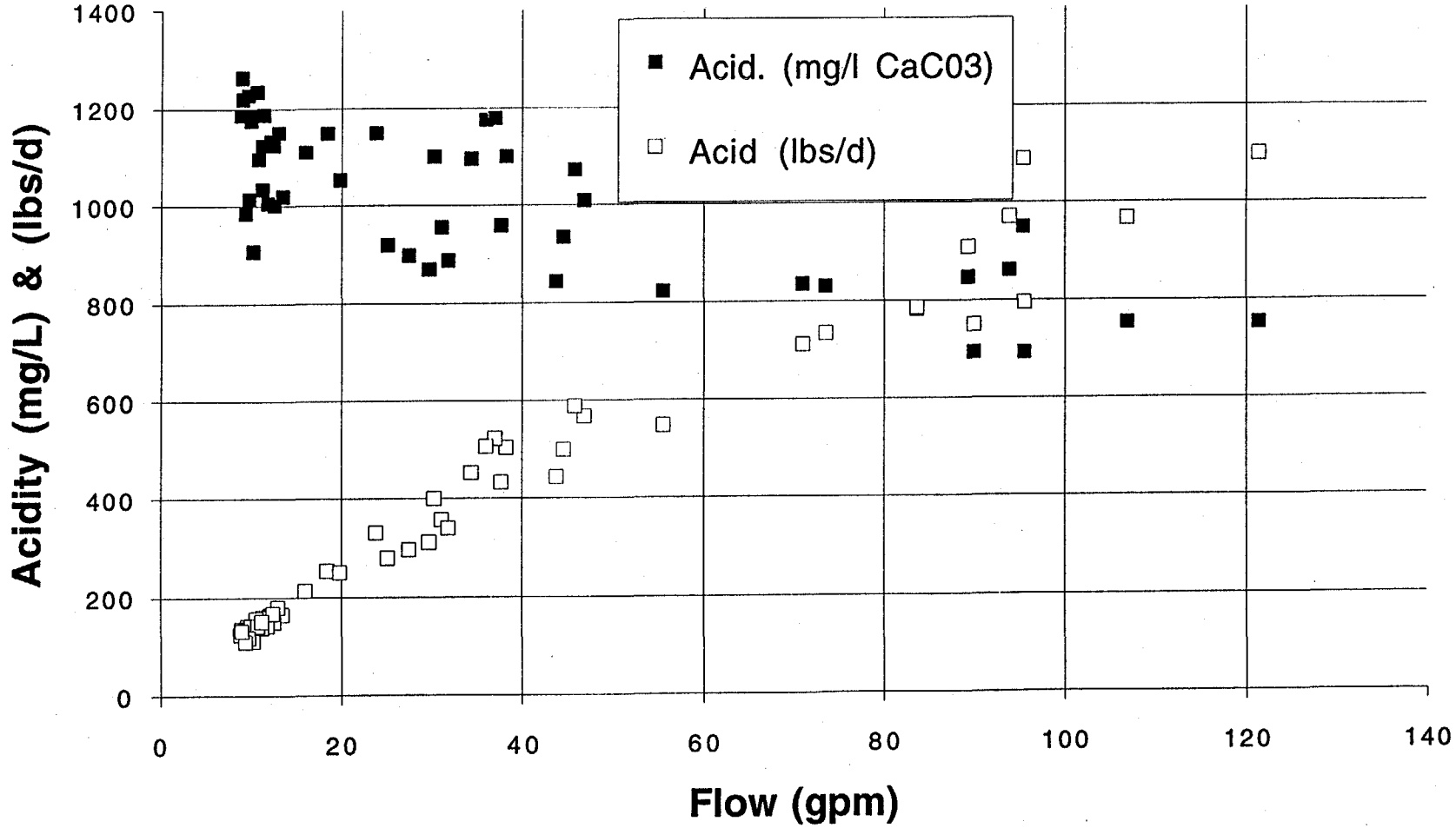

Figure 67. Acidity, Sulfate & Iron Vs Sample

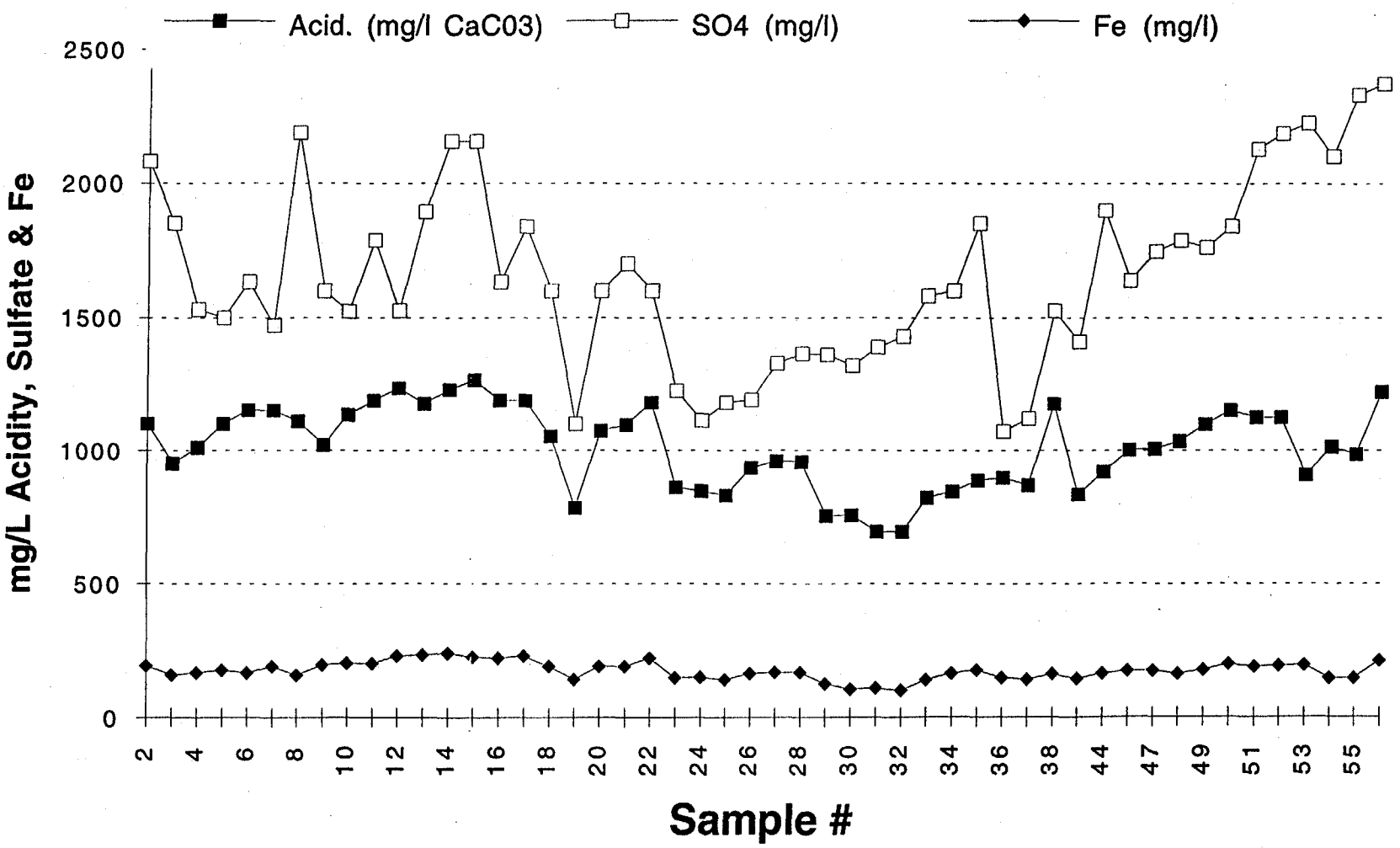

Figure 68. Al Vs Sulfate

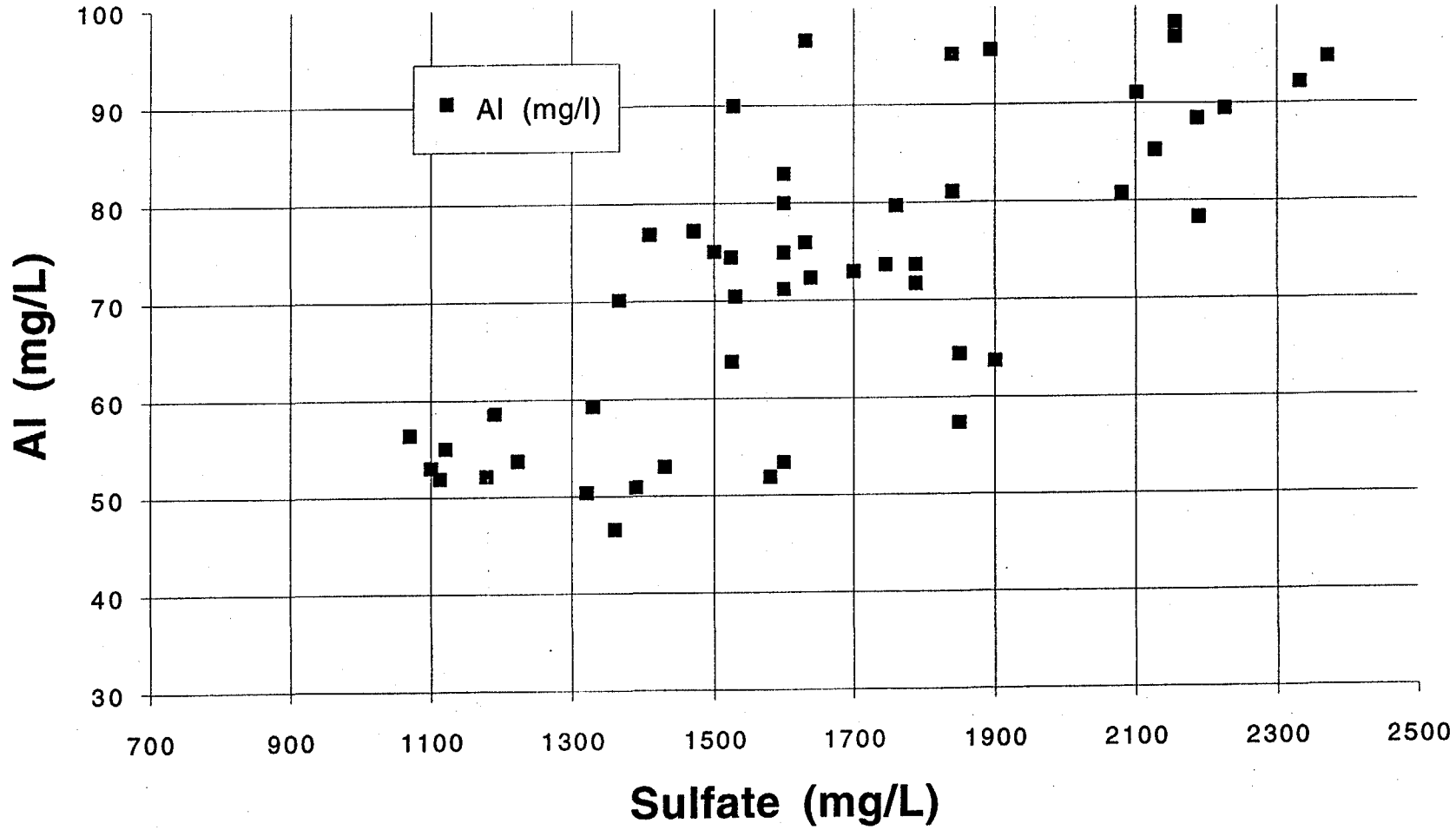

Figure 69. Iron Vs Acidity

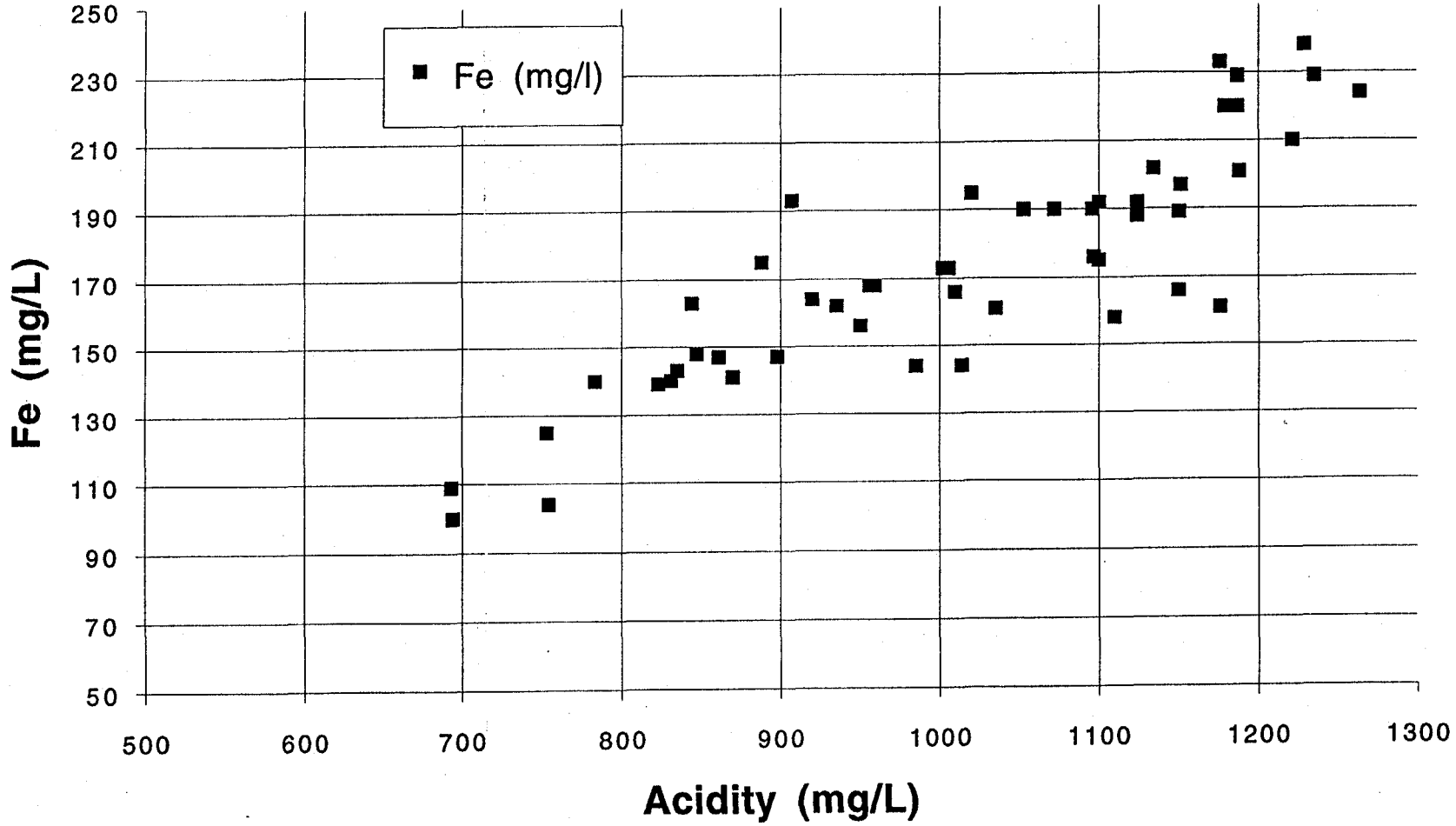

Figure 70. Ca, Fe, & Al Vs Sample

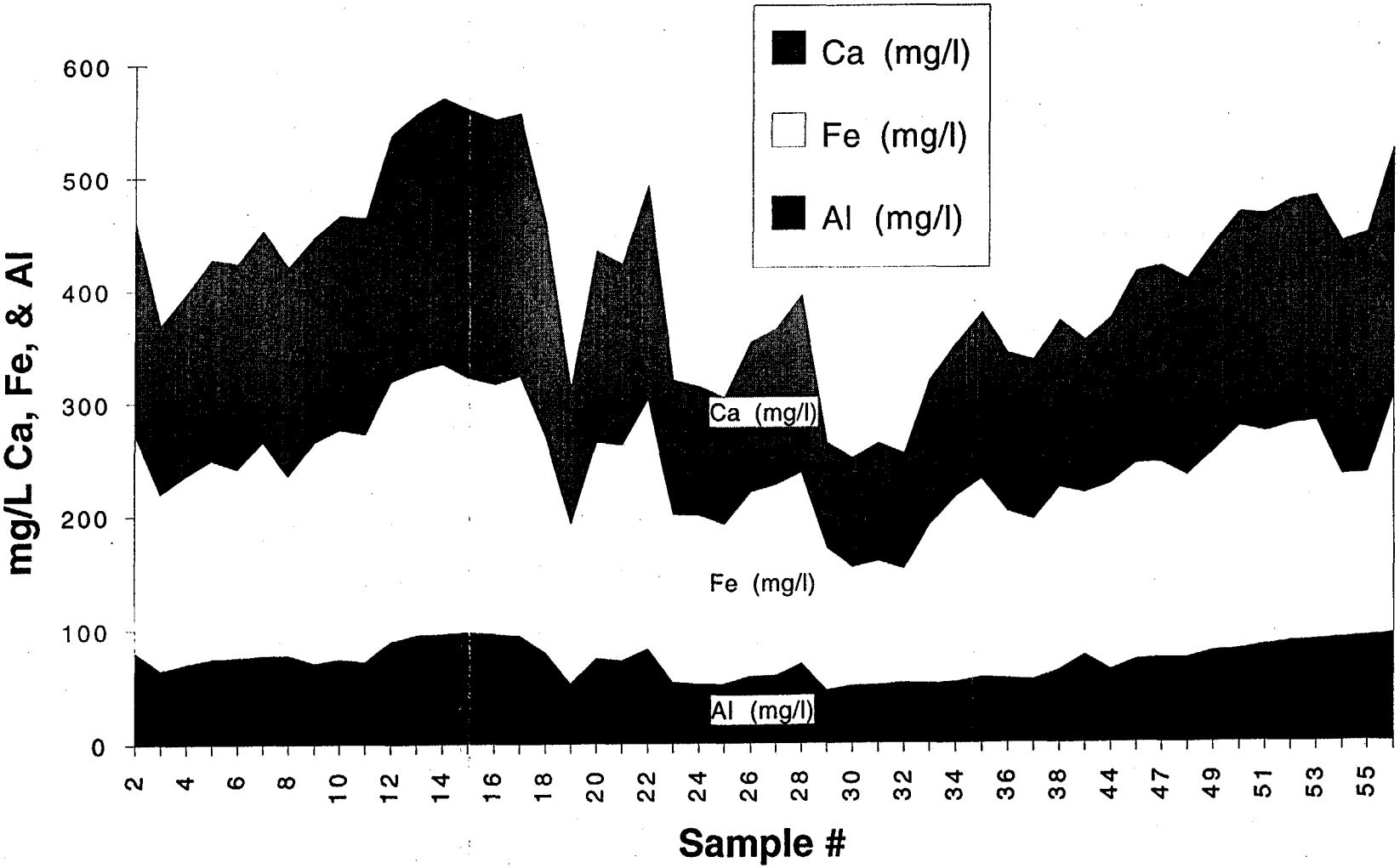

Figure 71. Flow Vs As, Se, & Pb

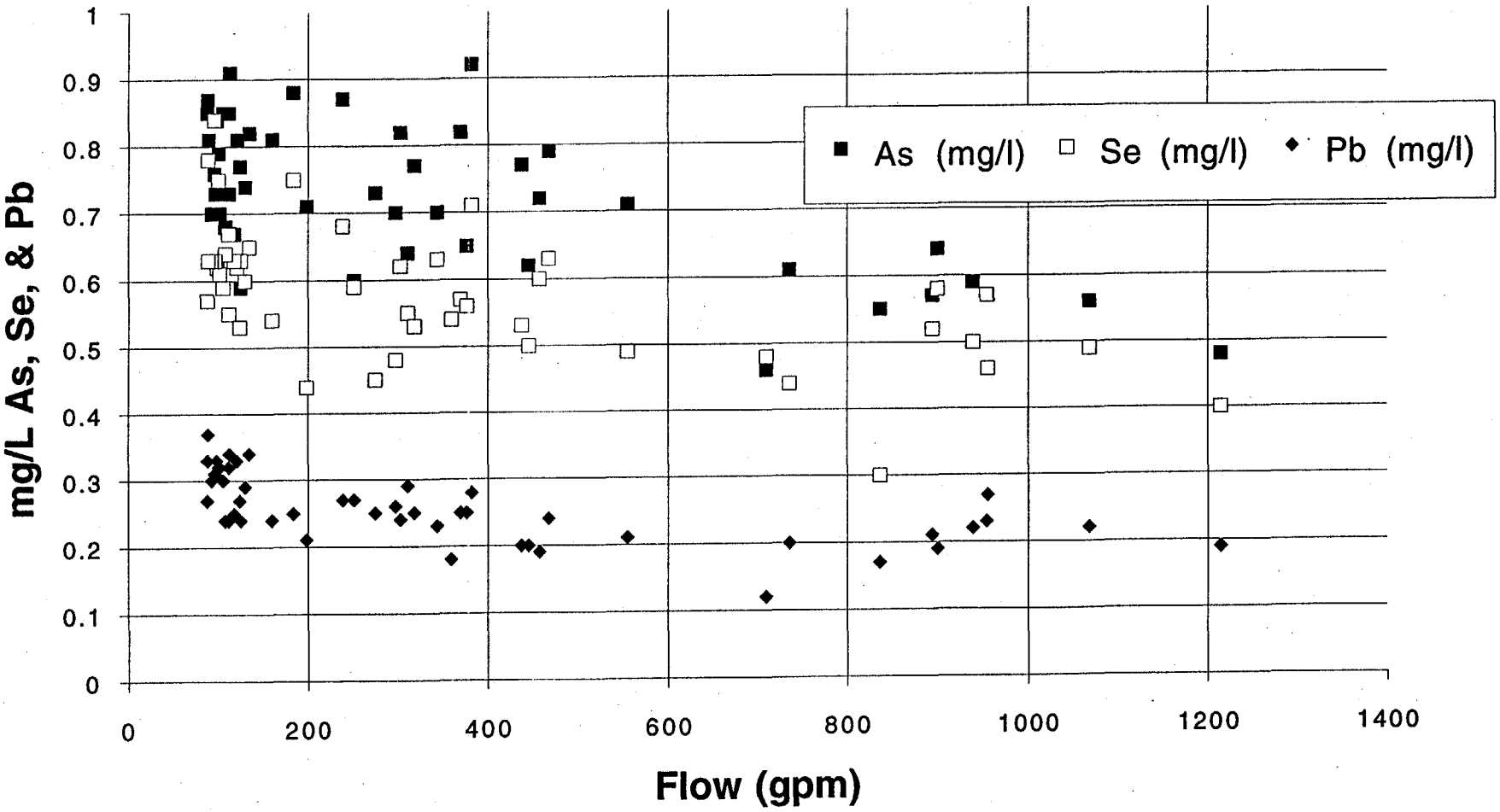

Figure 72. Flow Vs Pb Concentration and Pb Mass

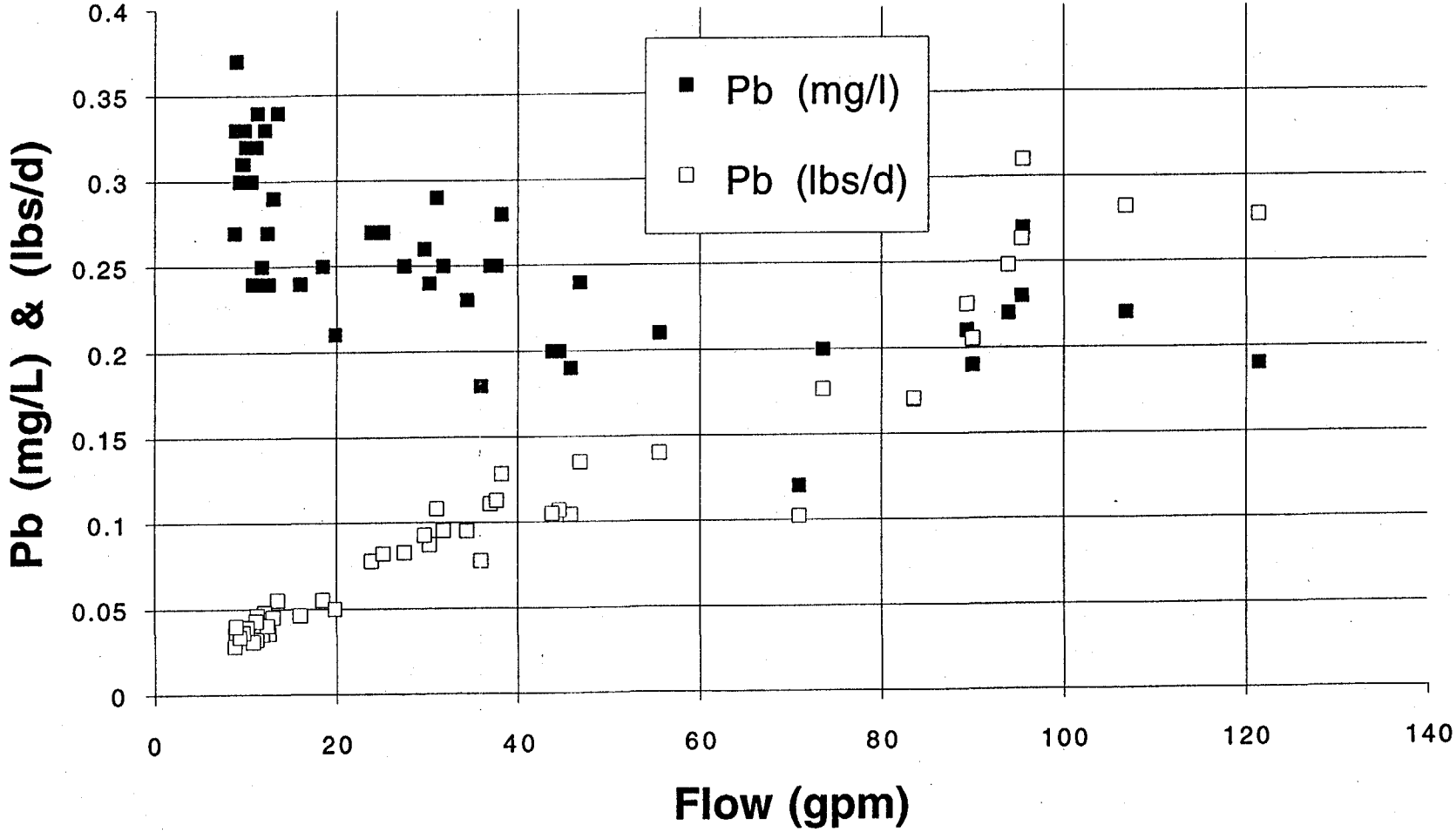

Figure 73. As, Se, & Pb Vs Acidity

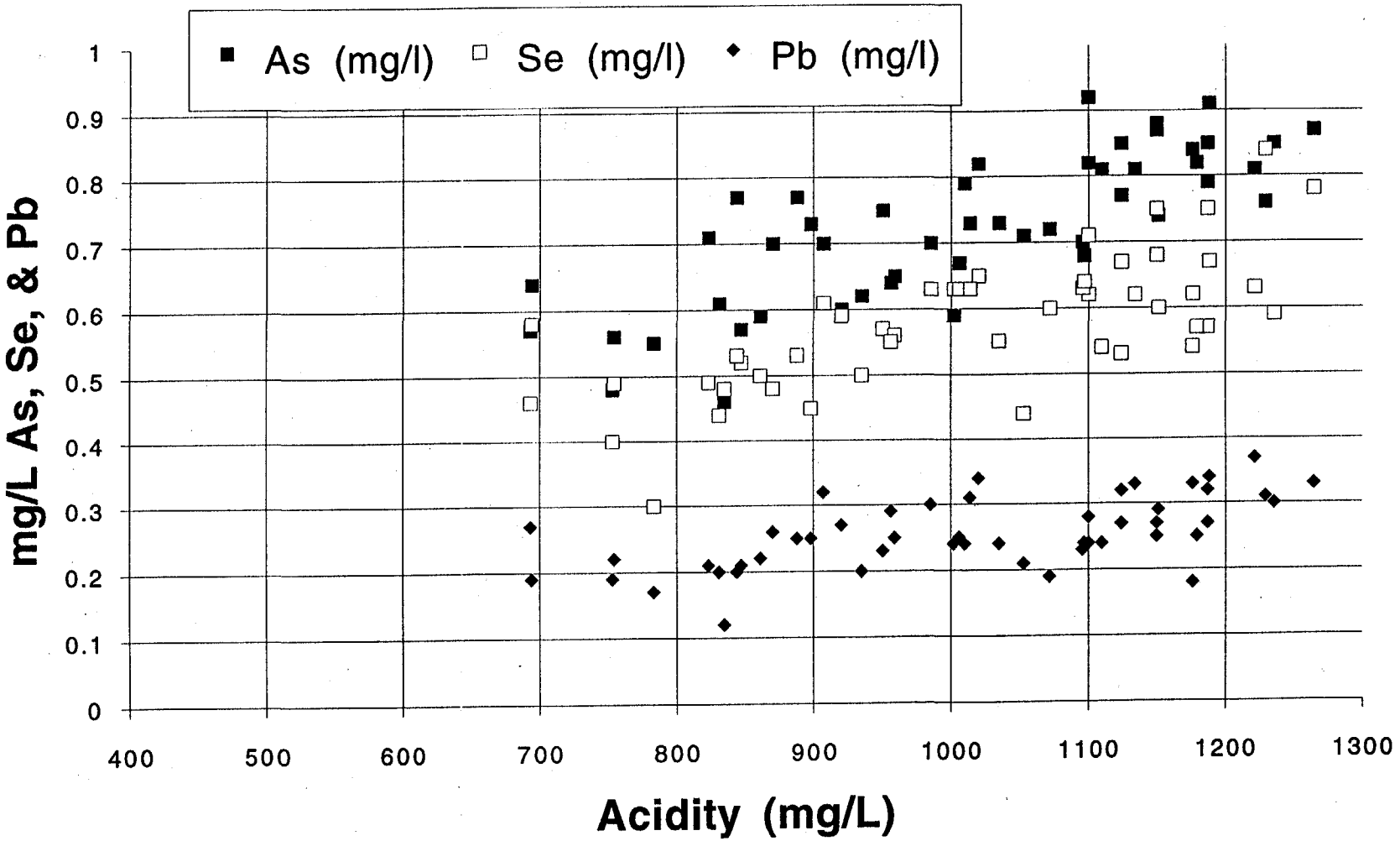

Conclusions

Sampling during the Phase 1 period has provided a good database of background water quality and quantity. Weekly average flow over the Phase 1 period varied from 8.8 to 121 gpm while precipitation ranged from 0 to 4.52 inches. Analyses of AMD from the Longridge Mine shows it to be typical in quality with respect to published data for AMD from the Upper Freeport Coal Seam. It is a relatively strong AMD with acidity, sulfate and iron averaging 1002, 1649, and 171 mg/L respectively. Environmentally significant trace elements are present including lead, selenium and arsenic levels averaging 0.251, 0.577, and 0.711 mg/L respectively. It was found that the concentration of the water quality parameters decreased significantly as flow increased. For example, the concentrations of acidity and iron fell about 38 and 49 % respectively as flow increased from 10 to 120 gpm. While the concentration of the contaminants fell with increased flow, the actual mass of contaminants released per day actual increased with flow. For example, the there was an 8 fold increase in the lbs/d of lead leaving the mine as the flow increased from 10 to 120 gpm. As may be expected, there was a general trend for the different contaminant concentrations to rise and fall together with changes in flow.

PNUEMATIC INJECTION

TASK 3B DESIGN OF PNUEMATIC ASH INJECTION DEVICE
TASK 3C BENCH-SCALE TESTING OF EJECTOR

Introduction

This project is undertaken to further develop the Burnett Ejector by designing, building and testing an improved supersonic nozzle which will be shockfree flow and to shroud the nozzles so as to induce additional air flow that transports the ash horizontally in the mine void. The project will develop the nozzles and shroud on a bench scale to optimize the performance with the ultimate goal of reducing the required amount of compressed air per ton of ash flow. These task are Tasks 3B and 3C from the Statement of Work for this Contract.

Purpose

The purpose of this work is to reduce the cost of injection of fluidized bed combustion by products into underground mine voids. The goal of this task was to improve the performance of the ejector by redesigning it to use less air for the same stowing capability or to increase the distance the material could be stowed using the same air flow as on the original design.

Background

The original design of the Burnett Ejector developed for the U.S. Bureau of Mines (*Burnett*) was tested on a NMLRC contract (*Burnett and Black*). The results of this project indicated that pneumatic injection of fluidized bed combustion by products into underground mines could be very cost effective and environmentally sound. Although the system appeared to be cost effective, it was known that the system could be further developed to reduce the highest cost element of the system operation, the cost of compressed air.

Methodology

The original ejector design tested on the NMLRC contract was designed for stowing gravel into underground mines through boreholes. It was meant to be a very simple low cost device. The supersonic nozzle design used on this ejector was a simple converging-diverging nozzle. This type of nozzle is simple to manufacture, but it has certain deficiencies. Shockwaves in the expanded flow can cause the flow to exit the nozzle in a non-parallel fashion which is detrimental to maximizing the horizontal distance the stowed material is thrown. To eliminate the shockwaves, the supersonic nozzle was redesigned with a contoured exit section which will insure that the flow is

parallel to the nozzle centerline.

Results and Discussion

Aerodynamic design

The aerodynamic properties of the supersonic nozzle were calculated. Figure 74 shows the nozzle contour design parameters for various mach numbers. The plot shows the nozzle shape downstream of the throat as a function of the throat diameter. For a converging-diverging supersonic nozzle the air is sonic at the throat. Therefore, the flow is determined by the throat radius. The extent of expansion and the mach number of the outlet air is determined by the exit radius and the pressure ratio across the nozzle. The nozzle throat diameter determines the airflow rate through the nozzle for a given pressure ratio. The nozzle throat and outlet diameter can be determined using the following equations. The conditions at the throat are determined from:

$$\frac{P_c}{P_0}=\left[\frac{2}{k+1}\right]^{\frac{k}{(k-1)}} \qquad \frac{\rho_c}{\rho_0}=\left[\frac{2}{k+1}\right]^{\frac{1}{(k-1)}} \qquad c_c=1 \tag{50}$$

Where:
T is the absolute temperature in ^{0}R
k is the specific heat ratio dimensionless
P is the absolute pressure in psi
ρ is the density lbm/ft^3
c is the critical sonic velocity ft/s
V is velocity ft/s
R is the gas constant ft lb/lbm ^{0}R

and the Subscripts:
$_0$ = conditions in the reservoir
$_c$ = critical condition at throat

The mass flow rate is an input variable to this equation set, and the throat area can be calculated from it using:

$$A_c=\frac{\dot{m}_{max}}{\rho_c V_c} \tag{51}$$

Where: m = mass flow rate lbm/s

The outlet area A is determined from the desired mach number using the following equation:

$$A = A_c\left(\frac{1}{M}\left(\frac{5+M^2}{6}\right)\right)^3 \qquad (52)$$

M = mach number at outlet
A = area at outlet

Mechanical design

A drawing of the three nozzles plus the original nozzle design are shown in Figure 75. The contour of the exit section was determined from the parameters shown in Figure 74. The nozzle exit contour was plotted on an Autocad® system and the parts were made directly from this software. All of the nozzles are sized for 50 ft^3/min at 100 psig. The throat diameter for all of the nozzles is 0.1774 in. The exit velocity is designed to be mach 2.1 for the C-V nozzle and nozzle number 1. The design mach number for nozzles 3 and 4 is 1.5 and 2.0 respectively. Performance of nozzles 1,2 and 3 provide an exit flow that is straight and parallel to the nozzle centerline.

Nozzle tests

A test fixture, shown in Figure 76, was designed to allow comparison of the original designed C-V nozzle and the new contoured nozzles. Thrust of each nozzle was measured on the test fixture by recording the load measured by the scale. The expected thrust of nozzle design number one was 3.38 lb-force/nozzle.

The test results of the four nozzles are shown in Table 4. All three of the contoured nozzles performed better than the original C-V nozzle design. The original C-V nozzle performed at 92% of its calculated thrust. This is to be expected since the flow coefficient was assumed to be unity, which is not possible. Nozzle number 1 (M=2.1) had 11% greater thrust than the original nozzle design. The other two nozzles had slightly less thrust. Based on these test results it can be concluded that nozzle number 1 (M=2.1) is the design to be used in the next phase of the development.

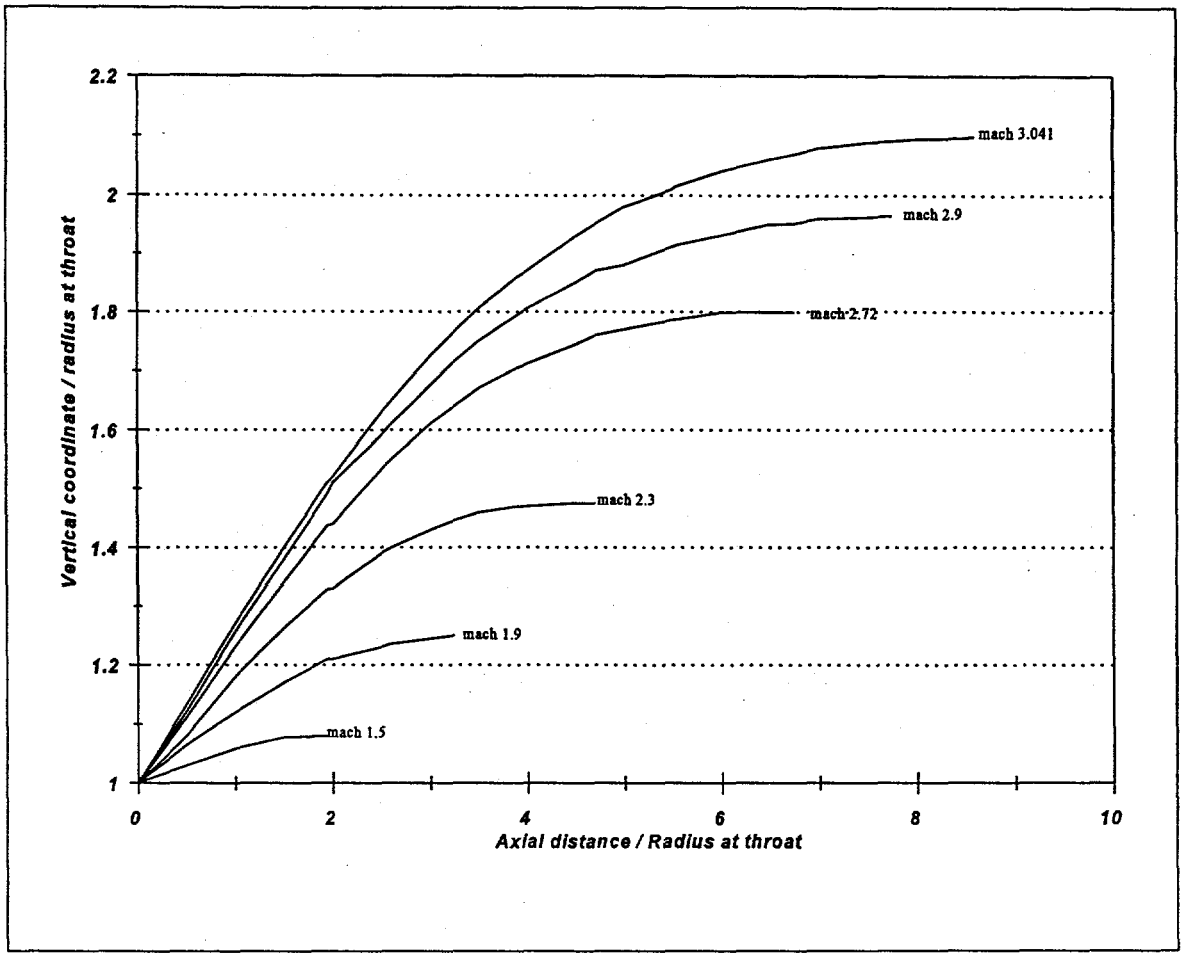

Figure 74 Isentropic nozzle data, wall contour vs. Exit mach number for sharp-cornered, axi-symmetric, isentropic, parallel exit flow nozzles (γ=1.4)

Table 4 Nozzle performance test results

Nozzle	Thrust lb	Ratio of Measured Thrust to Calculated Thrust	Ratio of Measured Thrust of Nozzle Tested to Measured Thrust of Original C-V Nozzle)
C-V (original)	3.05	.920	1.00
1-M=2.1	3.38	.995	1.11
2-M=1.5	3.12	.940	1.02
3-M=2.0	3.20	.960	1.05

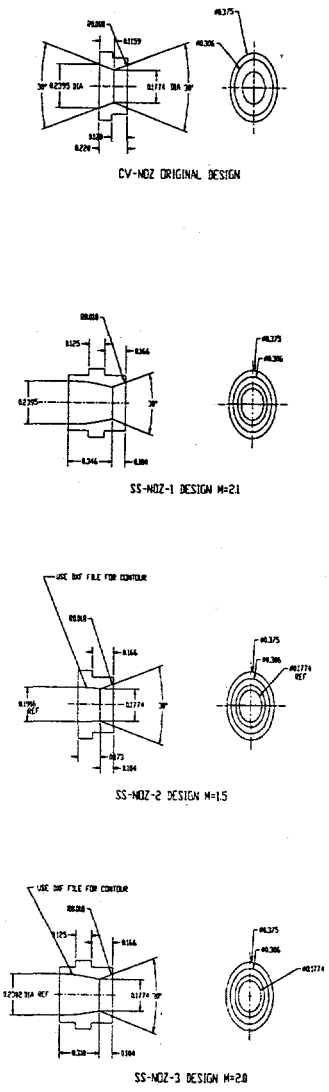

Figure 75 Drawings of the four nozzles designed, built and tested.

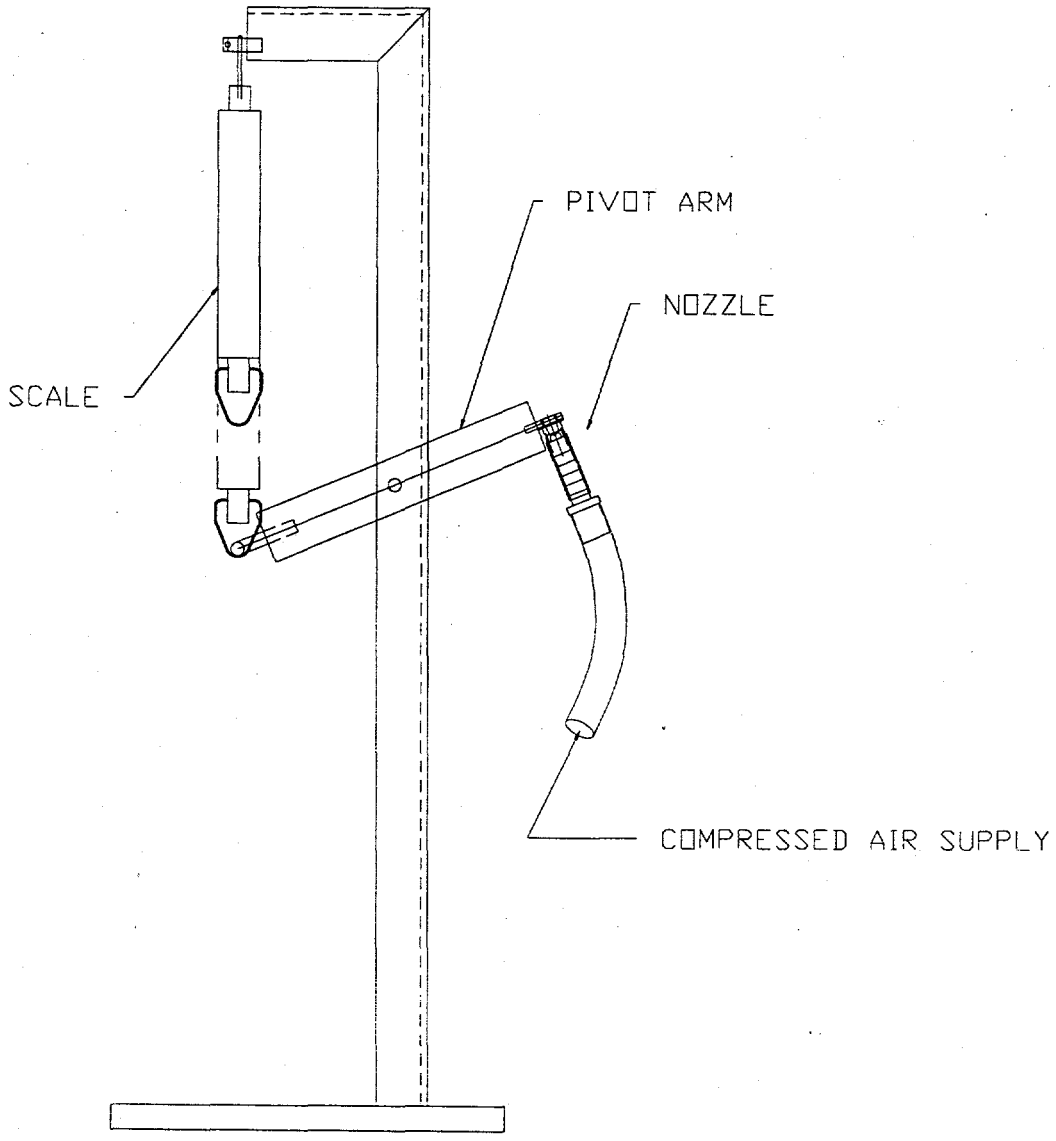

Figure 76 Nozzle Test Fixture.

Ejector design

The ejector uses a high velocity jet of air to intercept the material falling by gravity down the feed pipe. This jet of air in a volume of essentially still air such as found in a mine void will cause circulation of the air in that void. The velocity of this induced circulation, however, is low and needs to be as high as possible for good material transport.

Ejectors have been used for many purposes to move gasses and solids. Air blown through a set of supersonic nozzles mounted in a aerodynamic shroud can increase the total flow by at least a factor of two. That is, the flow through the nozzles induces an equal flow through the shroud. This concept can be applied to the ejector, as shown in Figure 77, to increase the flow of the jet. This additional flow contributes to an increased mass flow of air intercepting the falling material and creates a velocity in the mine void that is sufficient to transport material.

The full scale ejector was conceptually designed and is shown in figure 77. The ejector will have 30 nozzles for a 1,500 cfm ejector. The large number of nozzles is necessary to keep the ejector to a size that will fit down an 8-diam-borehole. The new nozzle L/D ratio (length over nozzle diameter) is significantly longer than the original design which requires scaling down of the nozzle and increasing the number of nozzles to achieve the desired air flow. The large number of nozzles has an additional benefit of insuring an even flow through the shroud which will aid in inducing up to 1,500 cfm of additional air.

Conclusions

The tests of the new contoured nozzles show that a performance improvement can be expected for the complete ejector. The changes to the ejector design will either allow the same stowing performance as the original ejector while using less compressed air or substantially improved stowing performance while using the same compressed air flow as the original ejector. This performance improvement will have a significant benefit to the overall cost of injecting ash in underground mines. Field tests in the spring of 1996 will demonstrate the actual improvement. The two changes over the original ejector design are:

1. improved supersonic nozzle insuring supersonic flow parallel to the nozzle centerline
2. shrouded nozzles allow induced air up to 100% of jet air which will enhance flow of ash in the mine void and allow ash transport to be increased substantially over the 100 ft achieved with the original ejector design.

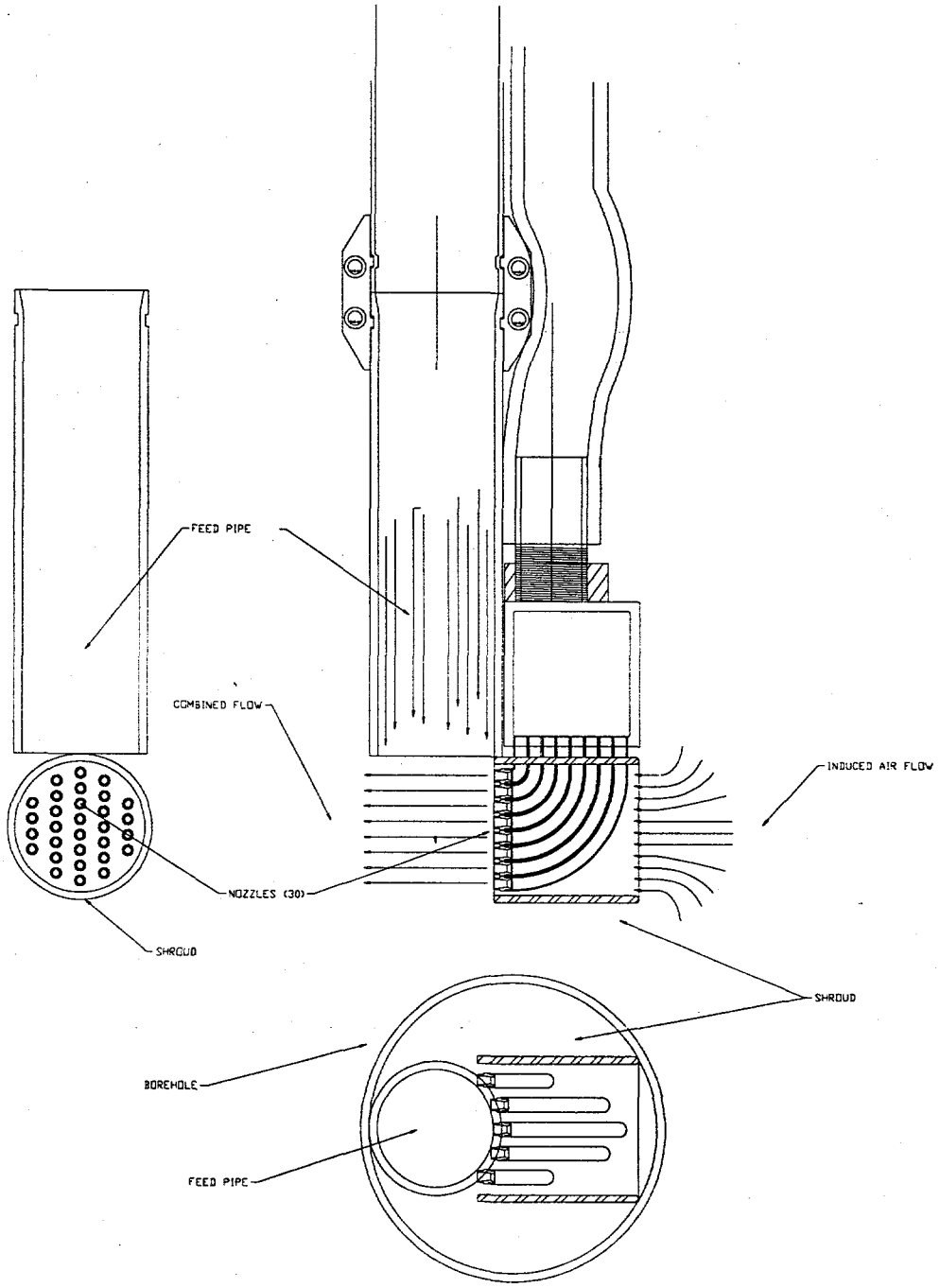

Figure 77 Three View Drawing of the Full Scale Ejector.

TASK 5 SUBSIDENCE CONTROL

Background

Adequate subsidence prediction, proper usage of damage mitigation techniques, rational mine backfill and mine design are essential prerequisites to control or minimize subsidence potential at abandoned and active mines. Inadequate pillar support due to deterioration of pillars causes the overlying strata to cave into the mine voids. This process proceeds upward and finally reaches the surface. In longwall mining, as soon as the mining operations are completed, surface subsidence might occur within a matter of a few days. In room-and-pillar mining, it takes much longer time for surface subsidence to occur. Subsidence is actually a function of the type of overlying strata, the depth of excavation and the method of mining. The present day commercial requirements have forced higher extraction rates and weaker pillar support in the mines thus, paving the way for larger subsidence potential in undermined areas.

In this study, Finite Element analysis was used for adequate subsidence prediction, and for obtaining the strength requirements of backfill grout. In this study, two actual mines were considered; one is referred to as the Fairfax mine while the other one is referred to as the Longridge mine. Figure 78 shows the location of the two mines in the state of WestVirginia. Computation of surface subsidence due to roof collapse was done at both the Fairfax and the Longridge mine. The analyses included a simulation of near total backfill to partial backfill to study the influence of backfill in the control of surface subsidence. Figures 79, 80, 81 and 82 show the location and area of grouting operations at both mine sites. The cross-sections selected for the Finite Element analyses are also shown in these Figures.

The Fairfax mine which is an active mine, is located in the Preston County in the state of WestVirginia. Due to mine voids approximately 225 feet below the surface, there is considerable potential for subsidence. The Longridge mine which is also an abandoned mine is also located in the Preston County, WestVirginia. In this mine, approximately 395,120 sq ft area of mine voids as shown in Figure 82 is to be backfilled. The mine voids are located at a depth of about 80 feet below the surface.

Objectives

The purpose of this project is to find the strength requirements of grout and grout backfill configurations to be used for mitigation of subsidence potential at the Fairfax and Longridge mines. The Finite Element Analysis was used to compute surface subsidence due to roof collapse, at selected cross-sections at both mine sites. The study also includes a comparisional study of the effect of 75%, 90% and 95% backfill of mine voids to control surface subsidence.

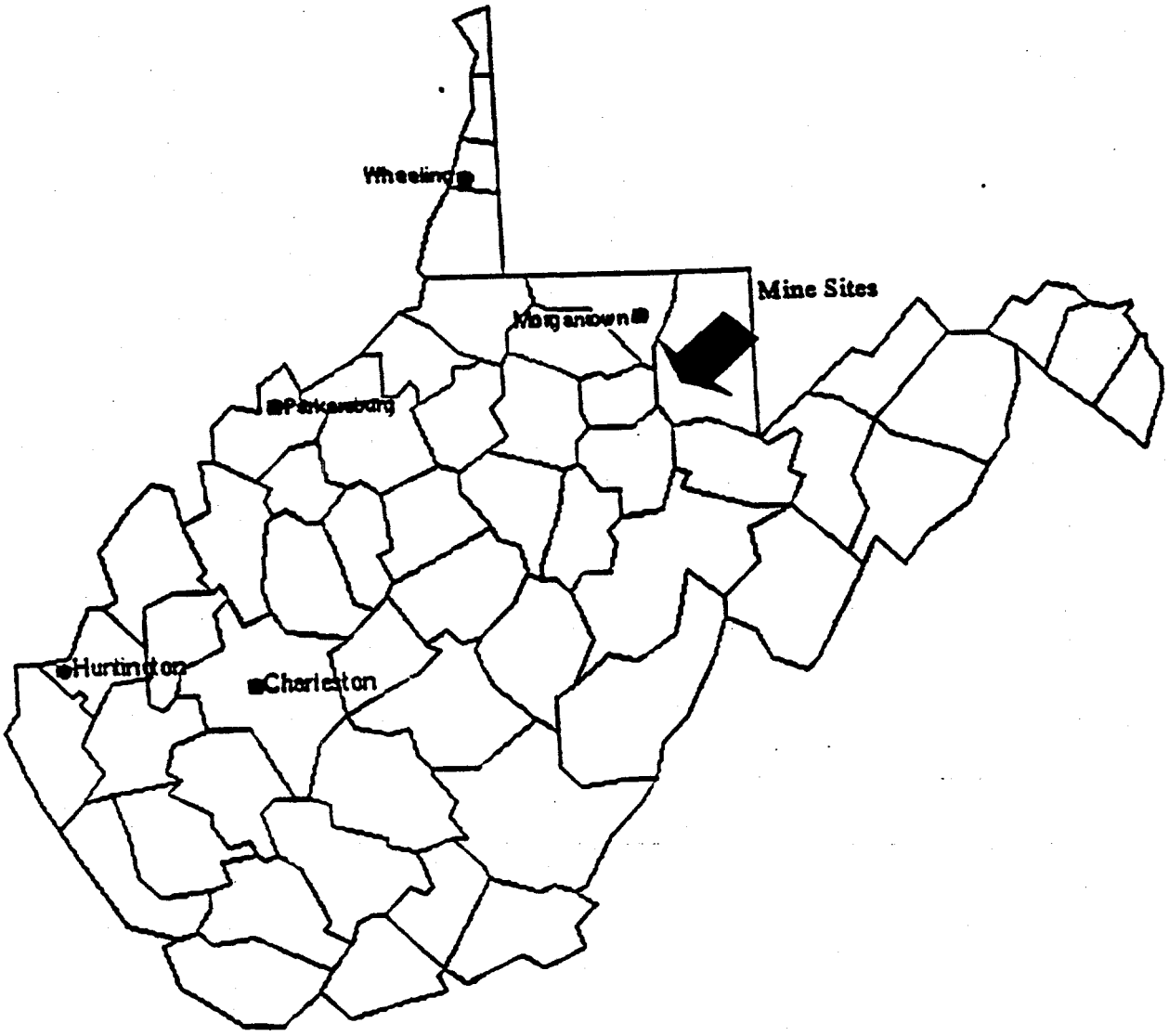

Figure 78: Map showing the location of Fairfax and Longridge mines in West Virginia

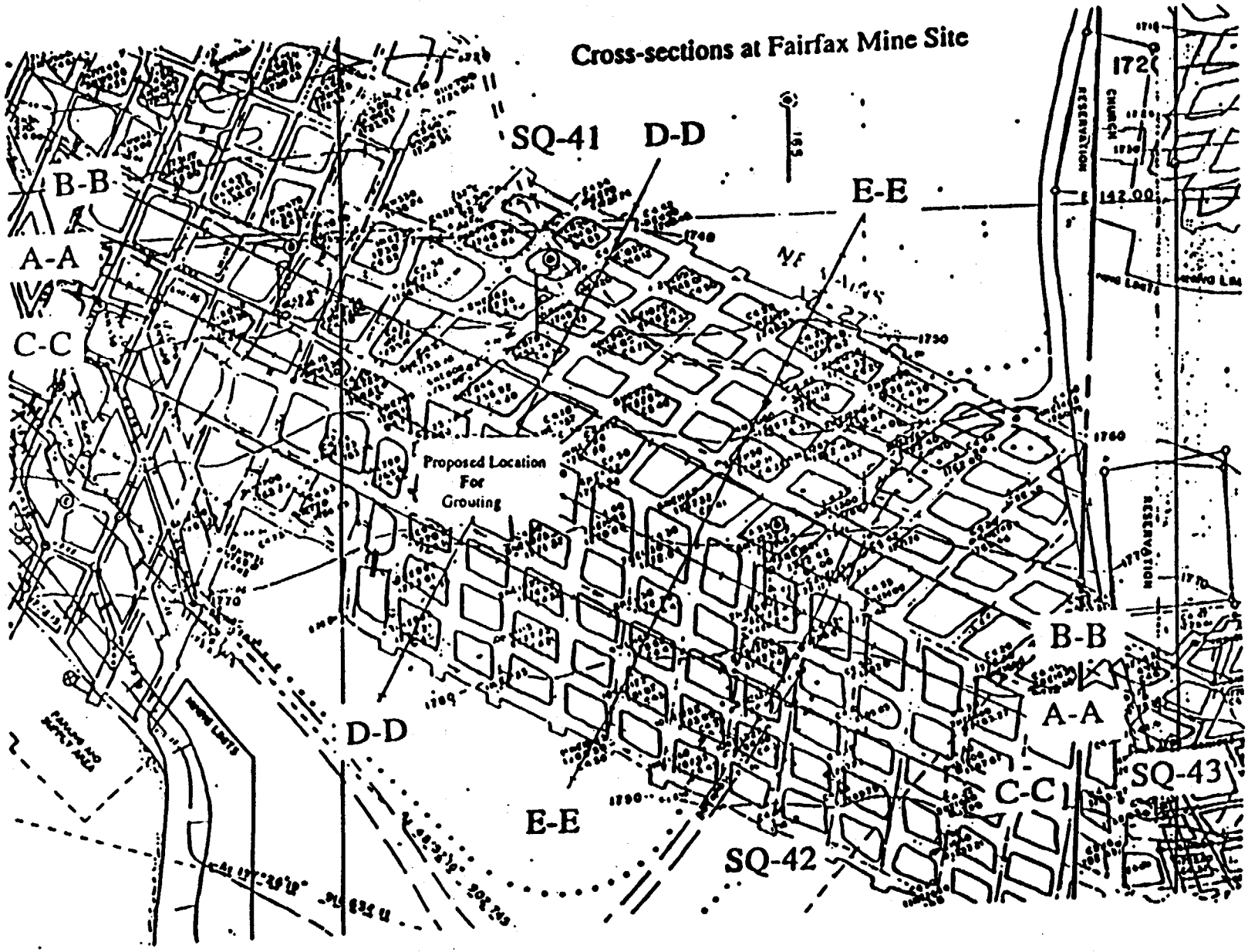

Figure 79 : Locations of cross-sections at Fairfax mine

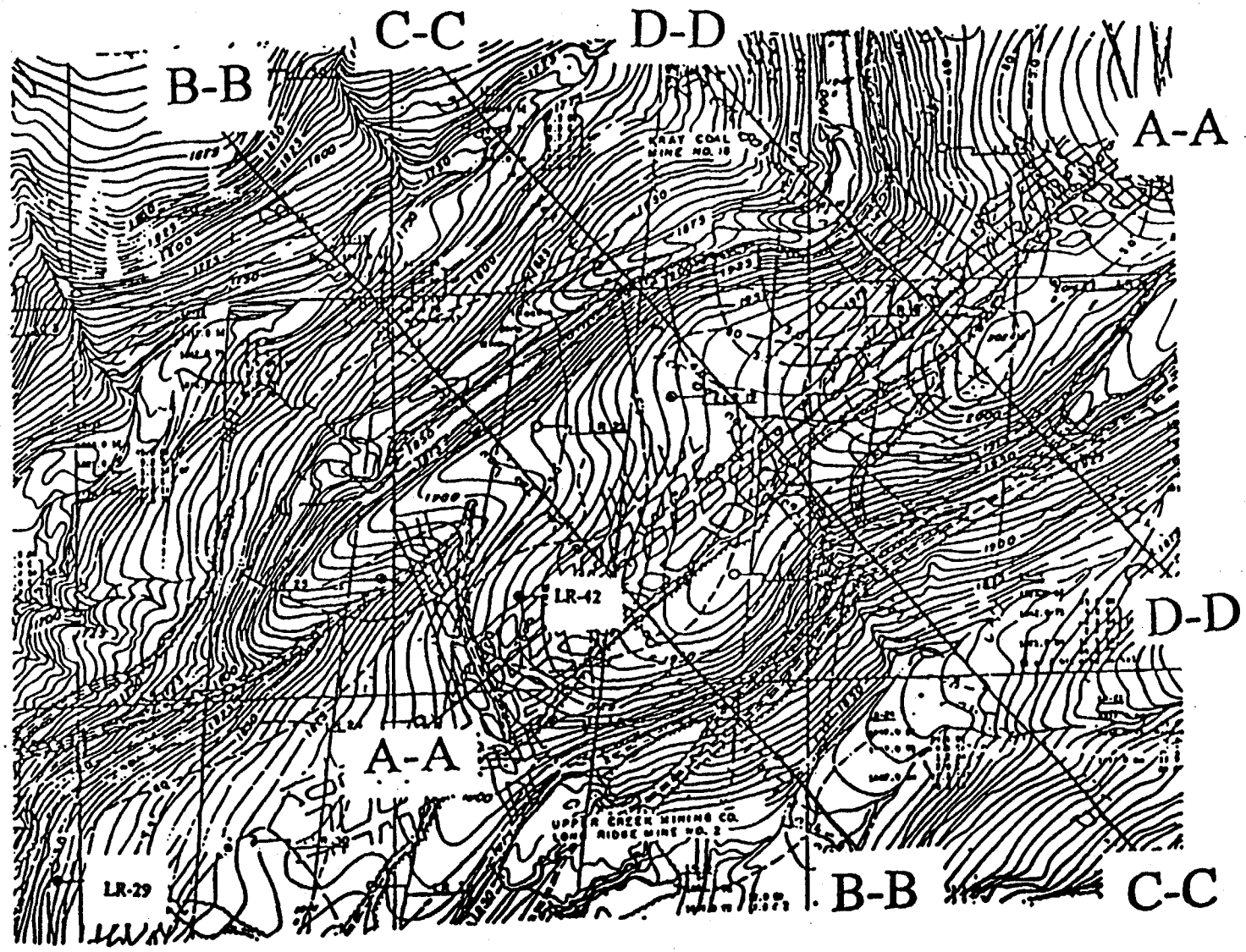

Figure 80 : Locations of cross-sections at Longridge mine

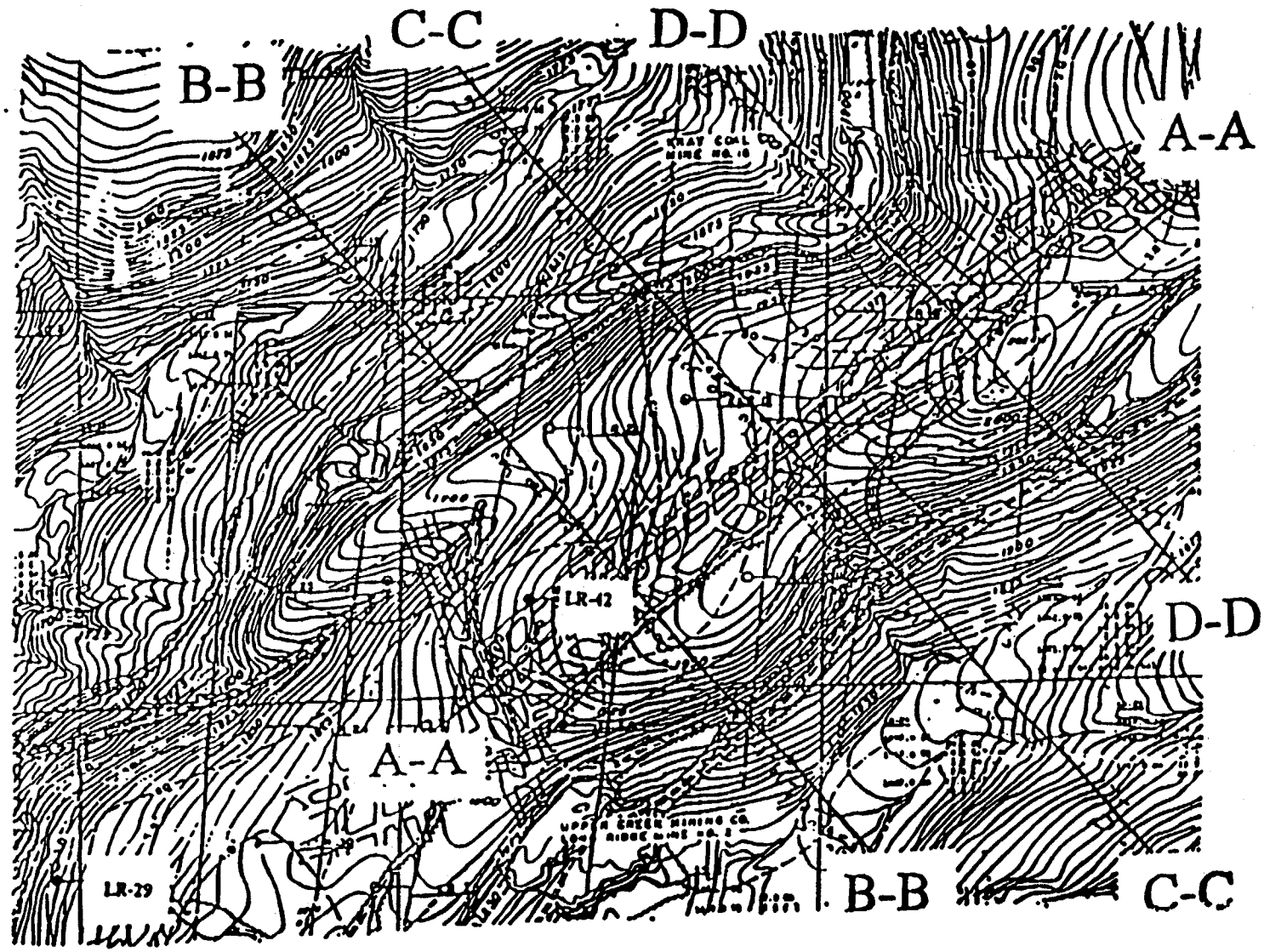

Figure 81 : Locations of core holes at Longridge mine

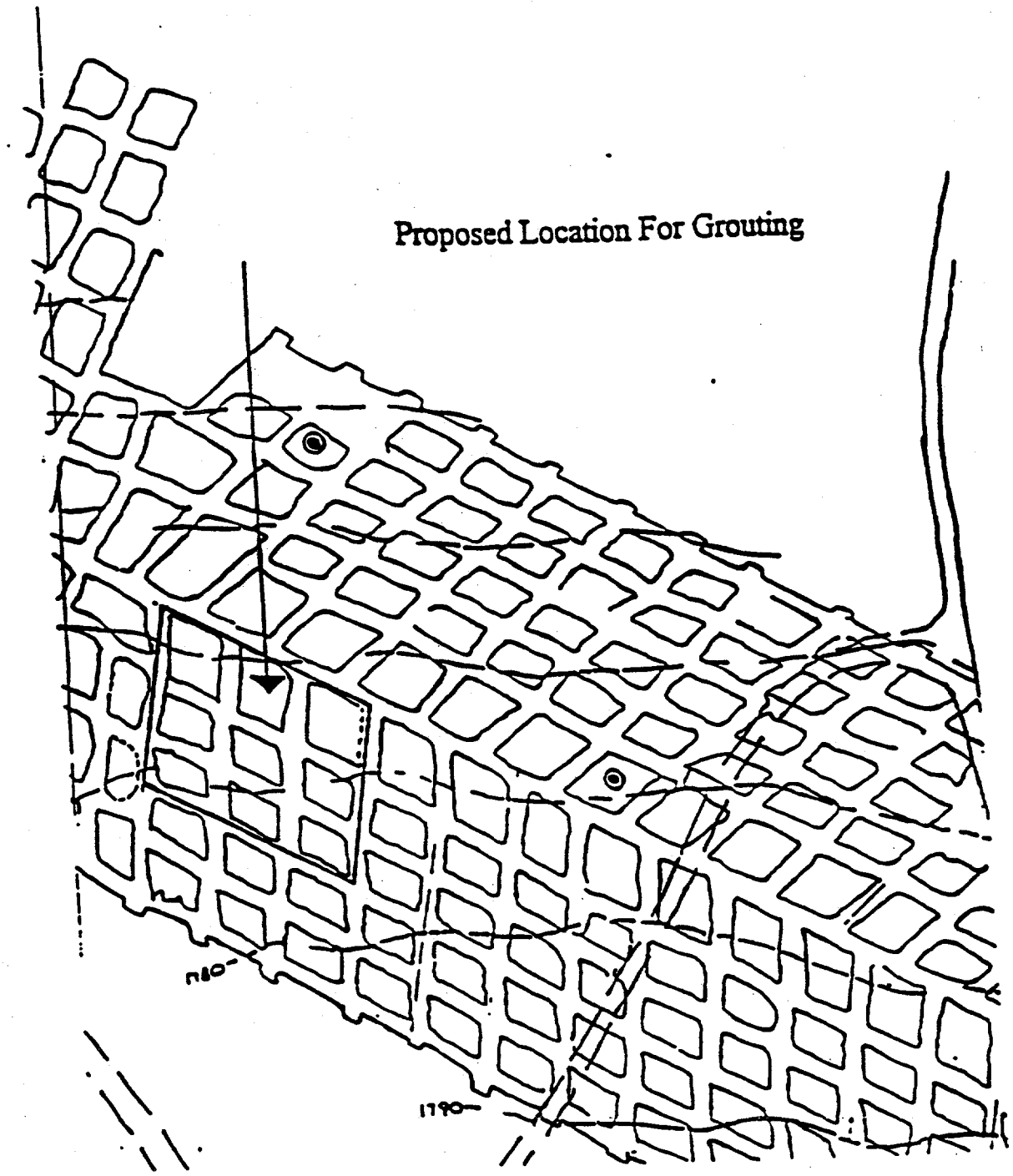

Figure 82: Proposed Location For Grouting

Scope of the Study

The scope of the study covers strength calculations for the grout (a mixture of Flyash, Bentonite and Water), which will be used at the Longridge mine site. An estimate of the volume of grout required for backfilling the mine voids made, based on the information extracted from the mine maps is included in this report. A study on the control of subsidence by using complete and partial backfill of mine voids is also presented in the report.

Site Description

Geologic and Geotechnical Characteristics

Figures 83, 84 and 85 show the soil and rock stratigraphy at core hole locations SQ 41, SQ 42 and SQ 43 at the Fairfax Mine; the locations of the core holes are shown in Figure 79. Information pertinent to these core holes was extracted from the bore hole logs obtained from the mining company. The geologic columns at these sites show that the thickness of soft clayey layers overlying the first layers of rock ranges from 19 to 28 feet. The rocks at the bedrock surface appear to be weathered. As shown in Figure 83, there is about 80 feet of weathered shale which can be fairly massive and uninterrupted. Immediately below the top soil is a layer of sandyshale of about 15 to 20 feet in thickness. The coal seam is located at approximately 225 feet below the surface. The thickness of the coal seam is about 5 feet. The coal seam has a dip of about 6^0 as can be seen in the contours shown in Figure 79.

The ground profile at the Fairfax mine is shown in Figures 86, 87, 88, 89 and 90. The profiles shown in Figures 86, 87 and 88 are along the longitudinal cross-sections A-A, B-B and C-C, respectively. The profiles shown in Figures 89 and 90 are along the transverse cross-sections D-D and E-E, respectively. The ground elevation starts increasing from a distance of 500 feet side and peaks at the center of the mine. The coal contours extended only upto a distance of about 500 feet on either side of the mine in the transverse direction. Therefore the thickness of the overburden could be determined only upto a certain distance on the basis of contour maps. The immediate roof comprises about 10 feet of sandyshale in the vicinity of core hole locations SQ 41 and SQ 42.

Figures 91, 92, 93 and 94 show the type of soils and rock that make up the overburden at core hole locations LR 29, LR 33, LR 34 and LR 42 of the Longridge mine, respectively. The geologic columns at these locations show the presence of fairly thin layers of clayey soils. The rock stratigraphy is not much different from the stratigraphy at the Fairfax Mine. There is about 50 feet of weathered gray sandstone below a 15 feet thick layer of sandyshale. The average thickness of the coal seam is about 7.5 feet, and is located at approximately 80 feet below the surface. The coal seam has a dip angle of about 6^0.

Figures 95, 96, and 97 show the ground profile at cross-sections A-A, B-B, and C-C of the Longridge mine, respectively. Cross-section A-A is along the Longitudinal direction of the mine. Cross-sections B-B, and C-C are transverse sections of the mine. The ground surface at the

Longridge mine is essentially a ridge that peaks at the center of the mine. The ground elevation drops rapidly from the center, and regions of outcrop can be seen at distances of about 500 feet from the center of the mine in transverse sections. The immediate roof is a fairly thick layer of weathered gray sandstone.

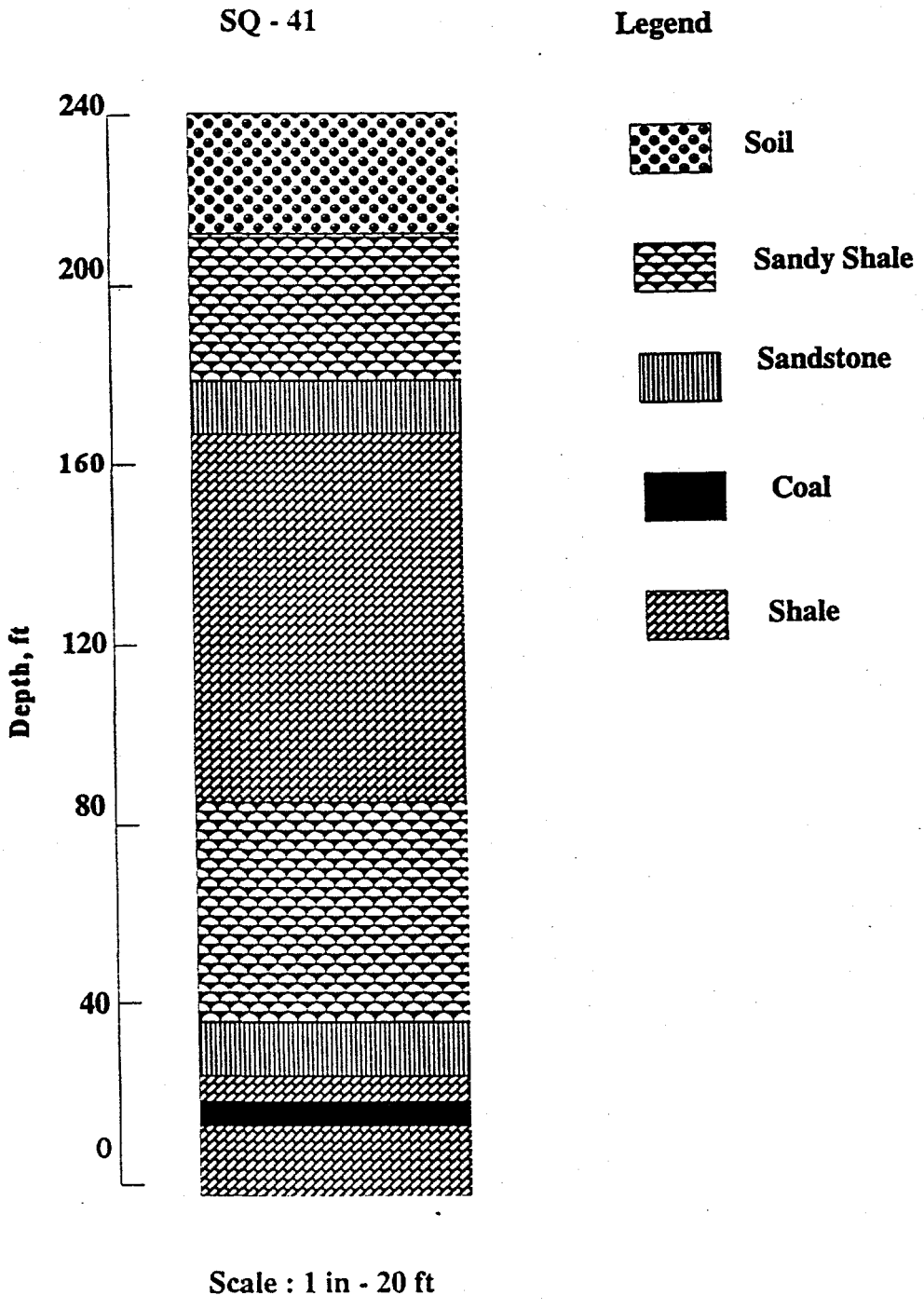

Figure 83 : Geologic column at location SQ-41 of the Fairfax mine

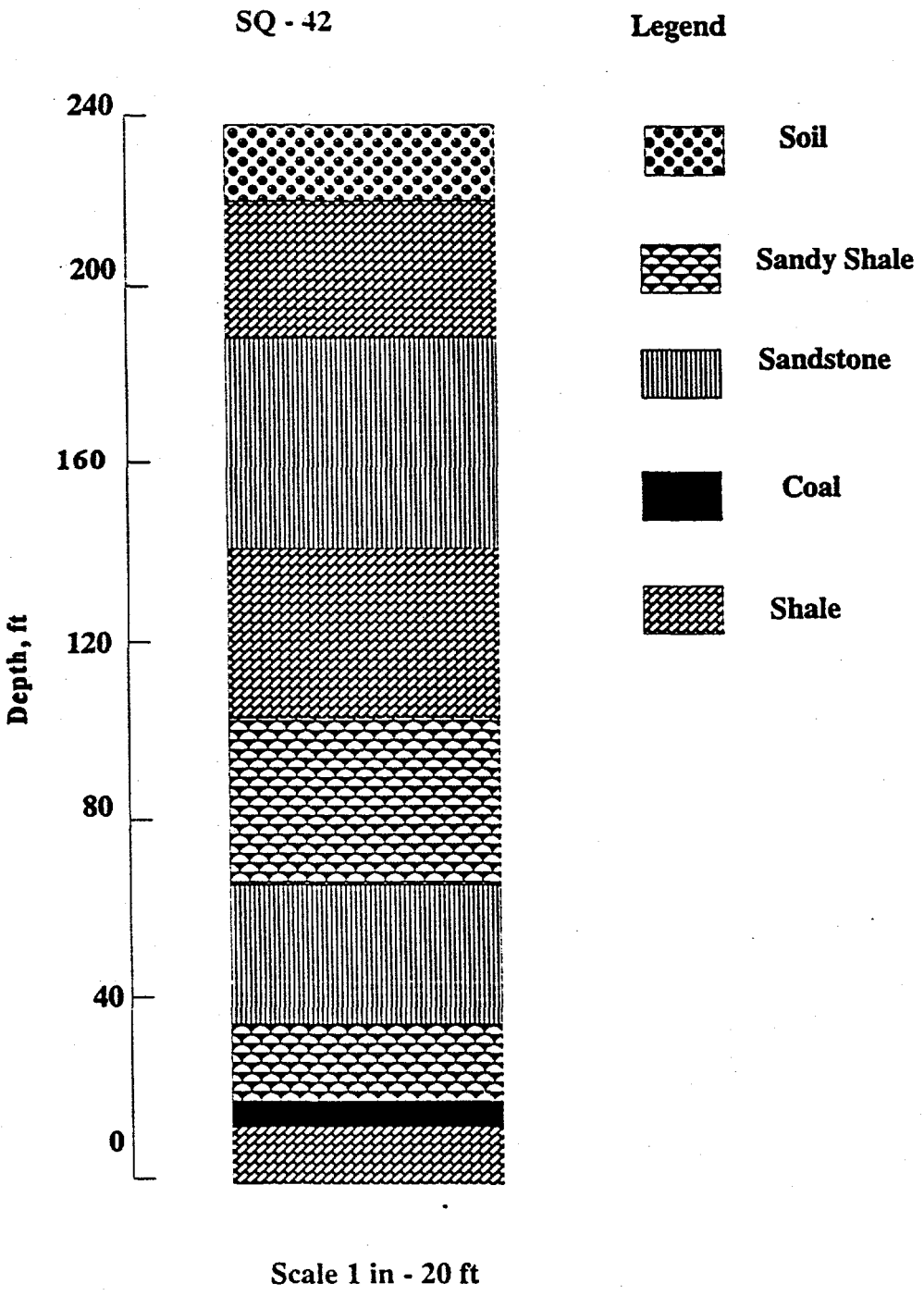

Figure 84 : Geologic column at location SQ42 of the Fairfax mine

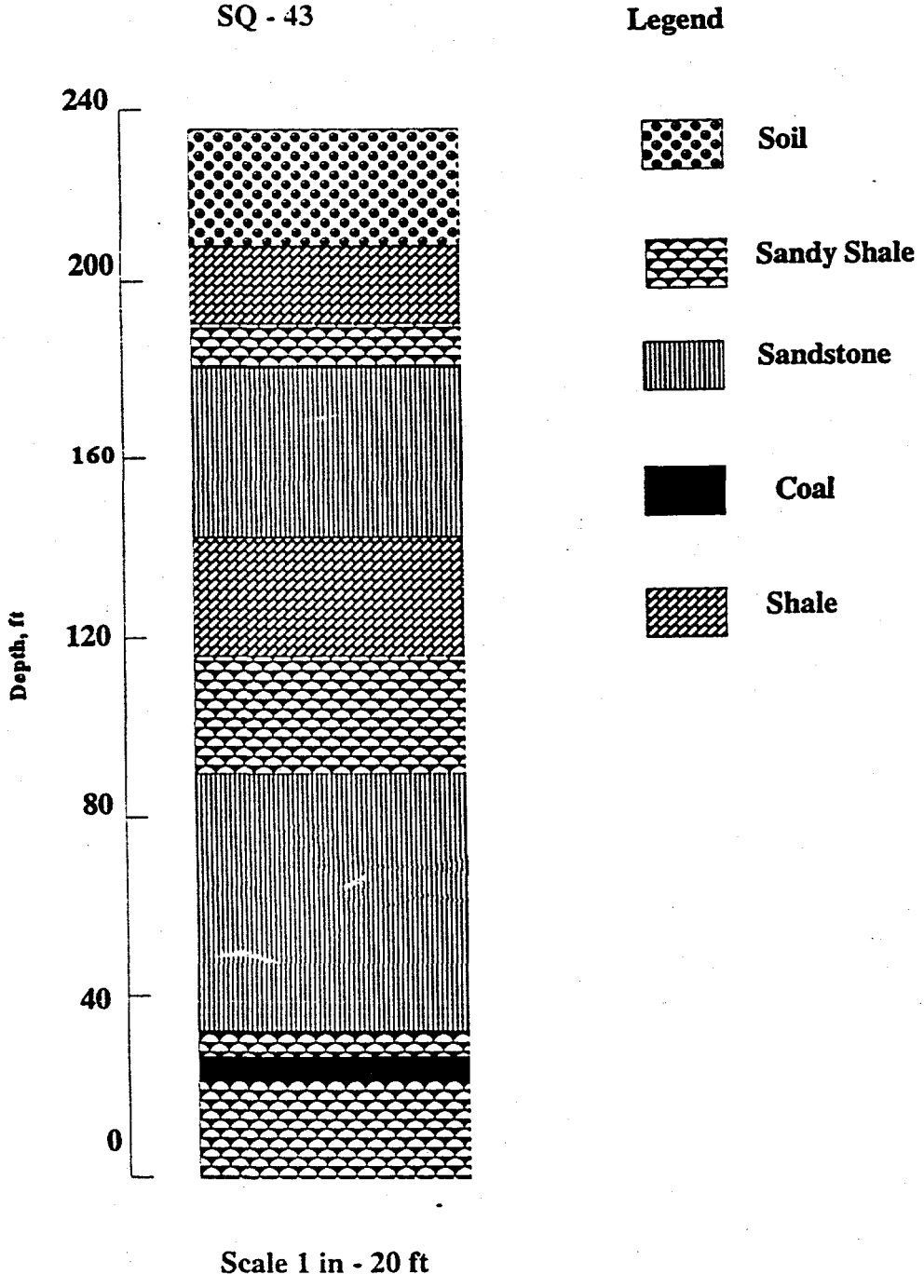

Figure 85 : Geologic column at location SQ-43 of the Fairfax mine

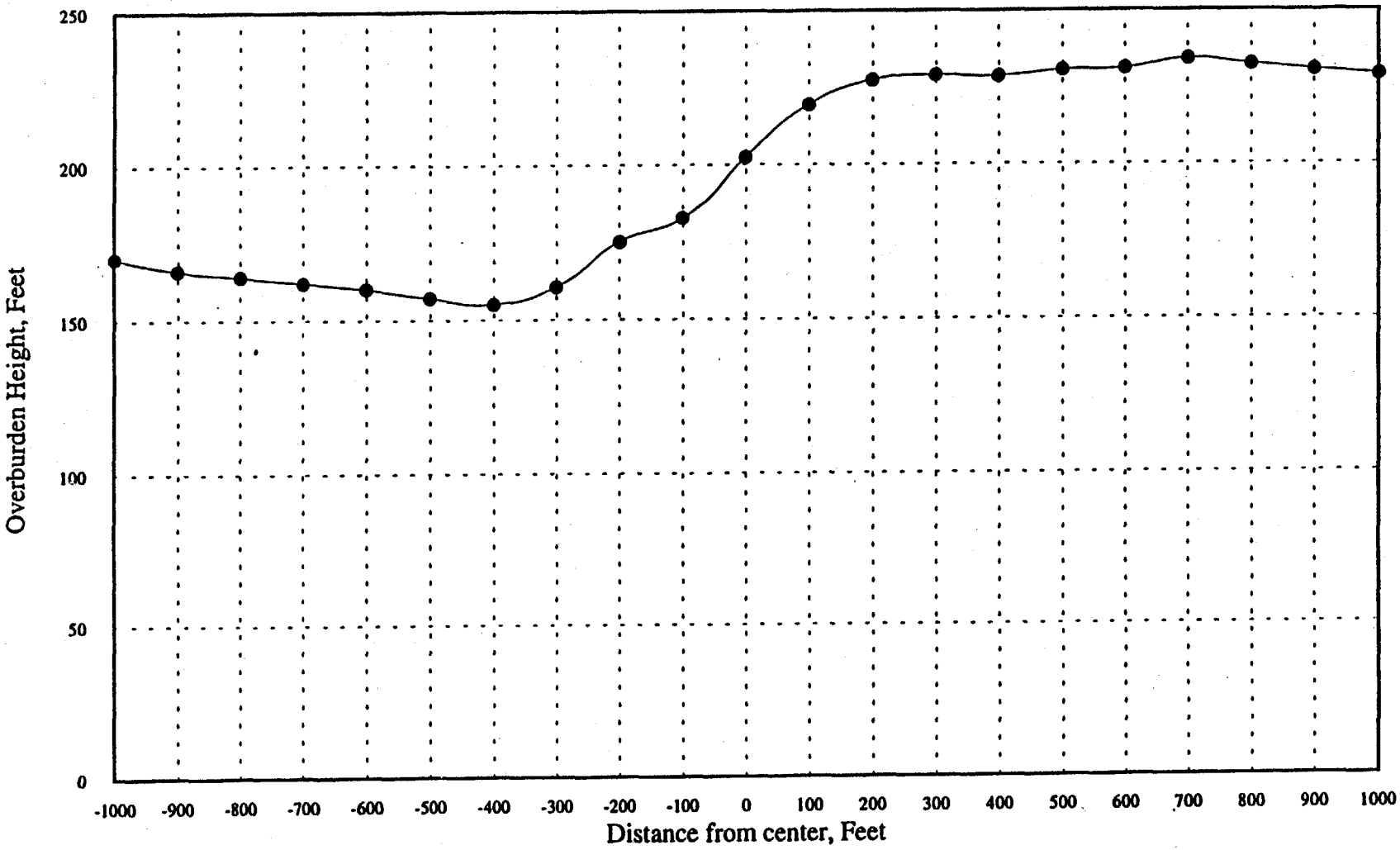

Figure 86 : Ground Profile At Section A-A Of Fairfax Mine

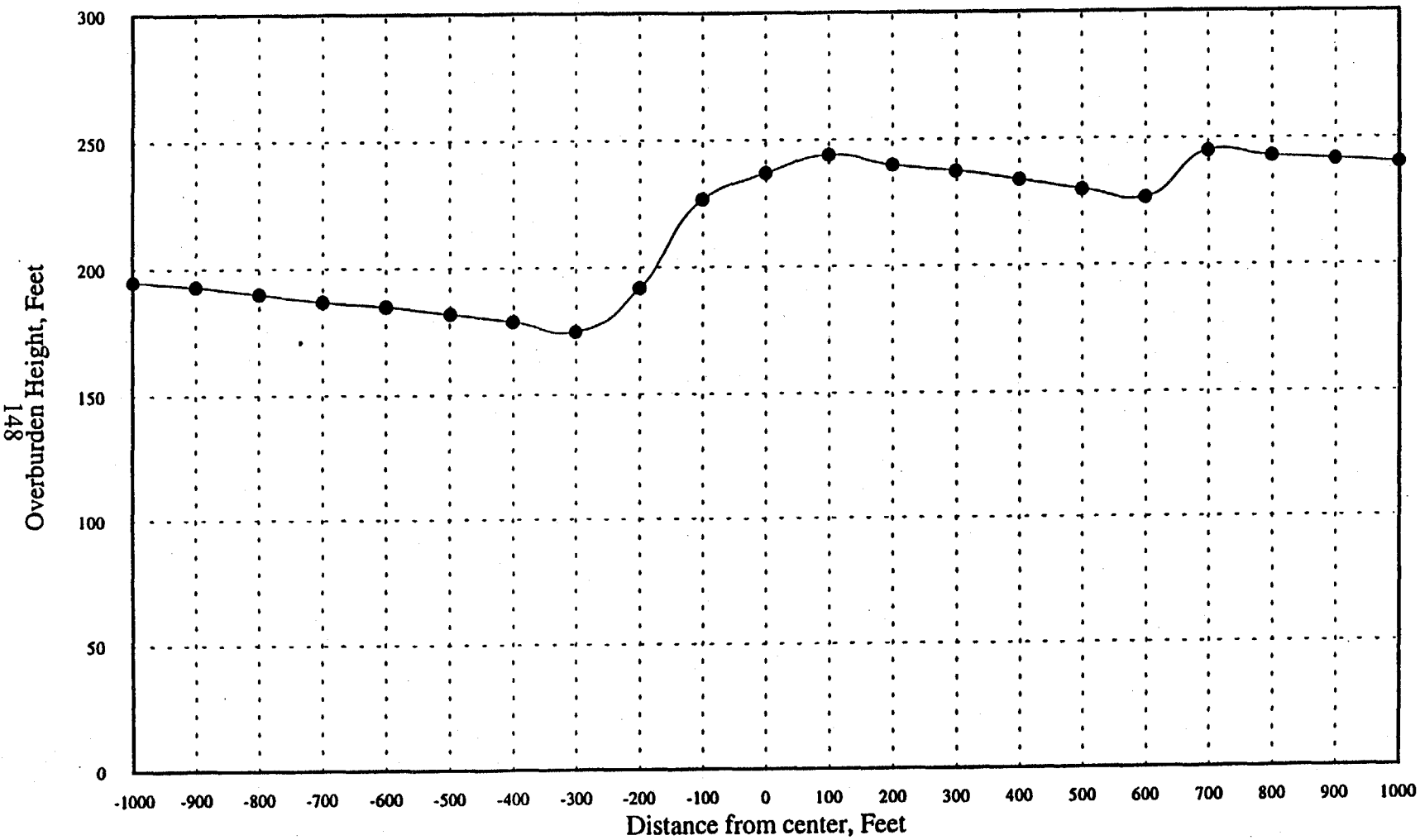

Figure 87 : Ground Profile At Section B-B Of Fairfax Mine

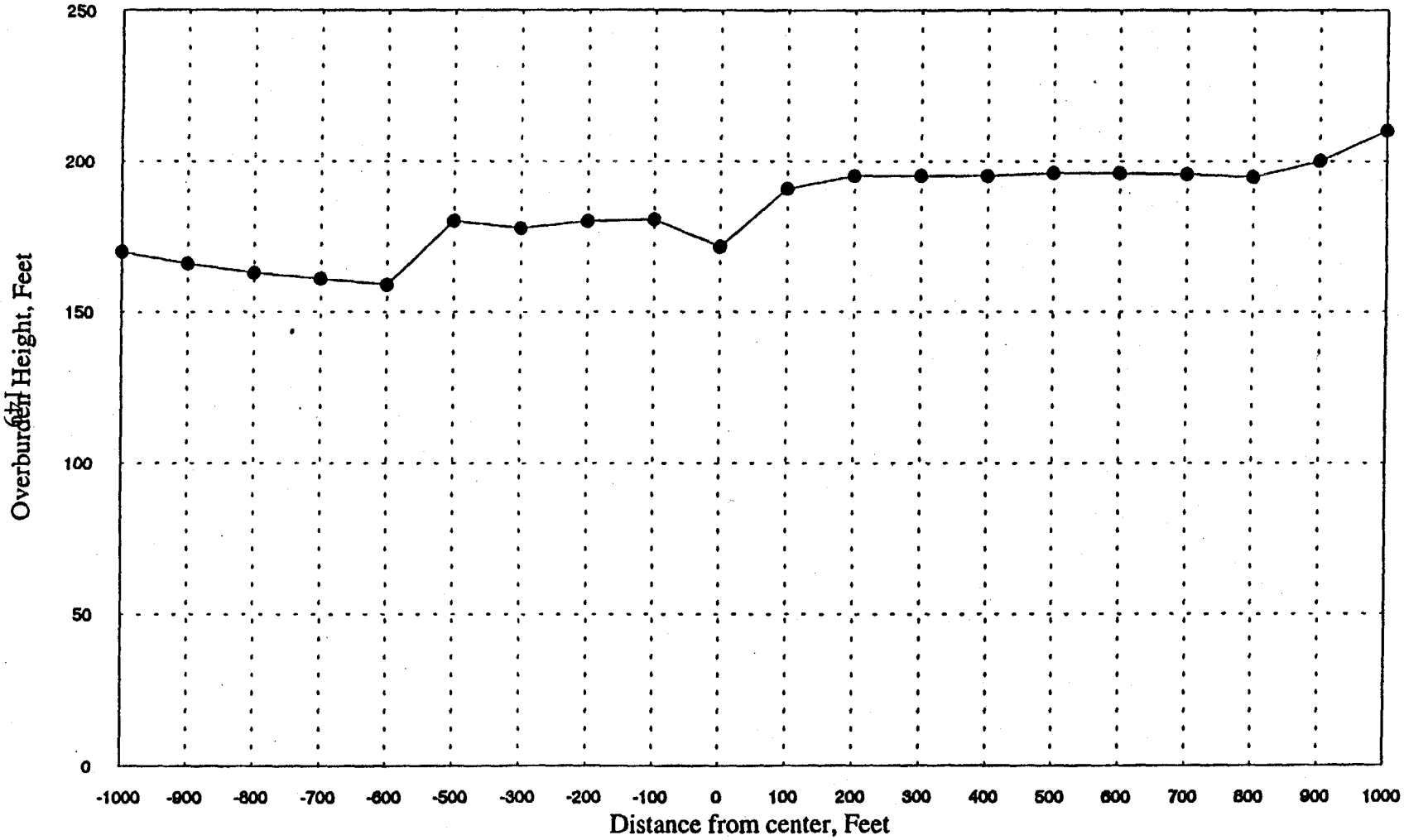

Figure 88 : Ground Profile At Section C-C Of Fairfax Mine

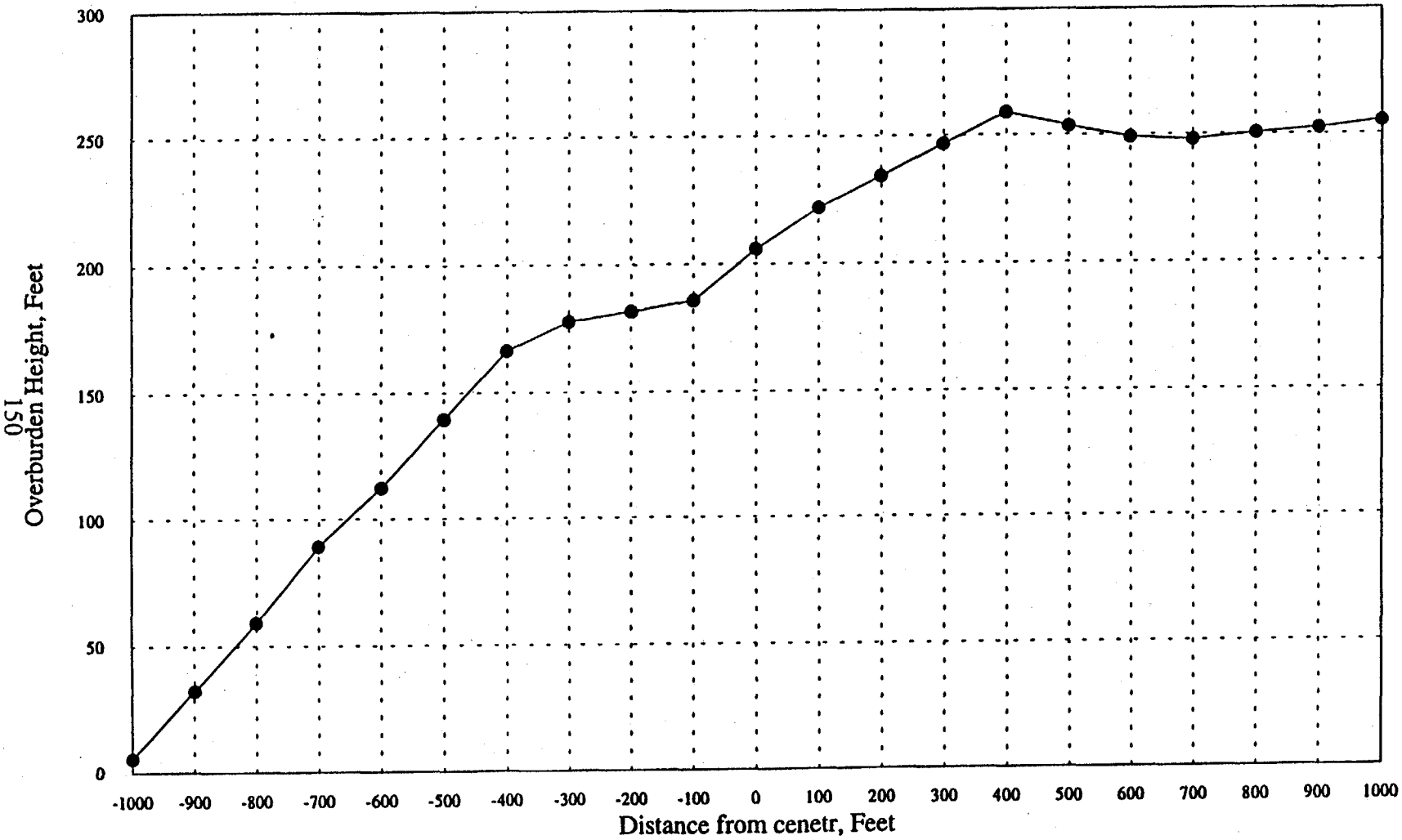

Figure 89 : Ground Profile At Section D-D of Fairfax Mine

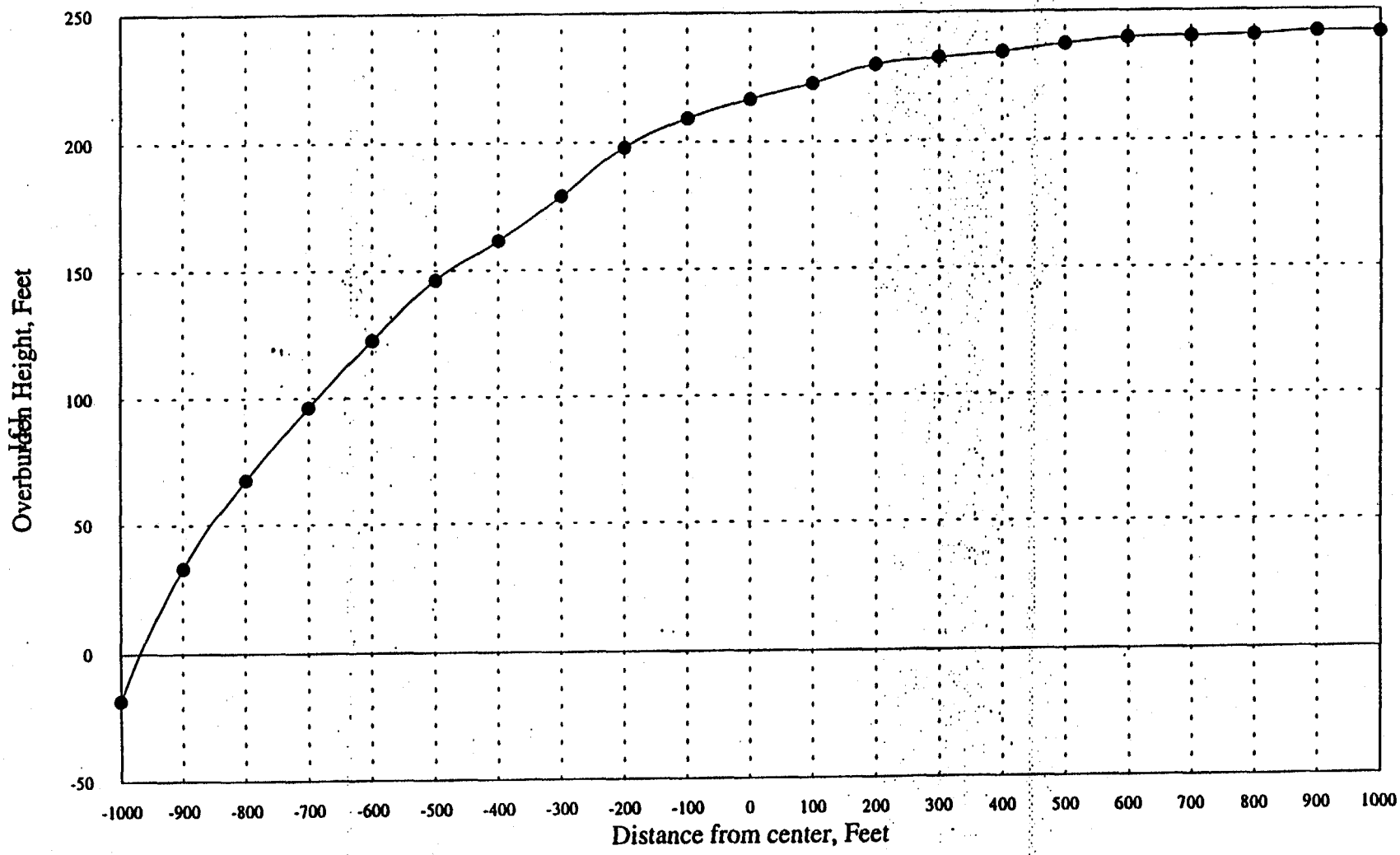

Figure 90 : Ground Profile At Section E-E of Fairfax Mine

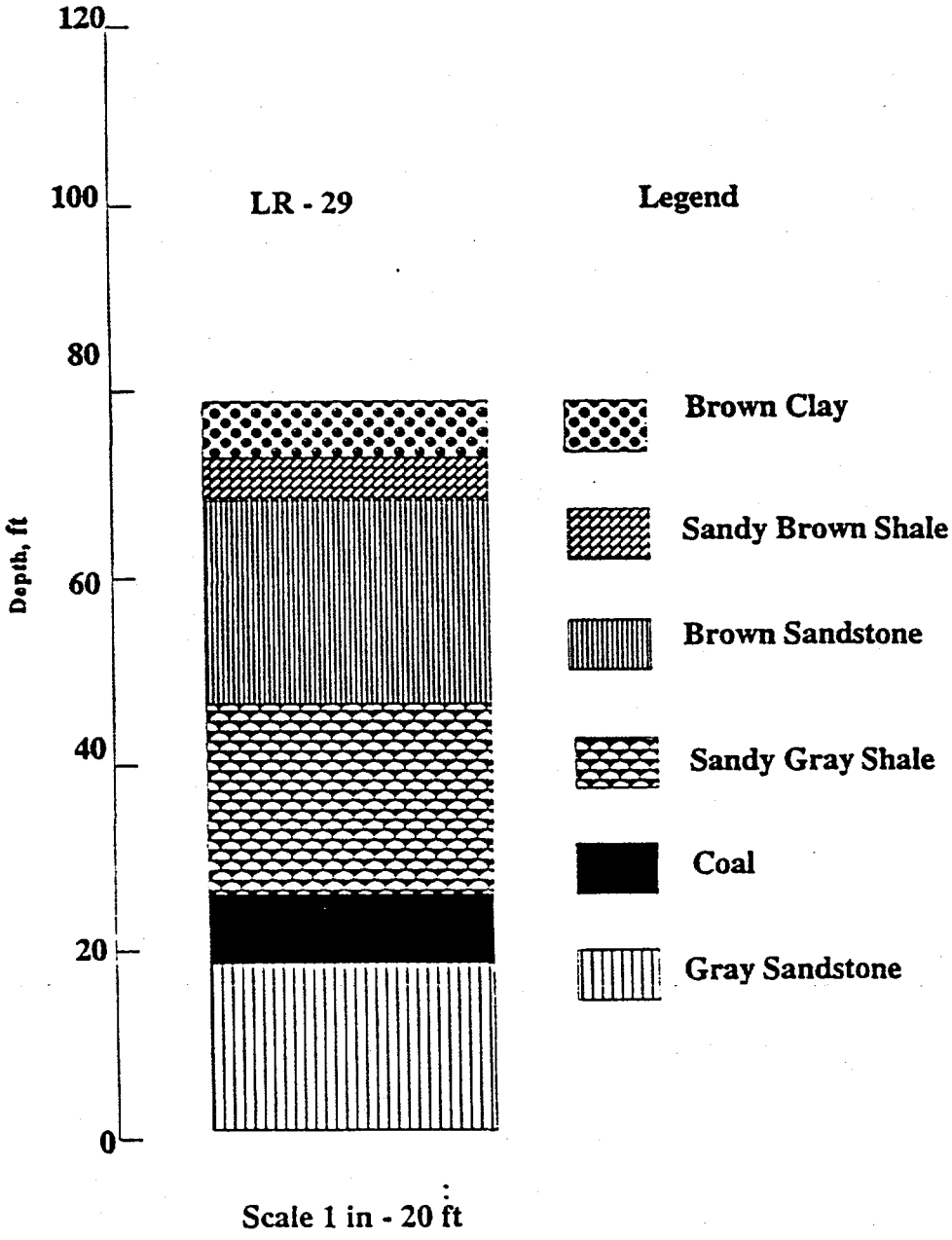

Figure 91 : Geologic Column at Location LR29 of the Longridge Mine

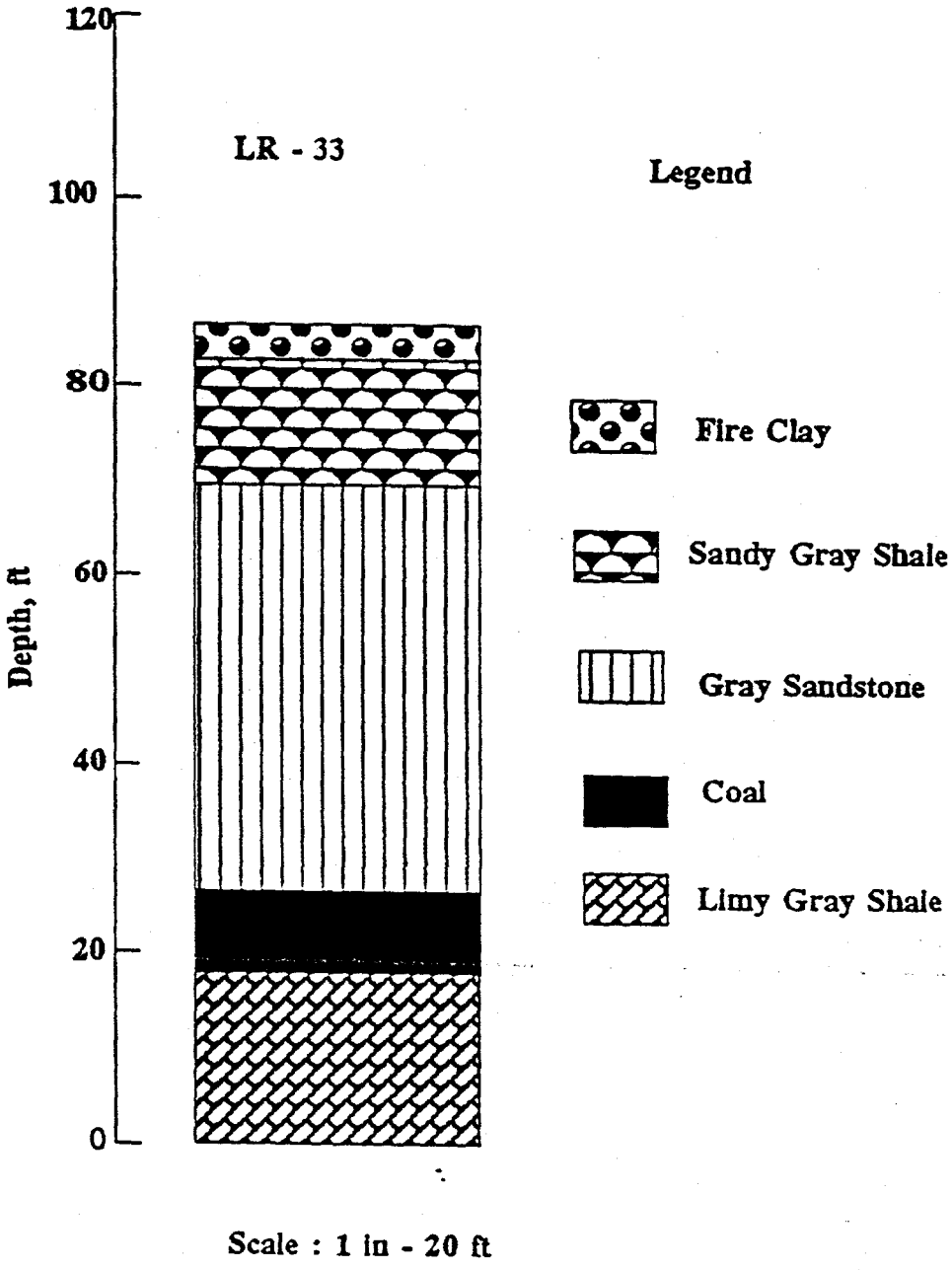

Figure 92 : Geologic column at location LR-33 of the Longridge mine

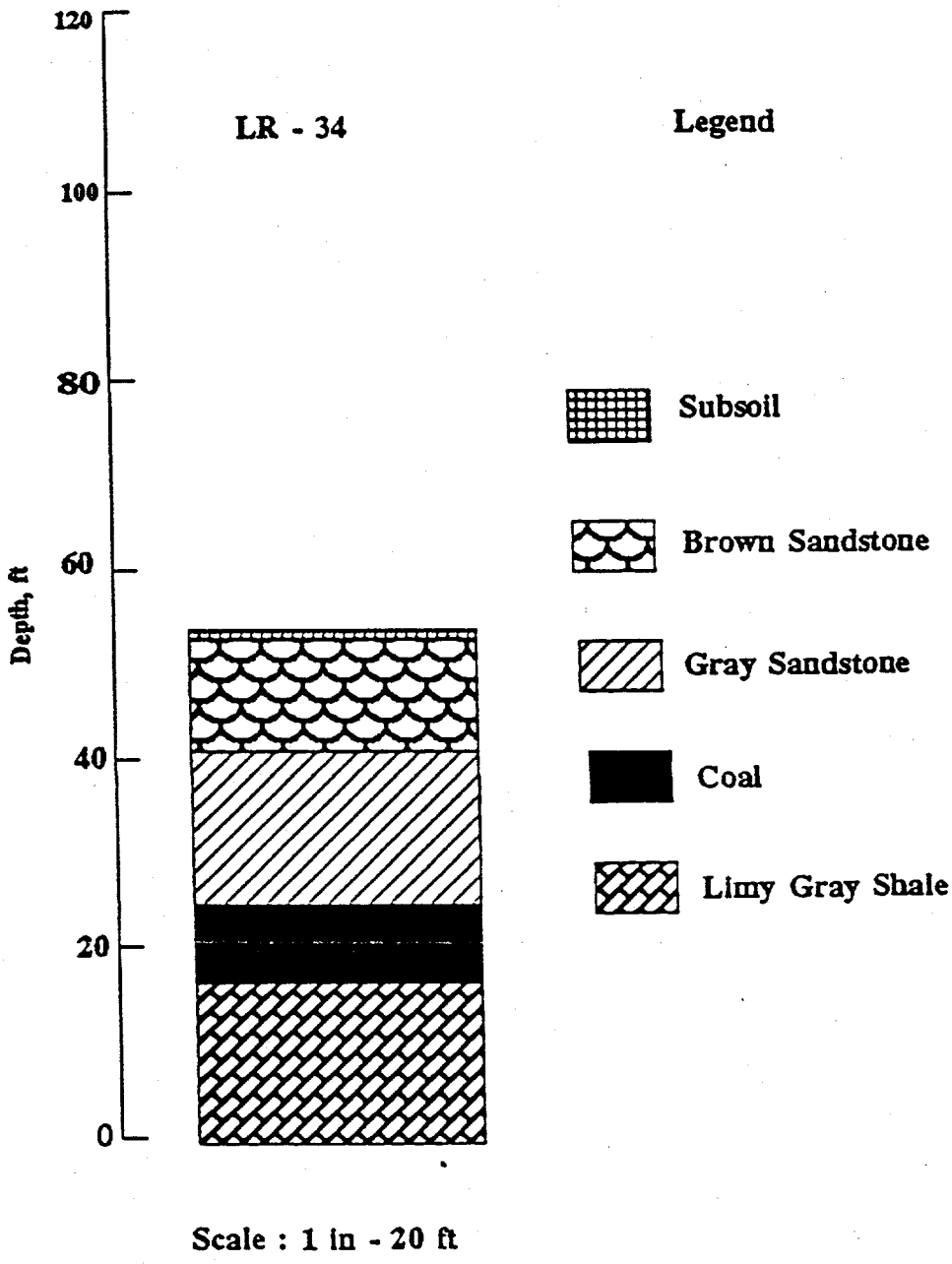

Figure 93 : Geologic column at location LR-34 of the Longridge mine

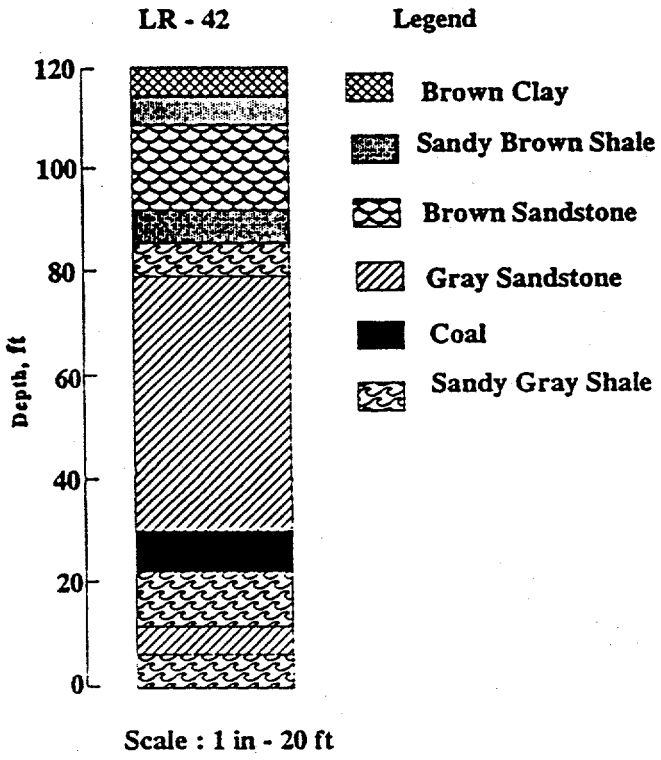

Figure 94 : Geologic column at location LR-42 of the Longridge mine

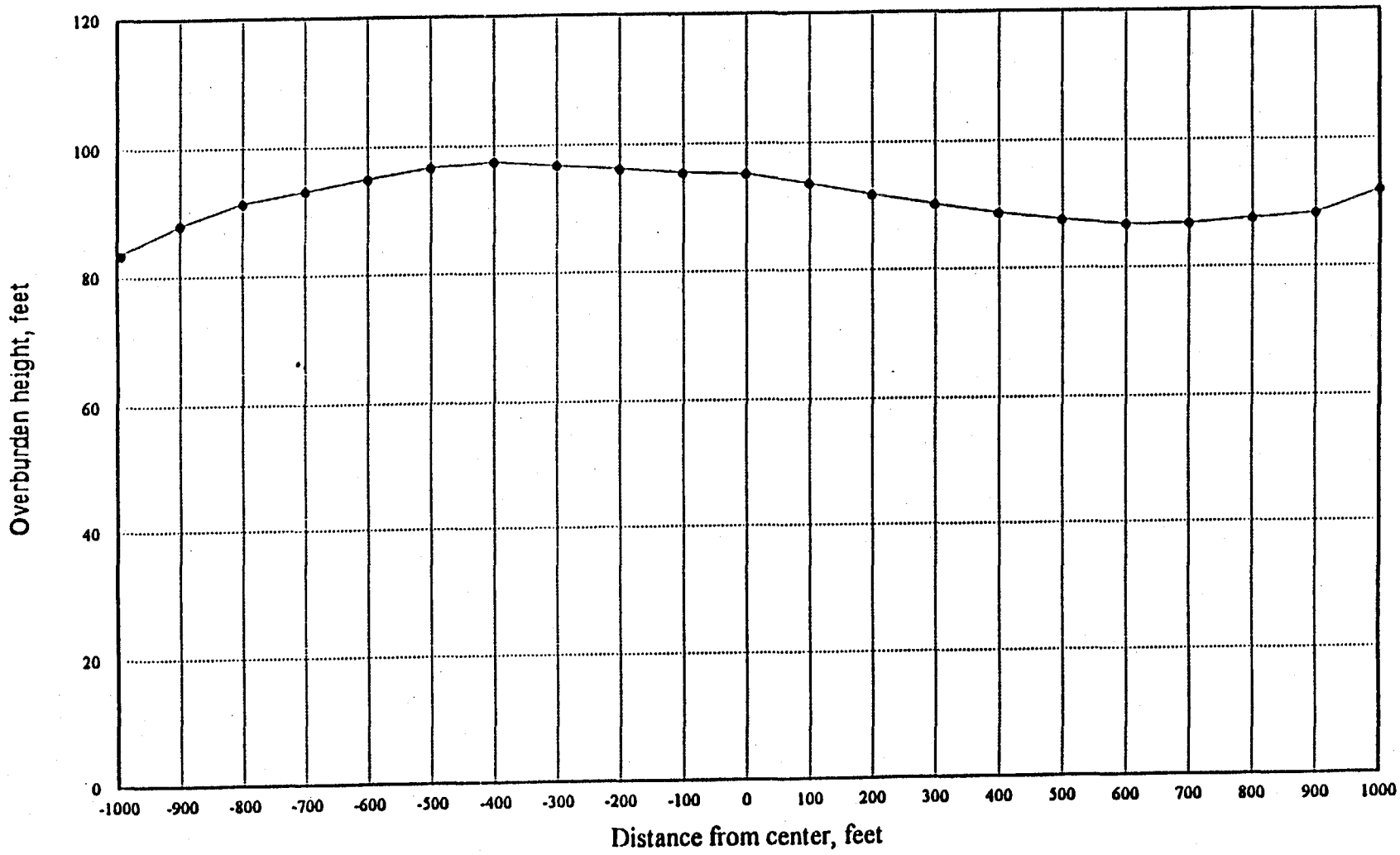

Figure 95 : Ground Profile At Section A-A Of Longridge Mine

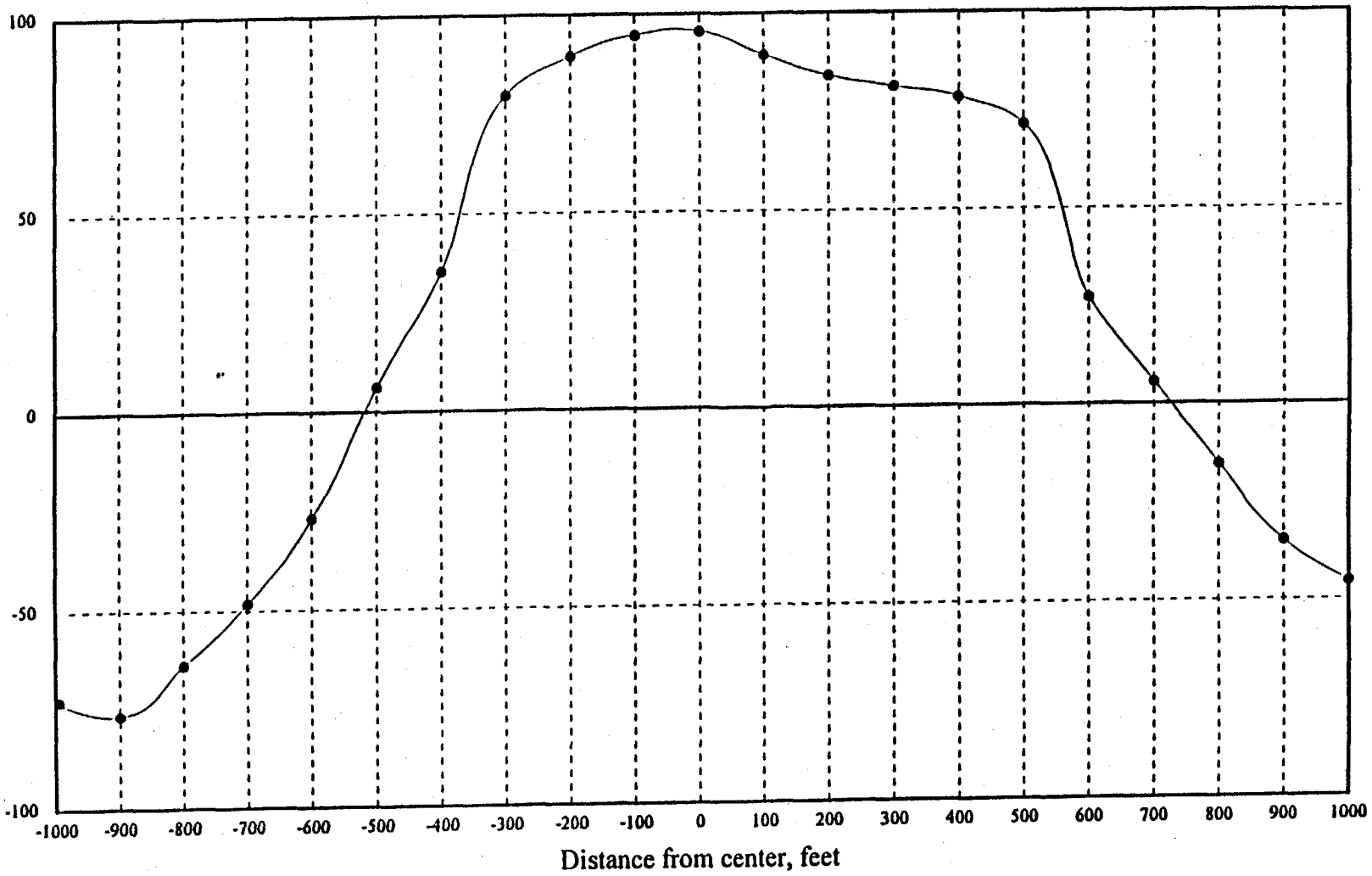

Figure 96 : Ground Profile At Section B-B Of Longridge Mine

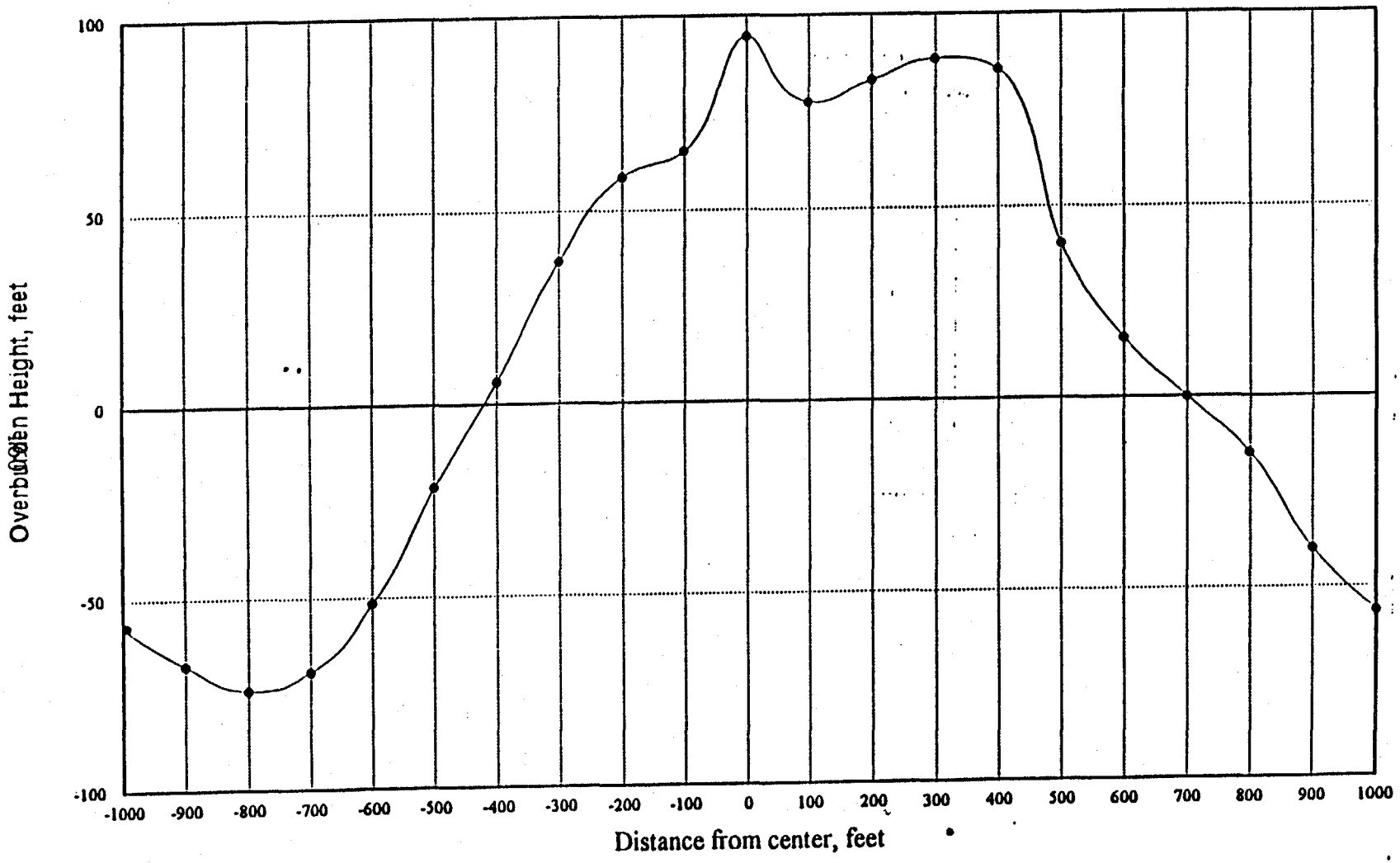

Figure 97 : Ground Profile At Section C-C Of Longridge Mine

Material Properties

Table 5 shows the material properties of the rock materials found in the overburden at the Fairfax Mine. The values are typical of weathered overburden. The material properties of the materials making up the overburden at the Longridge mine is reported in Table 6. Since measured values of rock properties at this mine was not available, the material properties were established on the basis of those reported in literature (Ward, 1992).

Literature Review

Subsidence is an adverse surface effect of underground mining operations. Excavation of solid material from the earth's surface disturbs the inherent state of equilibrium of the strata, and results in the creation of voids. Gravitational and/or tectonic forces, act on the strata surrounding the voids, and if the remaining support is insufficient for withstanding the weight of the overburden, the overlying rock mass fractures and collapses in to the voids. The resulting ground movement at the ground surface is termed as surface subsidence.

Information on subsidence prediction becomes more meaningful if some essential parameters such as angle of draw, width-to-depth ratio and slope of the subsidence profile are considered (Moebs, 1982). Table 7 includes definitions of terms frequently used in the literature.

Pillar Stability and Failure

Factors Affecting Pillar Stability

Pillar stability is a function of various factors such as the nature of the geology, the mining geometry, the type and magnitude of underground stresses, and other local effects such as the state of weathering of the overburden and the hydraulic conductivity of the rocks making up the overburden (Horino & Aggson). The overburden at Fairfax and Longridge mines comprises weathered rocks for considerable depths. These rocks have fairly high hydraulic conductivity values of the order 1×10 to 1×10^3 gallons/day/sq.ft (Todd, 1970). The flow of water through these rocks start the deterioration of roof, floor and pillars thus assisting roof collapse (Gray, et.al., 1977; Hartmann & Greenwald, 1941).

Pillar size and shape also affect pillar strength. The size of the pillar that should be tested for strength in laboratory should be representative of insitu pillars and should include all fractures and inhomogeneities . Hustrulid (1976) suggested the use of a critical width of 36 inches. The pillar strength is a function of the ratio of the least lateral dimension to the height (Crouch & Fairhurst, 1973).

Table 5 . Material properties used for the Analysis of Fairfax Mine

Rock Type	Elastic Modulus x 10^6 psi	Poisson's Ratio	Unit Weight pcf	Cohesion c psi	Internal Friction Φ deg	Tensile Strength psi	Coef. of e-pressure at rest k_o
Soil	0.007	0.30	120.0	2	20	2	0.50
Shale	0.960	0.15	160.0	2904.0	33.0	650.0	0.51
SandyShale	2.81	0.257	160.0	4260.0	31.4	15184.0	0.48
Sandstone	5.6	0.15	160.0	2336.0	28.0	851.0	0.46
Coal	0.180	0.30	83.0	1000.0	30.0	207.0	0.48

Table 6: Material Properties Used for the Analysis of Longridge Mine

Rock Type	Elastic Modulus x 10^6 psi	Poisson's Ratio	Unit Weight pcf	Cohesion c psi	Internal Friction Φ deg	Tensile Strength psi	Coef. of e-pressure at rest k_o
Soil	0.007	0.30	120.0	2.0	20.0	2.0	0.50
Shale	0.960	0.15	160.0	2904.0	33.0	650.0	0.51
Sandy Shale	2.81	0.257	160.0	4260.0	31.4	15184.0	0.48
Sandstone	5.6	0.15	160.0	2336.0	28.0	851.0	0.46
Coal	0.180	0.30	83.0	1000.0	30.0	207.0	0.48

Table 7: Definition of some general subsidence related terminology

Parameters that aid in the prediction of subsidence	Definition
Angle of draw	Angle subtended by the edge of the subsidence area with the edge of the mine, measured vertically as shown in Figure 3-1.
Maximum subsidence	Maximum computed value of subsidence at a section.
Subsidence coefficient	It is the ratio of the maximum subsidence to the seam thickness expressed as a percentage.
Width-to-depth ratio	It is the ratio of the width of a mined section to the overburden thickness.
Critical width	The width of a mine section that causes complete subsidence of a point on the surface.

Lowering of groundwater also leads to pillar instability. It is basically due to an increase in effective stress. Pillars are also largely non-homogeneous with different strength and elastic moduli at different locations (Mathur & Mikkilineni, 1982). The existence of non-homogenities lead to unequal deformation and subsequent instability.

The loading on a pillar is calculated by using the tributary area method (Peng, 1978). The concept involves calculation of the overburden weight in a "tributary area contributed by one half the width of the room on either side of the pillar" (Peng, 1978). The stress distribution on the pillars ranges from a minimum at the pillar periphery to a maximum at the core (Wagner, 1974). Pillars bear the maximum stress at the core due to lateral confinement of the material. As soon as the stresses exceed the yield strength of the pillar, the pillar fails.

Modes of Pillar Failure

Deterioration of pillars reduces its load carrying capacity and this causes eventual pillar failure. There are three common modes of pillar failure (Mathur & Mikkilineni, 1982):

1) Pillars undergo bulging at the mid-height if there is significant amount of flow. This allows separation of coal and results in decreased cross-sections.

2) The non-homogeneties present in the pillars, in the form of cleats, allow vertical spalling especially at the middle of the pillar as the cross-sectional area is reduced. This results in the formation of a "Waist".

3) The third mode of failure is shear failure along the weaker planes.

Pillar failure is a progressive phenomenon, as the excess loads are transferred to the neighboring pillars, thus triggering the collapse of adjacent pillars.

Roof Collapse

Roof collapse triggers surface subsidence. Mine roof is basically designed as a beam capable of withstanding a distributed load (Mathur & Mikkilineni, 1982). The instability in mine roof is a function of various factors such as the characteristics of materials comprising the overburden, the strength and deformation of the immediate and the main roof and fluctuations in moisture and humidity. Roof instability also depends on the presence of non-homogeneties (Mathur & Mikkilineni, 1982). It has been found that the presence of thin layers of shale in the immediate roof causes instability as compared to the presence of stronger strata such as sandstone.

Thus, it can be stated that physical properties, thickness, and the composition of materials in the immediate roof control roof stability. Figure 83 shows that the immediate roof at core hole location SQ-41 of Fairfax mine comprises a fairly thin layer of shale. Due to this nature of the immediate roof there exists a distinct possibility of roof instability at this mine. The main roof above

the immediate roof is a layer of sandstone. There is a possibility for the development an unbalanced stress field at the sandstone/shale interface due to differences in the moduli of the two materials. As compared to the Fairfax mine, the immediate roof at the Longridge mine is a 25 feet thick layer of sandy gray shale and hence there is a lesser possibility of roof instability.

Floor Failure

The thickness, physical properties and the composition of the materials in the underburden affect floor stability (Mathur & Mikkilineni, 1982). Due to weathering, the floor strata becomes relatively soft thus reducing the bearing capacity. Also, the presence of water reduces the floor stability considerably. The basic mode of failure is a bearing capacity failure, when the loads transferred by the pillars exceeds the bearing capacity of mine floor. The pillars in such a scenario, punch through the soft floor layers. Pillar punching is a function of pillar width, with larger pillar widths posing lesser threat of pillar punching.

Progressive Failure

The presence of a weak underburden immediately below the coal seam often results in a bearing capacity failure (pillar punching). The presence of water and non-homogeneties further contributes to this process. Pillar punching results in a gradual transference of loads to adjacent pillars and triggers a progressive failure.

Progressive failure halts as soon as a state of equilibrium is reached through a redistribution of loads. Further deterioration of pillars due to weathering, might start another cycle of progressive failure and the formation of a new state of equilibrium.

Mine Geometry and Layout

The amount of surface subsidence is related to the general geometry and the layout of the mines. Among other things, surface subsidence is related to seam thickness, the depth of coal seam, pillar width, panel width and design layout of room and pillars. Generally, subsidence is higher in mines with thicker coal seams. Subsidence potential is greater if coal is mined out from seams closer to the surface (Mathur & Mikkilineni, 1982). Larger extraction ratios and smaller pillar widths contribute to larger values of subsidence.

Presence of multiple seams also affects subsidence. In mines with multiple seams, the layout of pillars and the thickness of separation influences subsidence. Usually, lesser subsidence potential is noticed if pillars are designed to be directly above one another. In mines where pillar design is haphazard, the thickness of separation plays an important role in providing stability. A minimum separation of 50 feet is essential for stability (Mathur & Mikkilineni, 1982).

Bulking

The immediate and the main roof are subjected to high compressive and tensile stresses. The material comprising the roof might fail due to this stress field, and falls into the voids. This process is accompanied by volume change and is termed 'Bulking'. The subsidence of the surface may be stopped at an intermediate layer if significant bulking occurs in the mine.

In this study, the effect of bulking was considered in the subsidence modeling, by incorporating a bulking factor of 20% in the model. As the maximum subsidence in any mine is not equal to the seam thickness, it is expressed as a percentage of the seam thickness.

In the subsidence model, the prescribed roof displacements are multiplied by the 'roof displacement ratio 'p' to include the effect of bulking. The roof displacement ratio, p, is given by;

$$p = 1 - \alpha$$

where α = bulking factor.

Design Features in Room-and-pillar Mining

Mine Design

In the United States, room-and-pillar-mining has been extensively used in the past (Moebs, 1982). Solid pillars of coal (or mineral) are left as supports for holding the overburden, while extraction is being done. In other words, extraction of coal (or mineral) results in the creation of 'rooms'. The extraction rate in room-and-pillar mining was as low as 30% (Moebs, 1982). However, the rate has gone up in recent times (Moebs, 1982). Subsidence patterns and prediction methods over longwall mining is better understood, and is well documented. However, subsidence patterns over room-and-pillar-mining is somewhat complex and is a function of local geology, overburden thickness, physical properties of materials, presence of non-homogeneities and presence of stress fields (Ward, 1992). The water table as well as subsidence have to be accounted for in the mine design.

Room Design

Mine roof is designed as a beam supported on pillars. This is a criterion used for designing rooms. In other words, the maximum allowable span for stability of mine roof is one of the criteria for room design. Room design should take into consideration that sufficient space should be available for the operation of machinery. The average room dimensions are 40 ft x 40 ft x 5 ft in the Fairfax mine. The room dimensions in the Longridge mine are 30 ft x 30 ft x 7.5 ft as found from the mine maps.

Pillar Design

Pillars are basically designed by estimating the expected pillar loads from the overburden and equating it to the pillar strength. A factor of safety is included to account for local uncertainities in the geology. Some of the important factors that affect pillar design are the stress distribution in the pillars including horizontal stress component, deformation properties of pillars, roof stability, room design and other geologic factors. Pillars can be designed for either complete failure, i.e no yielding of pillars are allowed, or for yielding. Formulas for designing pillars are found in literature.

Grouting

For effective mitigation of surface subsidence, backfilling of mine voids with grout is one of the most practical and economical methods that is available today. As part of the efforts to minimize the adverse environmental impact of abandoned underground mining operations the backfilling of mine cavities with a grout was considered in this study. The grout consisting of a mixture of fluidized bed combustion ash, bentonite and water was selected for this purpose. The common types of grouts that are used include chemical and permament or cementatious grouts. Chemical grouts are used as support systems to stabilize soil in underground construction projects and are expected to perform for a period of one year. Chemical grouts are further classified as suspension type (ex; slag cement) and solution type (acid reactant). Suspension type grout has higher strength than solution type grout (Yonekura & Kaga, 1992). Strength of these grouts is a function of cement content. Cementatious grouts are used for permament stabilization of underground projects especially in mining operations.

Effectiveness of Grout as a Function of Rheology

Slump is a measure of grout mobility. Slump of a grout is a function of the shape of the particles and gradation. Grout mobility should be low for effective grouting especially in compaction grouting (Warner, 1992). Another important factor that evaluates the performance of grout is the setting time. Different setting times are necessary for different geologic conditions. Some of the other factors affecting the effectiveness of the grout are rate of injection, low confining pressure in shallow injections, proximity to down slope and presence of water. Lower injection rates, reduction in water content and addition of coarse aggregates increase the effectiveness of grout.

The Use of Bentonite in Grout

Bentonite is a promising sealing material that can be injected in fractures as it has fine particle size, very low permeability and a self-healing ability (Ran & Daemen, 1992). Bentonite increases the adhesive properties of the grout and keeps the grout suspension stable while pumping. Fractures ranging from 9 to 90 microns can be stabilized.

Methods Used in Backfilling

Hydraulic backfilling methods are of three kinds. 1) Controlled Flushing, 2) Blind Flushing, and 3) Pumped-Slurry Injection. Controlled flushing is used in accessible mines. The method

consists of building bulkheads around the periphery for confinement of the fill. One borehole for 4 acres is drilled from the surface to the top of the mine opening. Horizontal dispersal of slurry is done using large 90^0 pipe elbows. Horizontal dispersion is usually between 300 to 1000 feet. Blind flushing is used in inaccessible or flooded mines. The method consists of injecting slurry material until a conical pile builds up in the mine opening. Blind flushing requires closely spaced injection holes.

Pumped-slurry technique uses energy for injecting material. It is a closed system containing a dynamic suspension of slurry. Water from flooded mines may be used. The success of this technique depends on uninterrupted supply of energy sufficient to create enough velocity to keep the particles in suspension. This method requires less number of boreholes and is easier for use in inaccessible locations. Depending on strength requirements, selection of total or partial backfill can be chosen.

Methodology

Strength calculations are based on the fact that the grout after being injected into the mine void, should develop sufficient compressive strength to withstand the stresses caused by the overburden, along with the pillars. In effect, it should play the role of the excavated coal with its full strength. Traditionally, the vertical stress at the level of coal seam is calculated by multiplying the unit weight of the materials comprising the overburden with the respective thicknesses.

Source Code for Finite Element Analysis

The FORTRAN source code FEAGMEC (Finite Element Analysis in Geomechanics) written by Siriwardane, 1983 (Siriwardane, 1983, 1988, 1991, 1993) was used in this analysis. The output gives information on the stresses due to different loading conditions at any location in the ground. The output also provides the vertical and horizontal displacements due to overburden stresses, at any specified location in the ground.

Steps Involved in the Analysis

The steps involved in the analysis is given below.

- The ground profile, the geologic column and the material properties are established for a selected cross-section at the mine. A cross-section is selected for the analysis.
- The cross-section is discretized into a domain containing a finite number elements. The elements are generally four noded iso-parametric elements.
- The input for the program comprises the material properties, the nodal coordinate information, the element connectivity and the type of loading on the pillars.
- The input also includes information pertaining to the specified location in the ground where the stresses and the displacements are desired.

Finite Element Formulation : a Brief Review

A brief review of the steps involved in the Finite Element formulation is given below. Primarily, there are eight steps in a Finite Element Formulation. These steps are: 1) discretization, 2) selection of approximate model functions, 3) definition of the gradient-unknown relationship, 4) derivation of element equations, 5) derivation of global equations and the application of boundary conditions, 6) solution of primary unknowns, 7) solution of secondary quantities, and 8) interpretation of results. More details of the Finite Element formulation can be found elsewhere (Zienkiewicz, 1977).

Derivation of Element Equations

The governing differential equation in stress deformation problem for a one-dimensional element can be written as [29]:

$$AE\frac{\delta^2 U}{\delta x^2} = f(x)$$

where A is the area of cross-section, E is the elastic modulus and f(x) is the force acting on the body.

Element equations corresponding to this equation can be obtained by using one of the two methods.

a) Variational methods
b) Residual methods

Considering the variational methods, the element equations can be derived as:

$$[k](q) = (Q)$$

where [k] is the stiffness matrix for a single element, and (Q) is the load vector.

$$[k] = \int\int_v \int [B]^T[C][B]dV(Q) = \int\int_v \int [N]^T(y')dv + \int_s \int [N]^T[T']dS + (P)$$

The stiffness matrix obtained for each element above is assembled to form the global stiffness matrix. If the chosen element has n degrees of freedom, then the size of the element stiffness matrix would be of the order n x n.

The next step after the assembly of the local stiffness matrices, is the imposition of boundary conditions. The solution for primary unknowns can be obtained by using Gaussian elimination, after imposing the boundary conditions. The values of the primary unknowns obtained can be used for finding the secondary unknowns such as strain and stress at the element level. The results obtained are interpreted with the aid of computer graphics.

Results and Discussion

A quantitative assessment of subsidence potential beneath abandoned mines is essential for studying the adverse surface effects of underground abandoned mining operations. Reasonably accurate prediction of subsidence potential is possible with growing usage of numerical methods like the Finite Element method (Kutuk, et.al., 1994; Siriwardane, 1988, 1991, 1993). In this project, the subsidence computations are done for a two-dimensional idealization of the mine configuration. In other words, a plane strain analysis is performed for subsidence calculations at selected cross-sections.

Subsidence computations at both mine sites were done at selected cross-sections shown in Figures 79 and 80. The computations were done for 75%, 90% and 95% backfill of mine voids. Figure 98 shows grout backfill configurations. A bulking factor of 20% was considered to incorporate the effect of bulking of fallen overburden rock into mine voids.

Subsidence Computations at Section D-D of Fairfax Mine

The cross-section D-D of Fairfax mine is shown in Figure 79. The pillar configuration along this cross-section is shown in Figure 99. The procedure involved in the computations includes the discretization of the domain following the steps outlined in section 4.2. Roof collapse is modeled by prescribing displacements at the roof nodes. The Finite Element mesh used in this analysis is shown in Figure 100.

Due to symmetry, only one half of the mine is considered in the analysis. Figure 101 shows the computed subsidence profile at section D-D of the Fairfax mine. The profile shown in this Figure are for 75%, 90% and 95% backfill of mine voids.

Subsidence Computations at Section E-E of Fairfax Mine

Section E-E is a transverse cross-section as shown in Figure 79. The Finite Element mesh for this cross-section is shown in Figure 102. The computed subsidence profile is shown in Figure 103. At both cross-sections the values of maximum subsidence was almost equal for 75%, 90% and 95% backfill of mine voids. For 50% recovery of coal, the value of maximum subsidence was computed to be equal to 2.0 feet i.e. 40% of seam thickness of 5 feet.

Subsidence Computations at Section B-B of Longridge Mine

Pillar configuration at section B-B of Longridge mine is shown in Figure 104. The Finite Element mesh for this section is shown in Figure 105. The analyses was conducted in two phases. Initially, the ground profile was assumed to be horizontal. The computed subsidence profile for this analysis is shown in Figure 106. In phase two, the ground profile is the actual one as shown in Figure 96. The Finite Element mesh used in this analysis is shown in Figure 107. The computed subsidence profile is shown in Figure 108. The maximum value of subsidence was computed to be

equal to about 1.75 feet, i.e., is 23% of the seam thickness of 7.5 feet in both cases. The ground profile apparently had no significant influence on the maximum value of subsidence.

Subsidence Computation at Section C-C of Longridge Mine

The location of section C-C is shown in Figure 80. The pillar configuration is shown in Figure 109. The Finite Element mesh used in this analysis is shown in Figure 110. The computed subsidence profile is included in Figure 111.

In the analyses conducted at both mines, pillar dimensions were assumed as 20 ft x 20 ft to see the effect of uniform pillar dimensions. The assumed pillar configuration for Fairfax mine is shown in Figure 104. The computed subsidence profile for this analysis is shown in Figure 106. The assumed pillar configuration at Longridge mine is shown in Figure 112 and the computed subsidence profile is shown in Figure 113. The value of the maximum subsidence due to uniform pillar dimensions was found to be slightly higher than the maximum value of subsidence computed due to actual pillar dimensions.

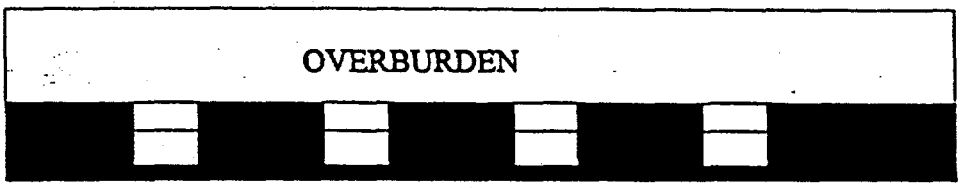

Figure 98 (a): 50% Backfill

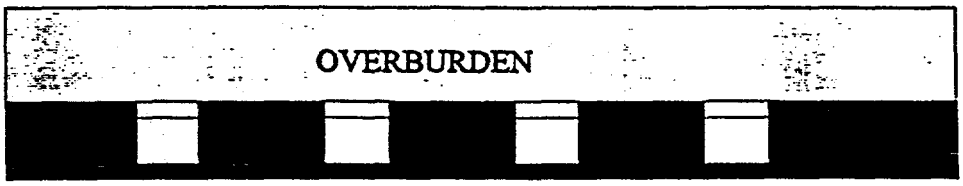

Figure 98 (b): 75% Backfill

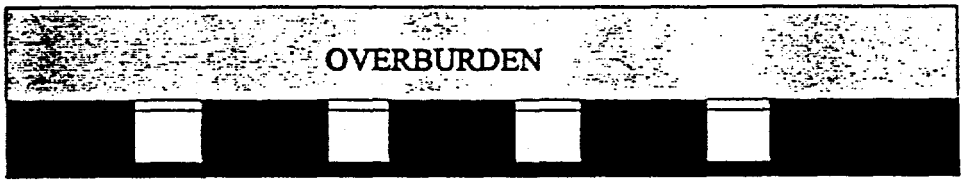

Figure 98 (c): 90% Backfill

Figure 98 : Actual Pillar Configurations at the Fairfax Mine Site

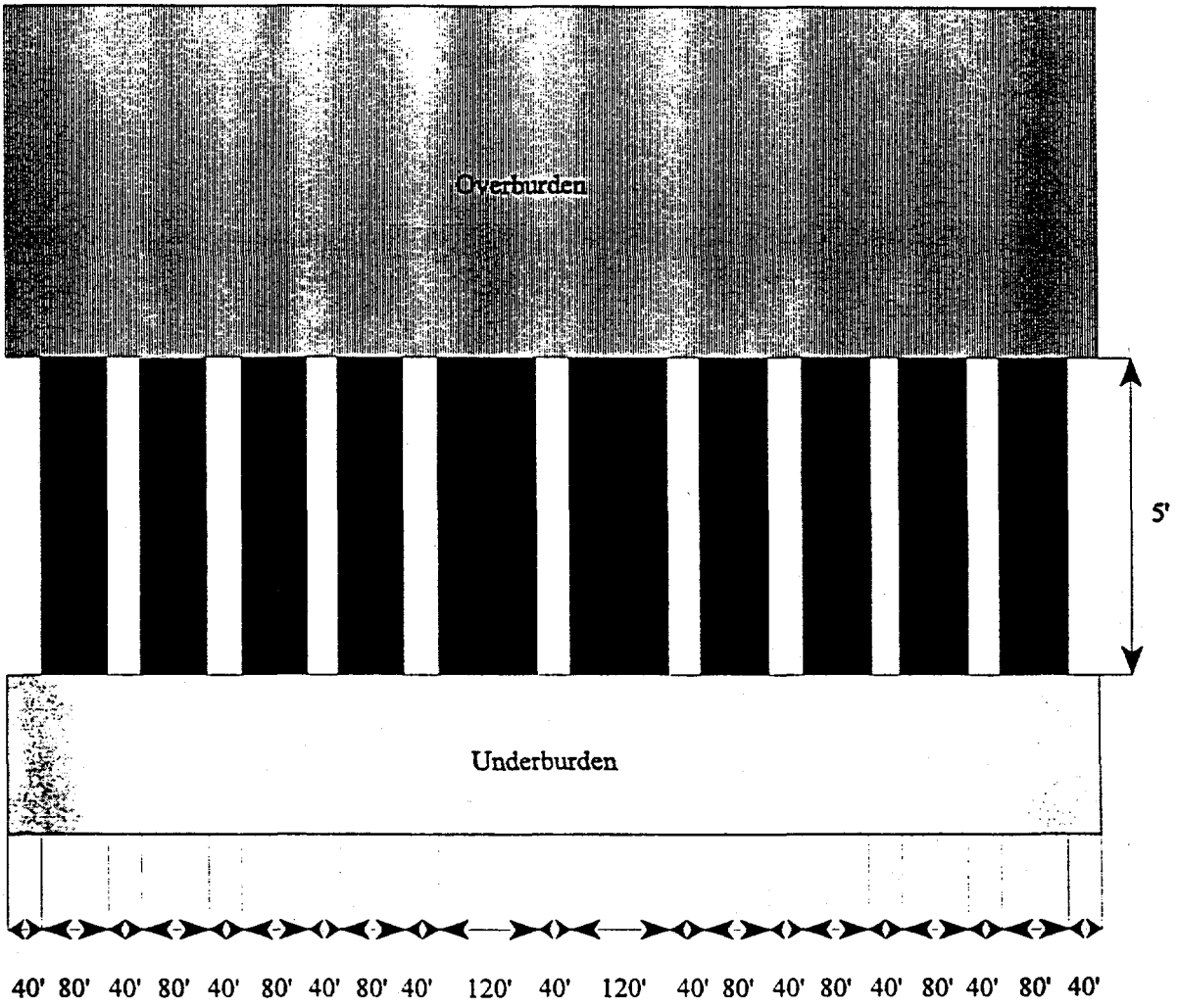

Figure 99 : Pillar Configurations at Section D-D of Fairfax Mine Site

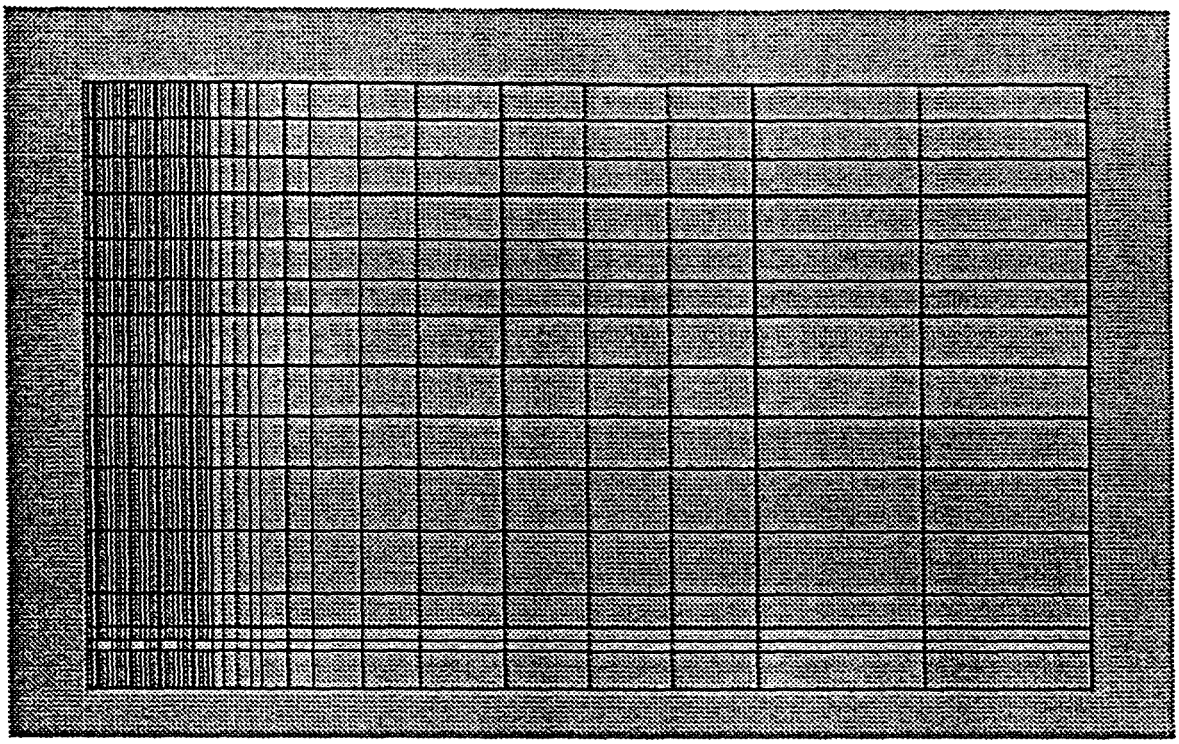

Figure 100 : Finite Element Mesh for Section D-D at Fairfax Mine

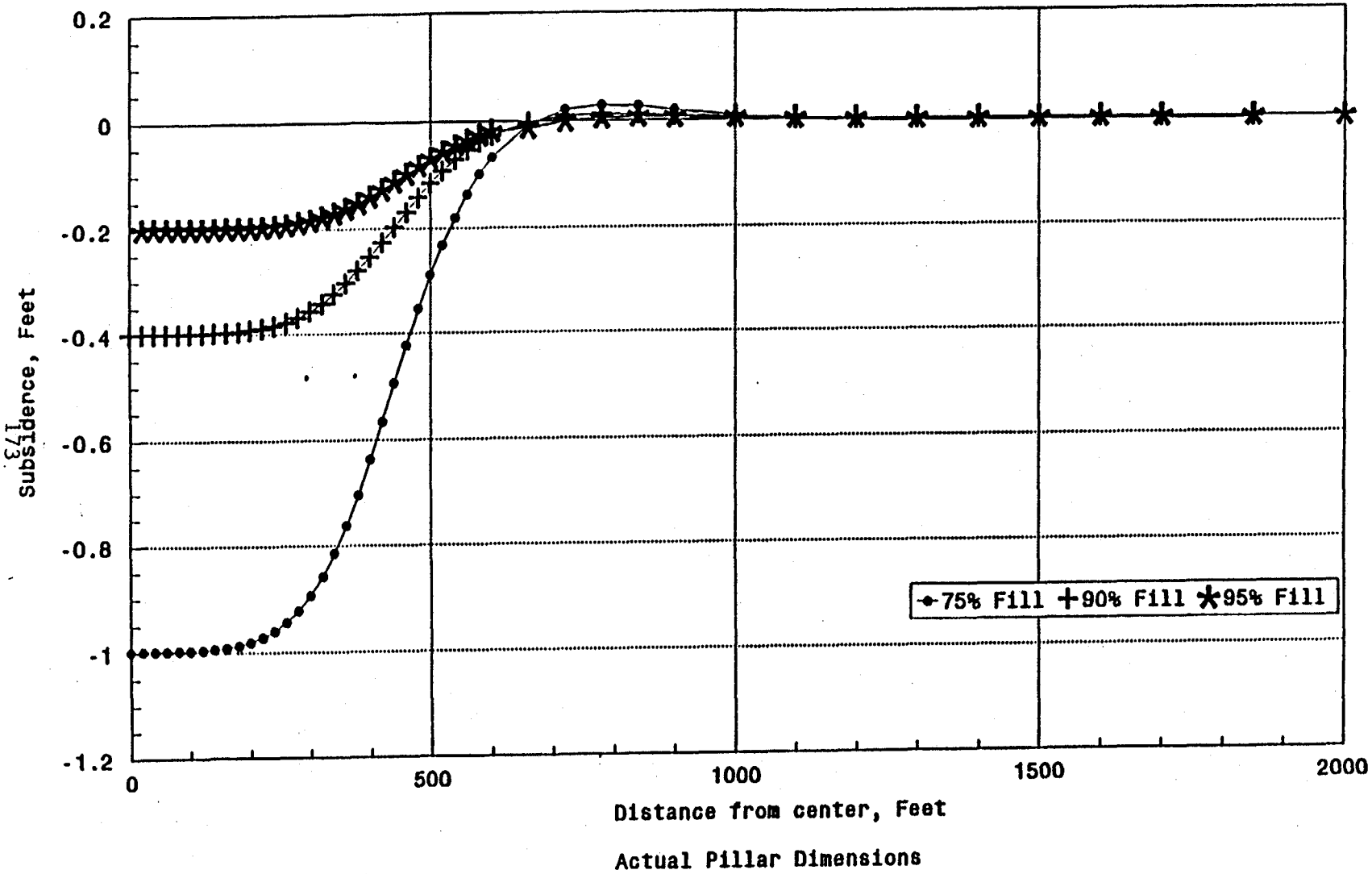

Figure 101 : Computed Subsidence Profile at Section D-D of Fairfax Mine Site

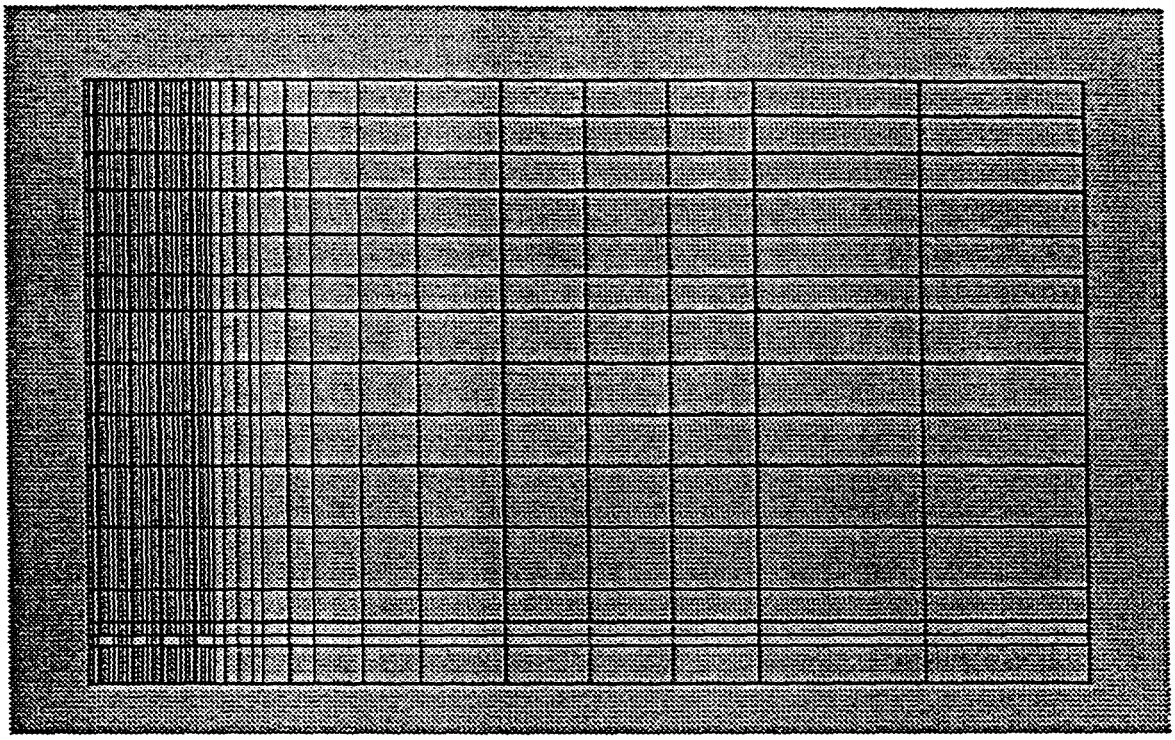

Figure 102 : Finite Element Mesh for Section E-E at Fairfax Mine

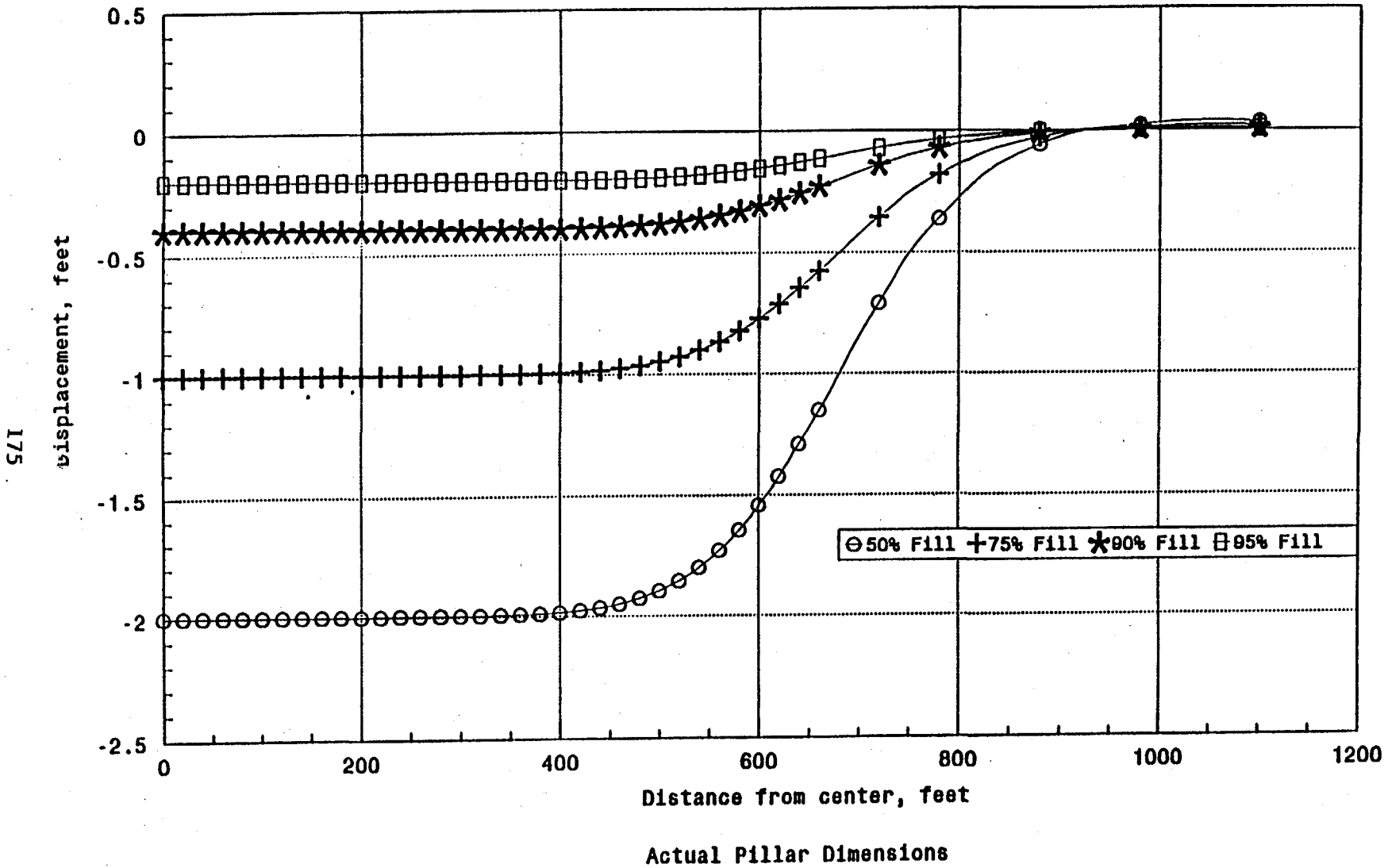

Figure 103 : Computed Subsidence Profile at Section E-E of the Fairfax Mine Site

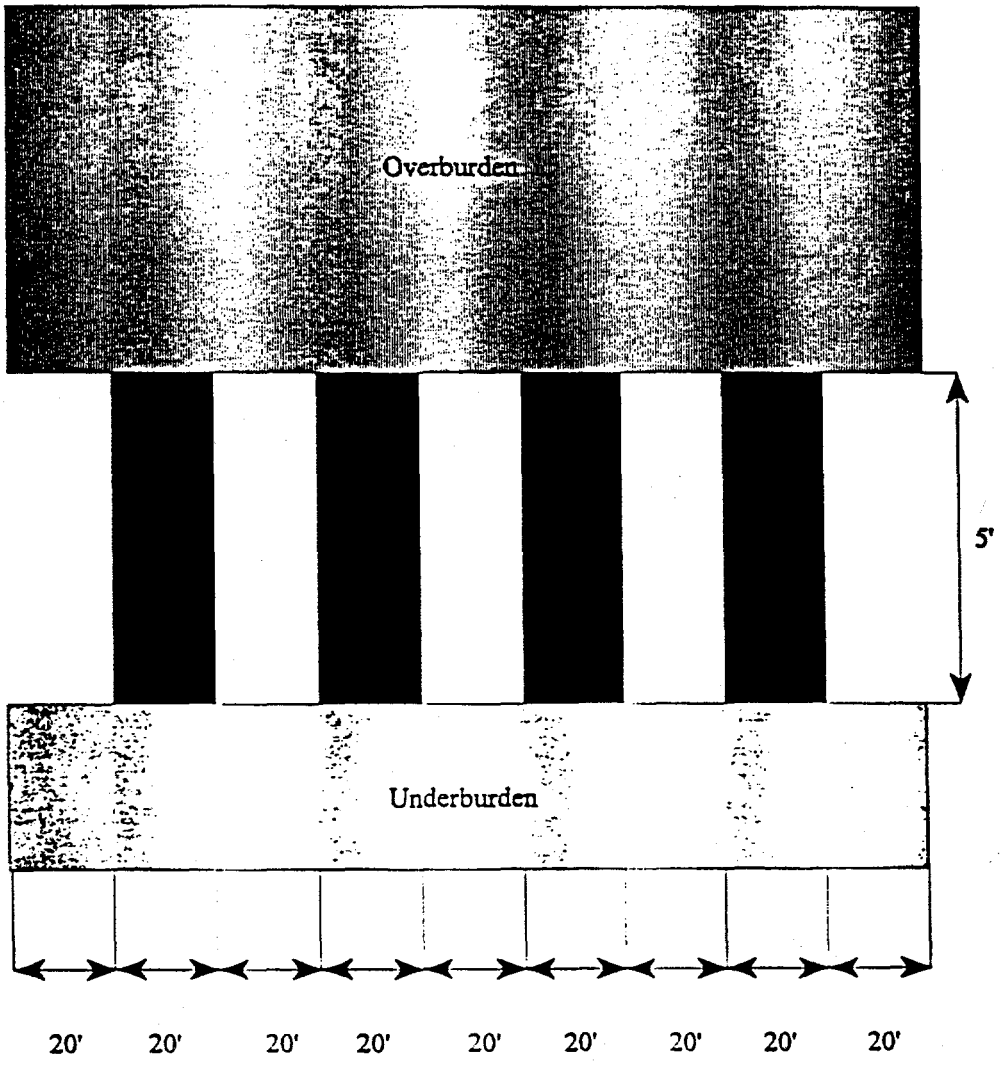

Figure 104 : Assumed Pillar Configurations at Fairfax Mine Site

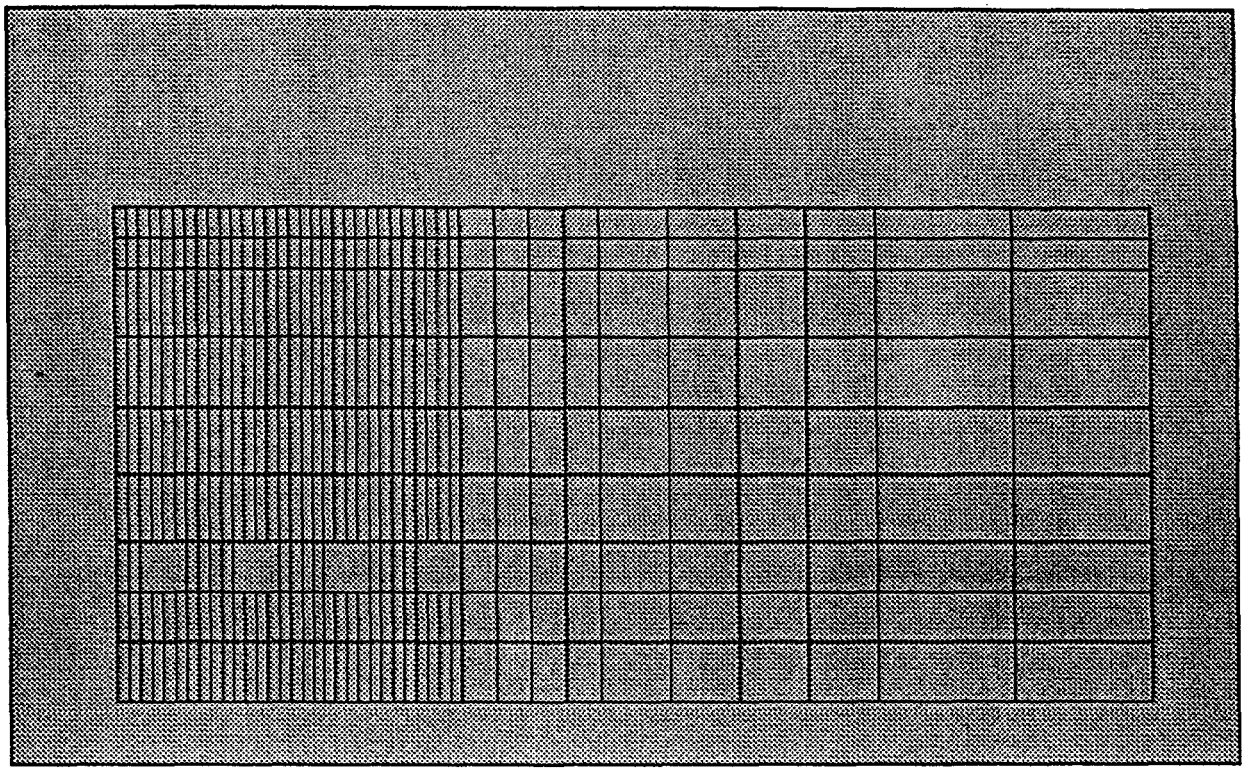

Figure 105: Finite Elelent Mesh for Section B-B with Horizontal Ground at Longridge Mine

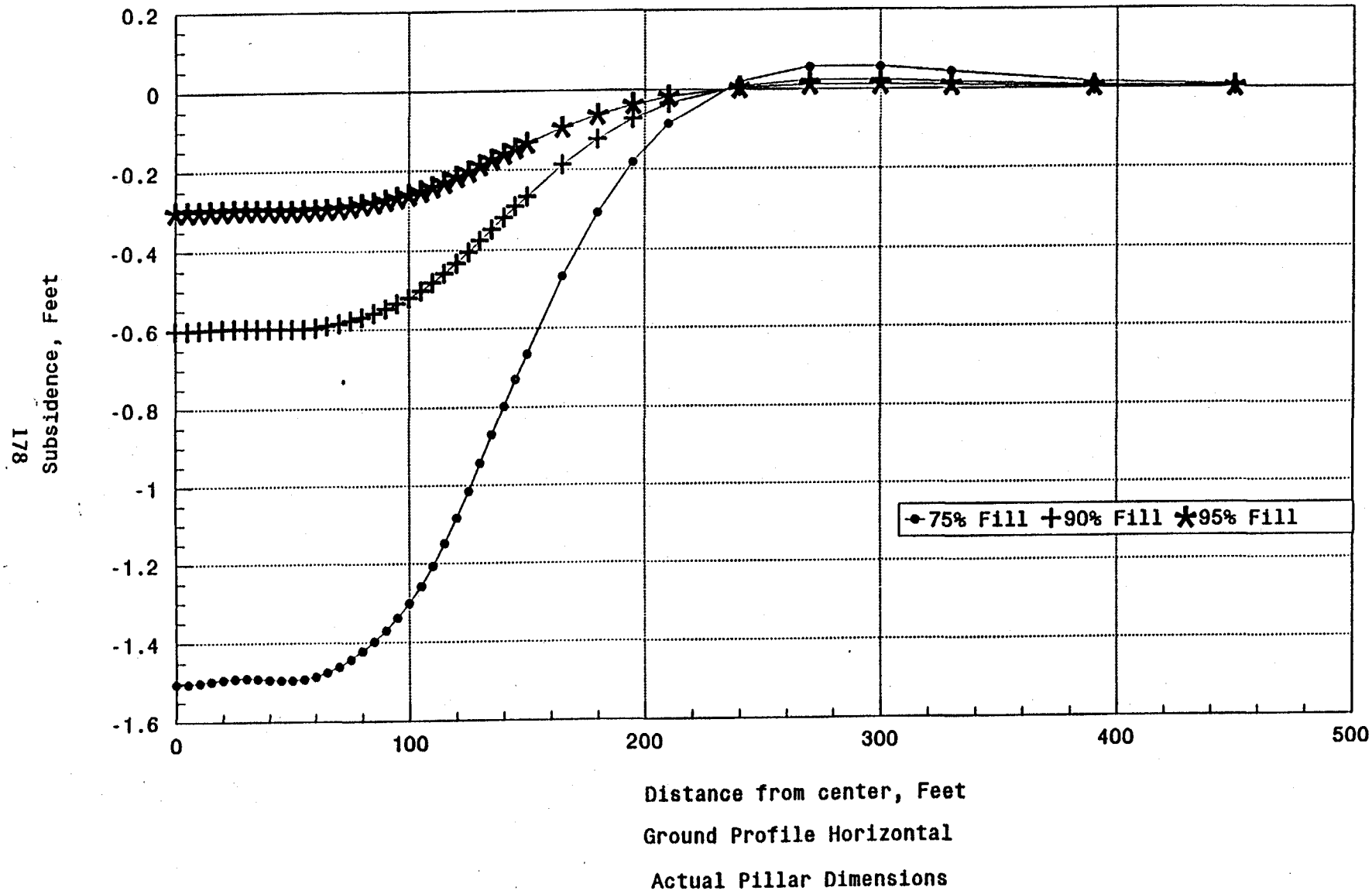

Figure 106 : Computed Subsidence Profile at Section B-B of Longridge Mine Site

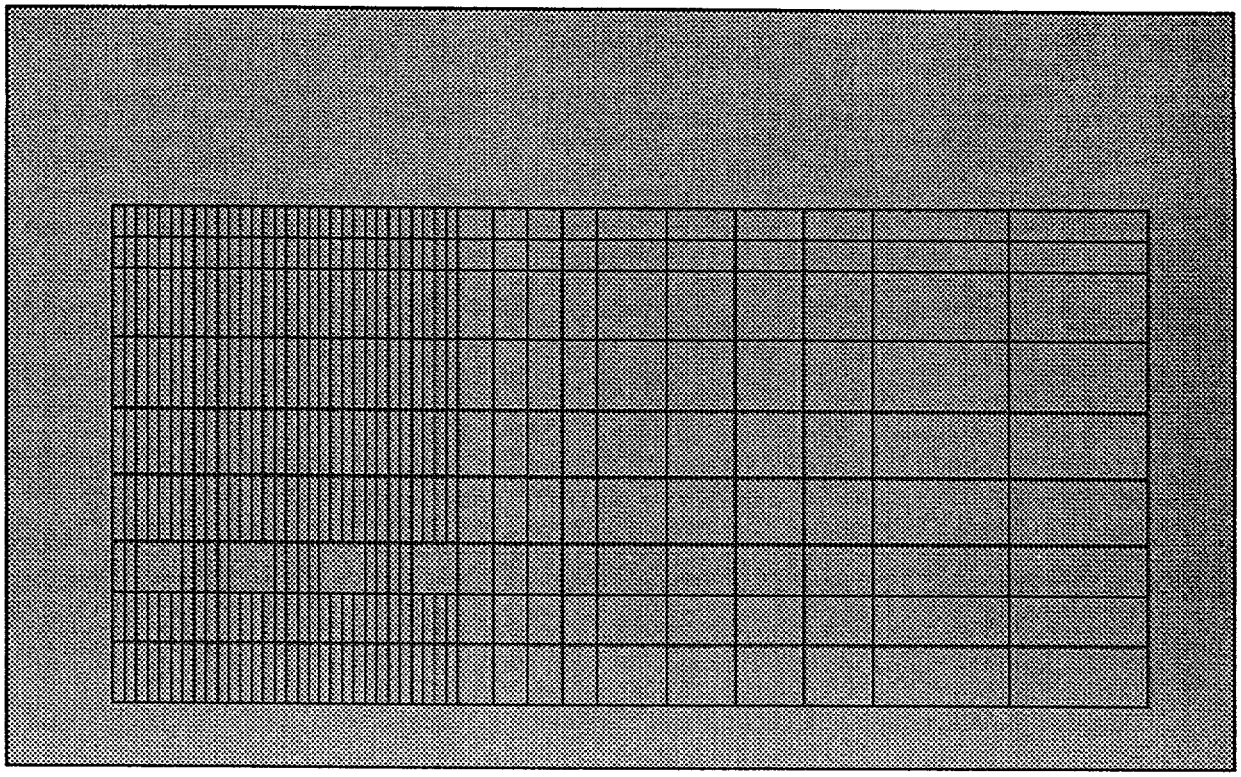

Figure 107:Finite Elelent Mesh for Section B-B with Horizontal Ground at Longridge Mine

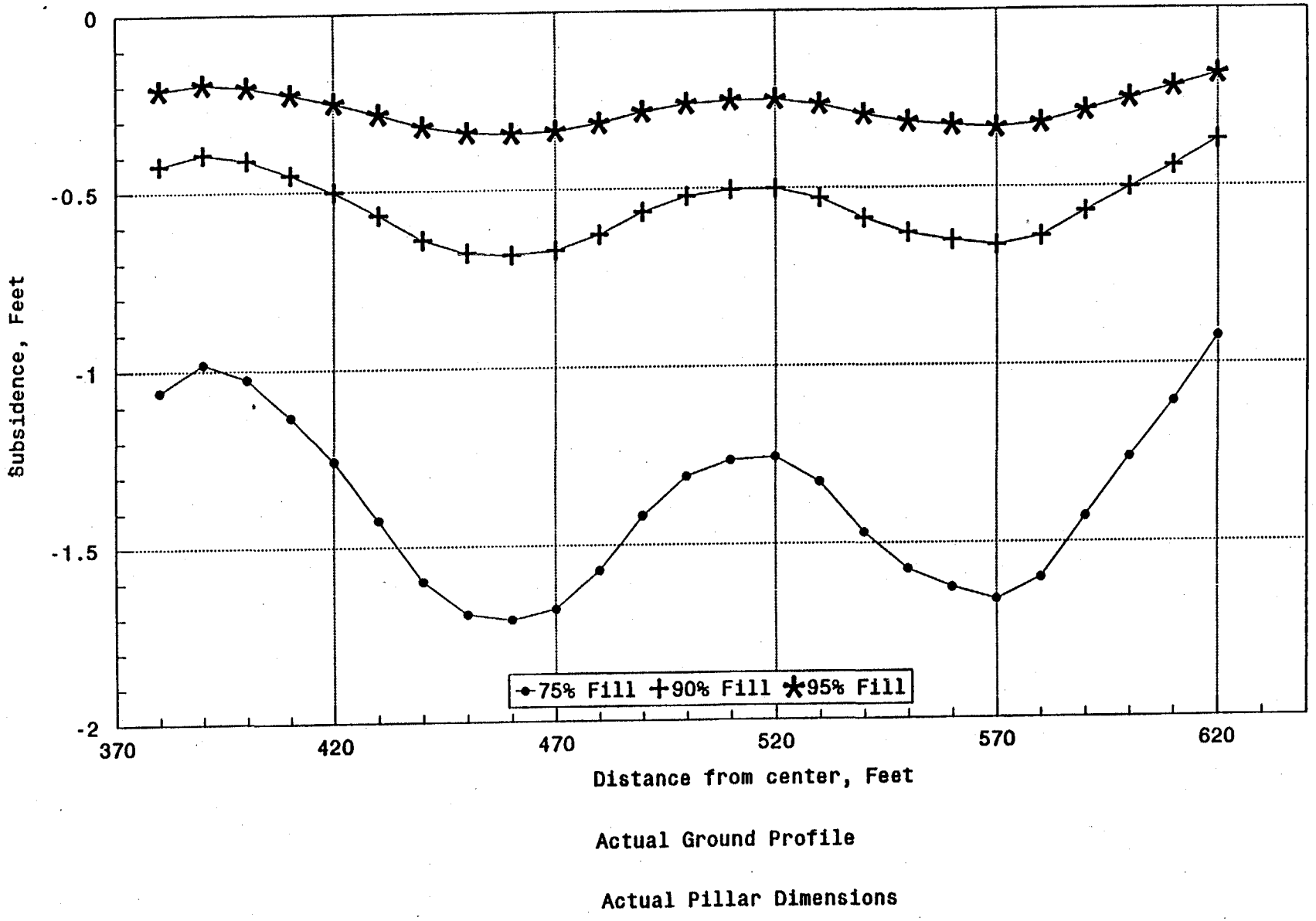

Figure 108 : Computed Subsidence Profile at Section B-B of Longridge Mine Site

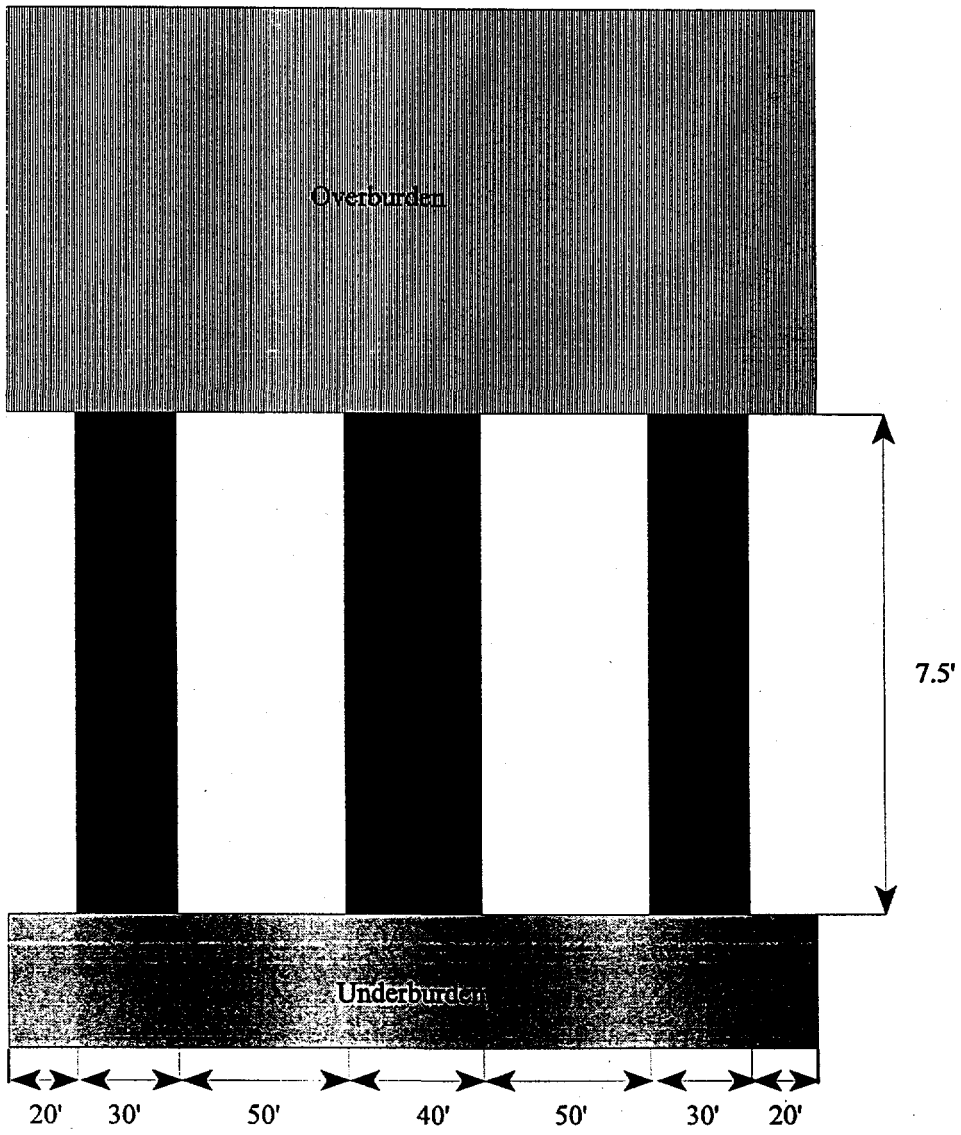

Figure 109: Pillar Configurations at Section C-C of Longridge Mine Site

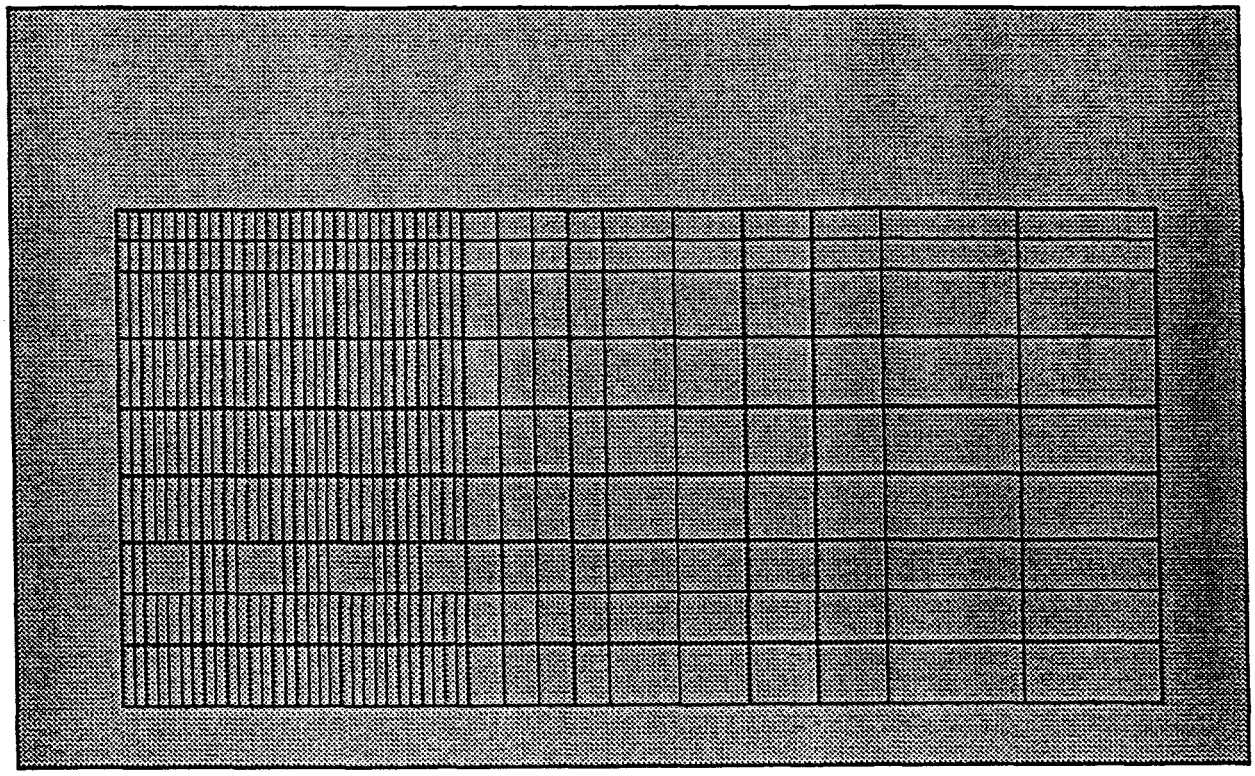

Figure 110: Finite Elelent Mesh for Section C-C with Horizontal Ground at Longridge Mine

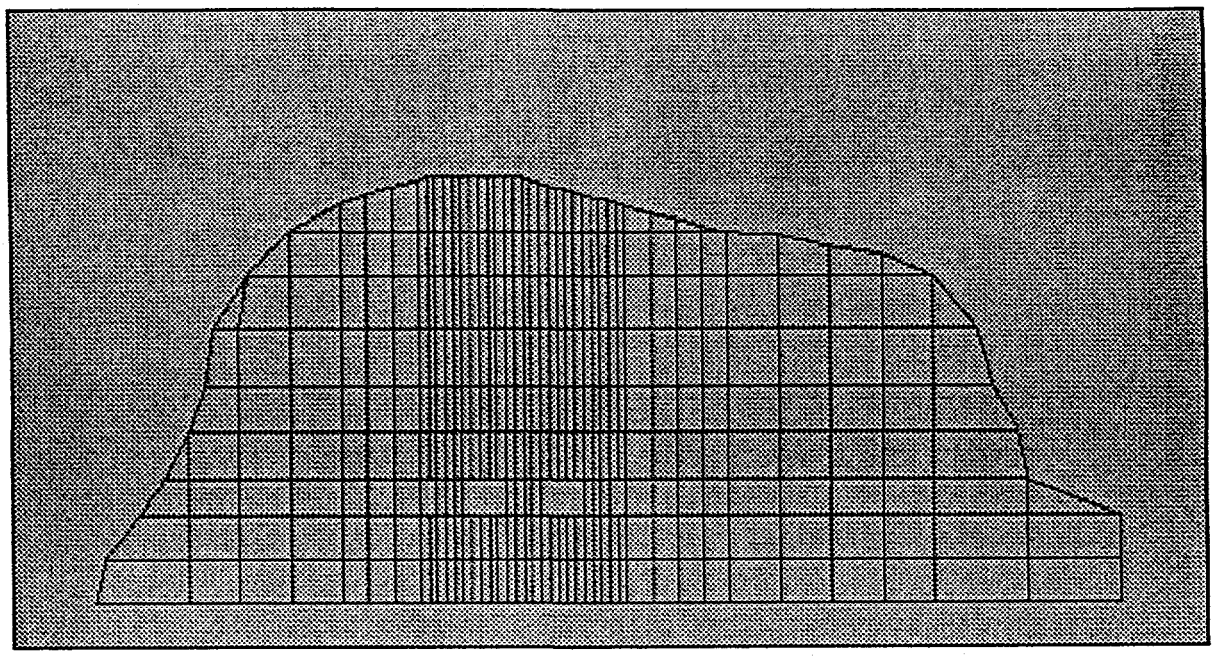

Figure 111: Finite element mesh used in the analysis of section c-c of the Longridge mine

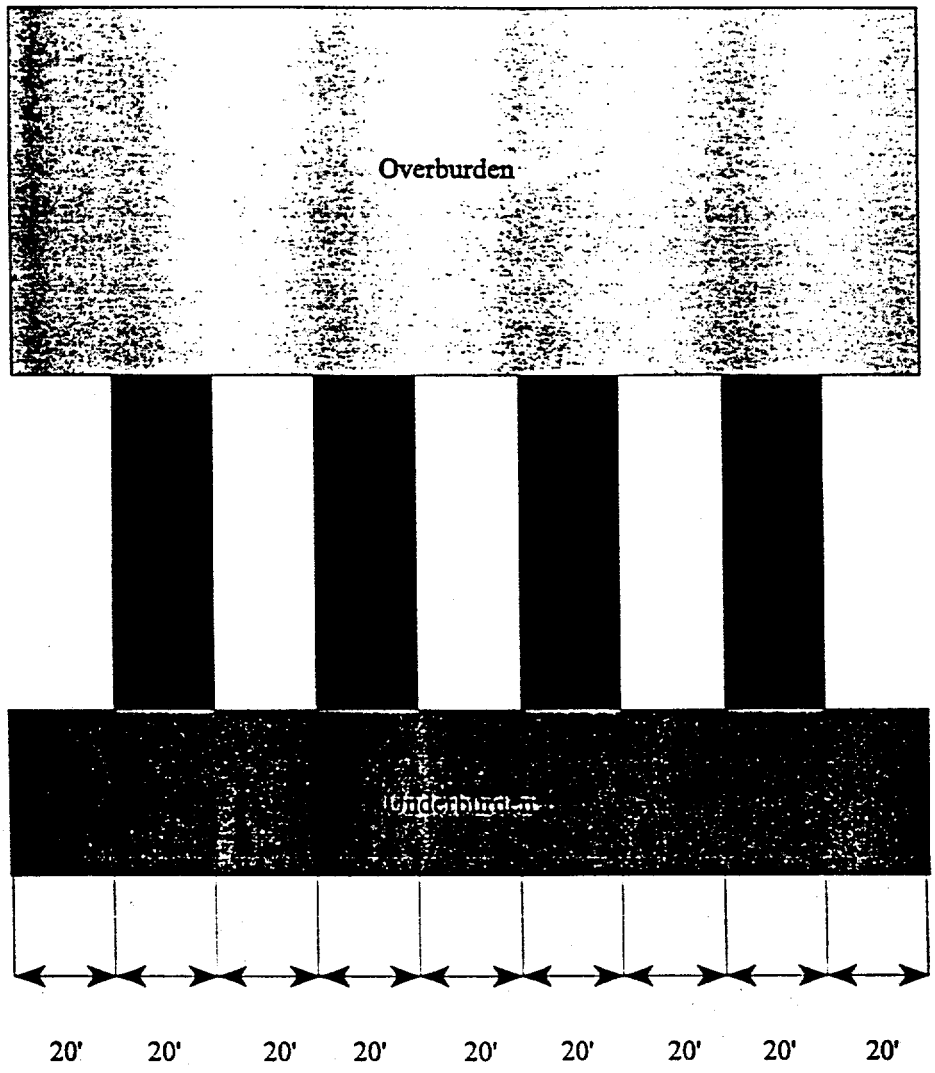

Figure 112 : Assumed Pillar Configurations at Longridge Mine Site

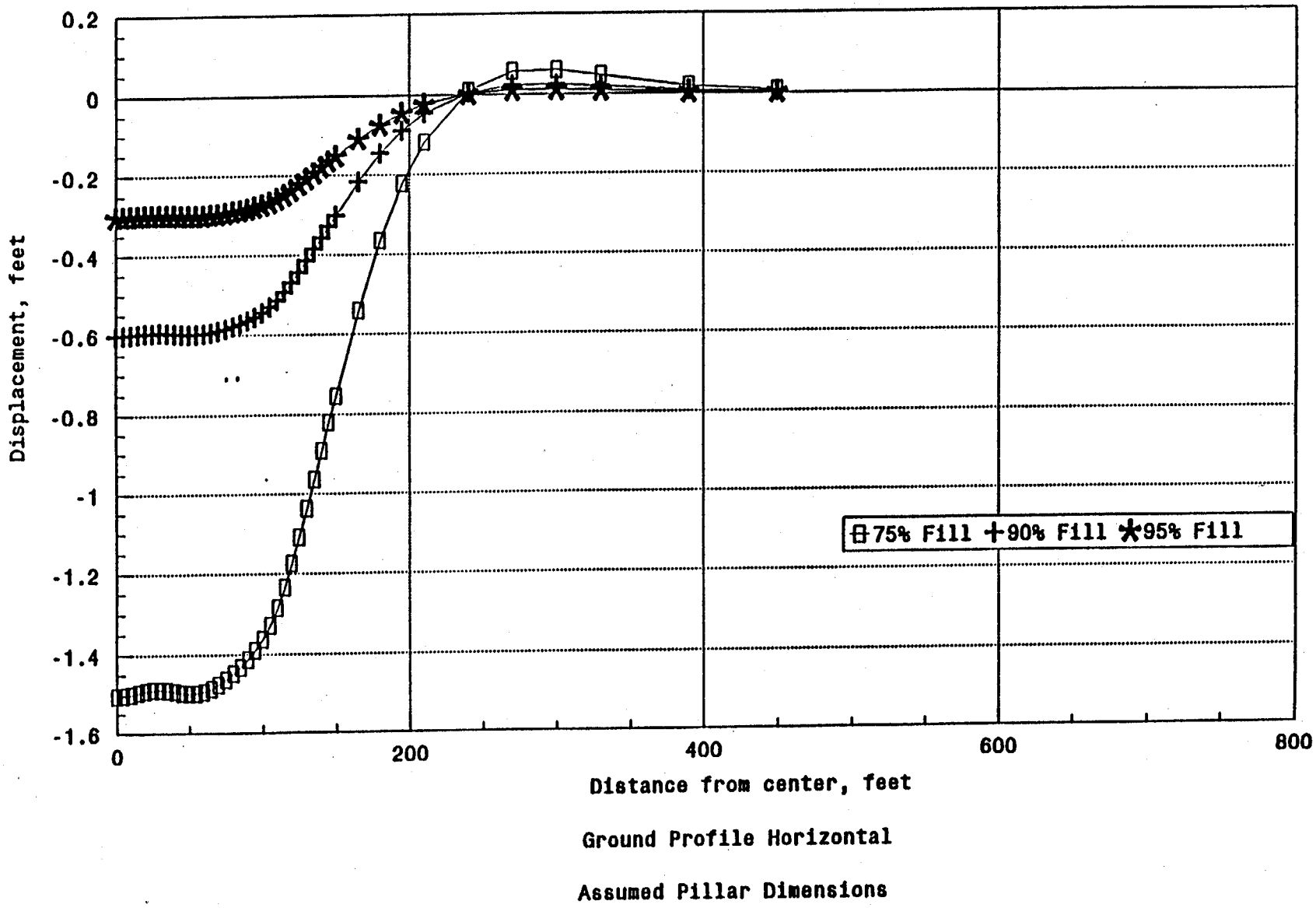

Figure 113 : Computed Subsidence Profile at the Longridge Mine Site

Grout Strength Requirements

Strength requirements of grout may vary with the method used for backfilling mine voids. The requirements are different for total backfill, partial backfill and for grout columns. Usually grout strength is estimated by calculating the stress caused by overburden at the level of coal seam by multiplying the thickness of the overburden with the respective unit weights. Insitu strength requirement varies from place to place and is a function of the following factors:

1) Local geology
2) Depth of coal seam
3) Stress orientations and Stress concentrations and,
4) The method used for placing grout.

Strength requirements found in the laboratory may have to be multiplied by a factor of safety to account for these uncertainties. Without accounting for any of these uncertainties, some preliminary calculations were done for calculating the grout strength requirements. Table 8 shows some of these preliminary study at Fairfax mine. Results of some preliminary calculations for Longridge mine are included in Table 9.

Summary and Conclusions

The results obtained from the Finite Element Analysis at the Fairfax and Longridge mines can be summarized as follows:

- The maximum value of the subsidence computed at the Fairfax mine was almost equal to the prescribed roof displacements in this analysis.
- The subsidence profiles were obtained for varying backfill configurations, i.e. for 75%, 90% and 95% backfill of mine voids.
- The larger the grout volume, the lesser the subsidence, as can be seen from the computed profiles.
- The effect of ground topography on the subsidence profile was not significant as can be seen from the computed values of maximum subsidence at section B-B of Longridge mine for both assumed and actual ground topographies.
- Preliminary calculations for grout strength requirements were performed by calculating the stresses at the level of the coal seam due to overburden height. In the present phase, detailed calculations for required grout strength are underway.

The required strength of grout should be multiplied by a factor of safety to account for the various uncertainties such as potential stress concentrations and segregation of the grout mix during placement as listed previously in this report.

Table 8 Expected Stress Levels On The Grout At Fairfax Mine Site

Core Holes	Stress In psf	Stress In psi
SQ-41	34495	239.54
SQ-42	35035	243.29
SQ-43	32815	227.88

Table 9 Expected Stress Levels On The Grout At Longridge Mine Site

Core Holes	Stress In psf	Stress In psi
LR-29	8982.5	62.37
LR-33	10488.5	72.83
LR-34	5456.25	38.51
LR-42	14905.5	103.51

TASK 6 CONTAMINANT TRANSPORT

Statement of the Problem

Acid Mine Drainage (AMD) is produced when sulphide minerals in waste rocks and coal measures are washed by groundwater in the presence of oxygen (Corbett, 1975). The Longridge Mine is an example where this phenomena occurs. The groundwater in the mine area flows through the mine reacting with the mineral pyrites in the presence of oxygen. This results in the outflow of AMD contaminated water from the mine.

Objectives of Study

The task on "Contaminant Transport and Acid Mine Drainage" is an endeavor to study the formation and propagation of AMD at the Longridge Mine. The aim of this task is to determine the flow patterns of the contaminant at the site. This task when accomplished is expected to provide information that will be useful in eradicating the AMD contamination problem at the mine.

Scope

This study will focus on the problem of AMD at the Longridge Mine. Given below are some factors that limit the scope of this study:

- The computer modeling will initially be limited to two-dimensional (multi-column, multi-layer, single row) simulations due to the complexity of the problem, and
- Unavailability of important computer modeling input parameters like groundwater table at the site and hydraulic conductivities would require some assumptions on these parameters.

AMD Phenomenon

Understanding the phenomenon of AMD production constitutes an important part of the this task. Permeability and location of underclays and coals greatly influence the groundwater flow in coal measures. The characteristic low permeability of clay severely restricts the downward flow of water. This causes the water to flow through the coals above, which are relatively more permeable. This is the first step of the AMD generation process (see Figure 114).

Deep mines serve as groundwater collection areas and provide unexpected flowpaths to the discharge points (Maryland, 1969). Groundwater flow patterns above the mine are greatly altered by deep mining. The mine roof often collapses into the cavity, which causes opening up

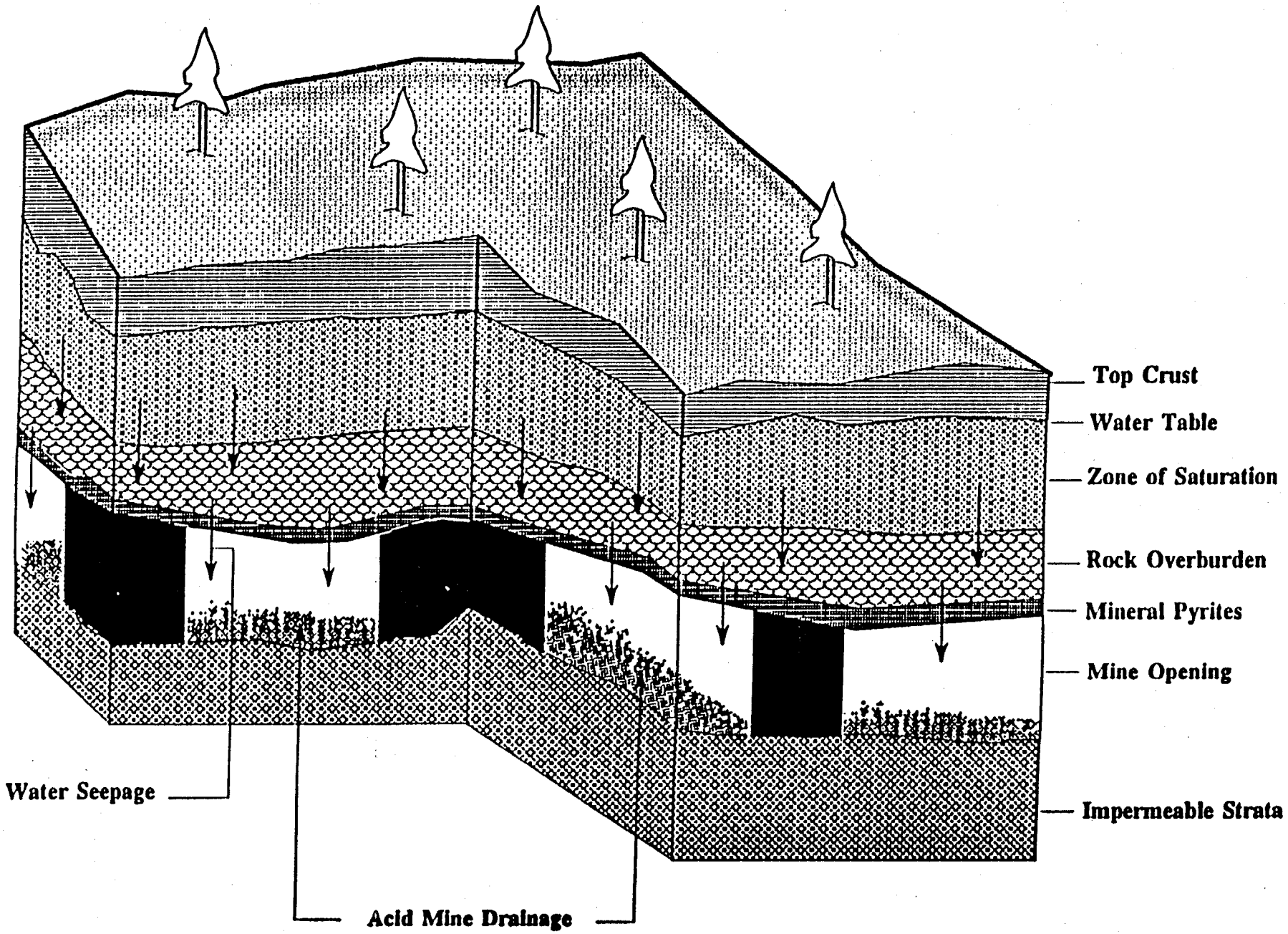

Figure 114 Schematic of Acid Mine Drainage

of overlying joint planes. These open joint planes often reduce the effectiveness of the overlying aquitards by providing vertical flowpaths which drain the overlying rocks. This water flows through the mine and acts as a transport medium for the soluble pyrite oxidation products.

AMD has many ill effects on the environment. Their production adversely affects man's water usage and water related facilities. Water with pH value lesser than 5 (acidic) kills aquatic life. Acid also dissolves concrete, corrodes most metals and increases water treatment costs. Toxic metal ions become highly soluble under highly acidic conditions. High sulfate concentration in AMD is a source of health hazards. Industrial water use is affected by the increase in acidity, hardness, iron and manganese.

There are some general methods of abatement of AMD. One of them is the prevention of formation of AMD at its source (e.g, mine sealing, reclamation of surface lands and waste piles, diversion of water from pollution sources.). Another method is by containing or isolating the polluted water or acid producing materials (e.g, deep well injection, surface and sub-surface impoundments). The third method is to disperse or dilute the pollutants to more acceptable levels (e.g, regulating waste discharges and diversion from one watershed to another).

Purpose

AMD (Acid Mine Drainage) is a common problem related to abandoned underground mines such as the Longridge Mine. Hundreds of gallons of contaminated water (AMD) flow out of the Longridge Mine every year causing a major environmental concern.

The production of AMD has many ill effects on the usage of water and water related facilities. This task is an attempt to study the groundwater flow patterns in the mine area and the propagation of contaminants after their formation. This study would help one in getting a thorough understanding of the problem of contamination from the mine. This task can be viewed as a step towards minimizing the production of the contaminants if not curbing it entirely.

Specific Objectives

The specific objectives of this task can be broadly listed as:

1. To understand the AMD and contaminant transport phenomena through literature review and other available data.
2. To study the groundwater flow patterns using computer software at the Longridge Mine in order to understand the AMD formation and transport process.
3. To study the spreading of the produced AMD using computer software.

Background

Literature Review

An elaborate literature survey was undertaken to identify and collect material relevant to Contaminant Transport and AMD. More than sixty relevant papers have been collected and a solid bank of references has been built for potential future use. This initial review of literature has greatly helped in comprehending the problem at hand and in developing a plan of approach for the task.

Source and Occurrence of AMD

Permeability and location of underclays and coals greatly influence the groundwater flow in coal measures. Many perched water tables are formed in coal measures because of these closely spaced underclays. The characteristic low permeability of clay severely restricts the downward flow of water. This causes the water to flow through the coals above, which are relatively more permeable.

Deep mines serve as groundwater collection areas by providing unexpected flowpaths to the discharge points (Maryland, 1969). The iron disulfide mineral pyrite is the greatest source of acid in coal measures. Pyrite is present in almost all coal and is found to be concentrated in the shaly portions of coal and the overlying carbonaceous shales. Pyrite is nearly insoluble until oxidized. Its oxidation products though are highly soluble. The crystal form of the pyrite and the presence of trace elements influence its oxidation potential.

The pyrite with low oxidation potential undergoes slow oxidation and does not produce much acid. The pyrite with high oxidation potential is termed 'reactive pyrite' and is responsible for most of the acid production.

Oxidation will certainly occur if the reactive pyrite is present in a non-flooded deep mine. Moisture is readily available as the air temperature is nearly constant and there is constant contact with ground water. More acidity is produced when the ferrous ion from the ferrous sulfate (in the above reaction) eventually oxidizes to the ferric state. The ferric ion precipitates under favorable conditions as a complex ferric oxy hydroxide called 'yellow boy'. Heavy yellow boy deposits are found associated with acid mine discharges (Maryland, 1969).

Oxygen in the mine may be either free oxygen or oxygen dissolved in water. The oxygen present in ground water is in trace amounts and is not responsible for significant acid production. The free air oxygen in deep mines is almost entirely responsible for pyrite oxidation.

High surface temperatures (about 105^0C) are favorable for acid production (West Virginia, 1985). Certain kinds of bacteria present in mine waters speed up the rate at which the acid forming reaction occurs. Pollution may also be caused by mine refuse piles resulting from the different mining activities.

Characteristics of Mine Water

The chemical alteration of water quality by coal mines begins with the exposure to the atmosphere of pyrite associated with coal during mining operations (West Virginia, 1985). The relatively insoluble exposed sulfide minerals are converted by oxidation, to sulfuric acid and iron compounds. Water coming into contact with these minerals dissolves the salts and transports the sulfuric acid which in turn dissolves other minerals.

The processes of water quality alteration depends upon:

1. The availability of air, water and iron sulfide minerals and the length of time water is in contact with the minerals.
2. Hydrologic, geologic and topographic features of the surrounding terrain and placement of mine with respect to them.
3. The type of mining method employed and whether the method is operationally active or inactive [9].

Table 10 shows the parameters and the range of values of concern for a water source affected by AMD.

Table 10: Indication of AMD (Maryland, 1969)

Parameter	Range of Values of Concern
pH	< 6
Acidity	sufficient to lower alkalinity below 20 mg/L.
Alkalinity	< 20 mg/L
Sulfates	> 250 mg/L
Hardness	>250 mg/L
Total Iron	> 1.0 mg/L
Manganese	> 1.0 mg/L
Aluminum	> 0.5 mg/L
Suspended Solids	> 250 mg/L
Dissolved Solids	> 500 mg/L

Impact on the Environment

Mine Drainage and associated conditions adversely affect man's water usage and water related facilities.

- Water with pH value lesser than 5 (acidic) kills aquatic life.
- Acid also dissolves concrete, corrodes most metals and increases water treatment costs.
- Yellowboy and strip mine silt clog drainage channels thus increasing flood potential.
- Toxic metal ions become highly soluble under highly acidic conditions.
- High sulfate concentration is a source of health hazards.
- Industrial water use is affected by the increase in acidity, hardness, iron and manganese.

These increase corrosion and scale formation in water using equipment. Navigational operations are affected by the acceleration of corrosion of barges and tow-boats. The overall maintenance and waste water treatment costs rise steeply as a result of ill effects of AMD (Maryland, 1969).

Abatement of AMD

A method of prediction of AMD called Acid Base Accounting is a chemical equilibrium approach in which the amount of acid that could be produced from iron sulfide minerals is compared to the amount of neutralizing minerals present. If the basic minerals present were insufficient to neutralize all the acid produced by the pyrite present then the overburden would be predicted to produce acid.

Detergents are used as ameliorants in cases where it is found that bacteria is actively involved in the acid production process (Batarseh, 1992). These detergents kill the bacteria. The technique of crushing limestone and spreading it in mines to counter the acidity produced by the toxic materials has been traditionally used.

Methodology

Study of AMD

The process of AMD production depends on several factors. The availability of air, water and iron sulfide minerals and the length of time water is in contact with the minerals play a role in determining AMD production rates. It is also affected by hydrologic, geologic and topographic features of the surrounding terrain and placement of mine with respect to them. The type of mining method employed also influences AMD production.

Table 10 shows the parameters and the range of values of concern for a water source affected by AMD. Literature was reviewed to identify the parameters in AMD contaminated waters and the their typical concentrations were noted. These values were compared to the contaminant levels of water flowing out of the Longridge Mine and drinking water standards (see Table 11). It was found that the outflow from the Longridge Mine could definitely be characterized as AMD contaminated water.

Hydrologic Computations

These computations were necessary in order to provide valuable input for the computer modeling phase. The catch basin for precipitation around the Longridge Mine area was approximated using the available surface and coal contour maps. With this information and the precipitation data at the site made available, the infiltration of precipitation into the ground at the Longridge Mine was calculated using the standard SCS (Soil Conservation Service) method (Haan & Bakersfield, 1978) (see Figure 115).

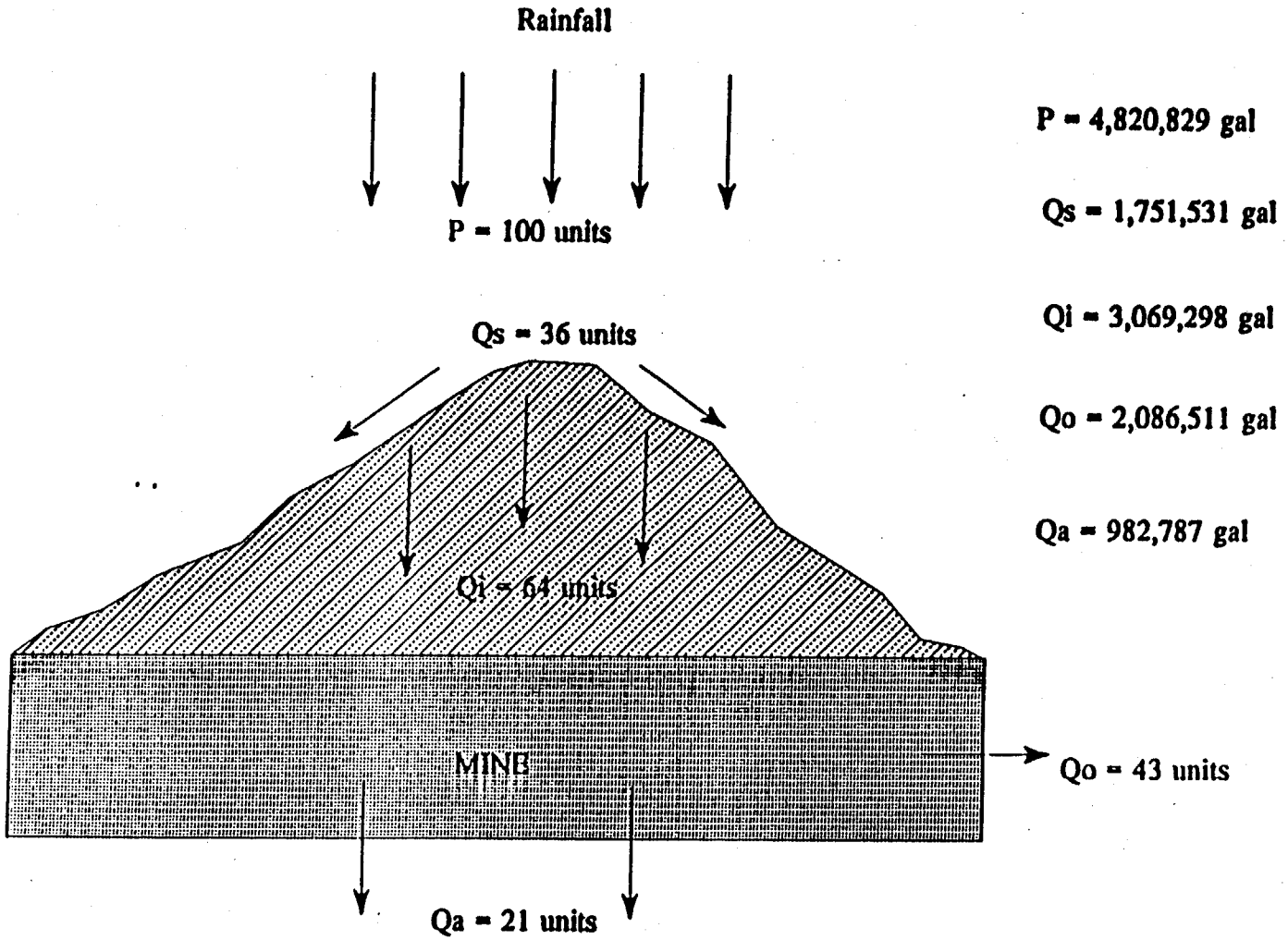

Figure 115 : Schematic of Average Monthly AMD at Longridge Mine

Table 11 : Comparison Of Parameters Of AMD At The Longridge Mine To Drinking Water Standards And Other Mine Water

Contaminant/Parameter	Drinking Water Standards	Highest AMD levels (from literature reviewed)	AMD levels in water from Longridge Mine*
pH	6.5-8.5	2.4	2.4
Acidity (mg/L)	-	35000	1264
Acid Load (lbs/day)	-	18283	967
Alkalinity (mg/L)	-	0	-
Total Iron (mg/L)	0.3	7600	238
Sulfate (mg/L)	<250	31000	
Aluminum (mg/L)	-	51	98.3
Manganese (mg/L)	<0.05	675	29.3
Turbidity (TU)	<5	36	-
Dissolved Oxygen (mg/L)	-	4	-
Total Solids (mg/L)	-	103.5	-
Total Hardness (mg/L)	-	13600	2190
Magnesium (mg/L)	-	2990	124
Calcium (mg/L)	-	507	238
Arsenic (mg/L)	0.05	-	0.92
Selenium (mg/L)	0.01	-	0.84
Lead (mg/L)	0.05	-	0.34
Barium (mg/L)	1.0	-	<0.05
Cadmium (mg/L)	0.01	-	<0.05

*The data shown in this table were not all collected on the same day. The table is a representation of the worst case scenario of each parameter from the data available. The data shown in this column was obtained from Dr. W. Sack who collected the data under a different task in the project.
**Reference-7

These infiltration rates were compared to the outflow data from the mine made available (see Table 12 and Table 13). These comparisons were useful in gaining an insight into the flow patterns at the site and in providing input for the computer modeling part of the task (see Figure 116).

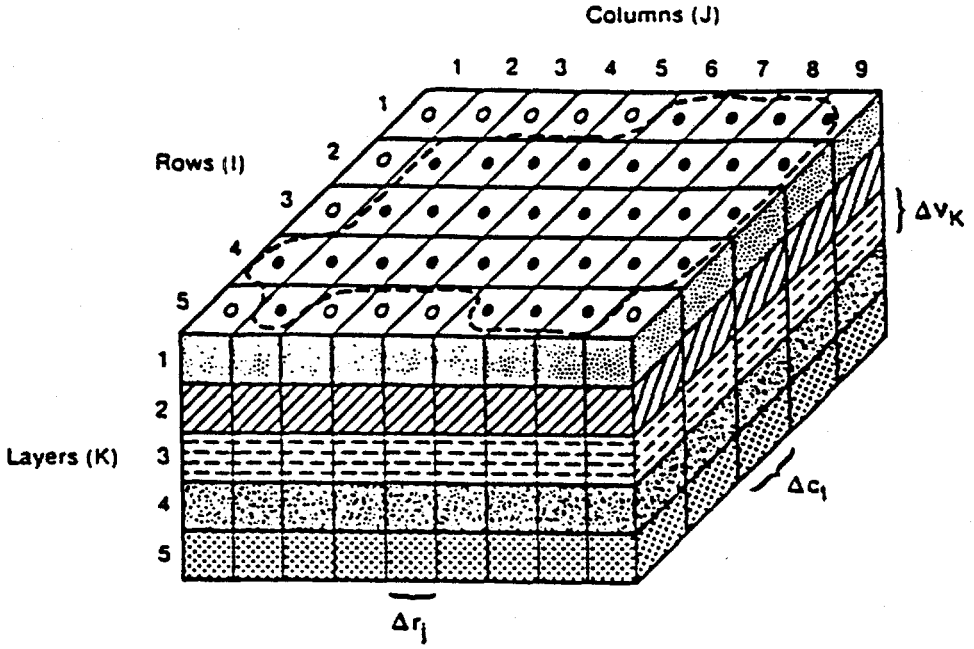

Explanation

----	Aquifer Boundary
•	Active Cell
0	Inactive Cell
Δr_J	Dimension of Cell Along the Row Direction. Subscript (J) Indicates the Number of the Column
Δc_I	Dimension of Cell Along the Column Direction. Subscript (I) Indicates the Number of the Row

Figure 116 : Schematic Descritization Used By MODFLOW [Reference-8]

Computer Modeling of Contaminant Transport

Appropriate computer software was identified for the modeling work involved in this task. MODFLOW, MT3D, MODELCAD and SURFER are the software packages identified for this purpose. A brief description of these models are given below.

MODFLOW

MODFLOW, a Modular Three-Dimensional Finite Difference Groundwater Flow Model, was developed by Michael G. McDonald and Arlen W. Harbaugh for the United States Geological Survey (1985). This model will be used as the basic modeling tool in this study.

MODFLOW is probably the most widely used groundwater modeling package. The model simulates groundwater flow in two and three-dimensions and has the capability to simulate a specific feature of a hydrologic system such as flow from rivers and flow into drains. Groundwater flow within the aquifer is simulated using a block centered finite-difference approach (see Figure 117).

Given below is a brief description of the governing equation and other conditions the MODFLOW code uses. The three dimensional groundwater flow equation through porous earth material maybe written as given below:

$$\frac{\partial}{\partial x}\left(K_{xx}\frac{\partial h}{\partial x}\right) + \frac{\partial}{\partial y}\left(K_{yy}\frac{\partial h}{\partial y}\right) + \frac{\partial}{\partial z}\left(K_{zz}\frac{\partial h}{\partial z}\right) - W = S_s\frac{\partial h}{\partial t} \qquad (1)$$

where,

K_{xx}, K_{yy} and K_{zz} are the values of the hydraulic conductivity along x, y and z directions (LT^{-1})
h is the potentiometric head (L)
W is a volumetric flux per unit volume and represents sources and/or sinks of water (T^{-1})
S_s is the specific storage of the porous material (L^{-1})
t is time (T)

Equation (1) depicts groundwater flow in a heterogeneous anisotropic medium, under nonequilibrium conditions. Baring some very simple flow systems, analytical solutions of equation (1) are possible, thus various numerical methods should be employed to obtain approximate solutions. One such approach is the use of finite-difference method, wherein the continuous equation described by equation (1) is replaced by a finite set of discrete points in space and time, and the partial derivatives are replaced by the differences in head values at these points. This leads to a series of equations whose solution yields values of heads at specific points and times (McDonald, et.al., 1985).

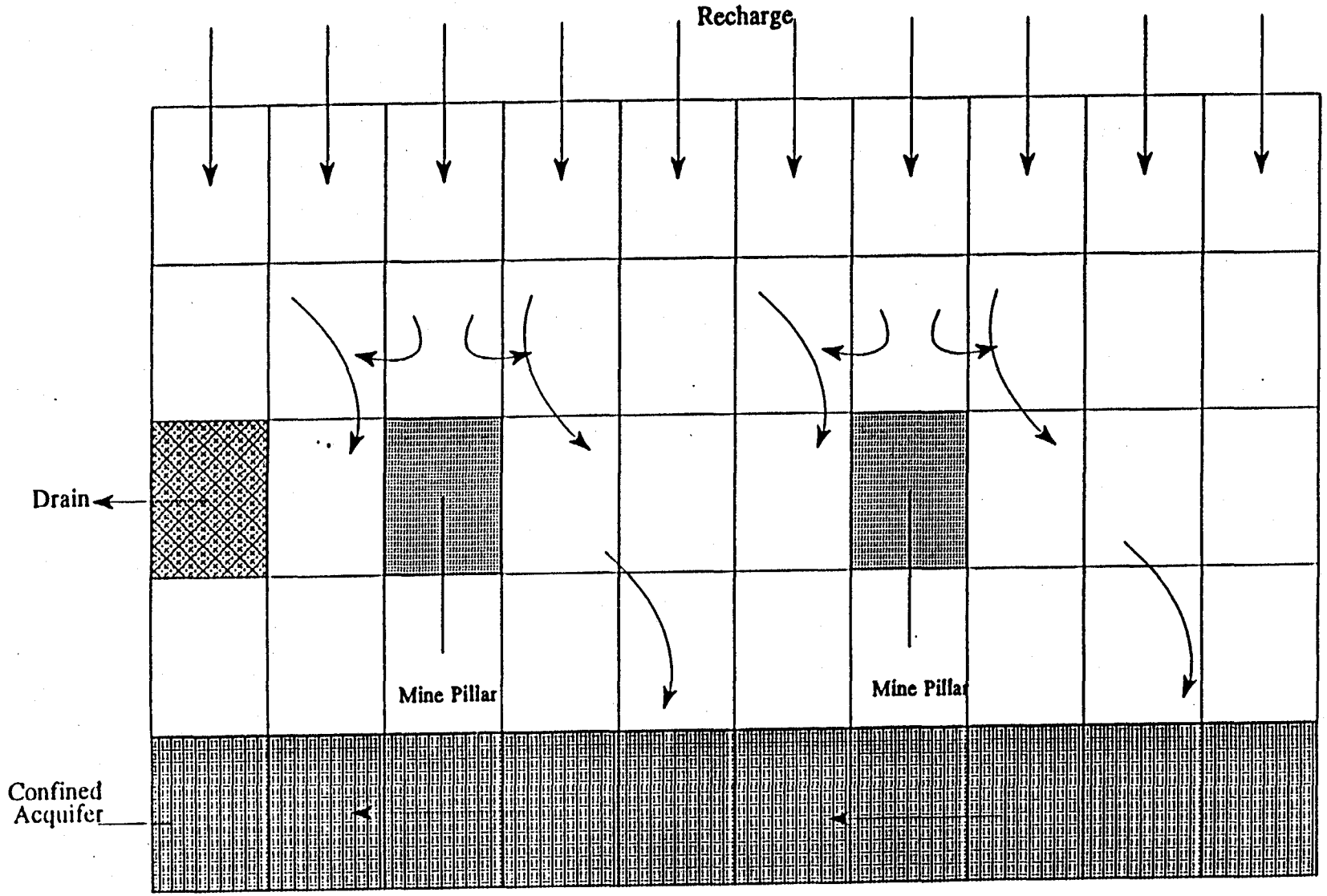

Figure 117 : Schematic of The Grid With The Flow Lines From The MODFLOW Simulation

Figure 117 shows a spatial discretization of an aquifer system with a mesh of cells, whose locations are described by rows columns and layers. An i, j, k indexing system is used. For a system consisting of n rows, n columns and n layers, the row index is I = 1, 2, 3... the column index is j = 1, 2 ,3...the layer index is k = 1, 2, 3... and so on.

Table 12: Flow Data At Longridge Mine

Month	Rainfall Vol.* (gal)	Infiltration Vol. (gal)	Outflow from Mine* (gal)	Losses (gal)
August '94	14,454,180	5,281,867.5	2,885,760	2,396,107.5
September '94	5,579,535	3,709,075	1,169,856	2,539,219
October '94	1,702,935	1,661,400	530,100	1,131,300
November '94	2,007,525	1,907,841	401,328	1,506,513
December '94	5,621,070	3,710,460	1,727,835.8	1,982,624.2
January '95	4,901,130	3,469,557	3,278,584.8	190,972.2
February '95	2,478,255	2,247,043.5	2,365,372.8	-118,329.3
March '95	2,796,690	2,451,949	3,881,336.4	-1,429,387.4
April '95	2,796,690	2,451,949.5	1,458,172.8	993,776.7
May '95	5,870,280	3,801,837	3,166,761.6	635,075.4
Average	4,820,829	3,069,298	2,086,510.8	982,787.13

* These columns are based in part on the data provided by Dr. W. Sack.

Table 13: Infiltration and Outflow Data At Longridge Mine As Percentages of Rainfall

Month	Rainfall Vol.	Runoff Vol. (as a %of rain)	Infiltration Vol. (as % of rain)	Mine Outflow* (as %of rain)	Losses (as%of rain)
August '94	100%	64%	36%	19.95%	16.58%
September '94	100%	33.52%	66.48%	20.97%	45.51%
October '94	100%	2.45%	97.55%	31.13%	66.42%
November '94	100%	4.97%	95.03%	19.99%	75.09%
December '94	100%	33.99%	66.01%	30.74%	35.27%
January '95	100%	29.21%	70.79%	58.33%	12.46%
February '95	100%	9.33%	90.67%	95.44%	-4.77%
March '95	100%	12.33%	87.67%	138.78%	-51.11%
April '95	100%	12.33%	87.67%	52.14%	35.53%
May '95	100%	35.24%	64.76%	53.94%	10.82%
Average	100%	36.33%	63.67%	43.28%	20.39%
Average without August	100%	20.67%	79.33	53.26%	26.07%

* This column is based in part on data provided by Dr. W. Sack.

MT3D

MT3D is a Modular Three-Dimensional Transport Model developed by C. Zheng (1990) of S. S. Papadopulos & Associates Inc. for the United States Environmental Protection Agency. In this study, the MT3D model will be used to investigate AMD contaminant transport. It can simulate advection, dispersion, sink/source mixing, and chemical reactions independently.

The MT3D transport model uses a mixed Eulerian-Lagrangian approach to the solution of the three-dimensional advective-dispersive reactive equation. It is intended to be used in conjunction with any block-centered finite-difference model such as MODFLOW and is based on the assumption that changes in the concentration field will not affect the flow field measurably. This allows a user to construct and calibrate a flow model independently. MT3D receives the hydraulic heads and the various flow and source/sink terms saved by the flow model (MODFLOW in this case), automatically incorporating the specified hydrologic boundary conditions. MT3D can accommodate the following spatial discretization and boundary conditions (Zheng, 1990):

- confined, unconfined or variably confined/unconfined aquifer layers
- inclined model layers and variable cell thickness within the same layer
- specified concentration or mass flux boundaries
- the solute transport effects of external sources and sinks such as wells, drains rivers, areal recharge and evapotranspiration.

The partial differential equation describing three-dimensional transport of contaminants in groundwater is as given below ;

$$\frac{\partial C}{\partial t} = \frac{\partial}{\partial x_i}[D_{ij}\frac{\partial C}{\partial t}] - \frac{\partial}{\partial x_i}(v_i C) + \frac{q_s}{\theta}C_s + \Sigma R_k \qquad (2)$$

where

C is the concentration of the contaminants dissolved in groundwater, ML^{-3}

t is time, T

x_i is the distance along the respective Cartesian coordinate axis, L

D_{ij} is the hydrodynamic dispersion coefficient, L^2T^{-1}

v_i is the seepage or linear pore water velocity, LT^{-1}

q_s is the volumetric flux of water per unit volume of aquifer representing sources (+) and sinks (-), T^{-1}

C_s is the concentration of the sources or sinks, ML^{-3}

θ is the porosity of the porous medium (dimensionless)

ΣR_k goes from k=1, N and is a chemical reaction term, $ML^{-3}T^{-1}$

The advective-dispersive-reactive equation [eqn. 2 above] describes the transport of miscible contaminants in groundwater flow systems. Most numerical methods for solving the advective-dispersive-reactive equation can be classified as Eulerian, Lagrangian or mixed Eulerian-Lagrangian. In the Eulerian approach, the transport equation is solved with a fixed grid method such as finite-difference or finite-element method. In the Lagrangian approach, the transport equation is solved either in a deforming grid or a deforming coordinate in a fixed grid. The mixed Eulerian-Lagrangian approach attempts to combine the advantages of both the approaches by solving the advection term with a Lagrangian method and the dispersion and reaction terms with a Eulerian approach (Zheng, 1990).

SURFER and MODELCAD SOFTWARE

MODELCAD is the proposed pre-processor for MODFLOW. MODELCAD provides a graphic visual interface to the user. It allows for convenient finite-different grid generation and easy methodical input of the various boundary conditions and other parameters. It then creates the input files to be fed into MODFLOW. It is an efficient and widely used pre-processor.

The post-processor to be used to obtain plots and contours in order to help interpret the output from MODFLOW is SURFER. SURFER also is an efficient and a widely used postprocessor.

A couple of two-dimensional test models were constructed and run using MODFLOW based on the hydrologic calculations made and using approximate values of the various geohydrologic parameters (see Figure 118).

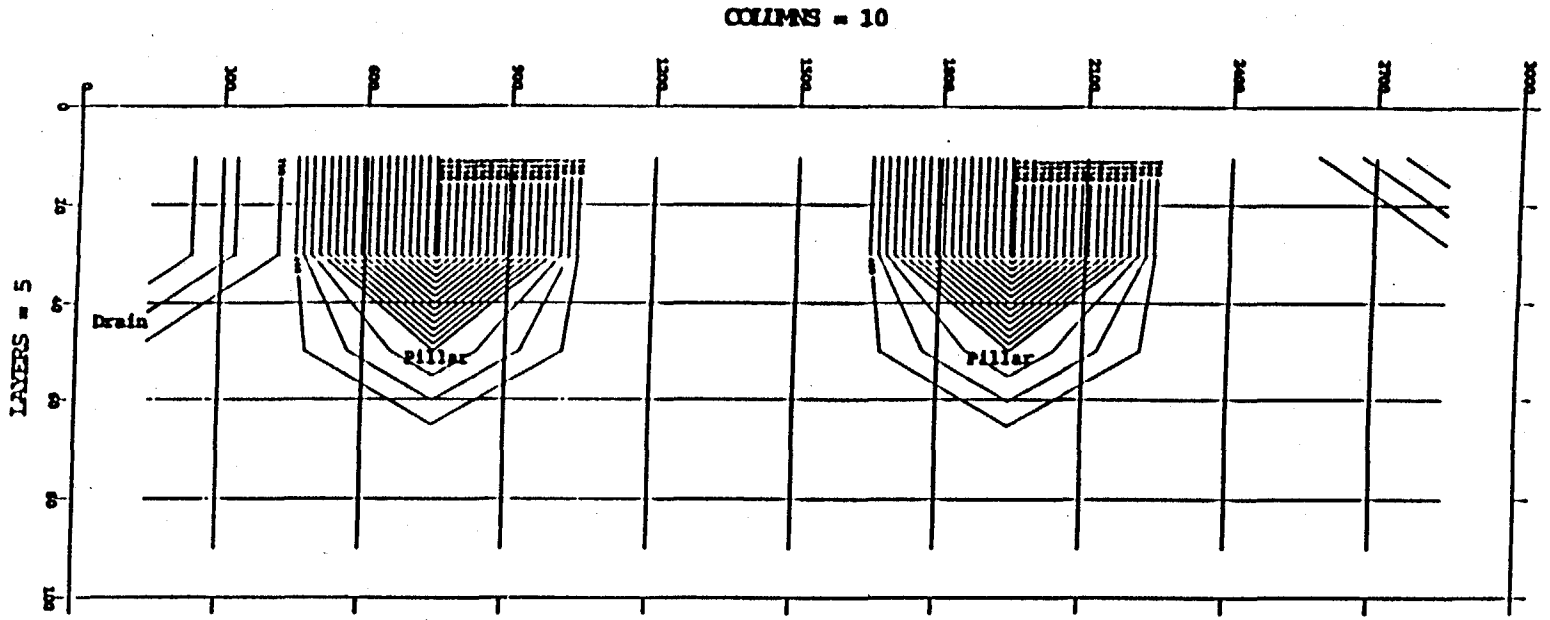

Figure 118 : SURFER Plot of The Fluid Heads Generated By The First Trial

MODFLOW Simulation

Results and Discussion

Given under is the summary of preliminary results obtained. These results were obtained from the initial study of AMD characteristics from literature and from the outflow data from the Longridge Mine made available:

- The outflow from the Longridge Mine maybe characterized as AMD contaminated water based on literature review (see Table 10 and Table 11).
- This outflow has very high contaminant concentrations and greatly exceeds the drinking water standards (see Table 11).

This initial study serves as the starting point for other studies under this task.

Hydrologic Findings

The hydraulic computations were made primarily to provide useful and necessary input for the subsequent modeling work. However, some useful observations were made at this stage of the task. It was found that not all the water infiltrating into the mine area was flowing out of the mine. This could mean that a part of the infiltration is being lost to the layers below the mine opening as seepage or to the groundwater table (see Table 13 and Figure 117) (Bedient, et.al., 1994). Though the calculations were approximate a fair picture of the geohydrologic system at the Longridge Mine was obtained (Freeze & Cherry, 1979). It should be noted that actual data pertaining to the groundwater table is not available at this mine site.

Computer Modeling Results

Having overcome the difficulties of acquiring the skills to use a computer software such as MODFLOW a couple of two-dimensional trial models were constructed and run (see Figure 117). Though approximate these models produced some interesting results. These outputs were plotted using SURFER (see Figure 119). Of particular interest in Figures 119 is the groundwater flow pattern around the mine pillars in the mine cavities.

Summary of Progress

The progress to date can be summarized as follows:

- A literature search has been conducted and more than 60 papers relevant to AMD and contaminant transport have been collected. A bank of over 175 references has been identified for potential future use in these areas.
- Standard levels of AMD have been established from reviewed literature and compared to the corresponding levels at the Longridge Mine.
- Hydrologic computations have been made to provide input for the modeling task.
- Relevant computer software has been identified for the computer modeling task and acquired in part.
- Some test problems were constructed and simulations were run using existing computer software.

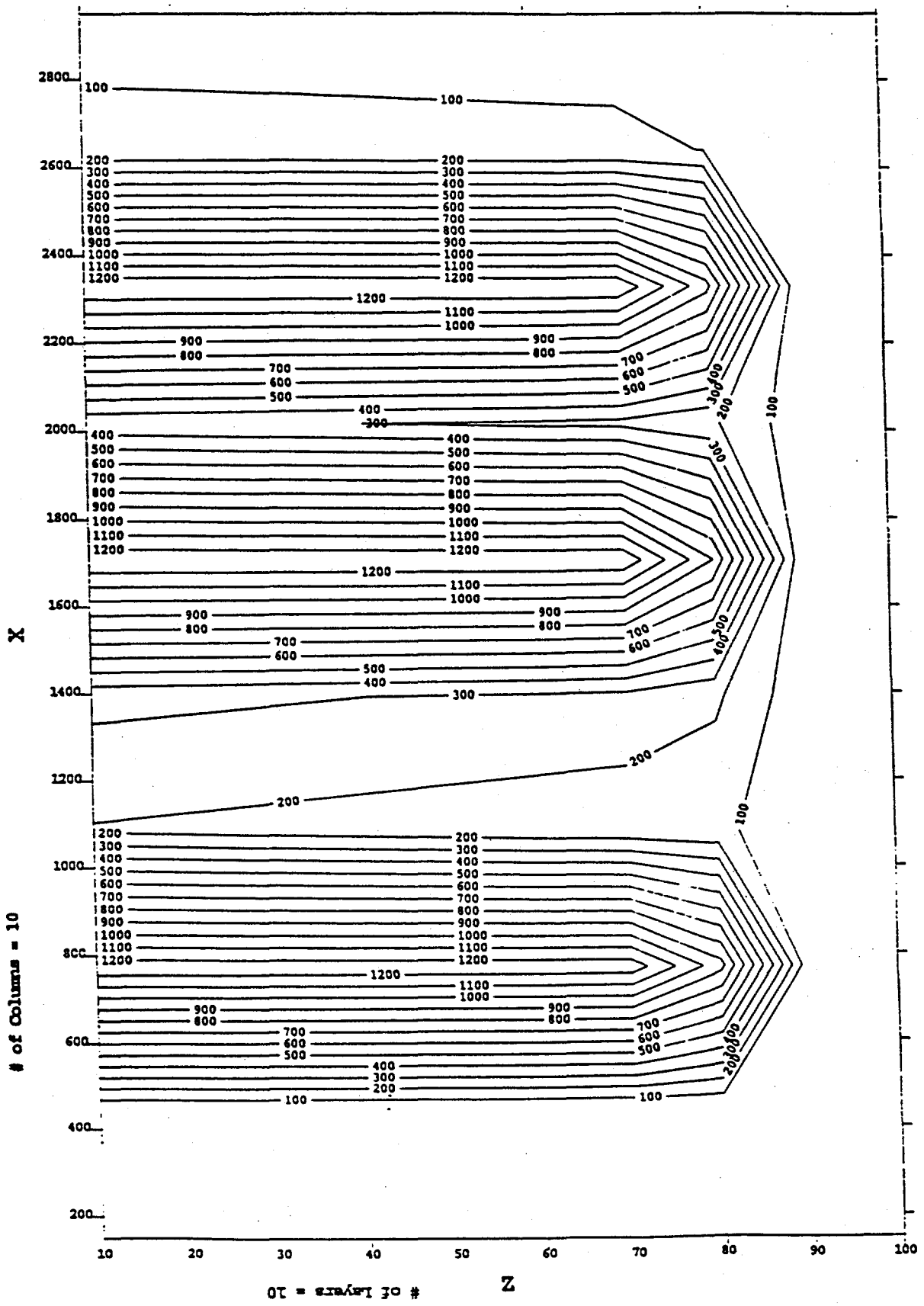

Figure 119 : SURFER Plot of The Fluid Heads Generated By The Second Trial MODFLOW Simulation

References

Barkat, O., R. Shaughnessy, and P.E. Clark, "A rheological Study of Cement Slurry", *Third Int. Symposium on Liquid-Solid Flows*, Presented at the Winter Annual Meeting of ASME, Illinois, Dec. 1988, p.115-120.

Barnes, H.A. and K. Walters, "The Yield Stress Myth?", *Rheol. Acta*, v.24, p.323-326, 1985.

Batarseh, Kareem., "Acid Mine Drainage", MS thesis, West Virginia University, West Virginia, 1987.

Batarseh, Kareem., "A Mathematical Model On The Role of Thiobacillus Ferro-Oxidans on Acid Mine Drainage", PhD thesis, West Virginia University, West Virginia, 1992.

Bedient, P.B., Rifai, H.S., and Newell, C.J., "Ground Water Contamination", PTR Prentice-Hall, Englewood Cliffs, NewJersey, 1994.

Burnett, M., "Development of a High Efficiency Ejector System," Final report on U.S. Bureau of Mines contract No. J0309012.

Burnett, M. and Black, D.C. "Determination of Engineering Requirements for Pnuematically Stowing Advanced Coal Combustion By-Products Underground." Final Report National Mine Land Reclamation Center, West Virginia University, 1994.

Bunn, T., A.J. Chambers, and C.M. Goh, "Rheology of Some Flyash Slurries", *Powder Handling and Technology*, v.3, n.3, p.221-226, Sept. 1991.

Cohen, Y. And A.B. Metzner, "Apparent Slip Flow of Polymer Solutions", *Journal of Rheology*, v.29, p.67-102, 1985.

Corbett, Don M., "Acid Mine Drainage Problem of The Patoka River Watershed, Southwestern Indiana", Water Resources Research Center, 1975.

Crittenden, John C., Neil J. Hutzler, David G. Geyer, Jacqueline L. Oravitz, and Gary Friedman. Transport of organic compounds with saturated groundwater flow: Model development and parameter sensitivity. Water Resour. Res., 22-3, 271-284, 1986.

Crochet, M.J. and K. Walters, "Numerical Methods in Non-Newtonian Fluid Mechanics", *Ann. Rev. Fluid Mechanics*, v.15, p.241-260, 1983.

Darby, Ron, "Determination and Utilization of Rheological Properties for Prediction of Flow Behavior of Pseudohomogeneous Slurries", Proceedings of the Ninth International Technical Conference on Slurry Transportation, Slurry Technology Association, Lake Tahoe, Nevada,

1984, p.107-115.

DePaoli, B., B. Bosco, R. Granata, and D.A. Bruce, "Fundamental Observations on Cement Based Grouts", Grouting, Soil Improvement, and Geosynthetics, Vol.1, ASCE Geotechnical Special Publication No. 30, New Orleans, Feb., 1992, p.474-485.

Freeze, R.A., and Cherry, J.A., "Groundwater", Prentice-Hall, Inc., Englewood Cliffs, NewJersey, 1979.

Govier, G.W. and K. Aziz, The Flow of Complex Mixtures in Pipes, Van Nostrad Reinhold Co., 1972.

Grim E., 1978. *Bentonites: Geology, Mineralogy, Properties and Uses,* Elsevier Scientific Pub. Co., New York.

Gupta,R.K., "Particulate Suspensions", *Flow and Rheology in Polymer Composite Manufacturing*, ed.S.G.Advani, Elsevier Science, Amsterdam, 1993, p.9-51.

Haan, C. T and B. J. Bakersfield., "Hydrology and Sedimentology of Surface Or Mined Lands", University of Kentucky, Lexington, 1978.

Håkansson, U., L. Hässler, and H. Stille, "Rheological Properties of Microfine Cement Grouts with Additives", Grouting, Soil Improvement, and Geosynthetics, Vol.1, ASCE Geotechnical Special Publication No. 30, New Orleans, Feb., 1992, p.551- 563.

Hanks, R.W. and K.H. Hanks, "The Importance of Yield Stress in Turbulent Slurry Pipeline Transport of Solids", Proceedings of the Ninth International Technical Conference on Slurry Transportation, Slurry Technology Association, Lake Tahoe, Nevada, 1984, p.117- 125.

Henderson, F.M., Open Channel Flow, Macmilian Publishing Co., 1966

James, T. J. (1984) "Characterization of Water Quality for Deep Mine Effluents of Upper Freeport and Bakersfield Coal Mines in Central Preston County, WV," MS Thesis, West Virginia University, Morgantown, WV.

Jeffrey,D.J. and A.Acrivos, "The Rheological Properties of Suspensions of Rigid Particles", *AIChE J.*, v.22, p.417-432, 1976.

Lawal, A., D.M. Kaylon, and U. Yilmazer, "Extrusion and Lubrication Flows of Viscoplastic Fluids with Wall Slip", *Chem. Eng. Comm*, v.122, p.127-150, 1993.

Lombardi, G., "The Role of Cohesion in Cement Grouting of Rock", 15th ICOLD, Lausanne, Q58, R13, p. 235-261, 1985.

Ludwig, J.C., Qin,H.Q., and Spalding, D.B., "The PHOENICS Reference Manual", CHAM TR/200, CHAM LTD., Wimbeldon Village, London, UK., 1989.

McDonald, Michael G., and Arlen W. Harbaugh "A Modular Three-Dimensional Finite Difference Flow Model", developed for USGS, 1985.

Maryland Department of Natural Resources.,"Mine Drainage Pollution Watershed Survey, Cherry Creek, Casselman River Watersheds, Garrett County, Maryland", Skelly and Roy, Baker-Wibberley and Associates Inc., prepared for Appalachian Regional Commission, 1969.

Mase, G.E and G.T.Mase, Continuum Mechanics for Engineers, CRC Press, 1992.

Metzner, A. B., and Otto, R. E., 1957. Agitation of Non-Newtonian Fluids, *A.I.Ch.E. Journal.* Vol. 3, No. 1, pp. 3 - 11.

Mori, H. and Y. Tanigwa, "Simulation Methods for Fluidity of Fresh Concrete", Memoirs of the School of Engineering, Nagoya University, V.44, n.1, p.71-133, 1992.

Nguyen, Q. D., and Boger, D. V., 1992. Measuring the Flow Properties of Yield Stress Fluids, *Ann. Rev. Fluid Mech.,* pp. 47 - 88.

O'Donovan, E.J. and R.I. Tanner, "Numerical Study of the Bingham Squeeze Film Problem", *Journal of Non-Newtonian Fluid Mechanics*, v.15, p.75-83, 1984.

Panda,D., A. Parida, J.S. Murty, and A.K. Mitra, "Transportation of Coarse Coal in a Fine Medium", *Int. J. Multiphase Flow*, v.20, n.1, p.171-176, 1994.

Patankar, S.V., Numerical Heat Transfer and Fluid Flow, Hemisphere Publishing Corp., Washington, 1980.

Patel,R.D., "Non-Newtonian Flows", pp 135-175, Handbook of Fluids in Motion, ed.N.P. Cheremisinof and R.Gupta, Ann Arbor, 1984, p.135-176.

Putnam, S.J., " Rheological Properties of Fluidized Bed Combustion Ash Grouts", Master's Thesis, West Virginia University, 1996.

Roache, P.J., "A Method for Uniform Reporting of Grid Refinement Studies", FED-Vol. 158, Quantification of Uncertainty in Computational Fluid Dynamics, ASME, 1993, p.109-120.

Sakuta, M., S. Yamane, H. Kasami, A. Sakamoto, "Pumpability and Rheological Properties of Fresh Concrete", Takenaka Technical Research Report, n.22, p.90- 97, Oct., 1979.

Schowalter, W.R., "The Behavior of Complex Fluids at Solid Boundaries", *Journal of Non-*

Newtonian Fluid Mechanics, v.29, p.25-36, 1988.

Skelland, A. H. P., 1983. Mixing and Agitation of Non-Newtonian Fluids, *Handbook of Fluids in Motio,*. Edited by N. P. Cheremisinoff and R. Gupta, Ann Arbor Science, Michigan, p.185

Skousen, J.G., and P.F. Ziemkiewicz (1995) "Acid Mine Drainage Control and Treatment," West Virginia University and the National Mine Land Reclamation Center, Morgantown, WV.

Silliman, W.J. and L.E. Scriven, "Separating Flow Near a Static Contact Line: Wall Slip at a Wall and Shape of a Free Surface", *Journal of Computational Physics*, v.34, p.287- 313, 1980.

Susquehanna River Commission.,"Coal Mine Drainage In The Susquehanna River Basin", Skelly and Roy, Pennsylvania, 1973.

Tattersall, G. H., and Bloomer, S. J., 1979. Further Development of the Two-Point Test for Workability and Extension of its Range. *Magazine of Concrete Research*, Vol. 31, No. 109. pp. 202-210.

West Virginia Geological and Economic Survey., "Stopping Acid Mine Drainage", West Virginia, 1985.

White, F.M., Viscous Fluid Flow, McGraw-Hill, Inc., 1991.

Yilmazer, U. And D.M. Kalyon, "Slip Effects in Capillary and Parallel Disk Torsional Flows of Highly Filled Suspensions", *Journal of Rheology*, v.33, p. 1197-1212, 1989.

Yoshimura, A.S. amd R.K. Prud'Homme, "Wall Slip Effects on Dynamic Oscillatroy Measurements", *Journal of Rheology*, v.32, p.575-584, 1988.

Zheng, C., "A Modular Three-Dimensional Transport Model for Simulation of Advection, Dispersion and Chemical Reactions of Contaminants in Groundwater Systems", S. S. Papadopulos & Associates Inc., Maryland, 1990.

Appendix-1
List of Collected Literature

Abriola, Linda M., George F. Pinder. A multiphase approach to the modeling of porous media contamination by organic compounds; 1.Equation Development. Water Resour. Res., 21-1, 11-18, 1985.

Aldous, P. J., and P. L. Smart. Tracing ground-water movement in abandoned coal mined aquifers using fluorescent dyes. Ground water. 26-2, 172-178, 1988.

Azimi-Zonooz, Ali., and Christopher J. Duffy. Modeling transport of subsurface salinity from a Mancos Shale hillslope. Ground Water. 31-6, 972-981, 1993.

Bassett, R. L., William R. Miller, John McHugh, and John G. Catts. Simulation of natural acid sulfate weathering in an Alpine Watershed. Water Resour. Res., 28-9, 2197-2209, 1992.

Booty, W. G., J. V. DePinto, and R. D. Scheffe. Drainage basin control of acid loadings to two Andirondack lakes. Water Resour. Res., 24-7, 1024-1036, 1988.

Chu, Wen-Sen., Eric W. Strecker, and Dennis P. Lettenmaier. An evaluation of data requirements for groundwater contaminant transport modeling. Water Resour. Res., 23-3, 408-424, 1987.

Corapciouglu, M. Yavuz., Arthur L. Baehr. A compositional multiphase model for groundwater contamination by petroleum products; 1. Theoretical Considerations. Water Resour. Res., 23-1, 191-200, 1987.

Cosby, B.J., G. M. Hornberger, R. F. Wright, J. N. Galloway. Modeling the effects of acid deposition: Control of long-term sulfate dynamics by soil sulfate adsorption. Water Resour. Res., 22-8, 1283-1291, 1986.

Crittenden, John C., Neil J. Hutzler, David G. Geyer, Jacqueline L. Oravitz, and Gary Friedman. Transport of organic compounds with saturated groundwater flow: Model development and parameter sensitivity. Water Resour. Res., 22-3, 271-284, 1986.

Dria, Myra A., Steven L. Bryant, Robert S. Schechter, and Larry W. Lake. Water Resour. Res., 23-11, 2076-2090, 1987.

Driscoll, Charles T., Noye M. Johnson, Gene E. Likens, and Michael C. Feller. Effects of acid deposition on the chemistry of headwater streams: A comparison between Hubbard Brook, New Hampshire, and Jamieson Creek, British Colombia. Water Resour. Res., 24-2, 195-200, 1988.

Dutton, Alan R., Brackish water in unsaturated confining beds at a Texas Lignite mine. Ground

Water. 23-1, 42-51.

Ebraheem, A. M., M. W. Hambuger, E. R. Bayless, and N. C. Krothe. A study of Acid Mine Drainage using Earth Resistivity measurements. Ground Water. 28-3, 361-368, 1990.

Enfield Carl G., Robert F. Carsel, Stuart Z. Cohen, To Phan, and David M. Walters. Approximating pollutant transport to Ground Water. Ground Water. 20-6, 711-722, 1982.

Faust, Charles R., John W. Guswa, James W. Mercer. Simulation of three-dimensional flow of immiscible fluids within and below the unsaturated zone. Water Resour. Res., 25-12, 2449-2464, 1989.

Freeberg, K. M., P. B. Bedient, and J. A. Connor. Modeling of TCE contamination and recovery in a shallow sand aquifer. Ground Water. 25-1, 70-80, 1987.

Herlihy, Alan T., Aaron L. Mills, George M. Hornberger, and Amy E. Bruckner. The importance of sediment sulfate reduction to the sulfate budget of an impoundment receiving Acid Mine Drainage. Water Resour. Res., 23-2, 287-292, 1987.

Herlihy, A. T., P. R. Kaufmann, M. R. Church, P. J. Wigington, Jr., J. R. Webb, and M. J. Sale. The effects of acid deposition on streams in the Appalachian Mountain and Peidmont Region of the Mid-Atlantic United States. Water Resour. Res., 29-8, 2687-2703, 1993.

Hornberger, G. M., B. J. Cosby, and J. N. Galloway. Modeling the effects of acid deposition: uncertainty and spatial variability in estimation of long term sulfate dynamics in a region. Water Resour. Res., 22-8, 1293-1302, 1986.

Hossain, M. Akhter., and m. Yavuz Corapcioglu. Modifying the USGS solute transport computer model to predict high density hydrocarbon migration. Ground Water. 26-6, 717-723, 1988.

Humenick, M. J., L. Jan Turk, and Michael P. Colchin, Methodology for monitoring Ground water at Uranium Solution mines, Ground Water., 18-3, 262-273, 1980.

Hutzler, Neil J., John C. Crittenden, John S. Gierke, and Amy S. Johnson. Transport of organic compounds with saturated groundwater flow: Experimental results. Water Resour. Res., 22-3, 285-295, 1986.

Huyakorn, Peter S., Michael J. Ungs, Lee A. Mulkey, and Edward A. Sudicky. A three-dimensional analytical method for predicting leachate migration. Ground Water. 25-5, 588-598, 1987.

Kaluarachchi, J. J., and J. C. Parker. An efficient finite element method for modeling multiphase flow. Water Resour. Res., 25-1, 43-54, 1989.

Kaluarachchi, J. J., J. C. Parker, and R. J. Lenhard. A numerical model for areal migration of water and light hydrocarbon in unconfined aquifers. Adv. Water Resour. 13-1, 29-40, 1990.

Lenhard, R. J., and J. C. Parker. Estimation of free hydrocarbon volume from fluid levels in monitoring wells. Ground Water. 28-1, 57-67, 1990.

Lowell, Robert P., Contaminant transport in a single fracture: Periodic boundary and flow conditions. Water Resour. Res., 25-5, 774-780, 1989.

Lynch, James A., C. Mark Hanna, Edward S. Corbett. Predicting pH, Alkalinity, and total acidity in stream water during episodic events. Water Resour. Res., 22-6, 905-912, 1986.

Mercer, James W., and Charles R. Faust. Ground-Water modeling: an overview. Ground Water. 18-2, 108-115, 1980.

Oberlander, Phil L and R.W. Nelson. An idealized ground-water flow and chemical transport model (S-PATHS). Ground Water. 441-449. 1984.

Osborne, M., and J. Sakes. Numerical modeling of immiscible organic transport at the Hyde Park landfill. Water Resour. Res., 22-1, 25-33, 1986.

Parker, J. C., R. J. Lenhard, and T. Kuppusamy. A parametric model for constitutive properties governing multiphase flow in porous media. Water Resour. Res., 23-4, 618-624, 1987.

Parker, J. C., J. L. Zhu, T. G. Johnson, V. J. Kremesec, and E. L. Hockman. Modeling free product migration and recovery at hydrocarbon spill sites. Ground Water. 23-1, 119-128, 1994.

Scheidegger, Andre., Christa S. Burgisser, Michal Borkovec, Hans Sticher, Hans Meessen and Willem van Riemsdijk. Convective transport of acids and basis in porous media. Water Resour. Res., 30-11, 2937-2944, 1994.

Sleep, B. E., and J. F. Sakes. Modeling the transport of volatile organics in variablly saturated media. Water Resour. Res., 25-1, 81-92, 1989.

Spayd, Steven E., Movement of volatile organics through a fractured rock aquifer. Ground Water. Vol. 23. 496-502. 1985.

Swistock, Bryan R., David R. De Walle, and William Sharpe. Sources of acidic storm flow in an Appalachian headwater stream. Water Resour. Res., 25-10, 2139-2147, 1989.

Sakes, J. F., S. Soyupak, and G. J. Farquhar. Modeling leachate organic migration and attenuation in groundwaters below sanitary landfills. Water Resour. Res., 18-1, 135-145, 1982.

Tim, Udayodara S., and Saied Mostaghimi. Modeling transport of degradable chemical and its metabolites in the unsaturated zone. Ground Water. 27-5, 672-681, 1989.

Toran, Laura, and Kenneth R. Bradbury. Ground-Water flow model of drawdown and recovery near an underground mine. Ground Water. 26-6, 724-733, 1988.

Turk, J. T , and D. H. Campbell. Estimation of acidification of lakes in the Mt. Zirkel Wilderness area, Colorado. Water Resour. Res., 23-9, 1757-1761, 1987.

Warfinge, Per., and Harald Sverdrup. Soil Liming as a measure to mitigate acid runoff. Water Resour. Res., 24-5, 701-712, 1988.

Watson, Ian., Contaminant analysis- flow nets and the Mass Transport equation. Ground Water. 22-1, 31-37, 1984.

Weiss, Jonathan S., and Allan C. Razem. Simulation of groundwater flow in a mined watershed in eastern Ohio. Ground Water. 549-560. 1981.

Zheng, C. 1990. MT3D: A Modular Three Dimensional Transport Model for Simulation of Advection, Dispersion and Chemical Reactions of Contaminants in Groundwater Systems. For USEPA, RSKERL, Ada, OK.